# Method Development and Mechanistic Investigation of Nickel-Catalyzed Reductive Coupling Processes

**by**

**Ryan David Baxter**

**A dissertation submitted in partial fulfillment**
**of the requirements for the degree of**
**Doctor of Philosophy**
**(Chemistry)**
**in The University of Michigan**
**2010**

**Doctoral Committee:**

**Professor John Montgomery, Chair**
**Professor Melanie S. Sanford**
**Professor Phillip E. Savage**
**Assistant Professor Anne J. McNeil**

## Dedication

This dissertation is dedicated to my mother, Laura Martens, and grandfather, Floyd "Ike" Isenhart. I would not have come this far without their support and influence, and will be forever grateful.

## Acknowledgements

I would like to thank my advisor, Professor John Montgomery, for his guidance and support throughout my time at the University of Michigan. I am especially appreciative of his willingness to allow me to explore and develop our chemistry with a level of independence that I was unlikely to be granted elsewhere. I firmly believe that my development as a scientist would have been stunted without the opportunity for such independence.

Thank you to my Montgomery group colleagues, past and present, for their continued support and thought provoking discussions. I'm grateful to have had such a level of support so close at hand. Thank you to Allison Knauff and Zack Buchan for proofreading early drafts of this dissertation and for providing valuable suggestions and advice.

Special thanks to committee member and rotation advisor Melanie Sanford and her students for allowing me access to their equipment and expertise during the exploratory period of my mechanistic work. This help was invaluable in guiding the direction of my final project.

Thank you to committee member Anne McNeil for helpful discussions and guidance regarding the acquisition and interpretation of kinetic data.

A very special thanks goes to my family and friends who've supported me, not only in the past five years of graduate school, but throughout my entire life. I've been fortunate enough to have a support network that should be the envy of any man, and I share my success with all of them.

I love my family.

I love my wife.

## Table of Contents

## List of Schemes

## List of Tables

## List of Figures

## List of Abbreviations

| | |
|---|---|
| *n*-Bu | butyl |
| *t*-Bu | *tert*-butyl |
| COD | 1, 5-cyclooctadiene |
| $^{o}$C | temperature in degrees centigrade |
| d | day(s) |
| Et | ethyl |
| equiv | equivalent |
| GCMS | gas chromatography mass spectrometry |
| h | hour(s) |
| *n*-Hept | heptyl |
| *n*-Hex | hexyl |
| Hex | hexanes/hexyl |
| IMes | 1, 3-bis-(1, 3, 5-trimethylphenyl)imidazol-2-ylidene |
| IPr | 1, 3-bis-(2, 6-diisopropylphenyl)imidazol-2-ylidene |
| Me | methyl |
| min | minute(s) |
| NHC | *N*-heterocyclic carbene |
| PCC | pyridinium chlorochromate |
| Pent | pentyl |

| | |
|---|---|
| Ph | phenyl |
| *i*-Pr | isopropyl |
| *n*-Pr | propyl |
| rt | room temperature |
| TBAF | tetrabutylammonium fluoride |
| TBS | *tert*-butyldimethylsilyl |
| THF | tetrahydrofuran |
| TLC | thin layer chromatography |
| Tol | toluene |

# Abstract

Many classes of standard organic transformations involve the coupling or cycloaddition of two different π-components to assemble a more functionalized product. Many such processes are amenable to the union of two complex fragments, thus allowing convergent approaches to complex organic molecules. A number of transition metal catalyst / reducing agent combinations are known to promote various reductive coupling processes. With respect to the nickel-catalyzed variants that are the subject of this thesis, many reducing agents have been employed, and the most widely used classes include silanes, organozincs, organoboranes, molecular hydrogen, and alcohols. The specific focus of this thesis will be the development and mechanistic investigation of nickel-catalyzed reductive processes involving the coupling of aldehyde and alkyne π-systems.

Utilizing trialkylsilanes as reducing agents in nickel-catalyzed aldehyde / alkyne coupling processes allows access to various silyl-protected allylic alcohols.[1] However, in some cases, dialkylsilane reducing agents promote a formal silylene transfer to offer direct access to oxasilacyclic products. This novel transformation was shown to be effective across a wide range of aldehyde / alkyne combinations as well as in the presence of chiral ligands to promote the first reported asymmetric transfer of a silylene synthetic equivalent.

Under specific catalytic conditions, aldehyde / alkyne reductive couplings can be promoted to yield α,β-unsaturated ketones in the absence of an external reducing agent

via alkyne-hydroacylation. Crossover data suggests that this coupling occurs via a previously unreported bimetallic mechanism. Intramolecular couplings proved to be facile under thermal conditions while intermolecular couplings required microwave heating.

Due to the interest of nickel-catalyzed reductive coupling processes developed in our lab and others,[2, 3] a detailed initial-rates study of the aldehyde / alkyne / trialkylsilane variant was undertaken to better understand the role of each reactive component. Along with kinetic data, crossover and kinetic isotope effects with respect to the silane reducing agent were examined. A complete kinetic profile was obtained, and a mechanism was proposed based on the experimental findings.

# Chapter 1

# Nickel-Catalyzed Reductive Couplings of Aldehydes, Alkynes, and Dialkylsilanes: A Novel Route to Oxasilacyclopentenes

## 1.1 Introduction

### 1.1.1 Nickel-Catalyzed Aldehyde/Alkyne Couplings

Allylic alcohols are synthetically useful building blocks for a variety of transformations including Claisen rearrangements,[4] hydroxyl-directed addition to alkenes,[5] and metal catalyzed π-allyl chemistry.[6] Because of this broad utility, considerable effort has been invested in the development of processes that provide access to allylic alcohols in good yield and with high levels of stereocontrol. Historically, the most common methods for the preparation of allylic alcohols have been the Nozaki Hiyama Kishi[7,8] coupling or metallation/addition reactions[9] involving synthesis of stereochemically defined alkenyl coupling components (Scheme 1). More recently, our research group,[1,2] and others,[3] have focused on developing catalytic methods that utilize the coupling of aldehydes and alkynes in the presence of a variety of reducing agents to offer direct routes to allylic alcohols and their analogues.

**Scheme 1.** Previous Methods for the Stereoselective Synthesis of Allylic Alcohols

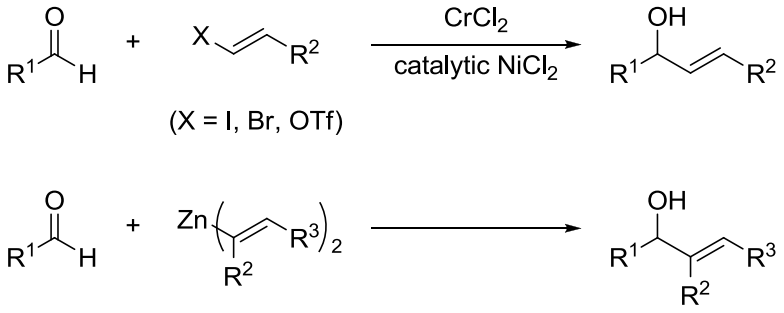


The nickel-catalyzed alkylative coupling (transferring a carbon substituent) of aldehydes and alkynes was first described by our group using organozinc reducing agents.[2] Using methodology previously developed for the intramolecular coupling of alkynyl enones,[10] derivatives of 5-hexynal were cyclized in the presence of $Ni(COD)_2$ and various organozinc reducing agents to afford cyclic allylic alcohols with stereodefined exocyclic tri- or tetrasubstituted olefins (Scheme 2). The methodology was tolerant of a variety of alkyne substitutions as well as various organozinc reducing agents.

**Scheme 2.** Nickel-Catalyzed Aldehyde/Alkyne Coupling with Organozinc Reducing Agents

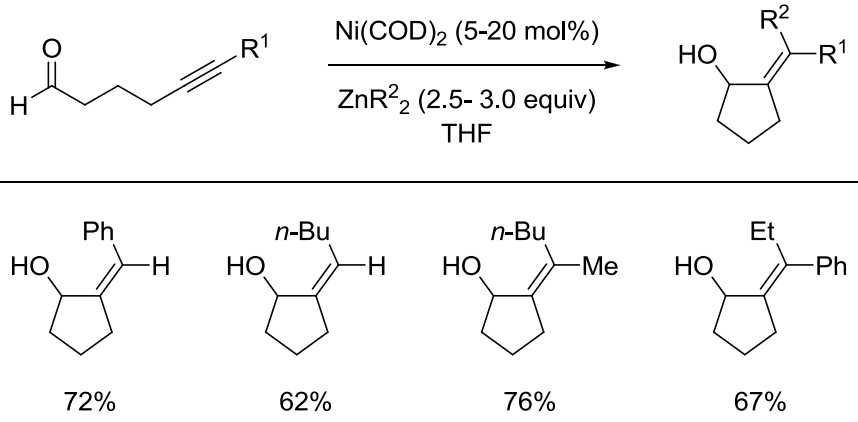


In the same report, reductive coupling (transferring a hydrogen substituent) could be promoted from identical starting materials using a $Ni(COD)_2/PBu_3$ catalyst system

with $ZnEt_2$ as the reducing agent. The change in mechanism from alkylative to reductive coupling was only observed using reducing agents bearing β-hydrogens and was rationalized by a change in the electronic environment of the nickel center in the presence of tributylphosphine ligands. The σ-donation from the phosphine ligands leads to an electron-rich metal center that likely suppresses the carbon-carbon bond forming reductive elimination pathway (Scheme 3). Under these specific reaction conditions, organozinc mediated reductive coupling was limited to intramolecular couplings only.

**Scheme 3.** Ligand Dependent Behavior of Nickel-Catalyzed Aldehyde/Alkyne Coupling

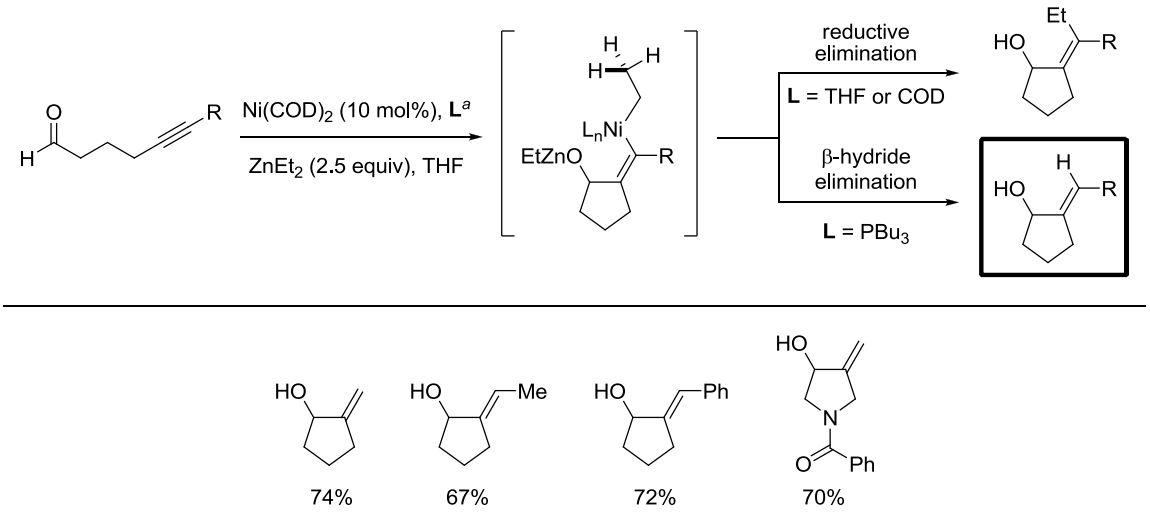


[a] 20 mol% of $PBu_3$ is used for reductive coupling.

A similar methodology was later developed by our lab to promote intramolecular aldehyde/alkyne couplings using trialkylsilane reducing agents as a more stable, non-nucleophilic alternative to zinc or zirconium reagents. This methodology was developed for the total synthesis of (+)-allopumiliotoxin 267A, (+)-allopumiliotoxin 339A, and (+)-allopumiliotoxin 339B.[11,12] High yields and excellent diastereoselectivities were

observed in the synthesis of bicyclic substrates (Scheme 4). However, the $PBu_3/Et_3SiH$ combination was not amenable for intermolecular reductive couplings.

**Scheme 4.** Couplings Towards the Total Syntheses of Allopumiliotoxins

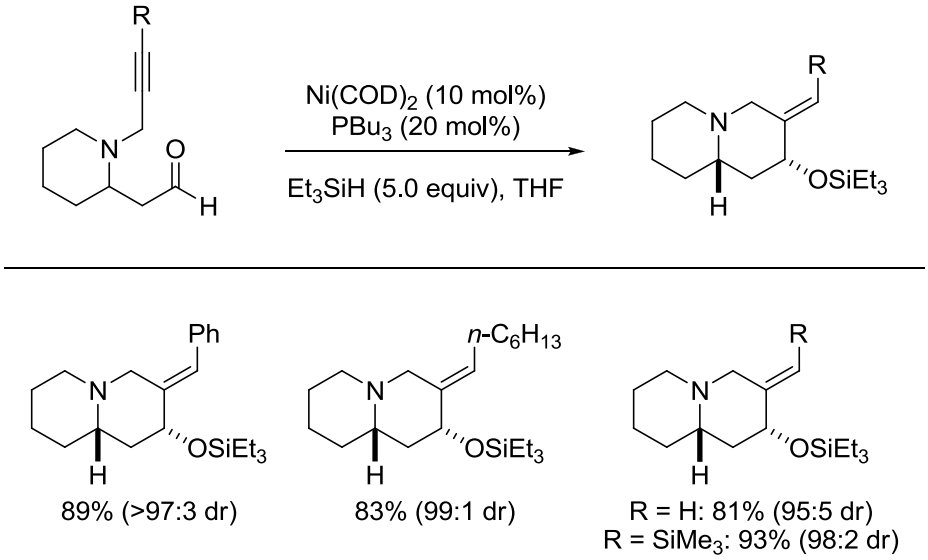


Related developments from Jamison and co-workers led to intermolecular reductive coupling of aldehydes and alkynes by utilizing trialkylborane reducing agents.[3] This process was most efficient for aromatic and internal alkynes, but was quite tolerant of various aldehydes (Scheme 5).

**Scheme 5.** Intermolecular Reductive Coupling Using Trialkylborane Reducing Agents

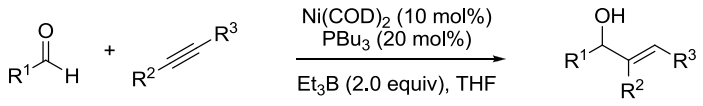


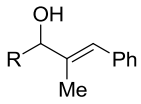

R = Ph: 77% (92:8 rs)
R = *n*-Pr: 85% (92:8 rs)

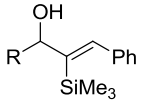

R = Ph: 49% (>98:2 rs)
R = *n*-Hept: 89% (>98:2 rs)

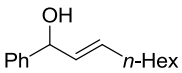

76% (96:4 rs)

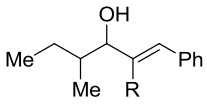

R = Me: 41% (94:6 rs, 66:34 dr)
R = $SiMe_3$: 31% (>98:2 rs, 58:42 dr)

Another important development from our lab regarding intermolecular reductive couplings of aldehydes and alkynes was the use of air- and bench-stable trialkylsilane reducing agents in combination with *N*-heterocyclic carbene (NHC) ligands to afford silyl-protected allylic alcohols (Scheme 6).[1]

**Scheme 6.** Nickel-Catalyzed Aldehyde/Alkyne Reductive Coupling with Trialkylsilanes

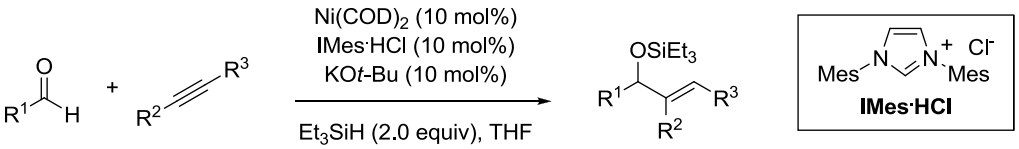


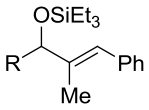

R = Ph: 84% (>98:2 rs)
R = *n*-Hex: 82% (>98:2 rs)

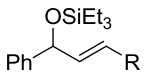

R = Ph: 72% (>98:2 rs)
R = *n*-Hex: 71% (>98:2 rs)

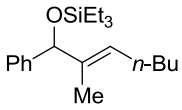

84 % (1.3:1)

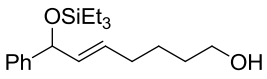

72 % (98:2)

Experimental evidence suggested that silanes of similar steric bulk but different molecular weight reacted with comparable rates, providing a handle for mechanistic study. To probe the role of the silane reducing agent in the coupling mechanism, $Pr_3Si$-H and $Et_3Si$-D were employed in equal amounts to determine if the relationship between the

silyl-hydride (or deuteride) and the alkyl group of the starting silane was maintained in the silylated products (Scheme 7).

**Scheme 7.** Nickel-Catalyzed Intermolecular Crossover Experiment

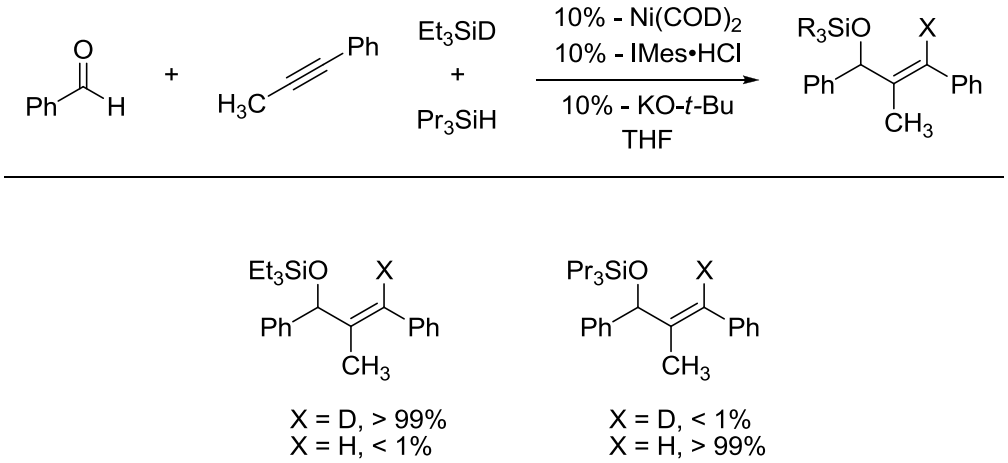


As illustrated above, both products are formed in comparable amounts, and with nearly complete retention of the relationship between the alkyl group and hydride/deuteride from the silane reducing agent. Based on this result, and the similarity in reaction rates between different silanes, a mechanism was proposed that involves rate-determining oxidative cyclization to metallacycle **1** followed by rapid σ-bond metathesis with the silane reducing agent leading to product after simple reductive elimination (Scheme 8).

**Scheme 8.** Proposed Mechanism for Nickel-Catalyzed Reductive Couplings of Aldehydes, Alkynes, and Trialkylsilanes

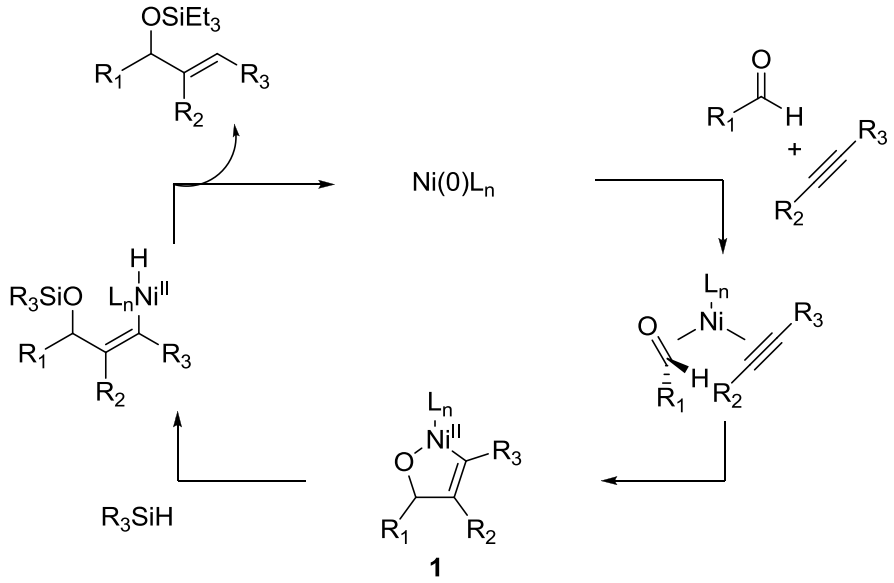


Based on this proposed mechanism, the identity of the silane reducing agent should not alter the efficacy of the coupling process as long as it is sufficiently reactive to reduce metallacycle **1**, leading to catalyst turnover. To expand the scope of the reductive coupling methodology, we sought to examine the use of dialkylsilanes as reducing agents to afford analogous silyl-protected allylic alcohols, but ones that still retained a reactive silicon-hydride bond (Scheme 9). The allylic alkoxysilane products, **2**, could then be used to promote the formation of oxasilacyclopentanes, **3**, through an intramolecular alkene hydrosilylation.

**Scheme 9.** Allylic Alkoxysilane Formation via Nickel-Catalysis

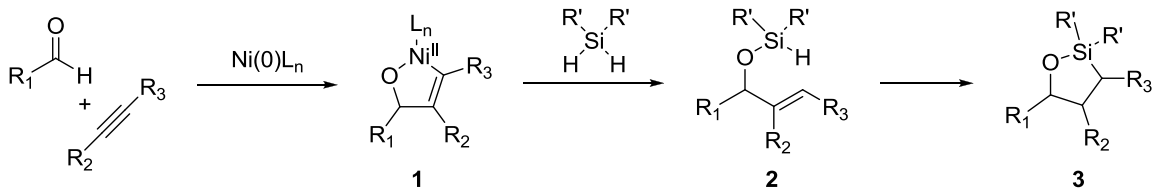

### 1.1.2 Preparation and Utility of Silacycles

#### 1.1.2.1 Silacycles as Synthetic Intermediates

Oxasilacyclopentanes and oxasilacyclopentenes are useful synthetic intermediates in a variety of organic transformations including oxidations, nucleophilic additions, and metal-catalyzed cross-couplings.[13,14] Since the development of the Tamao-Fleming oxidation in 1983, silicon-carbon bonds have been used as masked alcohols in a variety of settings.[15,16] This masked functionality was utilized in the synthesis of the C1-C21 subunit of the protein phosphatase inhibitor *tautomycin* by J. A. Marshall et al (Scheme 10).[17] The oxidation of a vinyl carbon-silcon bond leads to the formation of an enol intermediate which tautomerizes to a β-hydroxy ketone, completing the synthesis of the subunit.

**Scheme 10.** Silacyclic Intermediate in the Synthesis of the C1-C21 Subunit of *Tautomycin*

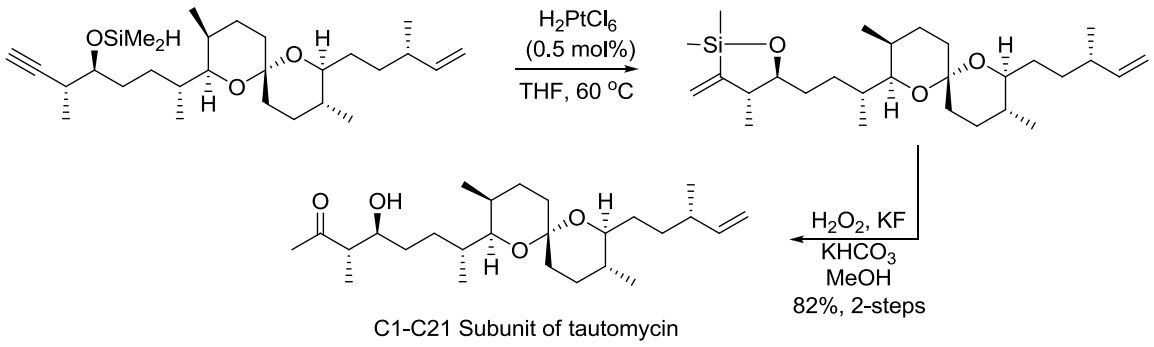


Oxasilacyclopentanes can also be used as electrophiles in nucleophilic substitution reactions (Scheme 11).[13] This strategy, combined with the Tamao-Fleming oxidation, allows access to highly functionalized 1, 3-diols through a straightforward two-step procedure.

**Scheme 11.** Nucleophilic Substitution/Tamao-Fleming Oxidation Sequence

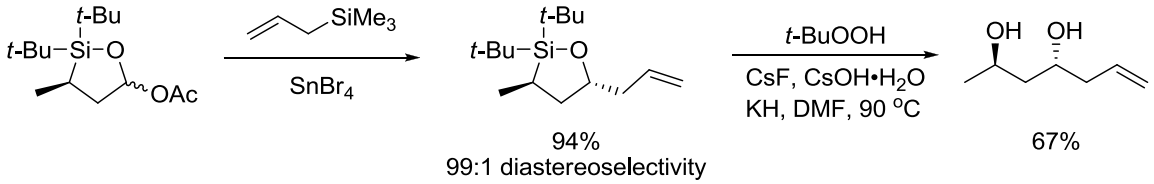


Utilizing the vinyl carbon-silicon bond of oxasilacyclopentenes as a coupling partner for reaction with aryl halides and transition metals has been a focus of the Denmark group in the last several years (Scheme 12). Combining a fluoride source, such as *n*-BuNF, with a palladium catalyst, Denmark et al. were able to promote couplings of various oxasilacyclopentenes and aryl iodides to yield highly functionalized allylic alcohols.[14]

**Scheme 12.** Pd-Catalyzed Cross Coupling of Oxasilacyclopentenes with Aryl Iodides

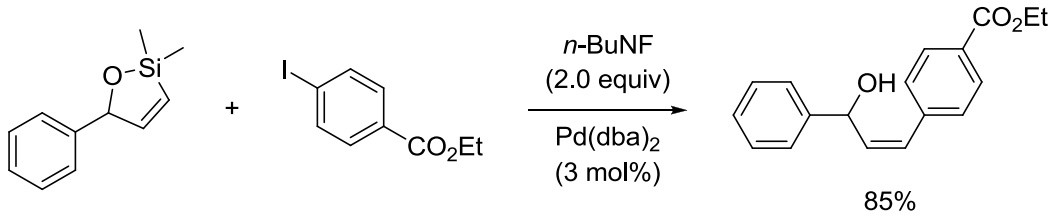


### 1.1.2.2 Silacycles via Hydrosilylation

Due to the synthetic utility of oxasilacyclopentanes and oxasilacyclopentenes, several methodologies exist to promote their formation from a variety of starting material/reagent combinations. Early methods of oxasilacyclopentane formation involved intramolecular hydrosilylation of an olefin via metal-catalysis using Ir, Pt, or Rh catalysts (Scheme 13).[18]

**Scheme 13.** Alkene Hydrosilylation via Rhodium Catalysis

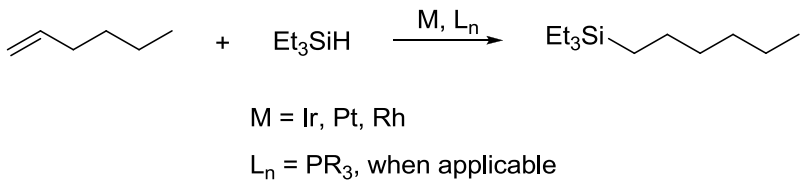


The generally accepted mechanism for alkene hydrosilylation, first described by Chalk and Harrod, involves oxidative cleavage of the Si-H bond by action of the metal catalyst, coordination of the alkene π-system to the metal center, and a migratory insertion/reductive elimination sequence which yields the silylated product and regenerates the active catalyst (Scheme 14).[19] This reaction sequence leads to silacyclic products when applied in an intramolecular setting with the silane tethered to the reacting π-system (an example of which is shown in Scheme 15).[18]

**Scheme 14.** Mechanism of Alkene Hydrosilylation

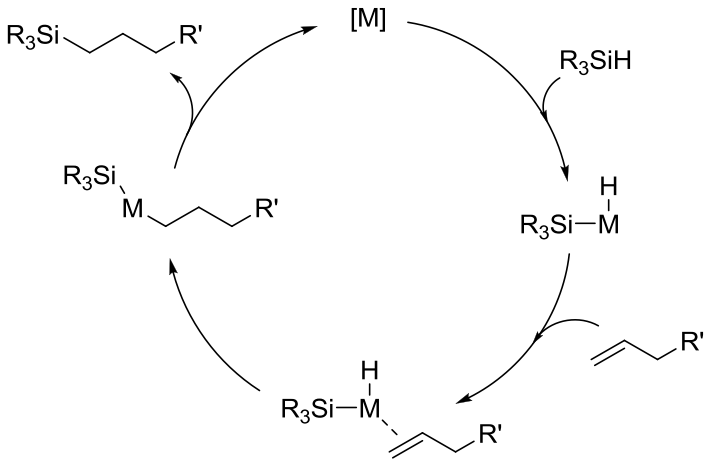

**Scheme 15.** Intramolecular Alkene Hydrosilylation Leading To Silacycles

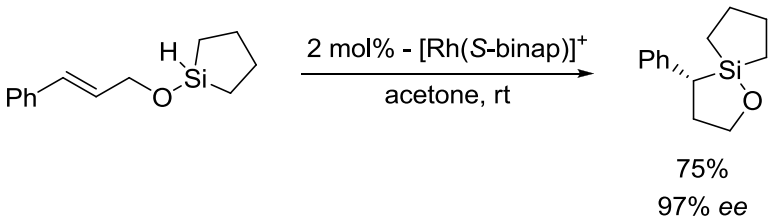


### 1.1.2.3 Silacycles via Silylformylation

Silylformylation, defined as the addition of $R_3Si$- and -CHO equivalents across various types of bonds, was first discovered by Murai et al., who developed the cobalt-catalyzed silylformylation of aldehydes, epoxides, and cyclic ethers.[20] This methodology was later expanded by Leighton et al. using rhodium catalysts pressurized with carbon monoxide to promote intramolecular silylformylations on alkenes to produce oxasilacyclopentanes (Scheme 16).[21] A similar strategy was also applied to the intramolecular silylformylations of alkynes in a tandem silylformation/allylsilylation process that is proposed to go through a silacyclic intermediate (Scheme 17).[22]

**Scheme 16.** Oxasilacyclopentanes from Intramolecular Alkene Silylformylations

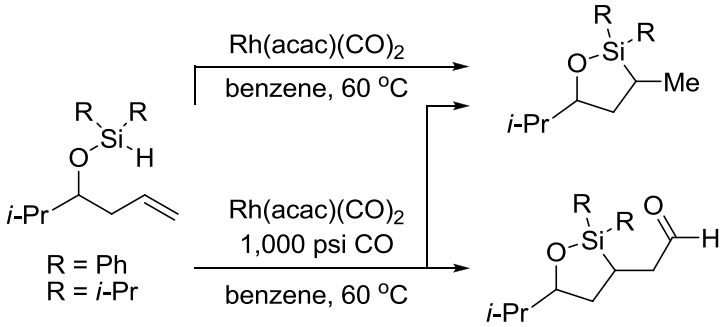

**Scheme 17.** Oxasilacyclopentane Intermediates in a Tandem Silylformation, Allylsilylation Sequence of Alkynes

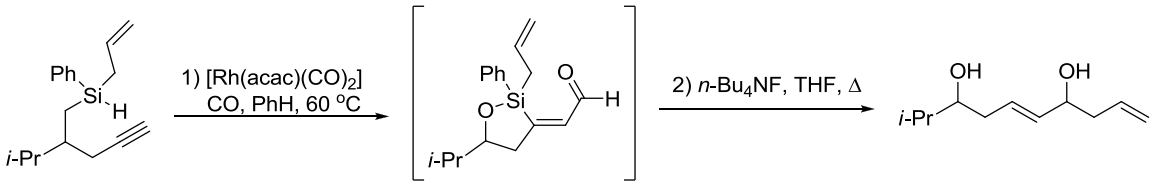


### 1.1.2.4 Silacycles via Cycloadditions of Silylene Equivalents

Perhaps the most robust strategy for the synthesis of oxasilacycles has been the cycloaddition of silylene equivalents primarily developed by the Woerpel lab.[23-25] This methodology involves the stoichiometric generation and purification of silylene transfer reagent **4** by the reduction of $(t\text{-Bu})_2SiCl_2$ in the presence of cyclohexene (Scheme 18).

**Scheme 18.** Generation of a Silylene Transfer Reagent from $(t\text{-Bu})_2SiCl_2$

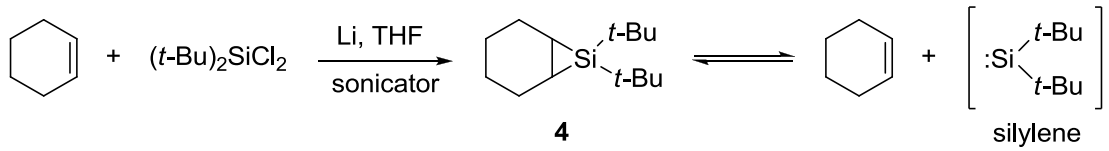


Reagent **4** can be transferred across the π-system of various alkynes[23] in the presence of carefully chosen silver-salts to generate a reactive silacyclopropene intermediate, **5**, which is capable of undergoing a metal-catalyzed ring expansion in the presence of carbonyls to yield oxasilacyclopentenes of various substitution (Scheme 19).

**Scheme 19.** Oxasilacyclopentenes via a Silylene Transfer, Ring Expansion Sequence

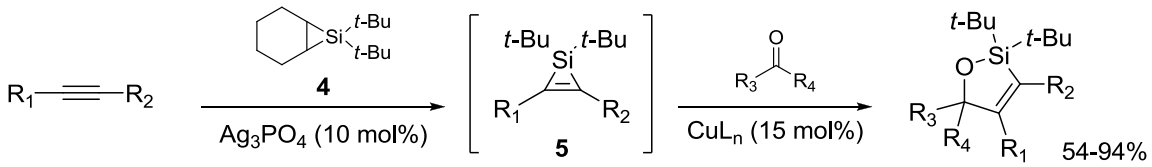


The mechanism by which intermediate **5** undergoes ring expansion with a carbonyl system in the presence of a copper catalyst has been the source of intense study.[25] NMR experiments and regiochemical probes support a mechanism by which intermediate **5** undergoes stereospecific ring opening by action of the copper catalyst to yield the vinyl-copper species **6**. Coordination of the carbonyl unit, followed by an oxidative addition/silylation sequence leads to the ring-expanded intermediate **7** before reductive elimination yields the oxasilacyclopentene product (Scheme 20).

**Scheme 20.** Silylene Transfer, Ring Expansion Mechanism

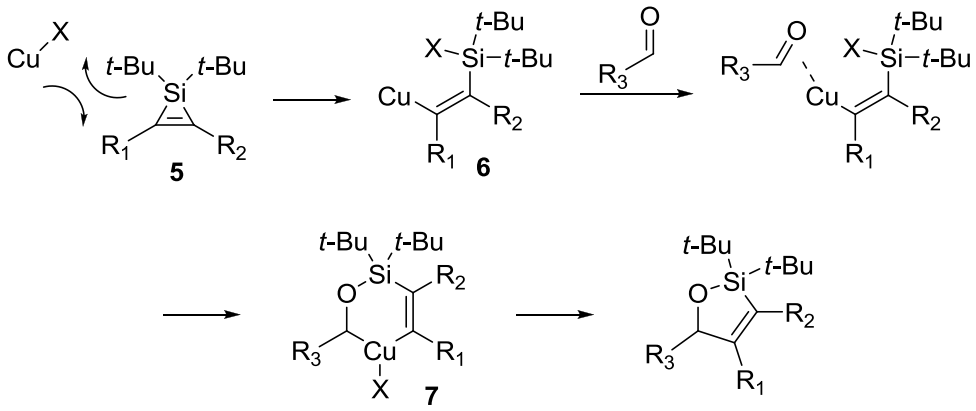


Very high levels of regioselectivity were noted for the formation of oxasilacyclopentenes via the sequence described in Scheme 19, with several examples achieving greater than 99:1 selectivity.[23] Such high levels of stereocontrol were rationalized by the minimization of steric interactions in the initial ring opening event

from **5** to **6**. This effect is illustrated in Scheme 21 with the silacyclopropenation of 1-phenyl-1-propyne followed by the carbonyl insertion of butyraldehyde. As shown below, the large substituents on silicon have a direct interaction with the vinyl substituent at the position distal to the bond which is breaking in transition state **8**. In all cases, this steric effect is minimized to produce the product which came from carbonyl insertion adjacent to the more sterically demanding group of the silacyclopentene (transition state **9**).

**Scheme 21.** Stereochemical Model for High Levels of Regiocontrol

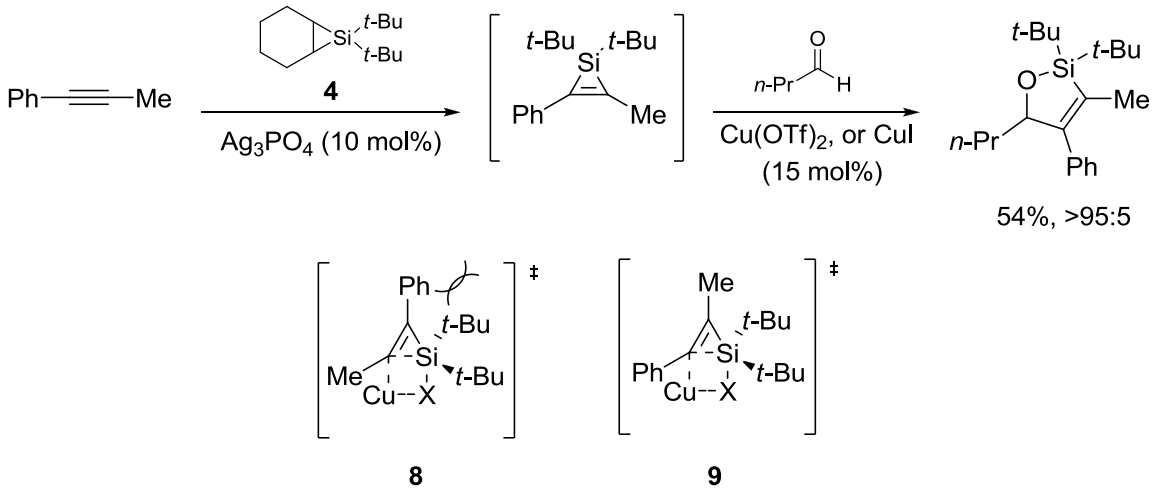


## 1.2 Results and Discussion

### 1.2.1 Nickel-Catalyzed Reductive Couplings of Aldehydes, Alkynes, and Dialkylsilanes

As discussed in Section 1.1, our group had recently expanded upon current methodology for the nickel-catalyzed reductive coupling of aldehydes and alkynes with the use of air- and bench-stable trialkylsilane reducing agents. In an effort to continue the development of this strategy, alkylsilanes of various composition were examined. Specifically, it was proposed that the use of dialkylsilanes would lead to analogous silyl-

protected allylic alcohol products (**2**), but retain a reactive Si-H bond that could be activated to promote intramolecular transformations such hydrosilylation or allylic transposition of the double bond (Scheme 22). Based on mechanistic understanding at the time, it was predicted that the identity of the silane reducing agent should not diminish the efficacy of the coupling process as illustrated in Scheme 7.

**Scheme 22.** Proposed Strategy for the Utilization of Dialkylsilanes in Nickel Catalysis

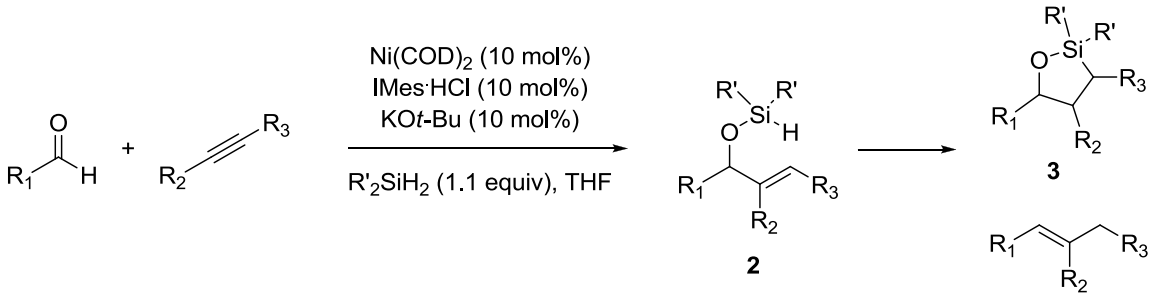


Initial efforts focused on simply replacing $Et_3SiH$ with commercially available $(t\text{-}Bu)_2SiH_2$ to explore the formation of products analogous to **10** (Scheme 23). This strategy was met with limited success and was hampered by low yields due to poor conversion. In all cases, large amounts of recovered starting material accounted for a significant portion of the mass balance of the reactions. Side-products were not observed in significant amounts, and it appeared that the reactions simply suffered from low reactivity.

**Scheme 23**. Initial Results of Ni(0)-Catalyzed Coupling of Aldehydes, Alkynes, and Dialkylsilanes

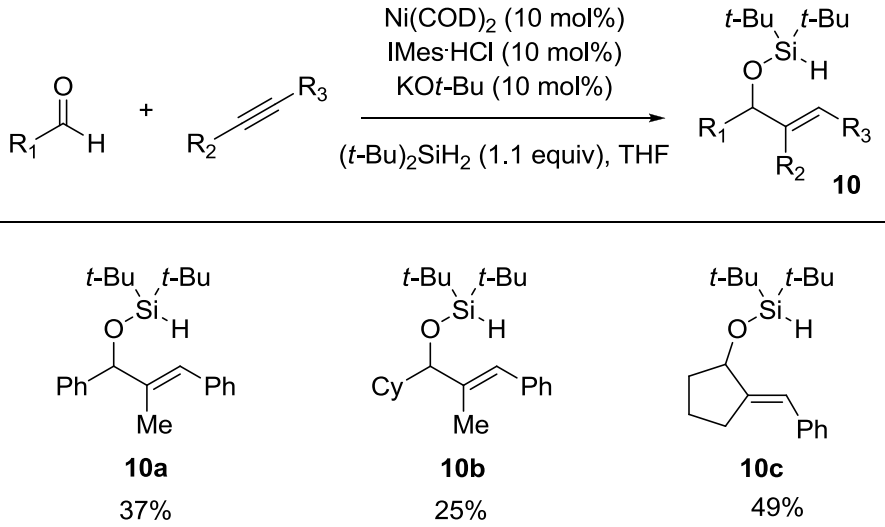


With these products in hand, studies with respect to the activation of the remaining Si-H bond were undertaken concurrently with reaction optimization efforts. It was proposed that nucleophilic activation of the silicon atom may promote an intramolecular hydride delivery to the conjugated alkene, allowing for an allylic transposition to take place, liberating the silicon group to yield a simple alkene product (Scheme 24).[26]

**Scheme 24.** Allylic Transposition via Intramolecular Hydride Delivery

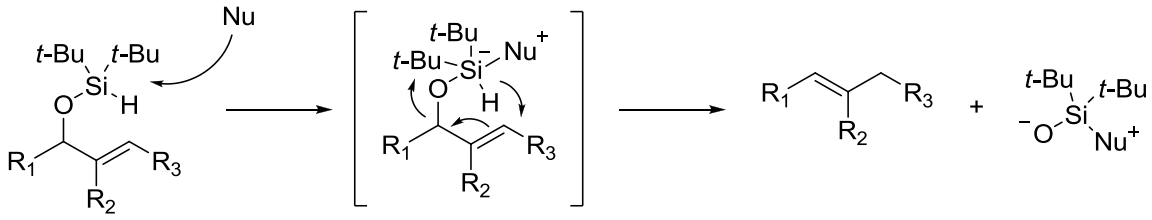


Listed below is a table of conditions examined for allylic transpositions in an effort to generate conjugated alkenes from allylic alkoxysilanes. For the purposes of

exploratory reactions, all conditions were examined using allylic alkoxysilane **10a** as starting material (Table 1).

**Table 1.** Conditions Examined for Allylic Transpositions of Alkoxysilanes

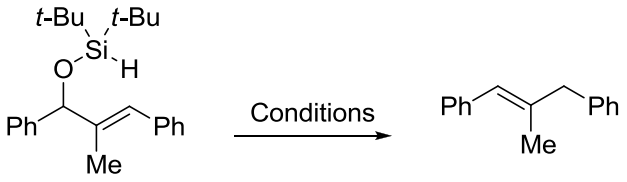


**10a** **11**

| Entry | Conditions | Result |
|---|---|---|
| 1 | Ti(O-*i*-Pr)$_4$, -78 $^{o}$C to rt | recovered SM only |
| 2 | Ti(O-*i*-Pr)$_4$ 25 - 45 $^{o}$C | recovered SM only |
| 3 | Ti(O-*t*-Bu)$_4$, rt | recovered SM only |
| 4 | *n*-BuNF, rt | deprotected alcohol only |
| 5 | CsF, -78 $^{o}$C to rt | recovered SM only |
| 6 | $BF_3$-OEt, -78 $^{o}$C to rt | decomposition + SM |
| 7 | TsOH, -78 $^{o}$C to rt | decomposition + SM |
| 8 | TMS-OTf, -78 $^{o}$C to rt | 60% - desired product |
| 9 | Acetic Acid, -78 $^{o}$C to rt | decomposition + SM |
| 10 | TMS-Cl, -78 $^{o}$C to rt | recovered SM only |
| 11 | HCl-$Et_2O$, rt | mixture of SM, product and decomposition |

As shown in Table 1, only one of several sets of conditions examined led to a significant yield of the desired alkene, which was formed as a complex mixture of isomers (entry 8). Control reactions incorporating stoichiometric amounts of 2,6-di-*tert*-butyl-4-methyl-pyridine as a Brønsted acid scavenger led to no formation of the desired product (Scheme 25). In fact, even catalytic amounts of 2,6-di-*tert*-butyl-4-methyl-pyridine (~10 mol%) were enough to quench the reactivity of TMS-OTf.

**Scheme 25.** 2,6-Di-*tert*-butyl-4-methyl-pyridine as an Acid Scavenger

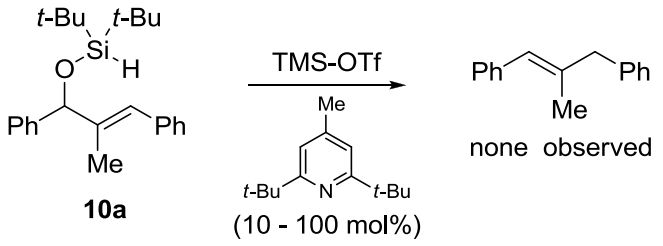


### 1.2.2 Concurrent Formation of Allylic Alkoxysilanes and Oxasilacyclopentenes

It was at this point in the efforts to optimize the formation of products analogous to **10a** that a unique result was discovered. Previous studies have shown $Ni(COD)_2$ to be tolerant of alkoxy Lewis acids in the context of reductive coupling reactions.[27] It was hoped that the use of $Ti(O\text{-}i\text{-}Pr)_4$, or similar Lewis acidic additives, would enhance the electrophilicity of the aldehyde coupling component, leading to greater reaction conversion. Surprisingly, in some cases the use of $Ti(O\text{-}i\text{-}Pr)_4$ led directly to the formation of oxasilacyclopentene product **12** while simultaneously increasing the yield of allylic alkoxysilane **10b** (Scheme 26).[28]

**Scheme 26.** Concurrent Formation of Allylic Alkoxysilanes and Oxasilacyclopentenes

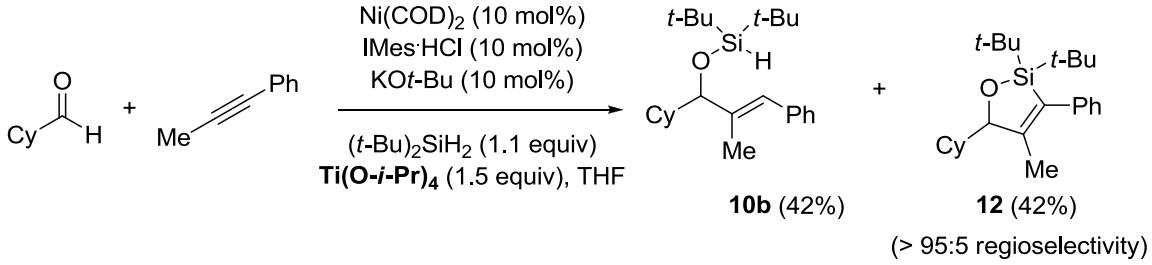


Control reactions showed that **10b** and **12** did not interconvert under the reaction conditions, suggesting that **12** is not formed via an intramolecular hydrosilylation-type

process from **10b**. Furthermore, GCMS analysis showed that **10b** and **12** were formed at nearly identical rates throughout the productive reaction. Since an initial goal of the methodological study was to promote the formation of oxasilacyclopentanes (analogous to **12**, but fully saturated), the focus of subsequent efforts involved favoring the production of **12** over **10b**. Extensive variation of order of addition, rate of addition, ligand structure, and solvent composition had little effect on the ratio of **10b** to **12**, which remained at nearly 1:1 regardless of substrates.

### 1.2.3 Lewis Acid Screening and Reaction Optimization

While procedural changes in the experimental setup had little effect on the ratio of **10b** to **12**, it was envisioned that the identity of the Lewis acid, which in most cases is necessary for the production of **12**, would have the largest impact on the product ratio. Several commercially available Lewis acidic reagents were examined in the coupling strategy to produce **12**, and their efficacy was judged based on the GCMS ratio of **10b** to **12** at the completion of the reaction (Table 2).

**Table 2.** Reaction Optimization: Lewis Acid Screening

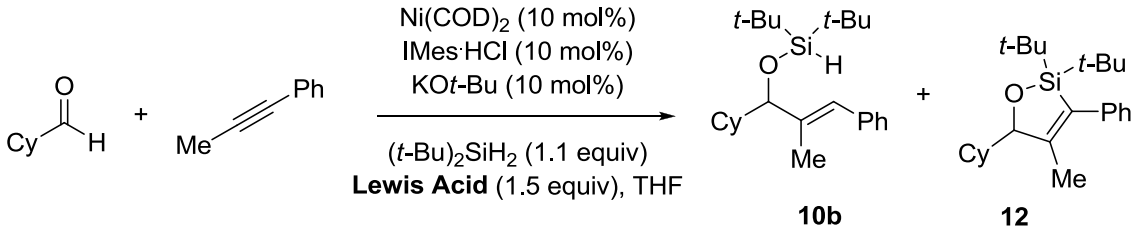


| Lewis Acid | Ratio **10b**:**12** |
|---|---|
| $Ti(O\text{-}Pr)_4$ | 1.:1.49 |
| $Ti(O\text{-}i\text{-}Pr)_4$ | 1:1.71 |
| $Ti(O\text{-}t\text{-}Bu)_4$ | 1:1.71 |
| $Al(O\text{-}i\text{-}Pr)_3$ | 1:1.72 |
| $Zr(OEt)_4$ | 1:1.71 |
| $TiF_4$ | N/A |
| $BF_3{:}OEt_2$ | N/A |
| $Sn(OTf)_2$ | N/A |
| $VO(OPr)_3$ | N/A |
| $Zn(OTf)_2$ | N/A |

Based on the results illustrated in Table 2, and due to its ease of use as a solid reagent, aluminum isopropoxide was chosen as the optimal Lewis acidic additive. A modest increase in selectivity was also noted when moving to a solvent of mixed composition containing an 8:1 ratio of THF to toluene, due to the increased solubility of $Al(O\text{-}i\text{-}Pr)_3$. It was clear based on the results of Table 2 that only alkoxy Lewis acid additives were effective in promoting the formation of **12**, a fact that would become important when rationalizing the proposed mechanism (discussed in Section 1.2.4).

At this point, even under the optimized reaction conditions, only modest yields were observed in the production of **12**, and always with concurrent production of **10b**.

However, switching to the much more reactive $Et_2SiH_2$ from $(t\text{-Bu})_2SiH_2$ led to the absence of products analogous to **10b**, although a new series of side-products were observed (Scheme 27).

**Scheme 27.** Aldehyde/Alkyne Coupling Reaction Using $Et_2SiH_2$

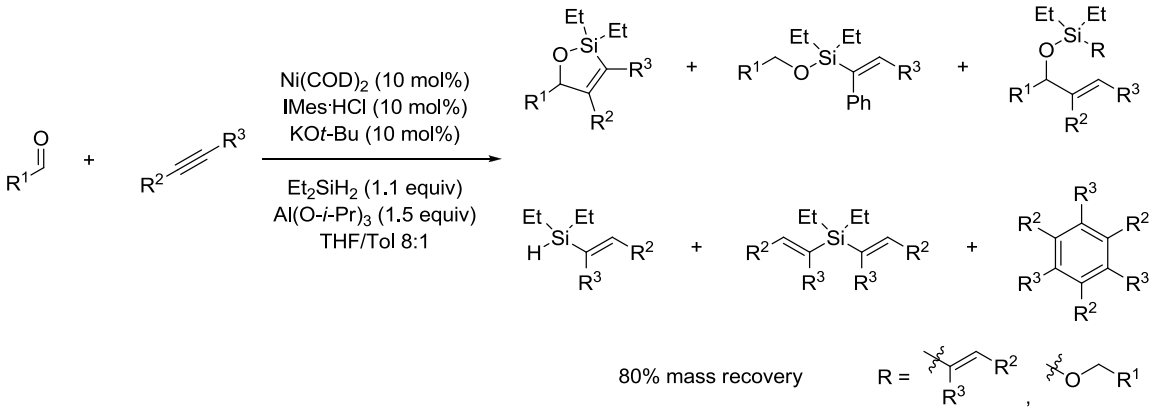


Although the reaction was a more complex mixture of products, the majority of undesired products appeared to be concentration dependent on the alkyne coupling partner, indicating that procedural manipulations could optimize the yield of the desired product. Simple slow-addition via syringe-drive of the alkyne and silane reagents led to synthetically useful yields of the desired oxasilacyclopentene (Scheme 28).

**Scheme 28.** Optimized Reaction Procedure for Oxasilacyclopentene Production

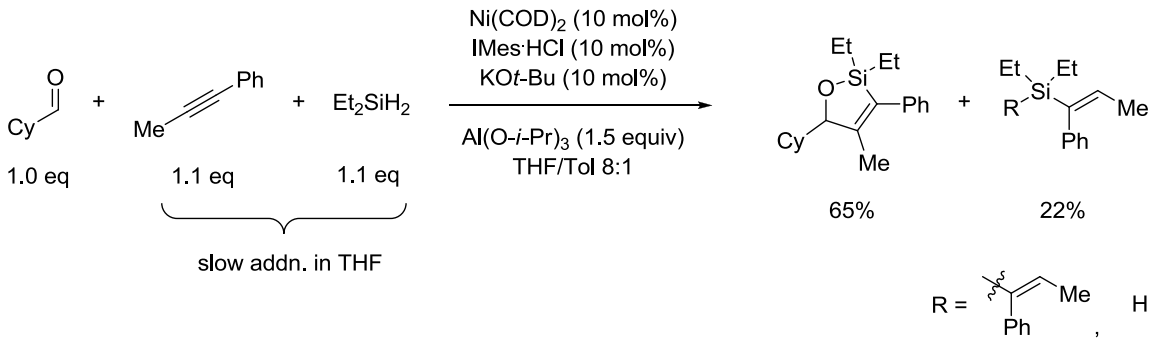


Further optimization could be achieved by using large excesses of both the alkyne and silane reagent, but was not synthetically useful due to its wasteful nature. The presence of side products, using the optimized procedure shown in Scheme 27, was substrate dependent and led to variance in isolated yields. As shown in Table 3, a variety of aldehyde/alkyne combinations were efficient coupling partners in the described methodology.

**Table 3.** Reaction Scope of Oxasilacyclopropene Formation by Nickel-Catalysis

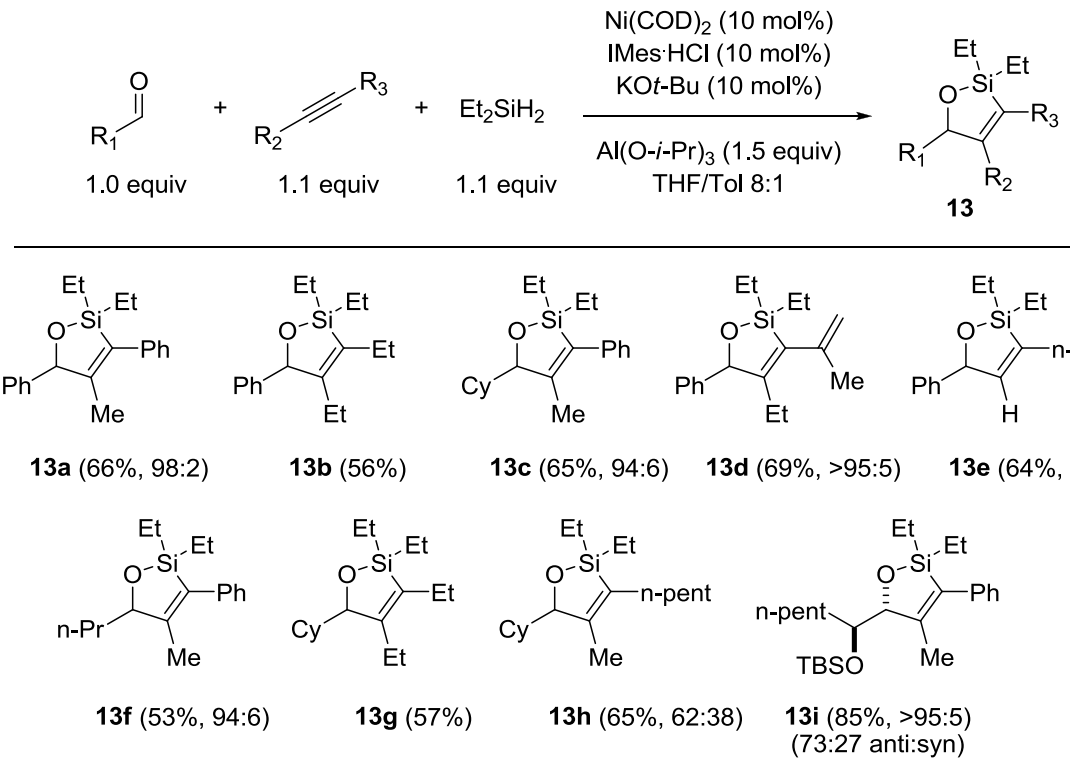


### 1.2.4 Proposed Mechanism for Nickel-Catalyzed Oxasilacyclopentene Formation

Although the net dehydrogenative silylene transfer from $Et_2SiH_2$ exhibits some similarity to the copper-catalyzed addition of silacyclopropenes to aldehydes, as reported by Woerpel, the scope and regioselectivity of the two procedures are markedly different. For example, couplings of butyraldehyde with phenyl propyne are highly regioselctive in both procedures. However, the nickel-catalyzed procedure produces compound **13f** whereas the copper-catalyzed silacyclopropene procedure affords an analogous compound as the opposite regioisomer (see Scheme 20). It is unlikely that the nickel-catalyzed procedure could go through silylene transfer directly to the alkyne in an analogous fashion to the copper-catalyzed procedure to yield the observed product

without suffering the same deleterious steric effects (depicted in **14**, Scheme 29). Additionally, omitting the aldehyde component in the nickel-catalyzed process involving $Et_2SiH_2$ leads to simple hydrosilylation of the alkyne, with no evidence of products derived from **14**.

**Scheme 29.** Nickel-Catalyzed Mechanism via Direct Silylene Transfer

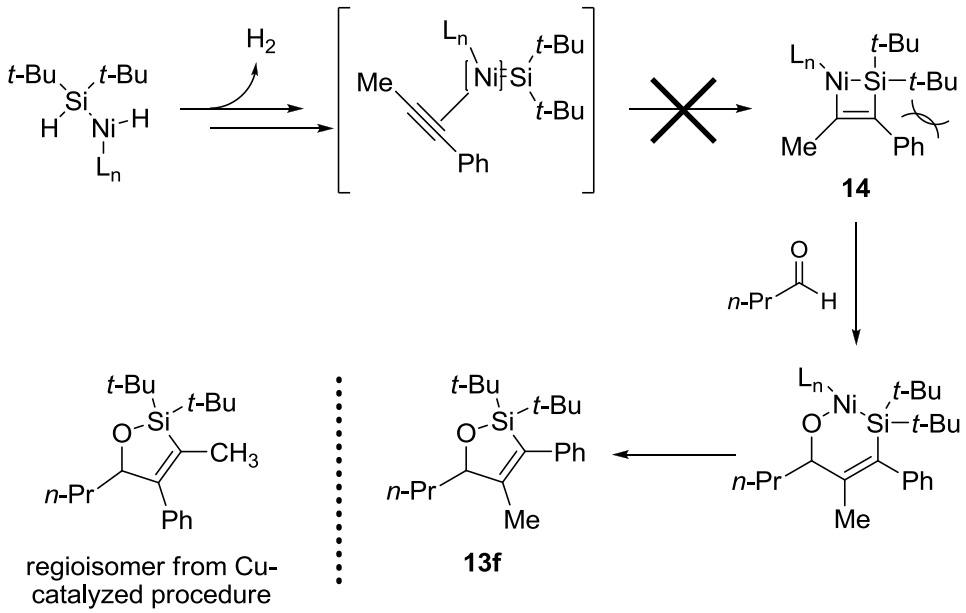


During the development of this methodology, it was noted that the regioselectivites observed in the oxasilacyclopentene products were essentially identical to those observed in the aldehyde/alkyne couplings with trialkylsilanes across a range of ligand structures.[1,11] These close parallels suggested to us the possibility of a common intermediate to these two nickel-catalyzed reaction classes, the latter of which cannot involve a silylene species. To illustrate this issue, the regioselectivity of the nickel-catalyzed couplings of cyclohexyl carboxaldehyde and 2-octyne with $Et_2SiH_2$ and $Et_3SiH$, using both IMes and IPr as ligand, was examined (Scheme 30).

**Scheme 30.** Regioselectivity of Aldehydes, Alkyne, Silane Couplings

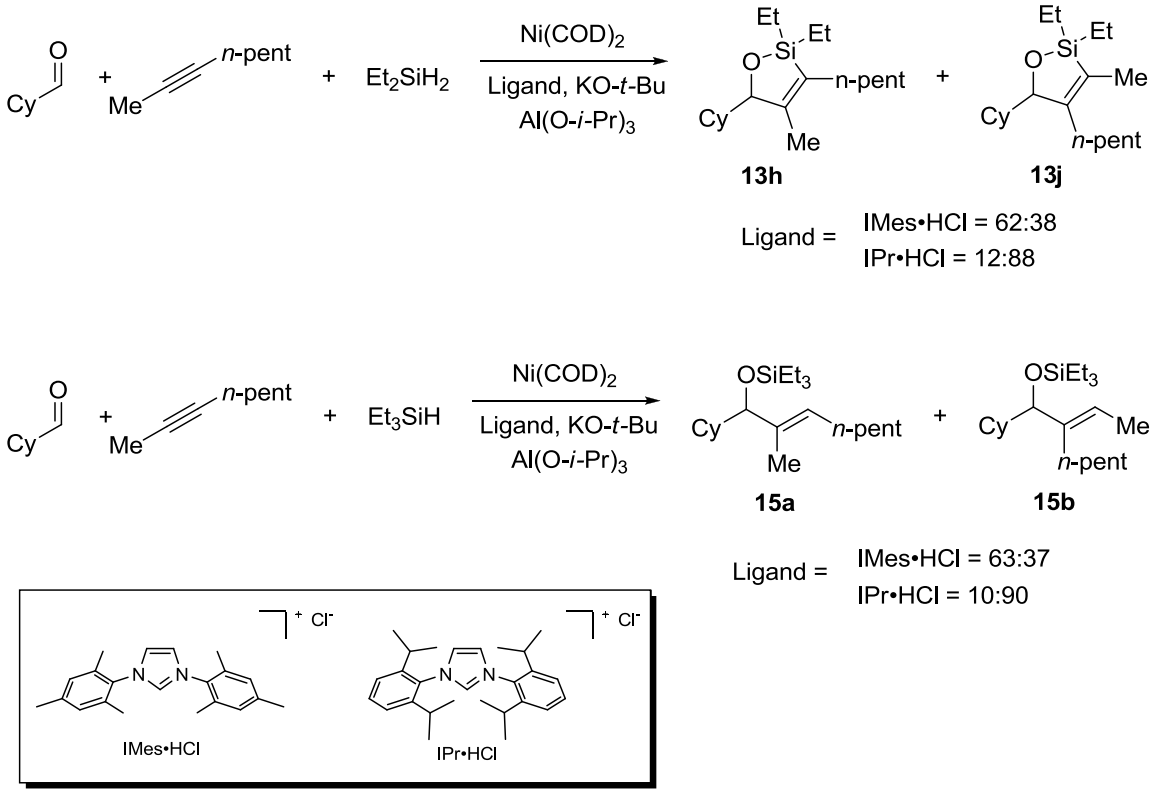


As illustrated in Scheme 30, the regiochemical outcomes of the separate nickel-catalyzed procedures are nearly identical. This result is consistent with a regiochemical defining C-C bond forming step which is common to both procedures. While the involvement of a nickel-silylene species cannot be definitively ruled out, a mechanistic framework that involves a common intermediate in the formation of both **2** and **17** seems the most likely based on their similar rates of formation and the regiochemical issues discussed above (Scheme 31). A potential mechanism may involve the formation of metallacycle **1**, setting the regiochemical outcome for either product **2** or **17**. Sigma-bond metathesis between the Ni-O and Si-H bonds from **1** would then lead to intermediate **16**. Simple reductive elimination would lead to allylic alkoxysilane product

**2**. However, a second sigma-bond metathesis, with extrusion of $H_2$ gas, could lead to a second metallacyclic intermediate with reductive elimination yielding oxasilacyclopentene **17**. As verification of this reaction sequence, the characteristic signal for $H_2$ at δ 4.5 in toluene-$d_8$ was observed in a sealed tube $^1$H NMR experiment. While the role of the Lewis acid is not definitively clear, disruption of the Ni-O coordination in intermediate **18** via Lewis acid coordination to oxygen, as depicted in **19**, may facilitate $H_2$ extrusion.

**Scheme 31.** Proposed Mechanism for Nickel-Catalyzed Oxasilacyclopentene Formation

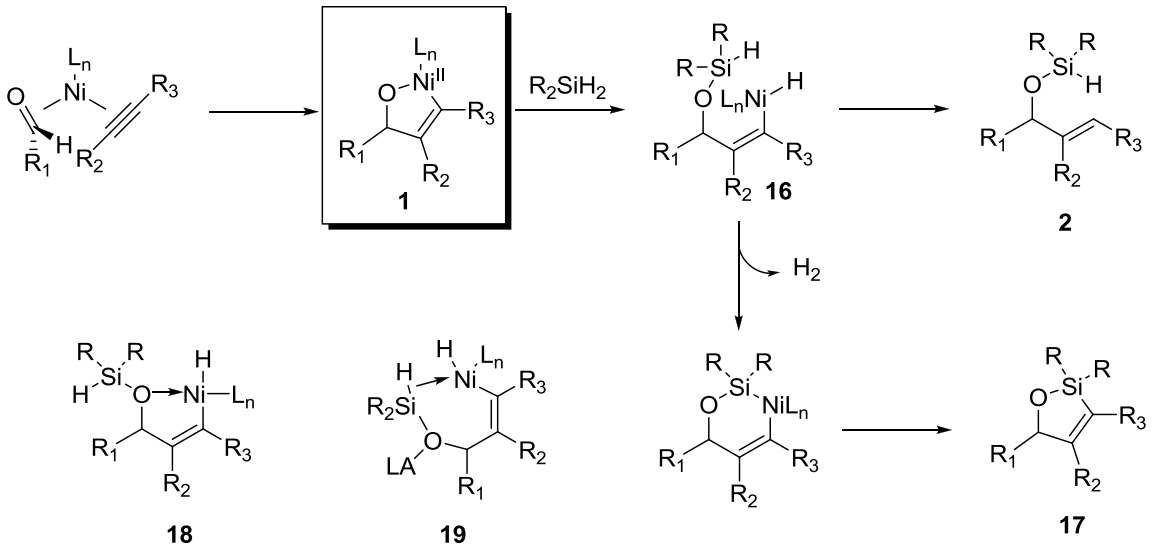


### 1.2.5 Asymmetric Induction and Synthetic Utility of Oxasilacyclopentenes

Due to the similarity of the procedures involving di- and trialkylsilanes, we sought to utilize a chiral NHC ligand recently developed in our lab to promote the first reported example of an asymmetric formal silylene transfer (Scheme 32).[29]

**Scheme 32.** First Reported Asymmetric Formal Silylene Transfer

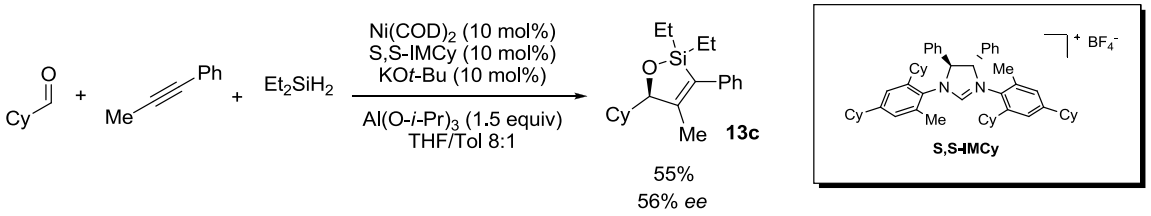


The preliminary example coupling cyclohexyl carboxaldehyde with phenyl propyne yielded a modest enantioselectivity of 56% *ee* in a 55% isolated yield. Although modest, this level of stereoinduction serves as an important benchmark as the first asymmetric transfer of a silylene synthetic equivalent.

To further provide support for the synthetic utility of the oxasilacyclopentenes formed by the described methodology, their efficiency as participants in subsequent synthetic transformations was explored. As shown in Scheme 33, the oxasilacyclopentenes produced by the described methodology were shown to undergo effective Tamao-Fleming oxidation, as well as Pd-catalyzed cross coupling; two very powerful transformations which showcase the synthetic utility of oxasilacyclopentenes.

**Scheme 33.** Synthetic Utility of Oxasilacyclopentenes

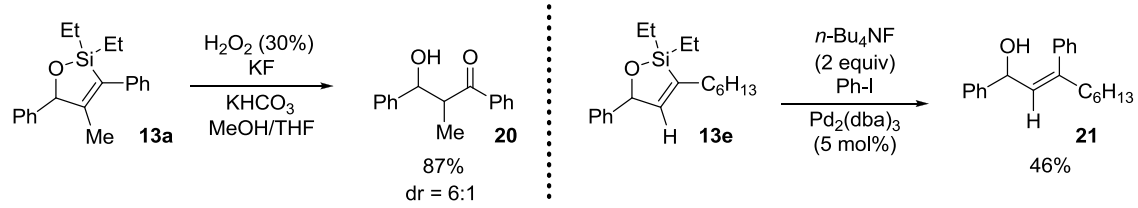

## 1.3 Summary of Nickel-Catalyzed Reductive Couplings of Aldehydes, Alkynes, and Dialkylsilanes

Nickel-catalyzed reductive couplings of aldehydes and alkynes has received much attention from the chemical community in the past decade as procedures have been continuously optimized to recently include the use of *N*-heterocyclic carbenes as ligands and air- and bench-stable silane reducing agents.[1] As an advancement of this development, the use of dialkylsilane reducing agents in an analogous procedure offers a simple and efficient route to oxasilacyclopentene products in a one-pot procedure. This new methodology takes advantage of the unique reactivity of dialkylsilanes to promote a formal silylene transfer as both hydrides are eventually lost through the coupling procedure. Based on the regiochemical similarities between the trialkyl- and dialkylsilane procedures, a mechanism involving a common intermediate was proposed. Synthetically useful silacycles were prepared by the procedure, and their synthetic utility was demonstrated by subsequent transformations. Additionally, the first asymmetric formal silylene transfer was reported using a chrial ligand developed in our lab.

# Chapter 2

# Nickel-Catalyzed Alkyne Hydroacylation

## 2.1 Introduction

The transfer of an acyl unit and a hydrogen atom across C-C multiple bonds to afford hydroacylation products represents a simple and atom-economical route to functionalized organic scaffolds via a powerful carbon-carbon bond forming transformation. Specifically, metal-catalyzed alkyne hydroacylation reactions offer a straightforward strategy for the synthesis of α,β-unsaturated ketones (enones) from robust starting materials (Scheme 34).

**Scheme 34.** α, β-Unsaturated Ketones from Alkyne Hydroacylation

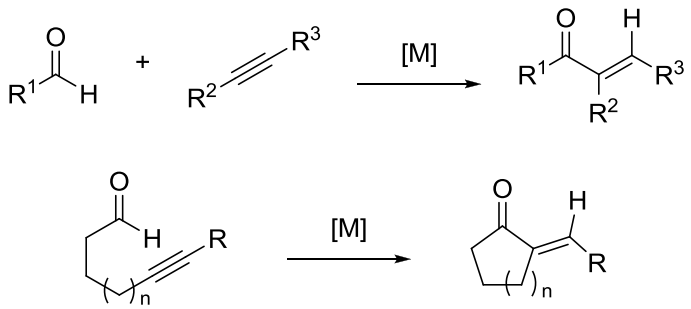


These α,β-unsaturated ketones can serve as key intermediates for the synthesis of biologically active compounds (such as prostoglandins)[30], or as natural product targets themselves (Scheme 35).[31,32]

**Scheme 35.** Enones in Natural Product Synthesis

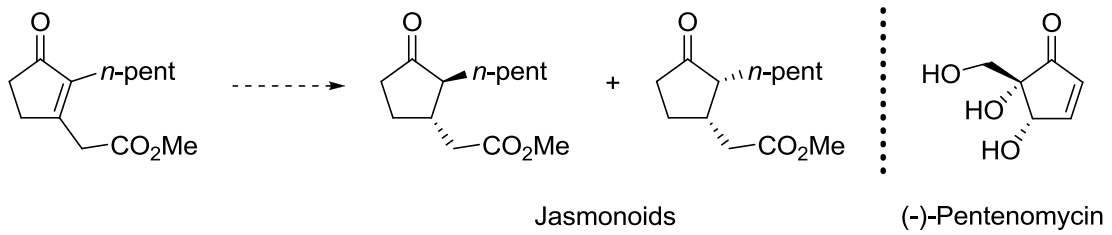


While methodologies to promote the inter- and intramolecular hydroacylation of various alkenes has been intensely studied, analogous hydroacylations involving alkynes has received less attention. In fact, certain well established strategies utilized for alkene hydroacylation were not effective in the setting of alkyne hydroacylation; a fact that was originally noted by Larock in 1980.[33] Whereas 4-alkenals underwent rhodium-catalyzed cyclization to afford hydroacylation products, analogous 4-alkynals were not effective (Scheme 36).

**Scheme 36.** Alkene Hydroacylation Methods Applied to Alkyne Hydroacylation

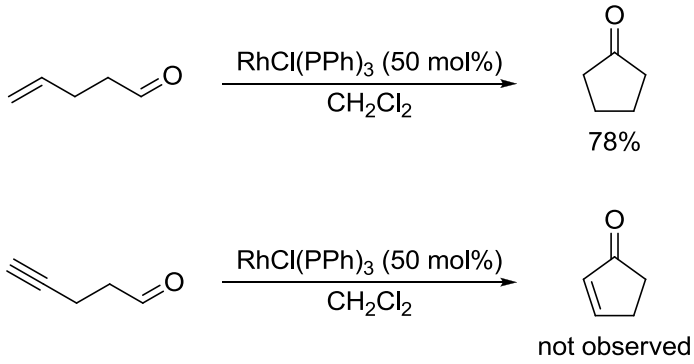


Perhaps the difficulty in promoting an intramolecular alkyne hydroacylation lies in the requirement for a trans addition of a metal hydride to the alkyne, assuming analogous mechanistic pathways for intramolecular alkene hydroacylation (Scheme 37).[34]

A mechanism involving trans addition of a metal hydride across alkenes has been supported by labeling and cross-over experiments, as well as computational studies.[35]

**Scheme 37.** Alkene/Alkyne Hydroacylation via a Trans Metal Hydride Addition

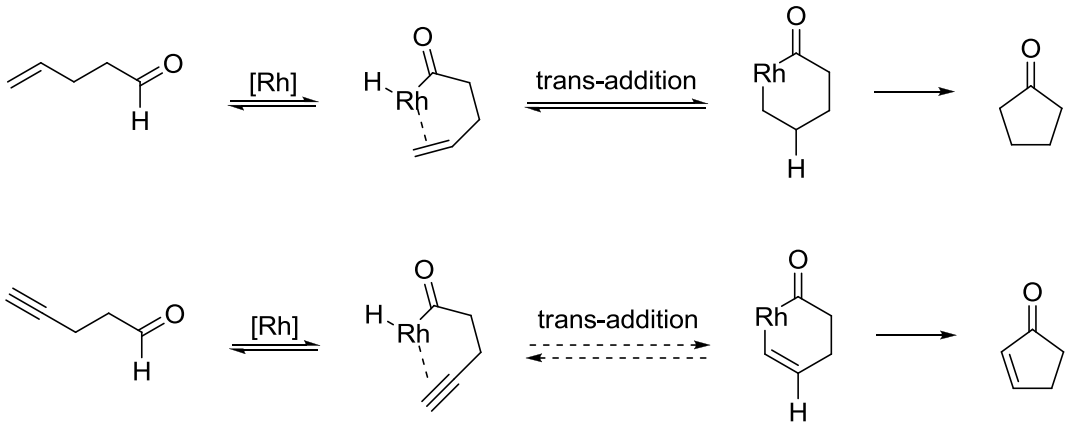


This limitation was overcome by Fu and coworkers when they presented a general strategy for intramolecular alkyne hydroacylations of various ynals using cationic rhodium catalysts (Scheme 38).[34] This result prompted the development of several strategies for the utilization of transition metals to promote both inter- and intramolecular alkyne hydroacylations; a select sampling of these methods will be discussed in Sections 2.1.1 and 2.1.2.

**Scheme 38.** Intramolecular Alkyne Hydroacylation via Cationic Rhodium Catalysts

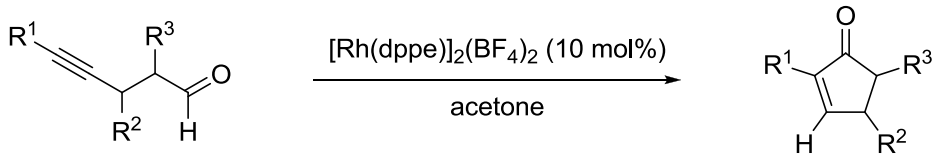


$R^1$ = alkyl, aryl, alkenyl, alkynyl
$R^2$ = alkyl, OMe, H
$R^3$ = alkyl, H

### 2.1.1 Previous Examples of Metal-Catalyzed Alkyne Hydroacylation

As stated in Section 2.1, methodologies for the inter- and intramolecular hydroacylation of alkenes were used as a springboard for the development of strategies for the hydroacylation of alkyne π-systems. Commencing with the pioneering work of Fu and coworkers (Scheme 38),[34] several noteworthy advances were made using primarily rhodium based catalyst systems. For example, during the study of the cyclization of various 5- and 6-alkynals, the Tanaka group discovered a complementary reactivity to the chemistry illustrated in Scheme 38. The use of a [Rh(BINAP)]$BF_4$ catalyst system led to the formation of *exo*-methylene cyclopentanones via *cis* metal hydride addition (Scheme 39).[36]

**Scheme 39.** *Exo*-Methylene Cyclopentanones via a Cis Metal Hydride Addition

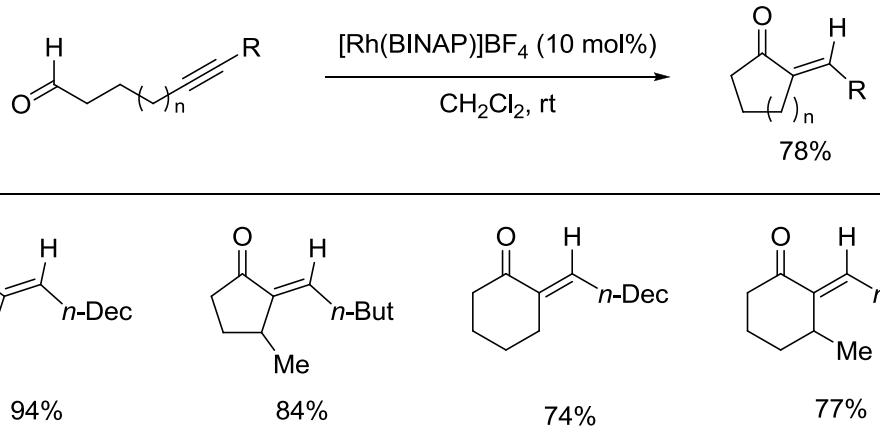


A similar rhodium-based methodology was developed by Jun and co-workers for promoting intermolecular alkyne hydroacylations.[37] In this procedure, a catalyst system generated from Wilkinson's catalyst, 2-amino-3-methylpicoline, and benzoic acid led to the coupling of alkyl and aryl aldehydes with terminal alkynes (Scheme 40). This procedure led to a mixture of branched and linear α, β-unsaturated enones.

**Scheme 40.** Intermolecular Rhodium-Catalyzed Alkyne Hydroacylation

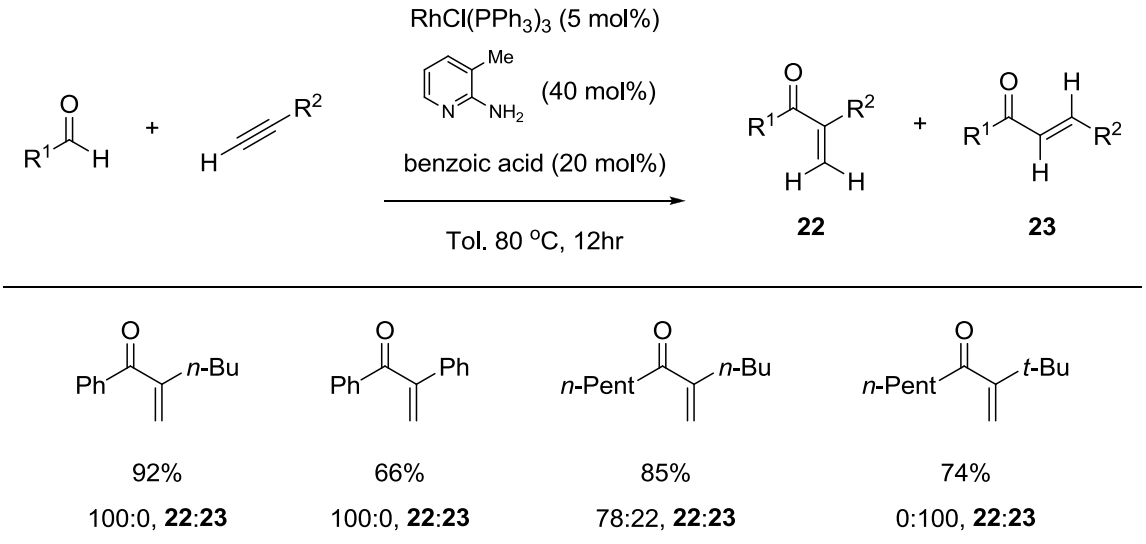

More recently, the Krische group has applied their ruthenium-catalyzed transfer hydrogenation chemistry to intermolecular alkyne hydroacylation.[38] Under carefully optimized reaction conditions, 2-butyne could be coupled with a variety of aryl aldehydes in good yield, although non-symmetrical alkynes suffered from poor regioselectivity, and non-aryl aldehydes were not discussed (Scheme 41).

**Scheme 41.** Intermolecular Ruthenium-Catalyzed Alkyne Hydroacylation

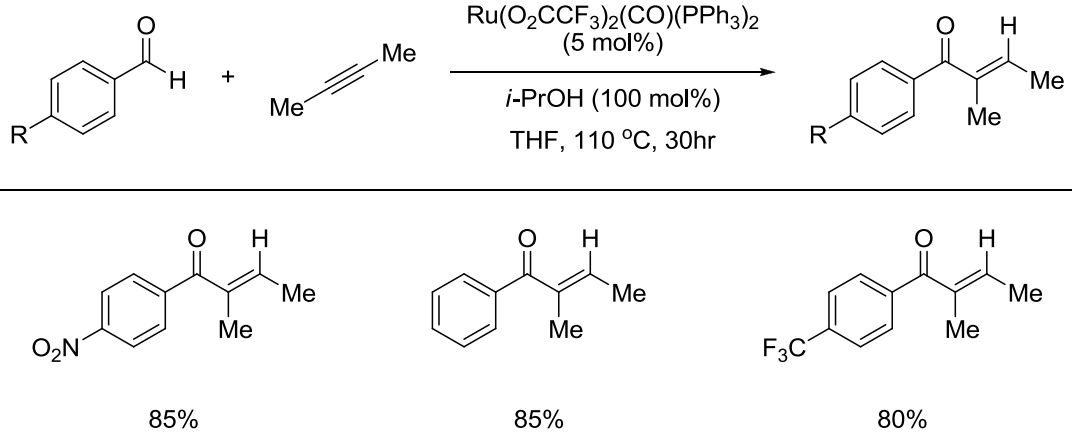


### 2.1.2 Previous Examples of Nickel-Catalyzed Alkyne Hydroacylation

Although methodologies for inter- and intramolecular alkyne hydroacylation are robust for metals such as rhodium and ruthenium, there have not been many reported examples utilizing nickel catalysts. An early report from Tsuda and co-workers in 1990 showed that a simple Ni(0)/*n*-alkylphosphine catalyst system could promote intermolecular alkyne hydroacylation under forcing conditions.[39] Reactions were performed in stainless steel autoclaves and heated to 80-150 $^{o}$C in THF (well past its boiling point of 65 $^{o}$C) to yield various α, β-unsaturated enones (**24**) with good *E/Z*

selectivity (Scheme 42). α, β; γ, δ-Dienones (**25**) were also occasionally formed as an undesired side-product, but their presence was substrate and ligand dependent.

**Scheme 42.** Nickel-Catalyzed Intermolecular Alkyne Hydroacylation

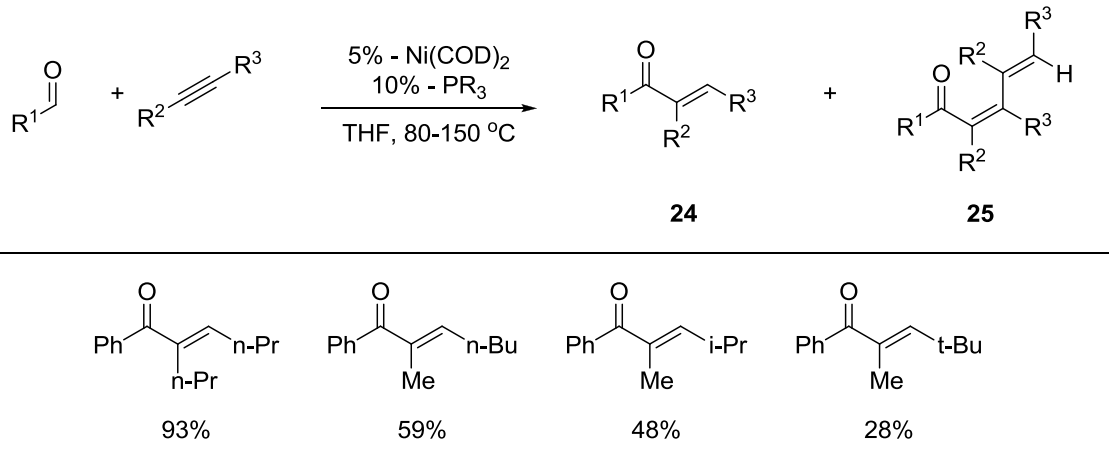


As illustrated in Scheme 42, the best alkyne coupling partners in the nickel-catalyzed hydroacylation strategy where symmetrical, aliphatic internal alkynes. Isolated yields dropped significantly when alkynes other than 4-octyne were explored. Extensive screening of trialkyl- and triarylphosphine ligands showed that *n*-alkylphosphines were the most efficient for promoting the formation of **24** over **25**. The optimum synthetic procedure involved a catalyst system comprised of P(*n*-$C_8H_{17}$)$_3$ with Ni(COD)$_2$ in a 2:1 ratio and heating to 100 $^oC$ for 20 hours in THF. Although no detailed mechanistic studies were discussed, Tsuda and co-workers proposed a mechanism involving the generation of an acyl nickel-hydride intermediate (**26**) as a key intermediate (Scheme 43).

**Scheme 43.** Proposed Mechanism for Nickel-Catalyzed Alkyne Hydroacylation

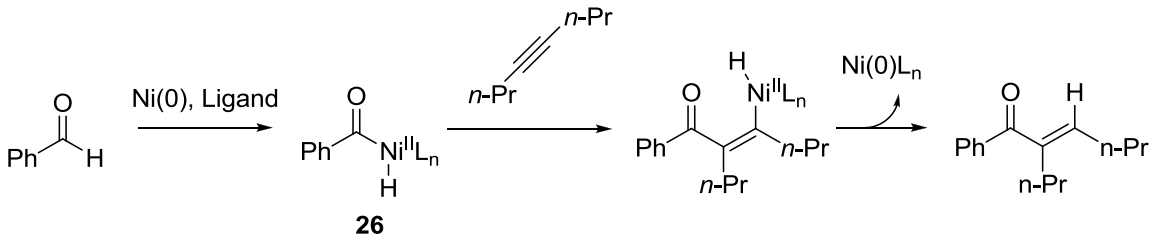


Although hampered by low substrate scope and the necessity for harsh reaction conditions, this methodology represents the only reported example of alkyne hydroacylation via nickel-catalysis.

Recent structural work by Ogoshi and co-workers described the formation of a dimeric oxametallacycle (**27**) generated from 2-butye, benzaldehyde, and Ni(0)/$PCy_3$ (Scheme 44).[40]

**Scheme 44.** Generation of a Stoichiometric Dimeric Nickelacycle

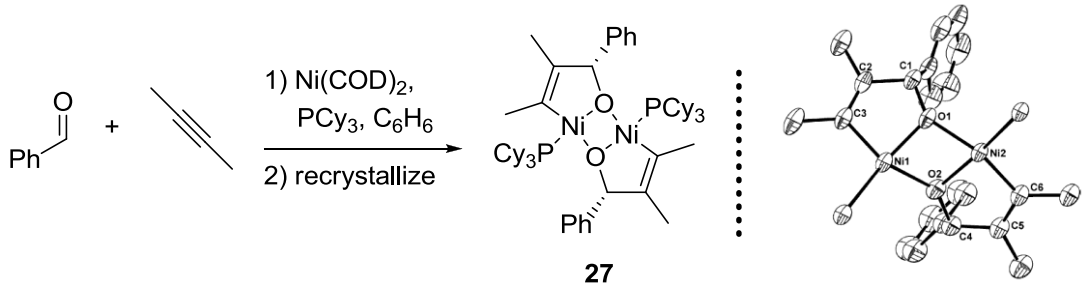


This crystalline material was shown to decompose to α, β-unsaturated enone **28** upon standing at room temperature for 48 hours (Scheme 45). It was proposed that **28** may be formed via a monomeric nickel-hydride intermediate from **27**, although it was specifically mentioned that such a transformation was previously regarded as unlikely.[39]

**Scheme 45.** α, β-Unsaturated Enone Formation from an Isolated Dimeric Intermediate

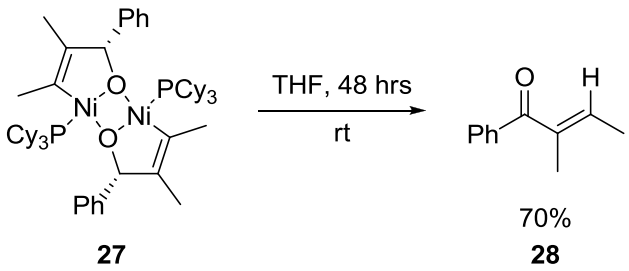


**27** **28**

## 2.2 Results and Discussion

### 2.2.1 Intramolecular Nickel-Catalyzed Alkyne Hydroacylation

Our lab's entry into the study of nickel-catalyzed alkyne hydroacylation came about in an indirect manner. In the mechanistic study of nickel-catalyzed reductive couplings of aldehydes and alkynes (discussed in Section 1.1) attempts were made to generate and isolate stoichiometric organometallic intermediates analogous to **27** in Scheme 44. Attempts by our lab to duplicate the synthesis of **27** to study its reactivity towards non-alkylative reducing agents were not met with success as only degradation products could be isolated.

Various aldehyde/alkyne combinations were examined in an effort to enhance the crystallinity of potential intermediates, including a variety of tethered aldehyde/alkyne ynal substrates. These tethered ynal substrates fared no better than previous substrate combinations when subjected to recrystallization conditions, but led to the formation of organic side-products after allowing the mother liquor to stand at room temperature for several hours (Scheme 46). These organic products were later identified by GCMS and NMR as α, β-unsaturated enone **31**, the product of an apparent alkyne hydroacylation reaction.

**Scheme 46.** α, β-Unsaturated Enone from an Ynal and Stoichiometric Ni/$PCy_3$

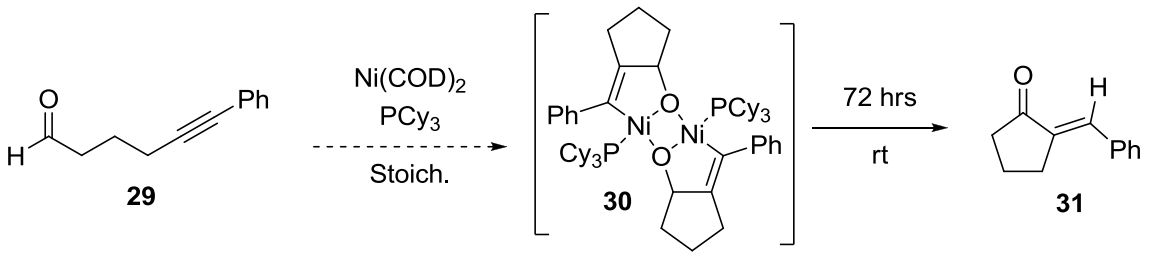


Based on the similarity of reagents and reaction conditions to the Ogoshi procedure, it's likely that **30** is formed *in situ* as a stoichiometric intermediate in the production of **31**.

Presuming the generation of dimeric metallacycle **30** by the combination of reagents described in Scheme 46, we believed that **31** may have arisen from a double β-hydride/reductive elimination sequence from **30** to yield two equivalents of the observed α, β-unsaturated enone (Scheme 47).

**Scheme 47.** Proposed Mechanism of Enone Formation from a Dimeric Intermediate

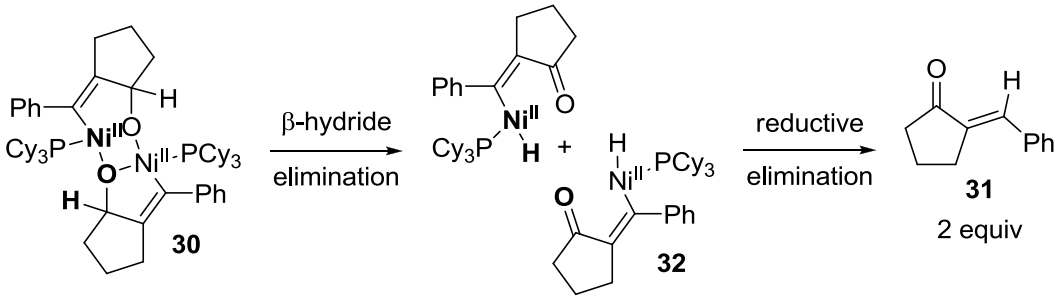


Based on this proposed mechanism for the generation of **31** via stoichiometric amounts of $Ni(COD)_2/PCy_3$, it was noted that a Ni(0) source is liberated via reductive elimination from nickel-hydride **32**, suggesting that the transformation may be rendered catalytic in $Ni(COD)_2/PCy_3$ under optimized reaction conditions. Because the initial observation of **31** resulted from allowing the stoichiometric mixture to stand at room

temperature for several hours, early attempts at developing a catalytic variant focused on enhancing the reactivity of the system by simple thermal heating. Initial results were promising, and an optimized procedure was quickly developed involving slow addition of substrate **29** (via syringe-drive) to a solution of the $Ni(COD)_2/PCy_3$ catalyst mixture heated to 45 $^oC$ in THF (Scheme 48)

**Scheme 48.** Optimized Procedure for Nickel-Catalyzed Intramolecular Alkyne Hydroacylation

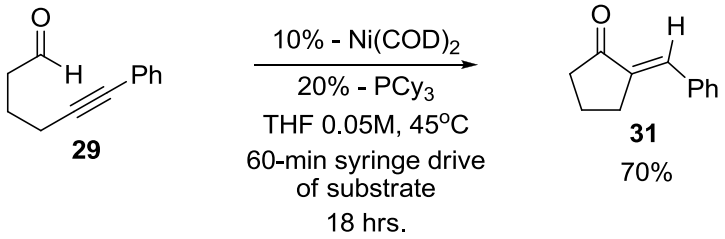


The optimized procedure was general for aryl 5-hexynals with various substitution on the aryl group, but was not directly amenable to ynals of varying length. For example, subjecting 7-octynal (**33**) to the optimized reaction conditions afforded poor yields of the desired enone and led to large amounts of recovered starting material (Scheme 49).

**Scheme 49.** Substrate Limitations of Hydroacylation Methodology

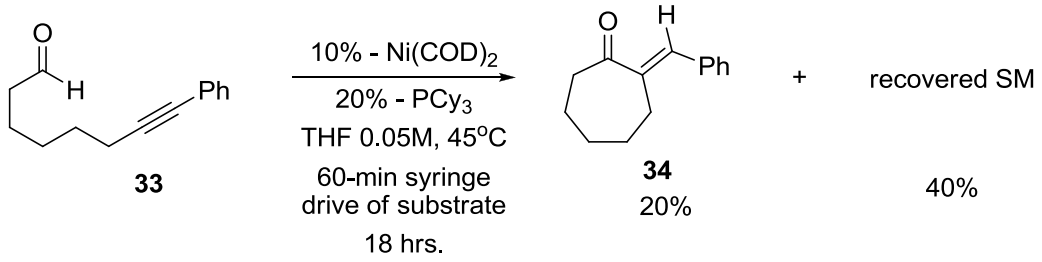


Based on this result, it was clear that the entropic bias of the substrates was playing a large role in the efficacy of alkyne hydroacylation by the currently optimized

procedure. To best overcome this limitation, optimization efforts were shifted towards developing an efficient method for intermolecular alkyne hydroacylations, where entropic effects will have minimal impact on reaction efficacy.

**Section 2.2.2 Intermolecular Nickel-Catalyzed Alkyne Hydroacylation**

Similar to the result illustrated in Scheme 49, intermolecular nickel-catalyzed alkyne hydroacylations suffered from poor conversions under thermal conditions (Scheme 50).

**Scheme 50.** Intermolecular Nickel-Catalyzed Alkyne Hydroacylation Under Thermal Conditions

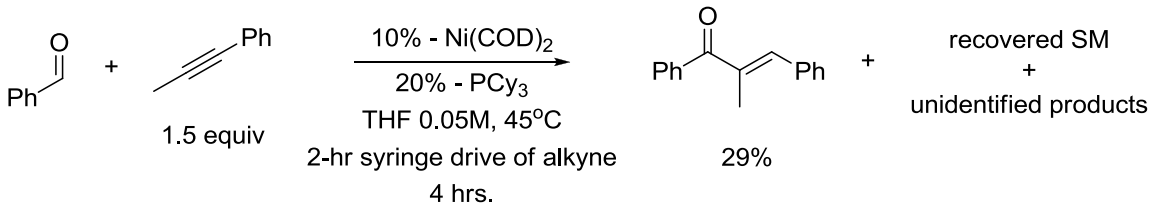


Following conditions similar to those optimized for the nickel-catalyzed hydroacylation of 5-hexynal, the hydroacylation of phenylpropyne with benzaldehyde yielded a complicated mixture of products including the desired enone, recovered aldehyde, and several organic products that were not identified. Screening several conditions varying solvent, temperature, and order/rate of addition showed that elevated reaction temperature along with slower addition of phenylpropyne led to modest gains in isolated yield. A brief ligand screen showed $PCy_3$ to be the optimum choice compared to traditionally used ligands for nickel (Scheme 51). In all cases, isolated yields were hampered by the presence of side-products arising from nickel-catalyzed alkyne self-condensation (trimerization products of varying regiochemistry).

**Scheme 51.** Ligand Screen for Intermolecular Nickel-Catalyzed Alkyne Hydroacylation

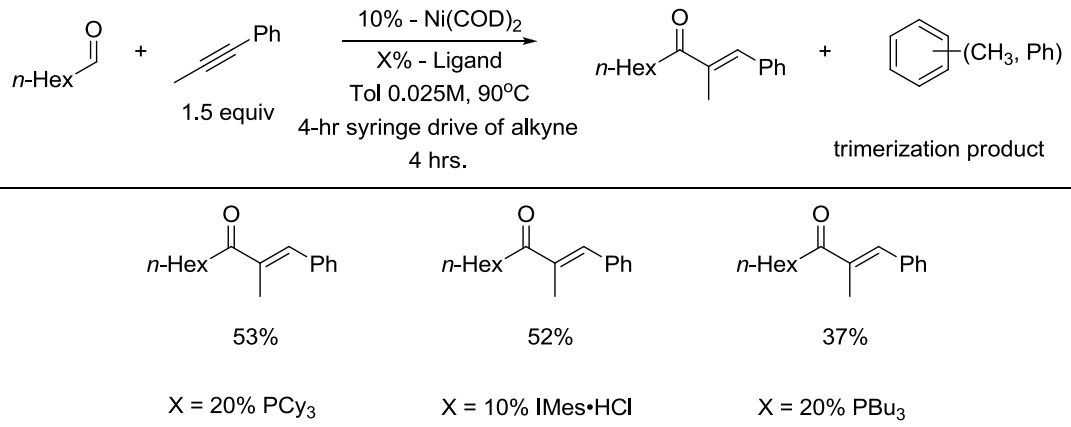


Since the optimum procedure to this point involved extensive thermal heating of the reaction mixture, microwave heating was explored as a means to increase reaction conversion while reducing overall reaction time. Under microwave heating conditions, $PCy_3$ was still shown to be the most effective ligand compared to IMes and $PBu_3$ based on yields calculated from GCMS integrations. The reaction of benzaldehyde with 4-octyne proved to be very efficient under microwave heating, leading to the highest isolated yield observed for the nickel-catalyzed procedure (Scheme 52).

**Scheme 52.** Intermolecular Nickel-Catayzed Alkyne Hydroacylation via Microwave Heating

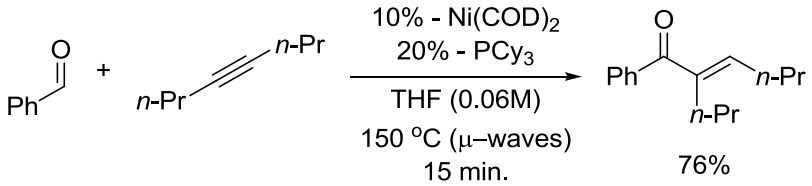


This initial result showed great promise, but it soon became evident that the methodology was extremely substrate dependent, as illustrated in Scheme 53. Much like the original report from Tsuda in 1990 (Scheme 42), symmetric aliphatic alkynes were the best coupling partners, and isolated yields dropped off significantly when examining

other substrates. Perhaps most intriguing is the fact that aliphatic internal alkynes bearing the same number of carbon units yielding such different results depending on the position of the alkyne triple bond (compare **35a** to **35b** and **35c** to **35d**).

**Scheme 53.** Substrate Scope of Intermolecular Nickel-Catalyzed Alkyne Hydroacylation via Microwave Heating

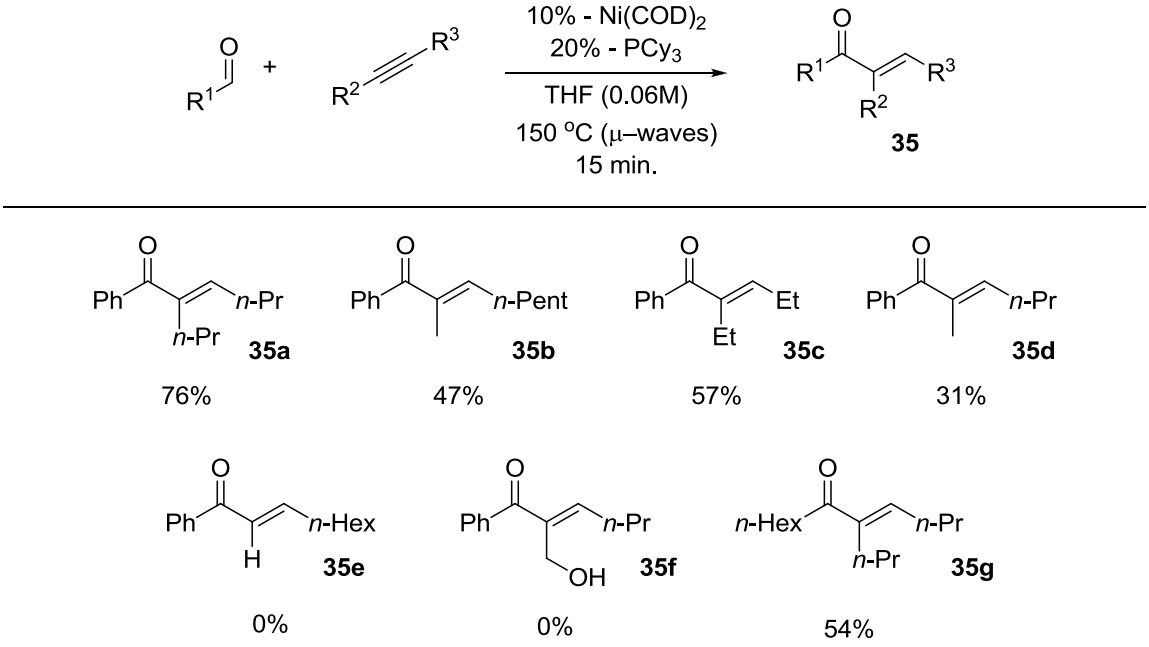


While this limitation is substrate scope is not currently understood, the procedure described in Scheme 53 represents the optimized method of promoting an intermolecular alkyne hydroacylation via nickel-catalysis.

### 2.2.3 Evidence for a Bimetallic Mechanism for Nickel-Catalyzed Alkyne Hydroacylation

Based on the initial observation of enone products (Section 2.2.1), it was believed that a dimeric metallacycle was a key intermediate in the nickel-catalyzed alkyne hydroacylations described above. To probe this hypothesis, crossover studies with ynals containing isotopic labels were undertaken (Scheme 54).

**Scheme 54.** Crossover Studies Comparing Isotopically Labeled Ynals

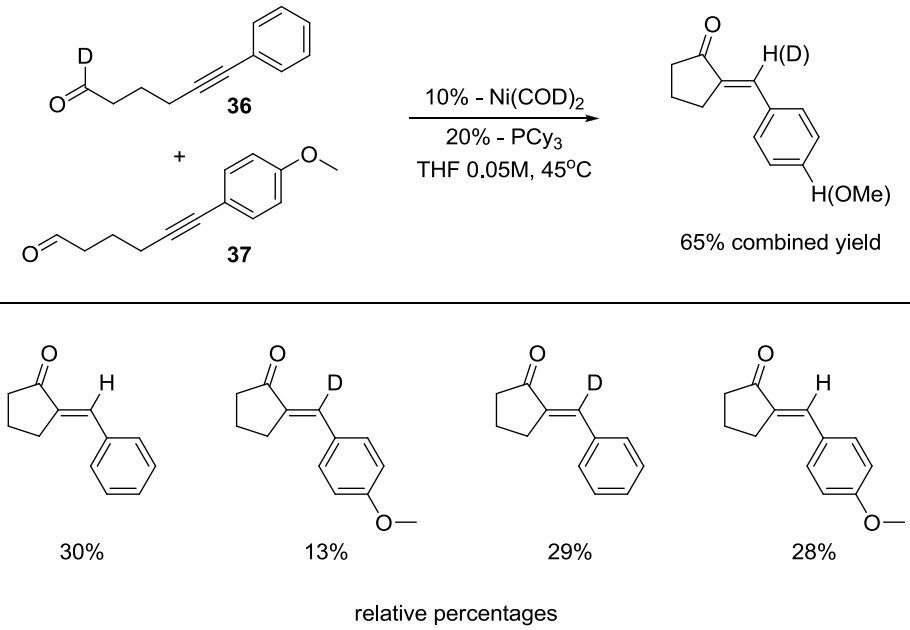


A one-to-one mixture of ynals **36** and **37** was subjected to the optimized nickel-catalyzed hydroacylation procedure under thermal conditions. The relative percentage of hydrogen incorporation at the vinylic position of each product was determined by NMR integration. As shown in Scheme 54, extensive scrambling of C-H and C-D was observed. This result is consistent with β-hydride elimination occurring from a hetero-dimeric intermediate formed from **36** and **37** (Scheme 55). It's unclear whether a dimeric intermediate is more likely to be formed directly through a bimetallic process, or by the combination of two monomers after oxidative cyclization as depicted in Scheme 55.

**Scheme 55.** Proposed Mechanism Involving a Dimeric Intermediate Leading to Observed Crossover Results

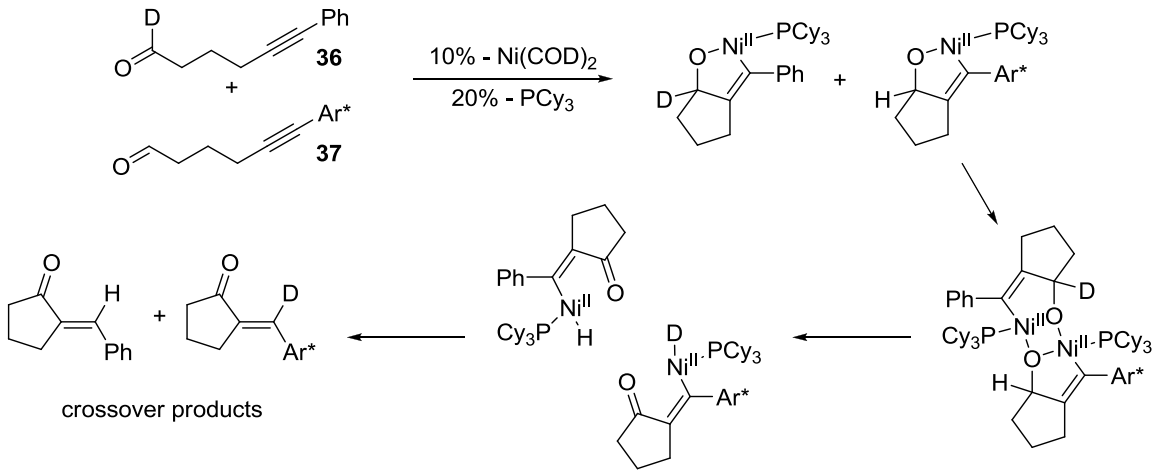


Visual inspection of DFT minimized ground-state structures suggested that β-hydride elimination from a dimeric metallacycle was geometrically favored over that from a monomeric metallacycle (Scheme 56). In monomeric nickel metallacycle **38**, it is difficult for the H-C-O-Ni bonding network to maintain the co-planar arrangement necessary for β-hydride elimination.[41] Conversely, dimeric nickel metallacycle **39** allows for the co-planar arrangement of the necessary atoms to allow for β-hydride elimination to occur across the central 4-membered oxanickelacycle.

**Scheme 56.** DFT Minimized Structures of Mono- and Dimeric Metallacycle Intermediates

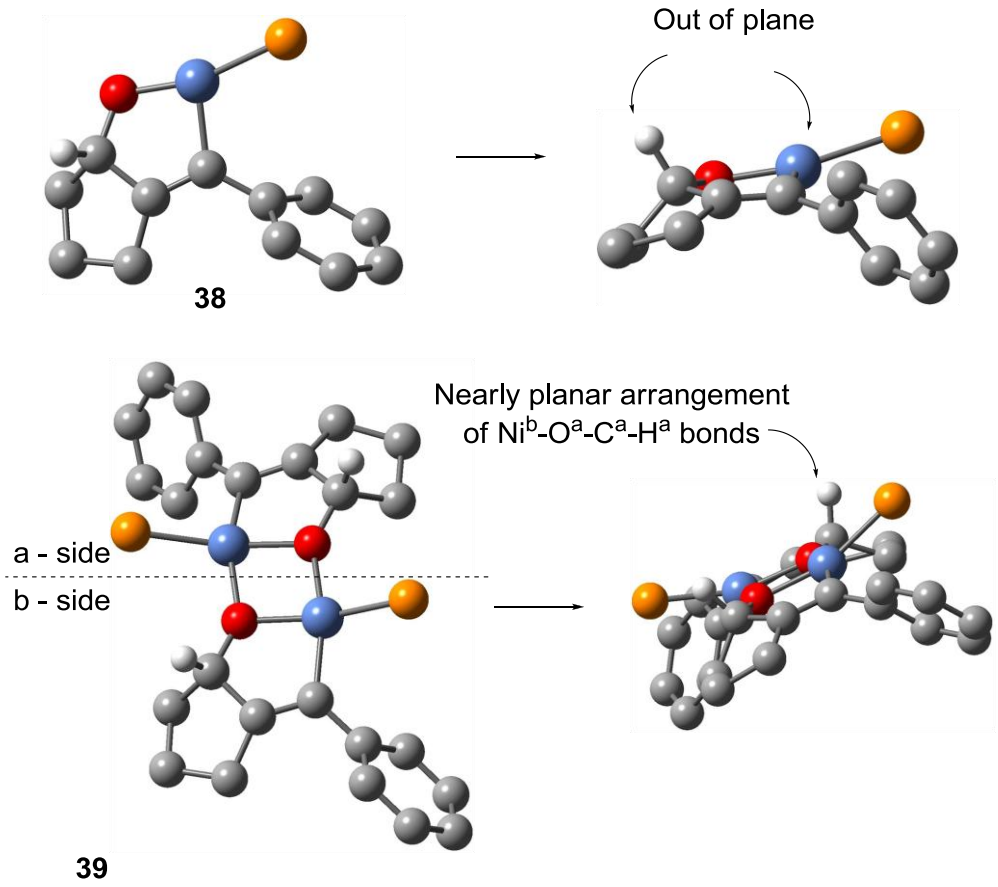


Crossover experiments, DFT calculations, and comparison to known hydroacylations from isolated dimeric metallacycles strongly suggest that the nickel-catalyzed alkyne hydroacylation methods described above contain a dimeric metallacycle as a key intermediate in the catalytic transformation.

**2.3 Summary of Nickel-Catalyzed Alkyne Hydroacylation**

Robust methodologies have been reported for alkyne hydroacylations using rhodium and ruthenium catalysts.[33-38] To date, only one account of nickel-catalyzed alkyne hydroacylations has been reported.[39] However, a novel methodology has been developed whereby intramolecular hydroacylations were performed under thermal conditions and intermolecular hydroacylations were performed under microwave

conditions. Limited substrate scope currently diminishes the generality of the developed methodology, but exhaustive optimization has not yet been completed. Crossover studies utilizing isotopically labeled ynals provide support for a bimetallic intermediate being generated during productive catalytic reactions. Visual inspection of DFT minimized structures of potential intermediates, along with comparison to known hydroacylation pathways from stoichiometrically generated and isolated dimeric structures also support a bimetallic reaction mechanism.

# Chapter 3

# Mechanistic Evaluation of Intramolecular Nickel-Catalyzed Reductive Couplings of Aldehydes, Alkynes, and Trialkylsilanes

## 3.1 Introduction

Nickel-catalyzed reductive and alkylative coupling reactions of two π-components have been extensively studied in the last two decades, with processes involving the hetero-coupling of differentiated polar and non-polar π-components encompassing the bulk of experimental efforts. Methodologies have been developed for nickel-catalyzed hetero-couplings of aldehydes, enones, ketones, or imines (as the polar π-component) with alkynes, allenes, or dienes (as the non-polar π-component).[1,42-45] A variety of reducing agents have been utilized in these nickel-catalyzed processes, with the most common classes including silanes, organozincs, organoboranes, and alcohols. Of these procedures, perhaps the most thoroughly studied is the nickel-catalyzed coupling of aldehydes with alkynes. Since the first reported example of nickel-catalyzed cyclization of ynals in 1997, many variants now exist that undergo either alkylative or reductive coupling. The methodology has been applied to both inter- and intramolecular couplings, allowing access to acyclic products as well as small or macrocyclic ring systems. In a typical nickel-catalyzed process, COD-stabilized zero-valent nickel, monodentate phosphine or *N*-heterocyclic carbene (NHC) ligands, and a reducing agent such as a silane, organozinc, or organoborane reagent are typically used. Several mechanistic

insights have emerged that shed light onto the subtle aspects that govern the reactivity and outcome of various nickel-catalyzed processes (discussed further in Section 3.1.1). Based on these protocols, methods have been developed that promote enantio- and regioselective couplings that proceed with very high levels of stereocontrol.

The first example of nickel-catalyzed aldehyde alkyne coupling described the alkylative cyclization of 5-hexynal derivatives with organozinc reducing agents to afford various allylic alcohols (Scheme 57).

**Scheme 57.** The First Reported Example of Nickel-Catalyzed Aldehyde/Alkyne Coupling

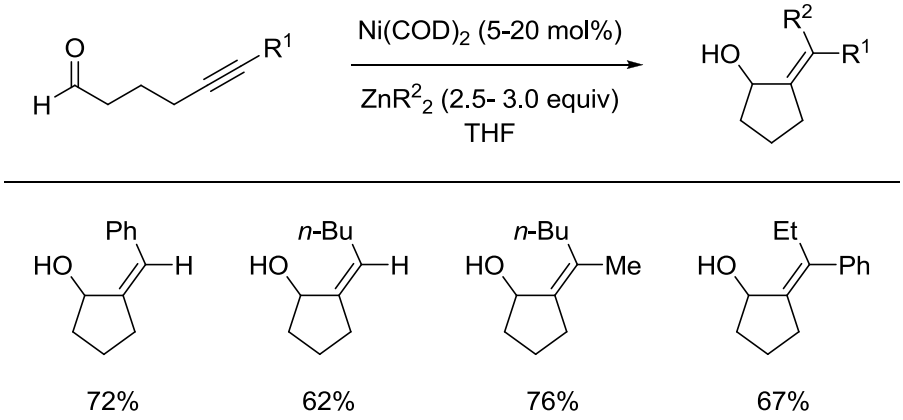


In the same report, it was noted that changing from an alkylative to a reductive coupling pathway could be promoted by pre-treating the Ni(0) catalyst with four equivalents of $PBu_3$, although an analogous effect not observed for intermolecular couplings (see Section 3.1.1 for mechanistic discussion). The intermolecular reductive coupling process was later developed by Jamison and coworkers using organoboranes as reducing agents, further expanding the scope and utility of the nickel-catalyzed process (Scheme 58).[3]

**Scheme 58.** Intermolecular Aldehyde/Alkyne Coupling Using Organoborane Reducing Agents

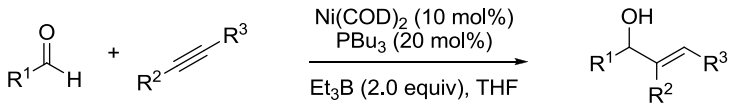


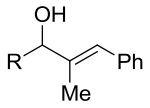

R = Ph: 77% (92:8 rs)
R = *n*-Pr: 85% (92:8 rs)

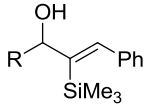

R = Ph: 49% (>98:2 rs)
R = *n*-Hept: 89% (>98:2 rs)

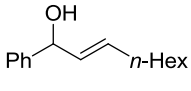

76% (96:4 rs)

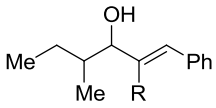

R = Me: 41% (94:6 rs, 66:34 dr)
R = $SiMe_3$: 31% (>98:2 rs, 58:42 dr)

Improvements in reducing agent stability and reaction efficiency in the intermolecular process were later reported by our group in 2004, utilizing *N*-heterocyclic carbenes (NHCs) as ligands along with air- and bench-stable trialkylsilane reducing agents to yield silyl-protected allylic alcohols (Scheme 59).[1]

**Scheme 59.** Intermolecular Aldehyde/Alkyne Coupling Using Trialkylsilane Reducing Agents

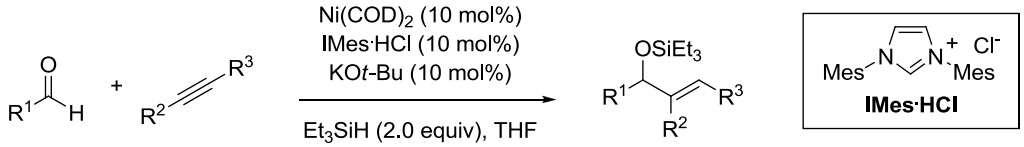


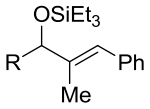

R = Ph: 84% (>98:2 rs)
R = *n*-Hex: 82% (>98:2 rs)

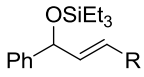

R = Ph: 72% (>98:2 rs)
R = *n*-Hex: 71% (>98:2 rs)

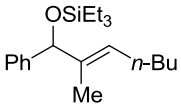

84 % (1.3:1 rs)

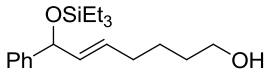

72 % (98:2 rs)

This reaction manifold was used to develop ligands for highly enantio- and regioselective reductive coupling processes. Sterically demanding chiral NHC ligands were developed to afford silyl-protected allylic alcohols with moderate to high levels of enantioselectivity (Scheme 60).[29] A highly ordered transition state was proposed to

explain the facial selectivity leading to such high levels of enantioselectivity (Scheme 61).

**Scheme 60.** Asymmetric Aldehyde/Alkyne Coupling Using Chiral NHC Ligands

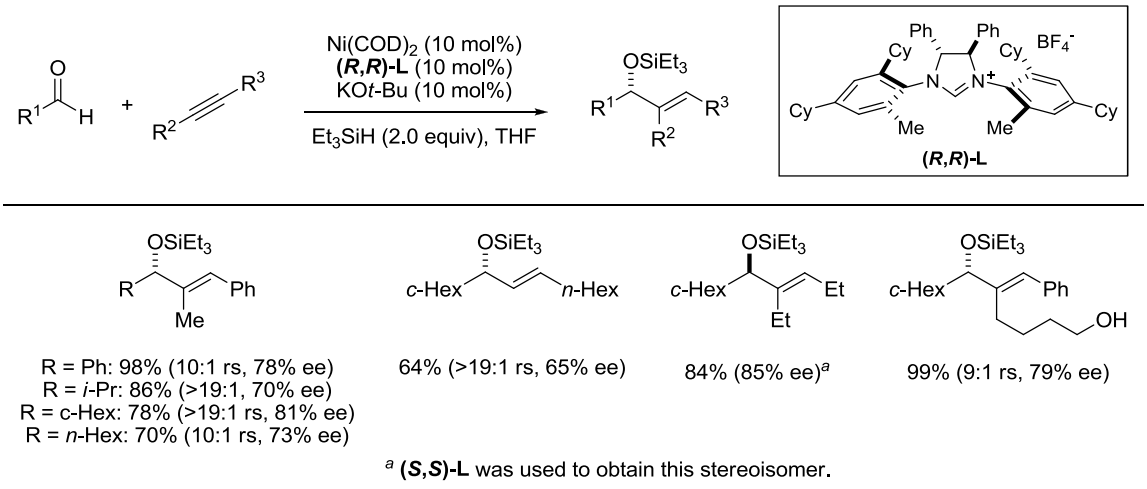


**Scheme 61.** Steric Model for Asymmetric Induction

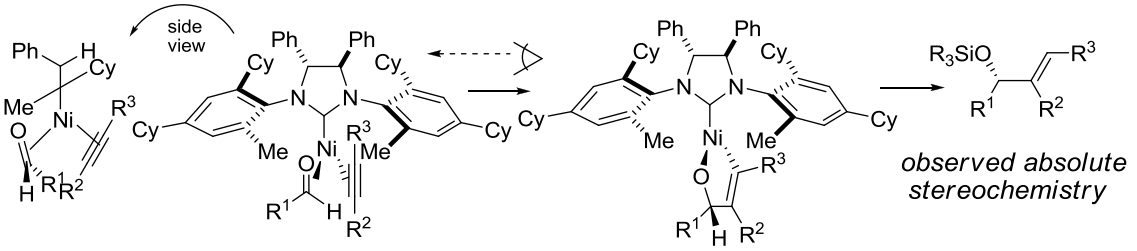


Using this steric model for substrate orientation during C-C bond formation, a series of NHCs were examined to develop highly regioselective couplings. Very high levels of regioselctivity, as well as the ability to effect a complete reversal of the regiochemical outcome, were achieved by utilizing a carefully chosen combination of ligands and reducing agents.[46]

**Scheme 62.** Highly Regioselective Aldehyde/Alkyne Couplings Using NHC Ligands

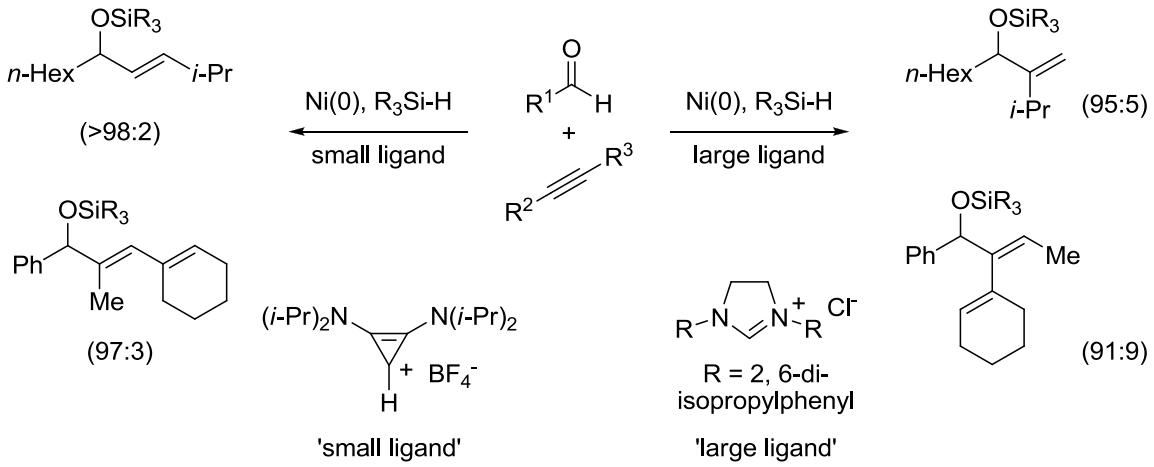


These varied and synthetically useful methodologies illustrate the impact that nickel-catalyzed aldehyde/alkyne coupling reactions has had on the chemical community in the last several years. As with any frequently used methodology or reaction class, there has been considerable effort devoted to elucidating mechanistic features. The following section describes the state of the art understanding of mechanistic intricacies related to nickel-catalyzed aldehyde/alkyne couplings.

### 3.1.1 Previous Mechanistic Work on Nickel-Catalyzed Reductive Couplings

Beginning with the first reported example in 1997, it was clear that this reaction class contained unique mechanistic features.[2] This was exemplified by the previously described change from an alkylative to a reductive coupling pathway when pre-treating the Ni(0) catalyst with four equivalents of $PBu_3$ (Scheme 63). It was proposed that either pathway could be accessed from intermediate **40**, which could undergo either direct reductive elimination (leading to alkylative product **41** with ethyl incorporation) or β-hydride elimination (leading to reductive product **42** with extrusion of ethylene gas). The

ability to change mechanism in the intramolecular system from an alkylative to a reductive pathway suggests that the electronic environment on the nickel-center plays an important role in chemical reactivity and reaction outcome.

**Scheme 63.** Ligand Dependent Change from an Alkylative to a Reductive Coupling Pathway

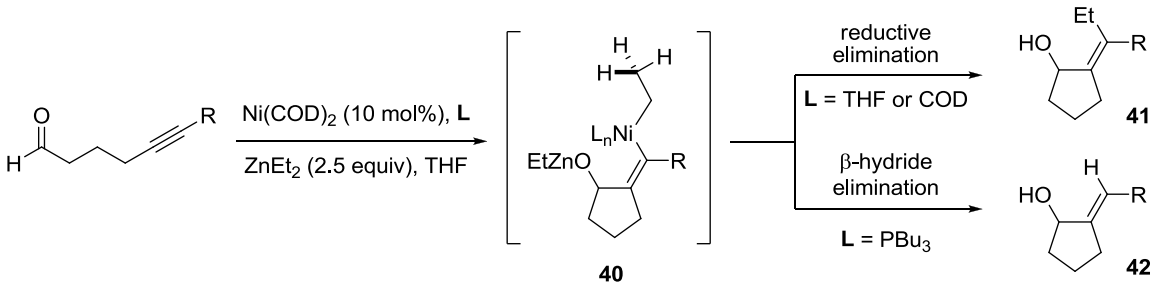


Based on previous reports from Buchwald[47] and Crowe[48] describing reductive couplings using titanium-based catalysts, it was speculated that oxametallacycles were involved in the transformations illustrated in Scheme 63, and that both cyclization products were derived from a common intermediate (structure **43** in Scheme 64).

**Scheme 64.** Proposed Mechanism for Ynal Cyclizations and Three-Component Couplings

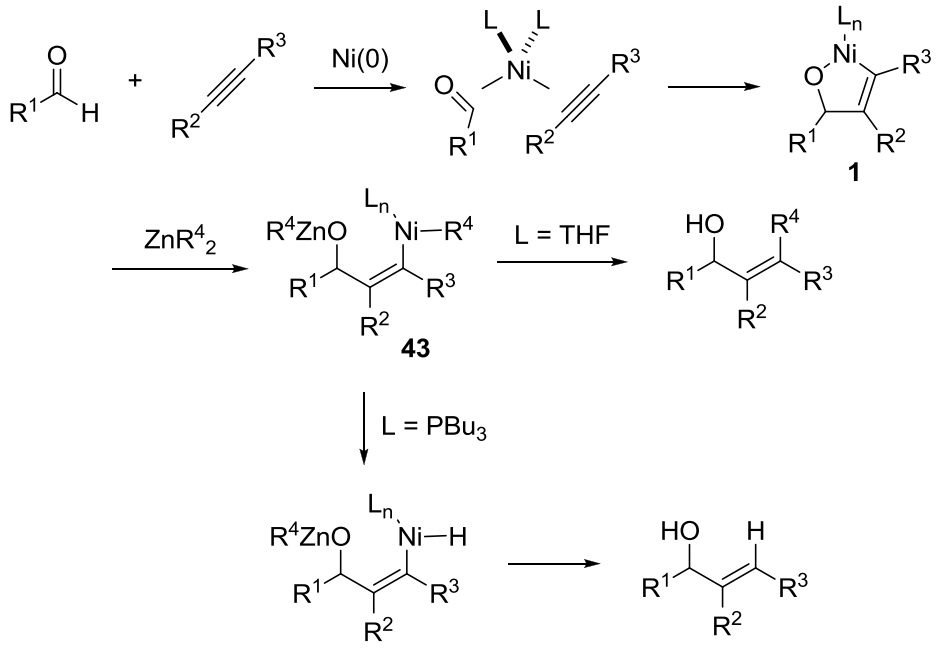


As discussed previously in Section 1.1 of Chapter 1, evidence for oxametallacycle intermediates was shown by comparing products formed from a competition reaction between $Pr_3Si$-H and $Et_3Si$-D reducing agents in the presence of nickel-catalysts. For the $Ni(COD)_2$/IMes catalyst system, results were similar in both inter- and intramolecular reductive couplings, with little or no crossover observed (results for the intramolecular variant shown in Scheme 65). Non-crossover products **45** and **46** were produced in 55% and 41% yield, respectively, and crossover products **44** and **47** were observed in <2% yield each, consistent with a mechanism involving metallacycle formation prior to involvement of the silane reducing agent (similar to the mechanism illustrated in Scheme 64). However, in the $Ni(COD)_2/PBu_3$ catalyst system, significant crossover was observed with **44**, **45**, **46**, and **47** produced in a 25:34:23:18 ratio. Although not fully understood at the time, this result implied that catalyst systems derived from *N*-

heterocyclic carbenes fundamentally differed from those derived from trialkylphosphines (a feature that will be addressed in the Results and Discussion section of this chapter).

**Scheme 65.** Intramolecular Crossover Results Comparing Phosphines with NHCs

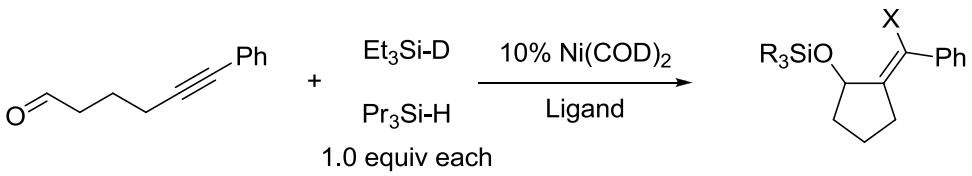


| | | | relative % | |
|---|---|---|---|---|
| R | X | product | IMes•HCl | $PBu_3$ |
| Et | H | **44** | <2 | 25 |
| Et | D | **45** | 55 | 34 |
| Pr | H | **46** | 41 | 23 |
| Pr | D | **47** | <2 | 18 |

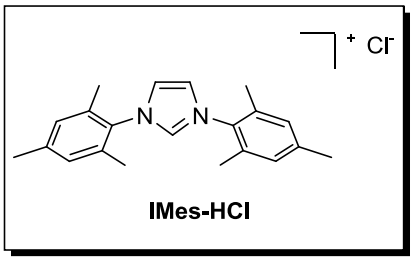


**IMes-HCl**

While the lack of crossover observed in the Ni(0)/NHC catalyst system is consistent with a metallacycle-based mechanism, there are other potential pathways that could lead exclusively to non-crossover products. An initial oxidative addition of the silicon-hydride bond to the nickel-catalyst could be followed by sequential insertions into the π-system of either the aldehyde or the alkyne (in any order) leading to the observed non-crossover products (Scheme 66).

**Scheme 66.** Non-Crossover Pathway via Initial Oxidative Addition of Reducing Agent to Ni(0)

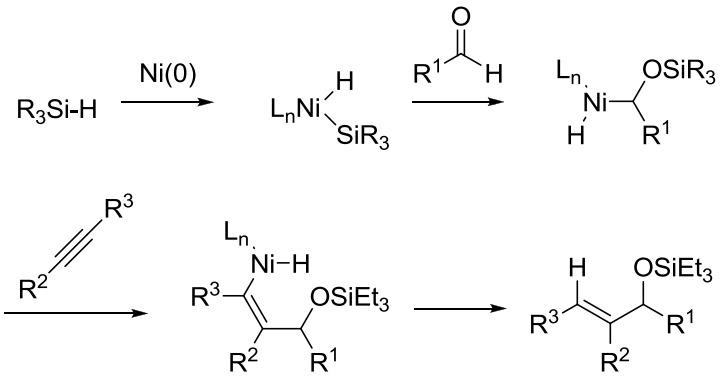


As discussed previously in Section 2.2.1 of Chapter 2, direct evidence for the existence of a nickel-metallacycle intermediate generated from an aldehyde and an alkyne was demonstrated by the Ogoshi group.[40] Ogoshi and coworkers were able to obtain a crystal structure of the dimeric oxametallacycle complex **27** generated from benzaldehyde, 2-butyne, $Ni(COD)_2$, and $PCy_3$ (Scheme 67).

**Scheme 67.** Generation of a Dimeric Oxametallacycle from an Aldehyde and an Alkyne

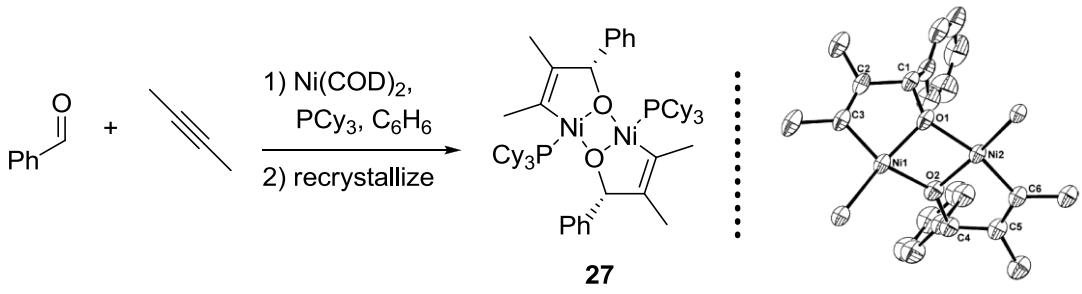


**27**

Although implicated as a reasonable intermediate for a variety of nickel-catalyzed processes, **27** was observed to undergo conversion to alkylative coupling product **48** at a rate that was much slower than what is observed for a productive catalytic experiment (Scheme 68).

**Scheme 68.** Reaction of Stoichiometric Dimeric Nickelacycle with $ZnMe_2$

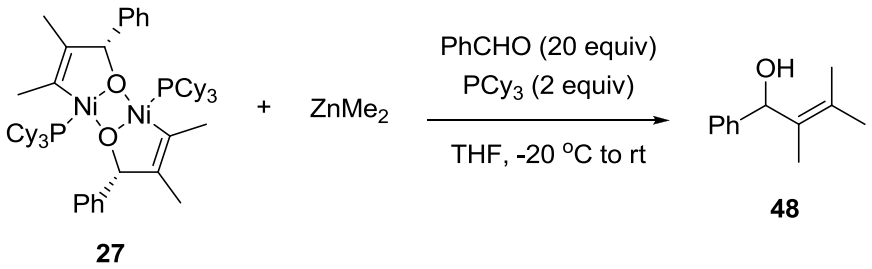


A rigorous computational study was undertaken by Houk and Jamison with respect to the nickel-catalyzed reductive coupling of aldehydes and alkynes with trialkylphosphine ligands and organoborane reducing agents to determine the most likely mechanism by which coupling occurs.[49] DFT calculations suggested that the most energetically feasible pathway for coupling involves rate-determining oxidative cyclization to metallacycle intermediate **52** in Scheme 69. Transmetalation to intermediate **53** after introduction of the borane reducing agent followed by β-hydride elimination to **54** leads to the expected allylic alcohol product after reductive elimination (Scheme 69). Due to the complex nature of the calculations, a model system involving $PMe_3$ and a simplified aldehyde and alkyne were used to identify a general mode of reactivity.

**Scheme 69.** DFT Calculated Mechanism for Aldehyde/Alkyne Reductive Couplings

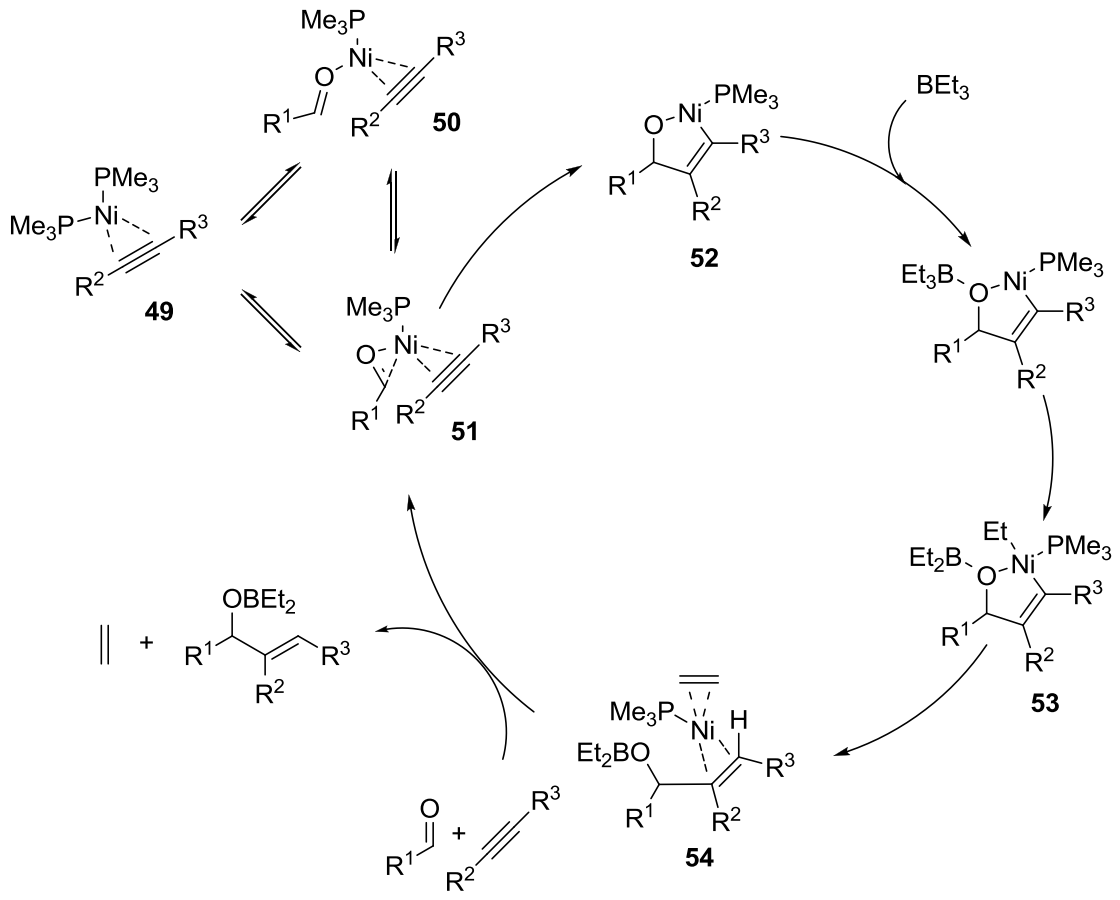


With all of the effort devoted to the development and mechanistic study of nickel-catalyzed aldehyde/alkyne couplings, it is surprising that no kinetic studies have been reported. While many of the studies described above support a metallacycle-based mechanism as the favored mode of transformation, direct experimental evidence has not been shown that can distinguish a metallacycle mechanism (such as that shown in Scheme 69) with an initial oxidative insertion of the reducing agent to the nickel-catalyst followed by sequential migratory insertions into the aldehyde and alkyne π-systems (shown in Scheme 66). For this reason, as well as unresolved questions surrounding ligand-dependent crossover effects, we sought to undertake a rigorous mechanistic study

of a nickel-catalyzed aldehyde/alkyne coupling process using trialkylsilane reducing agents. The primary tools for mechanistic elucidation would be the study of initial rates, DFT calculations, kinetic isotope effects, and crossover studies.

## 3.2 Results and Discussion

### 3.2.1 Probing the Viability of Dimeric Intermediates in Intramolecular Reductive Couplings of Aldehydes and Alkynes

A lingering issue left unresolved from the initial report of silane-mediated reductive couplings of ynals was the ligand-dependent crossover observed when comparing $PBu_3$ to IMes·HCl (Scheme 65).[1] Based on the structural work of Ogoshi described in Scheme 67, it was theorized that dimeric metallacyclic intermediates analogous to **27** could be responsible for the crossover effects observed. One potential sequence implicating a dimeric intermediate in the production of crossover products is illustrated in Scheme 70. Formation of monomeric metallacycle **55** could lead to **56** in a simple associative dimerization mechanism. Ligand dissociation from **56** followed by interaction with the silane reducing agent could lead to intermediate **57** where the relative positions of the silane alkyl group and hydride are scrambled between two separate substrate molecules, leading to the observed crossover products.

**Scheme 70.** Potential Role for Dimeric Intermediates Leading to Crossover

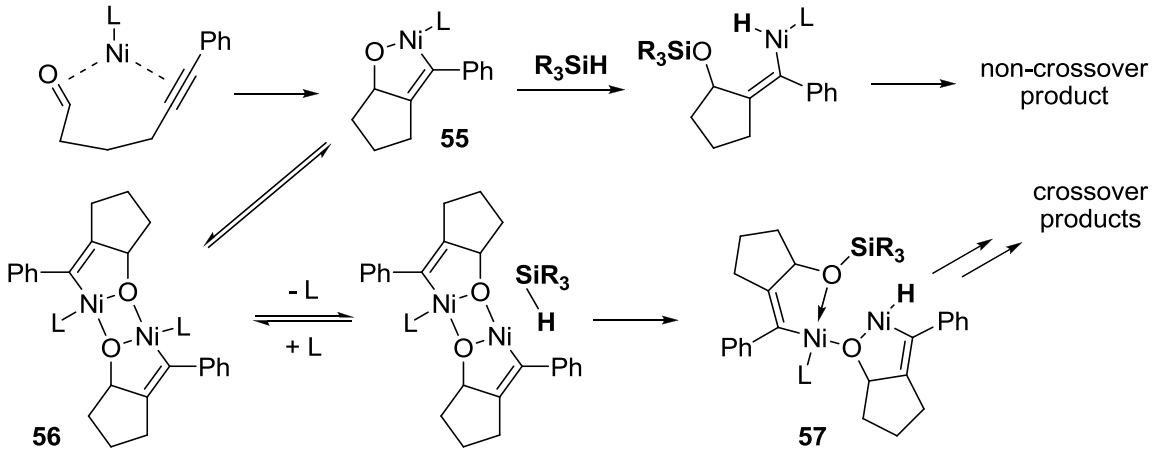


To determine the optimum ligand structure to probe these mechanistic possibilities, three catalyst/ligand combinations were screened (Scheme 71). While $Ni(COD)_2$/IMes is the preferred catalyst system for preparative experiments, the complete lack of crossover observed made it potentially difficult to study the mode by which crossover occurs. Also, the *in situ* generation of a potentially complex catalyst mixture could lead to difficulties in accurately describing the active catalyst participating in the coupling reaction. Whereas the $Ni(COD)_2/PBu_3$ catalyst system displays significant amounts of crossover, the intramolecular procedure requires high temperatures and extensive reaction times. Also, intermolecular couplings were not effective with the $Ni(COD)_2/PBu_3$ catalyst system, diminishing the generality of the procedure. However, a catalyst system comprised of $Ni(COD)_2/PCy_3$ was shown to be efficient at room temperature, was amenable to intermolecular couplings, and yielded a small yet significant amount of crossover. All catalyst/ligand combinations yielded similar kinetic isotope effects comparing H/D product ratios from a reaction using three equivalents each of $Et_3SiH/Et_3SiD$. This result suggests a similarity in the timing of the Si-H bond

cleavage with respect to the rate-determining step of the catalytic procedure, irrespective of ligand identity.

**Scheme 71.** Ligand Screening for Mechanistic Study

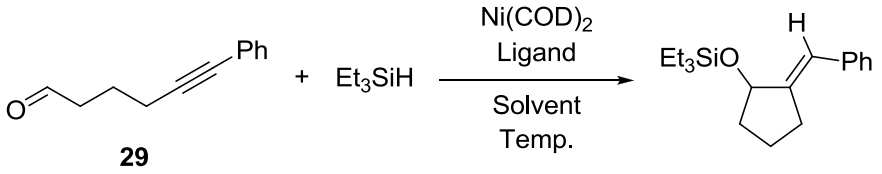


| Catlyst System | Temperature | % Crossover Observed | $k_H/k_D$ |
|---|---|---|---|
| 10%-$Ni(COD)_2$<br>10%-IMes•HCl<br>10%-KO-*t*-Bu | rt | < 2% | 1.04 |
| 10%-$Ni(COD)_2$<br>20%-$PBu_3$ | 45 °C | 42 - 50 % | 1.04 |
| 10%-$Ni(COD)_2$<br>20%-$PCy_3$ | rt | 11% | 1.04 |

As described in Scheme 70, if dimeric metallacycle **56** is formed via a simple dimerization from **55**, it was proposed that varying the steric environment of the ynal substrate would have an effect on the propensity to generate dimeric intermediates, thus affecting the amount of crossover observed. To probe this effect, ynal substrates of varying tether length were synthesized to correlate the steric influence of the methylene spacers in **29** to the amount of crossover observed. As illustrated in Scheme 72, crossover results comparing 5, 6, and 7-membered ring products displayed a decreasing amount of crossover with increasing ring size, diminishing altogether in the 7-membered case.

**Scheme 72.** Substrate Dependent Crossover: Varying Ring Size

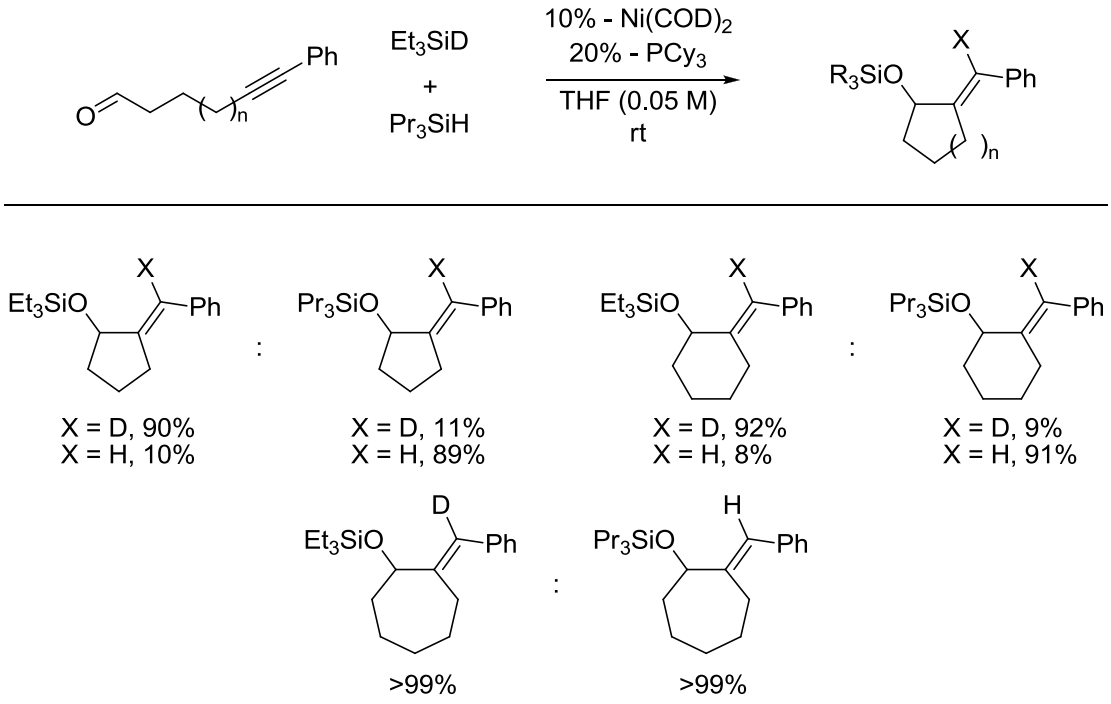


Not surprisingly, the trend in diminishing crossover also follows the trend in decreasing reaction rate, with the 5-membered ring cyclization occurring much faster than either the 6, or 7-membered cyclizations.

Crossover effects of various substrates were also examined at several reaction temperatures. Across the range of temperature studied, the extent of crossover observed was directly correlated to decreasing temperature, consistent with catalyst aggregation effects leading to crossover (Scheme 73).

**Scheme 73.** Temperature Dependent Crossover

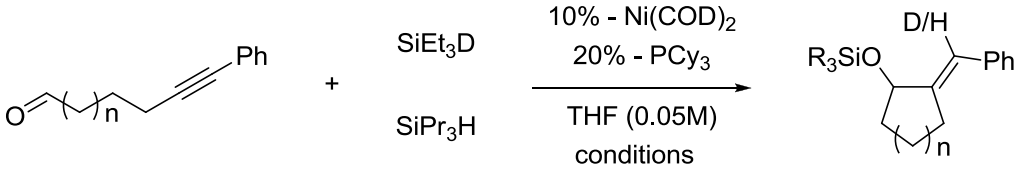


| n | conditions | R | H/D% |
|---|---|---|---|
| 1 | -25 °C | Et | 43/57 |
| | | Pr | 57/43 |
| | 0 °C | Et | 18/82 |
| | | Pr | 65/45 |
| | 45 °C | Et | 6/94 |
| | | Pr | 94/6 |
| 2 | -25 °C | Et | 38/62 |
| | | Pr | 54/46 |
| 3 | -25 °C | Et | 15/85 |
| | | Pr | 87/13 |

For comparison purposes, similar effects were examined in the intermolecular coupling of benzaldehyde with 3-hexyne (Scheme 74). As illustrated below, a standard reaction run at room temperature yields a very small amount of crossover. However, significant crossover effects are observed at much lower temperatures, although the intermolecular reaction is very sluggish under these conditions.

**Scheme 74.** Temperature Dependent Crossover in Intermolecular Coupling

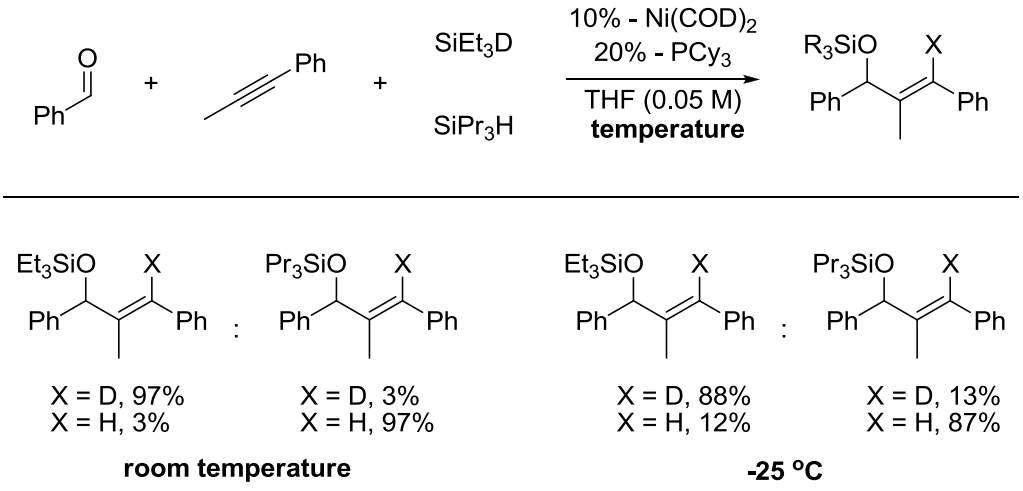


### 3.2.2 DFT Calculations of Proposed Intermediates

While there is direct evidence for the stoichiometric generation and isolation of dimeric metallacycles from $Ni(COD)_2/PCy_3$, a series of ground state DFT calculations were undertaken to compare the relative energies of mono- and dimeric metallacycle coupling pathways. The reaction sequence involving oxidative cyclization of ynal substrate **29** to monomeric metallacycle **38** was examined as the general sequence for the monomeric coupling pathway (Scheme 75). $PMe_3$ was used in place of $PCy_3$ as the ligand for nickel in order to simplify the calculations.

**Scheme 75.** Model System for DFT Calculations: Monmeric Pathway

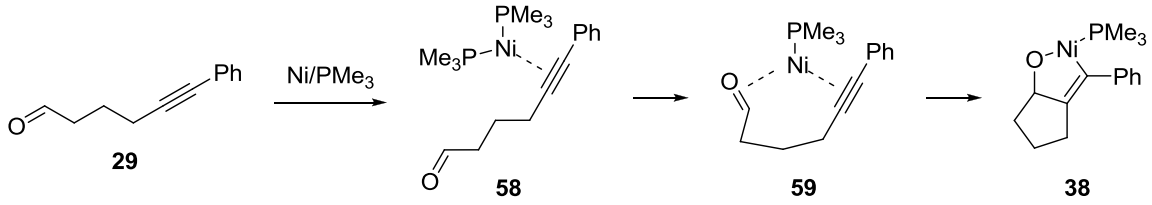

Ground state calculations revealed that the transformation from intermediate **58** to **38** is only slightly energetically favorable by a value of 0.2 kcal/mol. While $\Delta G^{\neq}$ values were not calculated, the ground state energy of intermediate **59** is only 3.7 kcal/mol higher than that of **58** (Scheme 76).

**Scheme 76.** Ground State Energies of Proposed Intermediates: Monomeric Pathway

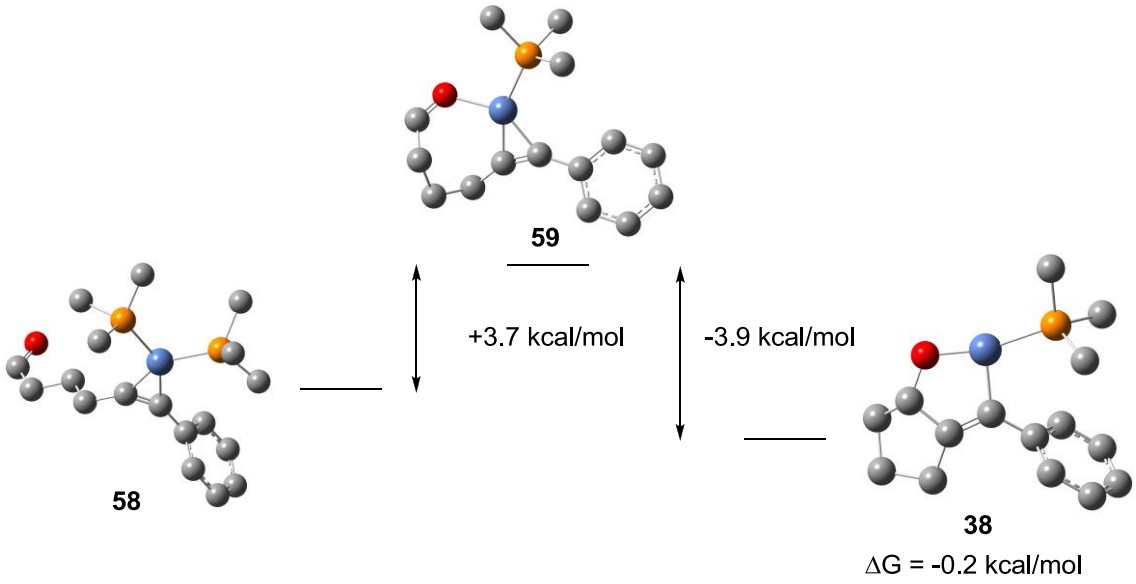


Conversely, when comparing the relative energies of intermediates along an analogous reaction pathway involving the generation of a dimeric metallacycle, a very large change in energy is observed (Scheme 77). Dimeric metallacycle **39** may be formed via a number of reaction sequences, although the sequence and timing of the dimerization process is not obvious. For ease of comparison, ground-state energies were calculated from a reaction sequence analogous to the one shown in Scheme 70 involving dimerization of two equivalents of monomeric metallacycle **38** to **39**.

**Scheme 77.** Ground State Energies of Proposed Intermediates: Dimeric Pathway

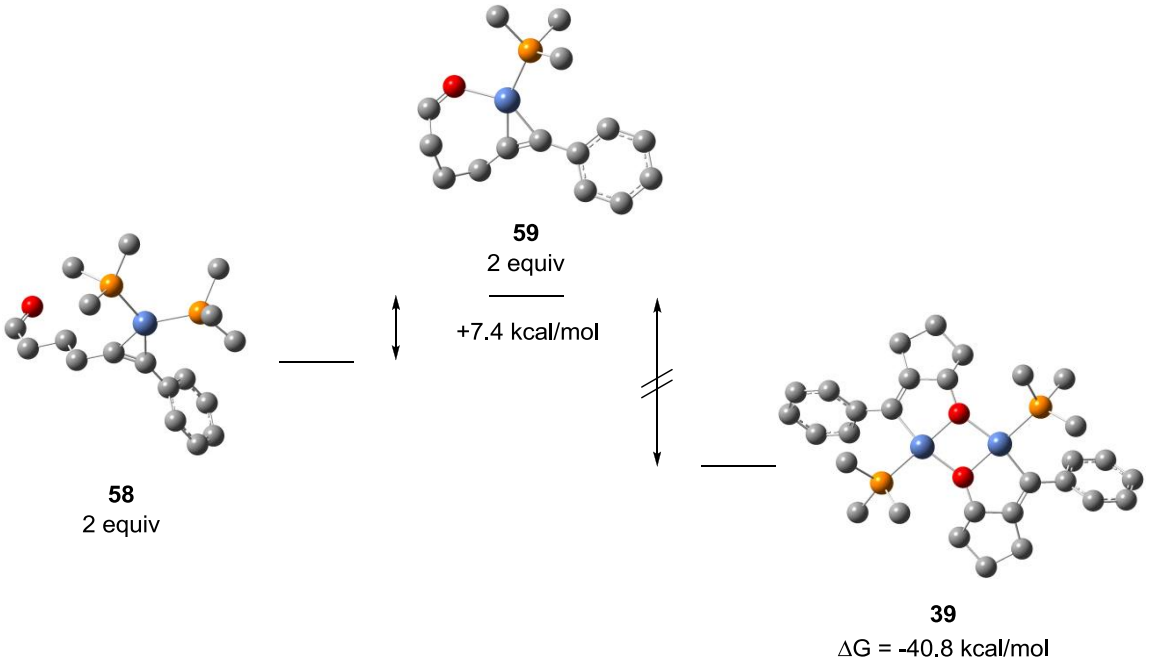


As shown in Scheme 77, the dimerization of two equivalents of **59** to **39** is a very energetically favorable process. To probe whether such thermodynamically stable intermediates are kinetically competent in the catalytic transformation of substrate **29** to the observed reductive coupling product, a series of mixing experiments were undertaken. Based on the experimental procedure reported by Ogoshi, it was theorized that pre-mixing substrate **29** with a stoichiometric amount of $Ni(COD)_2/PCy_3$ would rapidly lead to the *in situ* generation of **30** (Scheme 78).

**Scheme 78.** Stoichiometric Generation of Dimeric Metallacycles *In Situ*

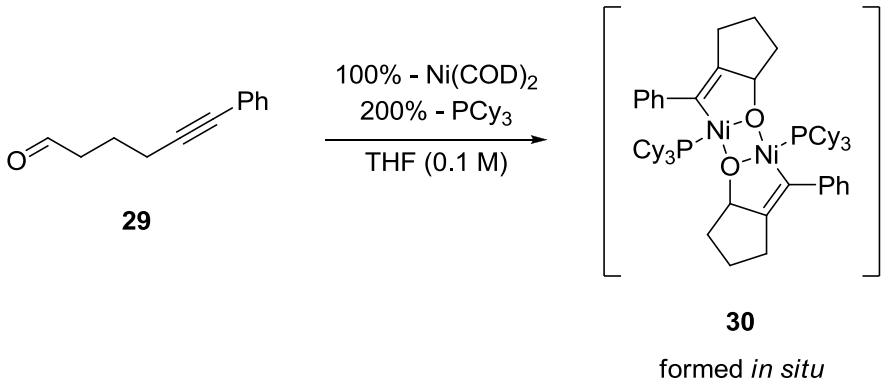


**29**

**30**

formed *in situ*

Treating the resulting reaction mixture with various amounts of silane reducing agents yielding no desired product after several hours at room temperature (Scheme 79). In fact, the only organic product observed from these experiments was the alkyne-hydroacylation product **31** discussed in Scheme 48 of Section 2.2.1.

**Scheme 79.** Treatment of a Dimeric Metallacycle Generated *In Situ* with $Et_3SiH$

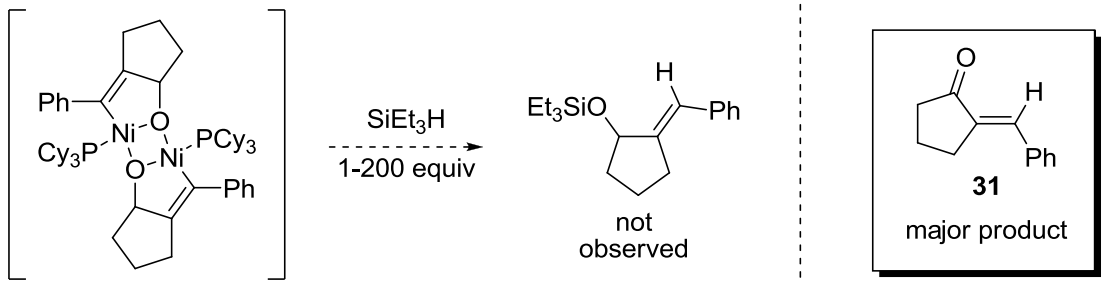


**30**

formed *in situ*

A similar effect was observed in an experiment involving catalytic amounts of $Ni(COD)_2/PCy_3$. In all cases, pre-mixing the catalyst mixture with substrate **29** in the absence of a silane reducing agent effectively shuts down the reaction to produce the

desired product. While the DFT calculations suggest that the formation of dimeric intermediates is highly energetically favorable, subsequent mixing experiments suggest that if formed *in situ*, they are not kinetically competent in silane-mediated transformations to yield the expected silyl-protected allylic alcohols. This data does not conclusively discount the presence of dimeric oxametallacycles in the catalytic production of silyl allylic alcohols, but it does suggest that if they are allowed to form in large concentrations, such that the majority of the $Ni(COD)_2/PCy_3$ present is consumed, they are unreactive towards silane reducing agents known to promote reductions in the catalytic process.

Following this work, a collaboration with the Houk group was initiated to fully evaluate transition state barriers involving the formation of dimeric intermediate as they relate to the production of crossover products. That work in progress will not be fully described in the context of this thesis, but will likely be co-published with experimental contributions by our research group.

### 3.2.3 Preliminary Kinetic Results Using *In Situ* IR Monitoring in Real-Time

In an effort to gain insight into the timing or nature of Si-H bond cleavage in nickel-catalyzed reductive couplings of aldehydes and alkynes, an initial-rates study was undertaken with respect to the intramolecular cyclization of ynal **29** using a $Ni(COD)_2/PCy_3$ catalyst system and $Et_3SiH$ reducing agent. We envisioned the elucidation of a complete kinetic profile as the most straightforward method to distinguish between initial oxidative addition of the silane Si-H bond to Ni(0) (Scheme

66), and the generally favored metallacycle mechanism involving oxidative cyclization of the aldehyde and alkyne with Ni(0) (Scheme 64 and Scheme 69).

Due to the rapid rate of reaction, concentration and temperature were modified from the preparative procedure for the cyclization of **29** to simplify the acquisition of rate data. The exact reaction conditions for preliminary study involved the reductive cyclization of 0.05 mol/L of ynal **29** (half the concentration used in preparative experiments) at 0 $^{o}$C in the presence of 1.0 equivalent of $Et_3SiH$ (Scheme 80).

**Scheme 80.** Experimental Conditions for the Kinetic Study of Nickel-Catlyzed Ynal Cyclizations at 0 $^{o}$C

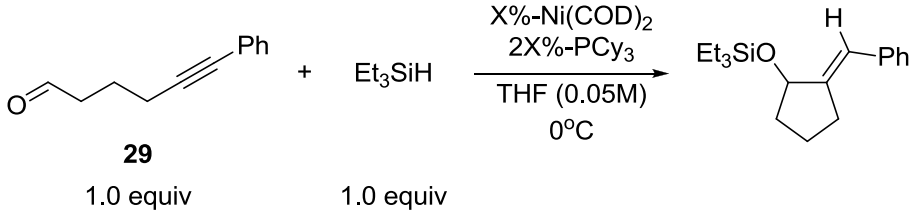


Tracking the disappearance of **29** in the presence of 10 mol% $Ni(COD)_2$ in real-time via *in situ* IR monitoring yielded the reaction progression shown in Figure 1, measured as absorbance units per second. Systematic variation of the concentration of the $Ni(COD)_2/PCy_3$ catalyst mixture yielded the data shown in Figure 2. Using these data, changes in initial-rate with respect to changes in the concentration of $Ni(COD)_2/PCy_3$ were used to assign a reaction order for the concentration of cataylst in the coupling reaction (represented as $[Ni(COD)_2]$ for the remainder of this discussion). Fitting the curve shown in Figure 2 to the equation y = ax^b suggested a non-linear dependence of reaction rate on $[Ni(COD)_2]$. A value of 1.71 ± 0.08 was calculated for the reaction order in $Ni(COD)_2$.

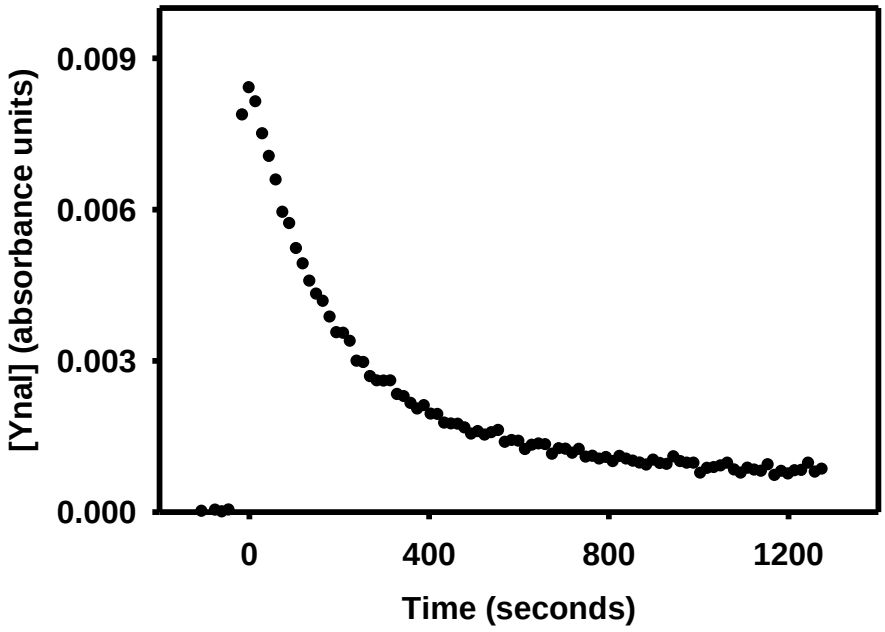


**Figure 1.** Reaction Progression as Measured by Starting Material Consumption

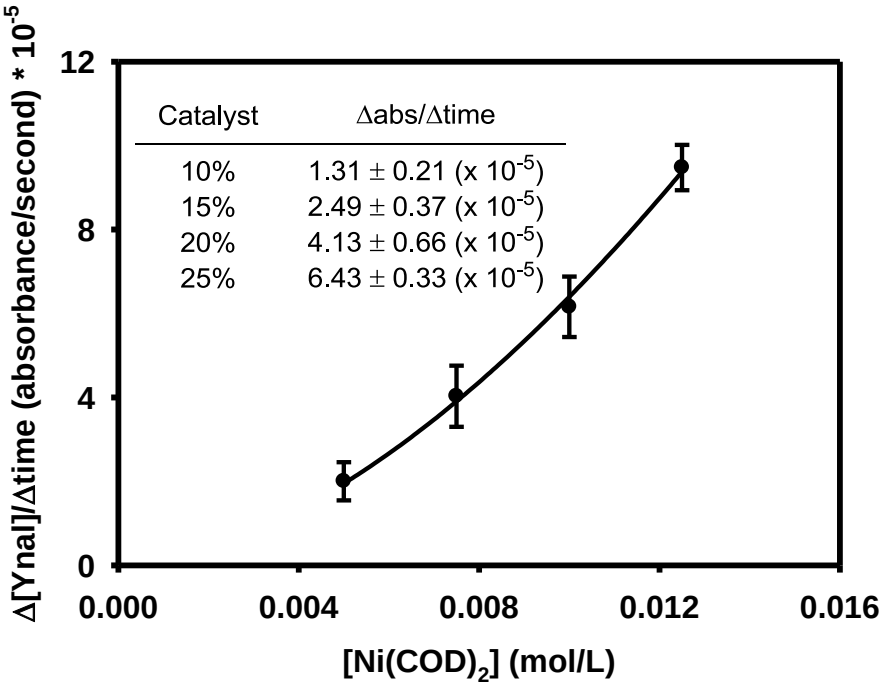


**Figure 2.** Graphical Depiction of Initial Rate Dependence on $[Ni(COD)_2]$

Depending on the resting state of the catalyst, this result could be consistent with the formation of dimeric metallacycles similar to those discussed in the previous section. However, upon closer inspection of the reaction progressions used to calculate rate data, it became clear that the very fast rate of reductive cyclization was becoming problematic for kinetic interpretation. Reactions run at high catalyst loadings yield a small number of early data points from which to calculate initial rates, and the absolute values of the calculated rates varied significantly depending on which data points are included. For example, Figure 3 represents the reaction progression of a reductive cyclization with 25 mol% catalyst loading. A rate calculated from the first three data points of the reaction gives a value of $5.68 \times 10^{-5}$ (abs/sec). However, a rate calculated from the second through fourth data points yields a value of $7.28 \times 10^{-5}$ (abs/sec), a significant amount of variation. In addition to this variation, the reaction has passed greater than 50% conversion by the time the fifth data point is registered, well beyond the point of reaction that is normally considered for initial rates.

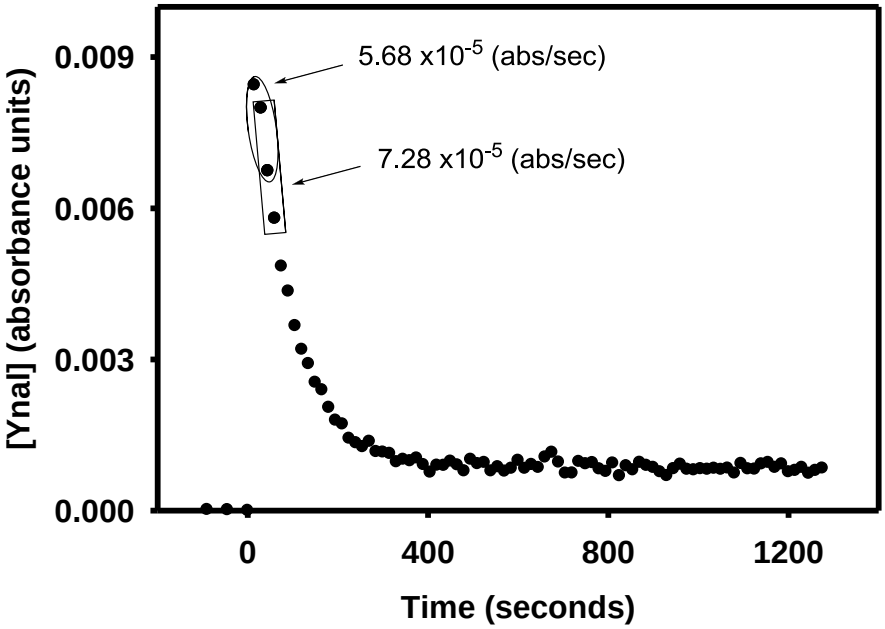


**Figure 3.** Reaction Progression with 25 mol% Catalyst Loading

Another limitation of this procedure was identified when examining the dependence of reaction rate on [$Et_3SiH$]. It was shown that using super-stoichiometric amounts of $Et_3SiH$ led to the formation of an undesired side-product (**60** in Scheme 81).

**Scheme 81.** Formation of an Undesired Side-Product at High $Et_3SiH$ Concentrations

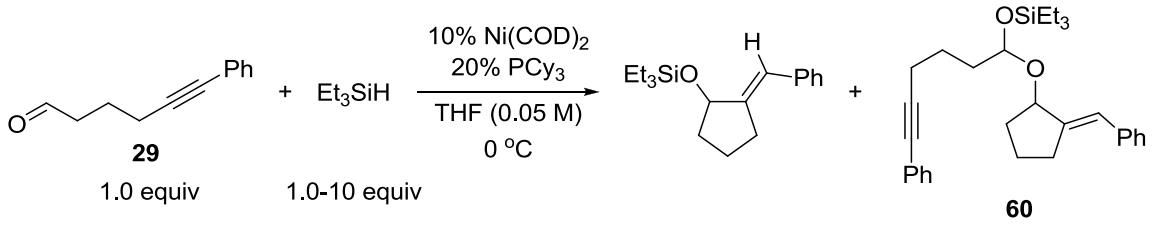


The formation of **60** did not allow for accurate measurements of initial rates, as starting material consumption could not be cleanly correlated to the formation of the

desired product. As shown in Figure 4, no clear rate dependence was observed with varying [$Et_3SiH$].

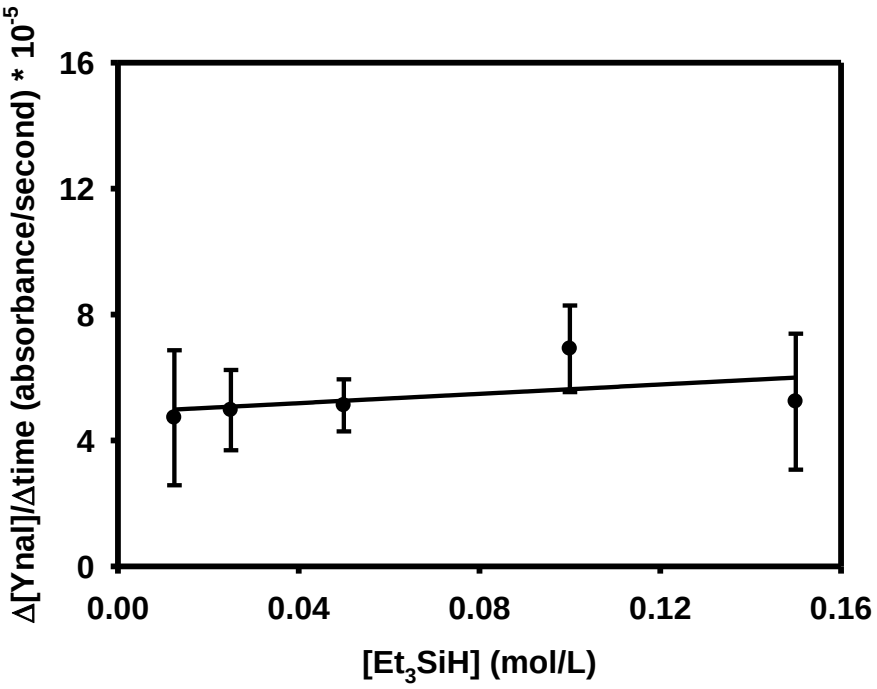


**Figure 4.** Rate Dependence on [$Et_3SiH$]

It was clear that several problematic issues were confounding the analysis of initial rates under the conditions described in

Scheme **80** and Scheme 81. To address these issues, subsequent kinetic analyses were performed under synthetically relevant conditions known to be optimum for the clean production of desired product in high yield in the absence of undesired side-products.

### 3.2.4 Mechanistic Investigation Under Synthetically Relevant Conditions

The optimized preparative reaction conditions involve the cyclization of 0.1 M of **29** in the presence of 2.0 equivalents of $Et_3SiH$ in THF at room temperature (Scheme 82).

**Scheme 82.** Experimental Conditions for the General Preparative Procedure

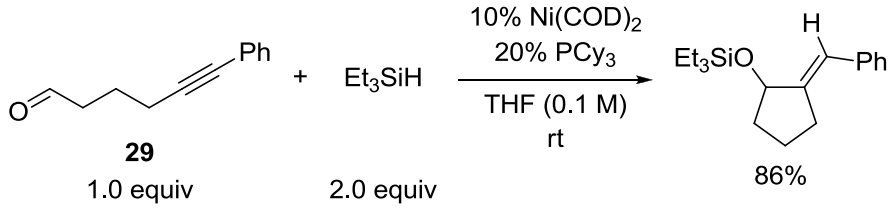


Reactions run under these conditions were extremely fast and required cooling to - 25 $^{o}$C to allow for adequate data collection. Following this modified experimental procedure, the amount of data collected was increased by a factor of ten compared to the procedure discussed in the previous section (compare Figure 3 and Figure 5).

Under the conditions described in Scheme 83, the reaction rate was shown to have a linear dependence on [Ni(COD)$_2$] between 10-25 mol% catalyst loading (Figure 6). Initial rates of reactions using less than 10 mol% catalyst loading were not included in this analysis due to inconsistent reaction conversion.

**Scheme 83.** Experimental Conditions for the Determination of Rate Dependence on [Ni(COD)$_2$] at - 25 $^{o}$C

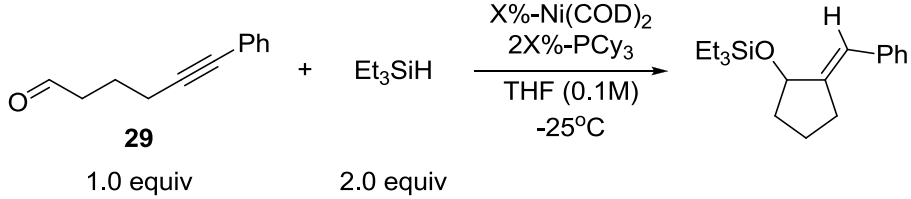

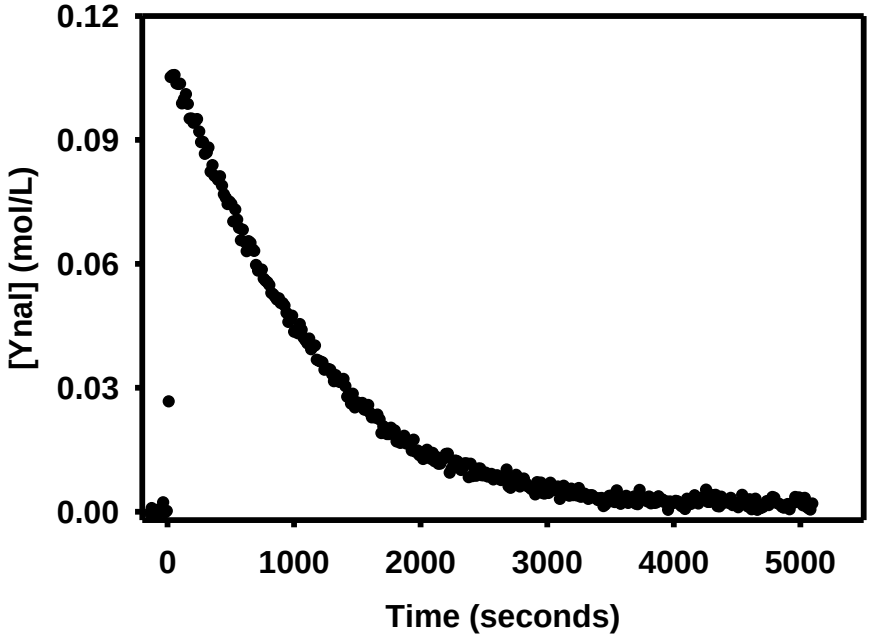


**Figure 5.** Reaction Progression Under Synthetic Conditions at - 25 $^{o}$C

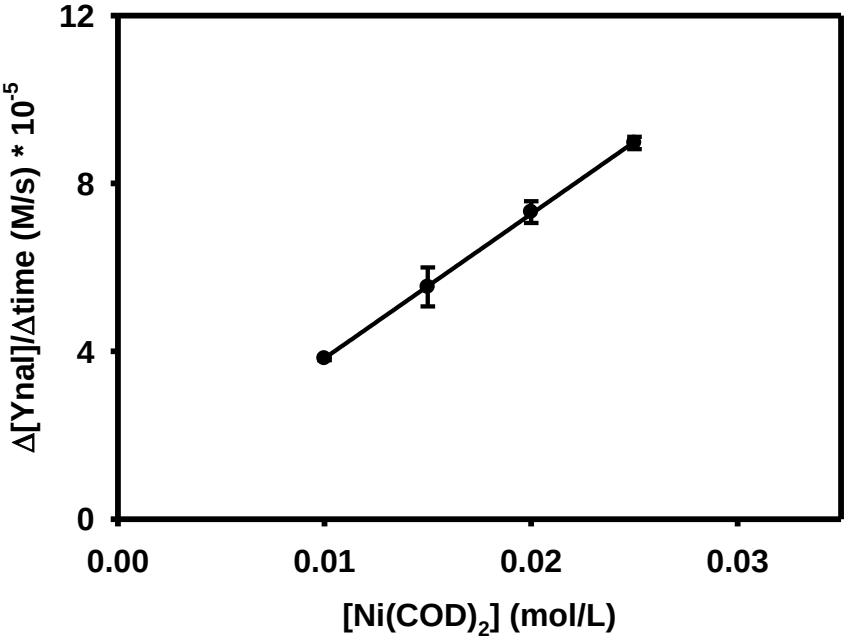


**Figure 6.** Initial Rate Versus [Ni(COD)$_2$]

Unlike the results discussed in the previous section, it's clear that even at high catalyst concentrations there is adequate data to calculate initial rates. An overlaid plot of reaction progression at various values of [$Ni(COD)_2$] illustrates the increase of reaction rate with increasing [$Ni(COD)_2$] (Figure 7).

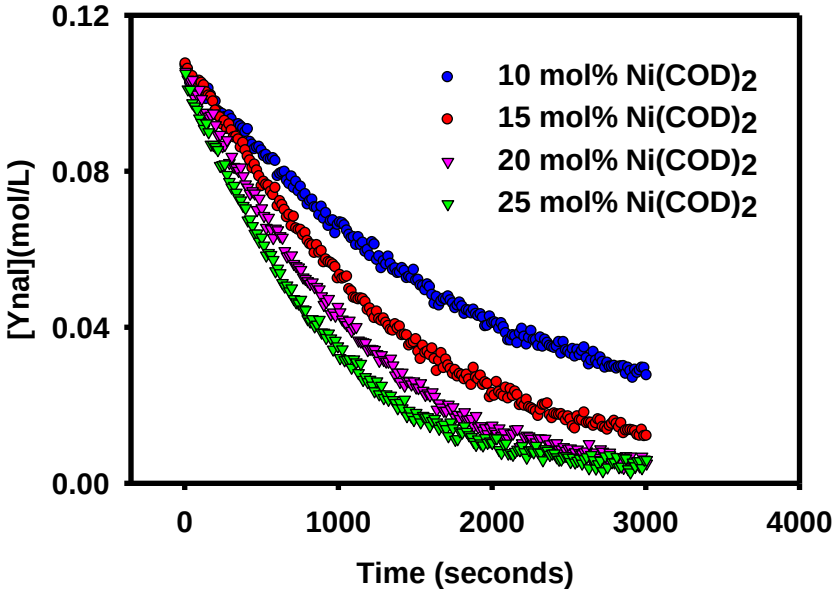


Figure 7. Overlaid Reaction Progressions at Varying [$Ni(COD)_2$]

Under the conditions described in Scheme 84, the reaction rate was shown to have a linear dependence on [Ynal **29**] between 0.5-1.25 equivalents (Figure 8). This rate dependence is clearly illustrated by overlaying reactions run at different values of [**29**] to demonstrate how the reaction rate changes with changing [**29**] (Figure 9).

**Scheme 84.** Experimental Conditions for the Determination of Rate Dependence on [Ynal] at - 25 $^{o}$C

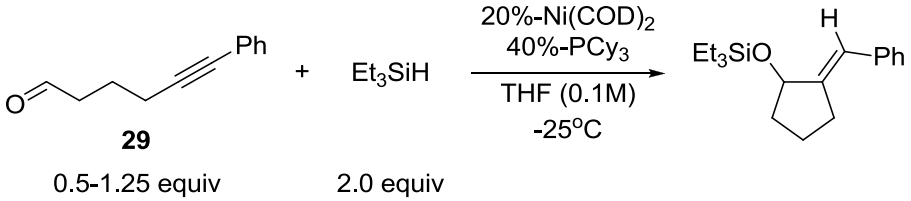


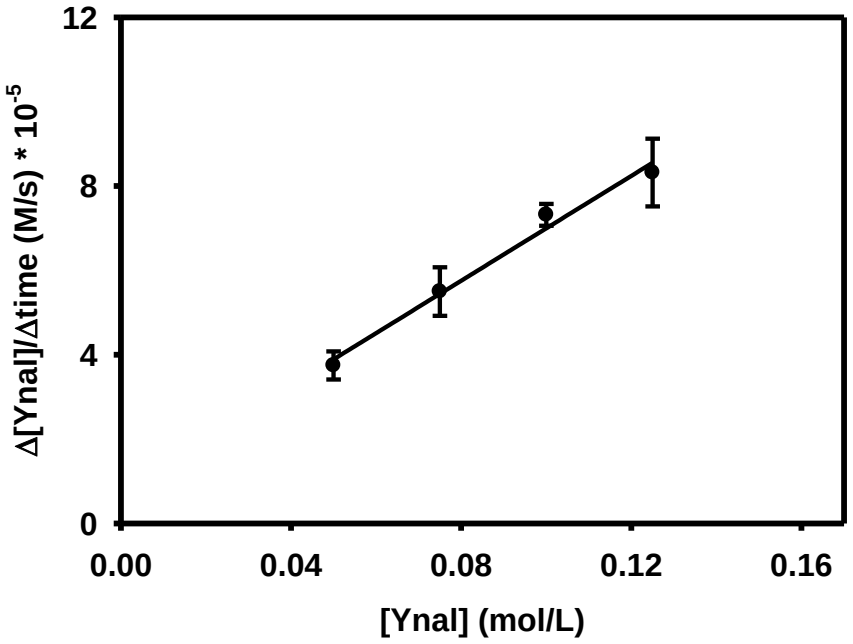


**Figure 8.** Initial Rate Versus [Ynal]

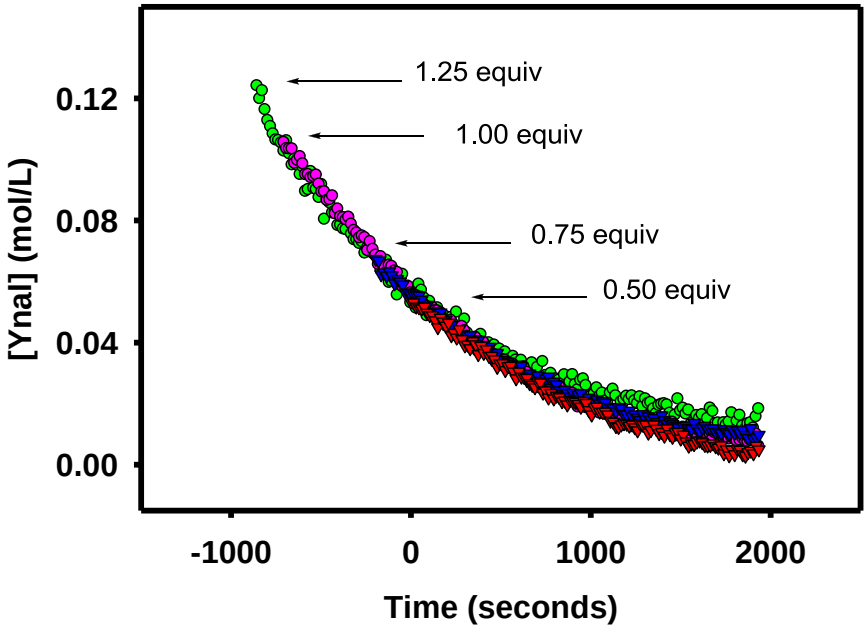


**Figure 9.** Overlaid Reaction Progressions of Ynal

However, when examining higher concentrations of ynal **29**, strange effects began to emerge. As shown in Figure 10, a clean reaction progression was not observed. Reactions run in excess of 1.25 equivalents of **29** appeared to involve a slow initiation period followed by increasing reaction rate before leveling off to a slow conversion to product. While the origin of these effects remains unknown, they were consistently observed when examining reactions run with 1.5-2.0 equivalents of **29**. Large excesses of $Et_3SiH$ did not have an effect on the strange rate behavior observed at high [**29**], suggesting that the effect is a result of the overall concentration of **29**, not the relative ratio of [**29**] to [$Et_3SiH$].

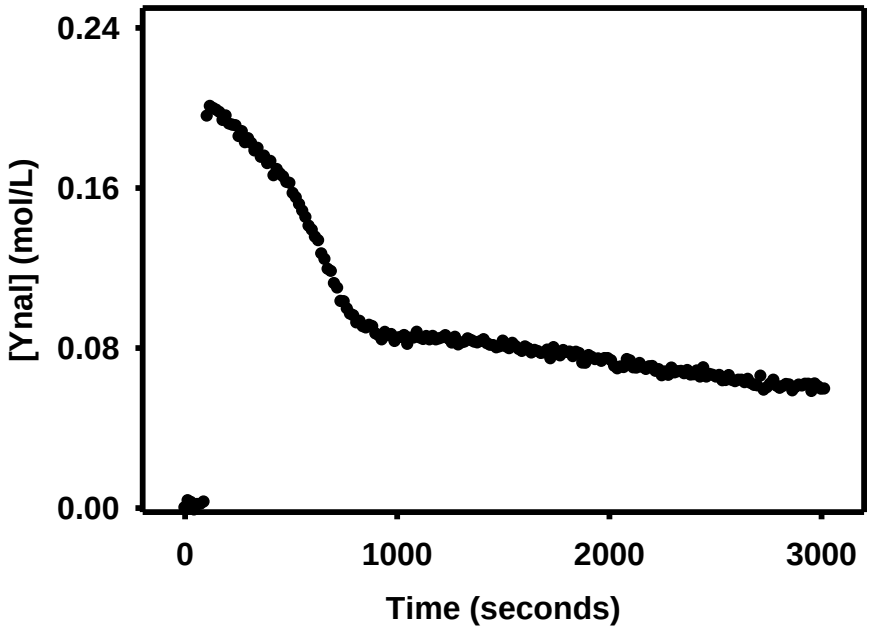


**Figure 10.** Reaction Progression at High Concentration of Ynal

Under the conditions described in Scheme 85, the reaction rate was shown to have zero-order dependence on [$Et_3SiH$] between 1.0-4.0 equivalents (Figure 11). This effect is especially clear by examining overlaid reaction progressions at various [$Et_3SiH$] to show no change in reaction behavior across a four-fold concentration range (Figure 12)

**Scheme 85.** Experimental Conditions for the Determination of Rate Dependence on [$Et_3SiH$] at - 25 $^oC$

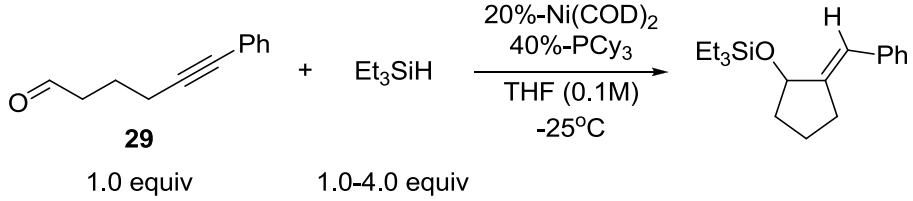

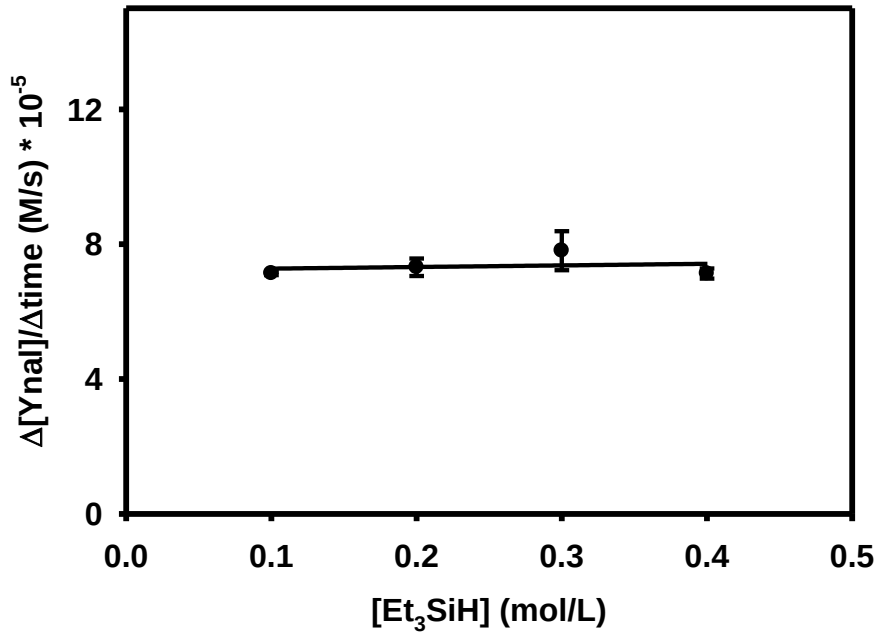


**Figure 11.** Initial Rate Versus [$Et_3SiH$]

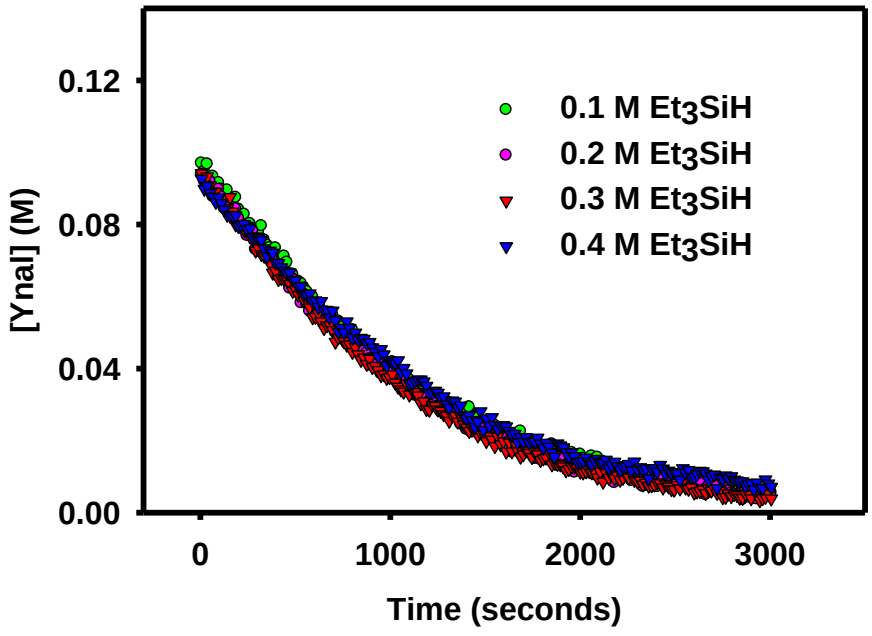


**Figure 12.** Overlaid Reaction Progressions at Varying [$Et_3SiH$]

A first order dependence of reaction rate on [$Ni(COD)_2$] and [**29**] combined with a zero-order rate dependence on [$Et_3SiH$] could be consistent with either a metallacycle-based mechanism or a fast initial oxidative addition of Si-H to Ni(0) followed by substrate incorporation (equations 1 and 2, respectively, in Scheme 86).

**Scheme 86.** Kinetically Indistinguishable Mechanisms

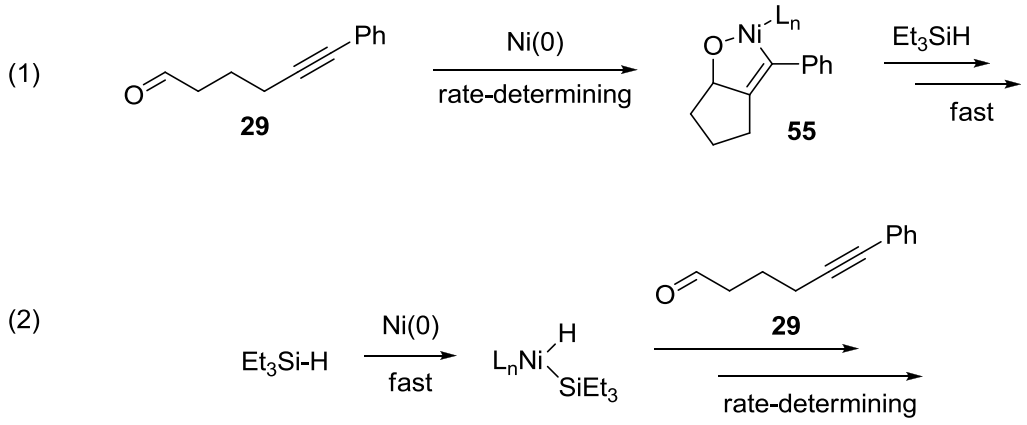


To examine the possibility of a very rapid reaction between $Et_3SiH$ and Ni(0) as an initial step in a productive reaction sequence, $Et_3SiH$ was treated with a stoichiometric amount of $Ni(COD)_2/PCy_3$ as the concentration of $Et_3SiH$ was monitored via *in situ* IR spectroscopy. No consumption or change in the silicon-hydride stretch (2100 $cm^{-1}$) was observed on the timescale of a productive catalytic reaction (Figure 13). These observations are most consistent with a rate-determining addition of the $Ni(0)/PCy_3$ catalyst to substrate **29**, followed by a rapid sequence involving $Et_3SiH$ (equation 1 in Scheme 86).

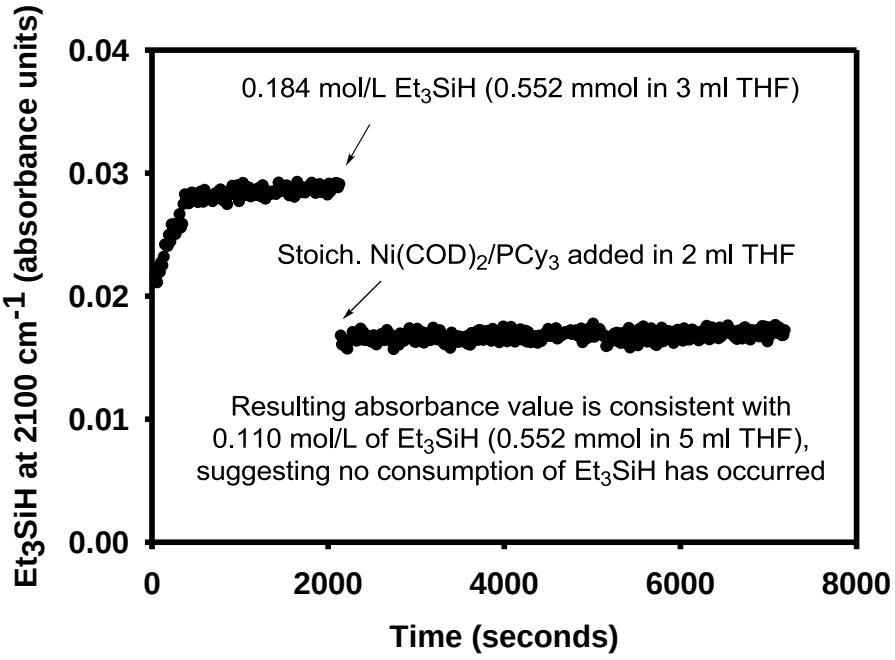


**Figure 13.** *In Situ* Monitoring of Si-H Stretch with Stoichiometric $Ni(COD)_2/PCy_3$

To further distinguish between the mechanisms described in Scheme 86, kinetic isotope effect studies were undertaken to gain insight into the Si-H bond cleavage process (Scheme 87). No significant competition kinetic isotope effect was observed for the silane mediated reductive cyclization of **29** with $Ni(COD)_2/PCy_3$ at 45 $^oC$ ($k_H/k_D$ = 1.00). To compare this outcome against a reaction that likely does involve direct oxidative addition of Si-H to Ni(0), the competition kinetic isotope effect was determined in the hydrosilylation of aldehyde **61** under the same reaction conditions. The hydrosilylation of **61** under these conditions proceeded with an inverse kinetic isotope effect ($k_H/k_D$ = 0.75). If the steps involved in aldehyde hydrosilylation are reversible, then an inverse kinetic isotope effect may be the result of an equilibrium isotope effect.[50-52] This stark difference in isotope effects suggests that a common mechanism for irreversible consumption of the silane is not involved.

**Scheme 87.** Kinetic Isotope Effect Studies of Reductive Cyclization and Aldehyde Hydrosilylation

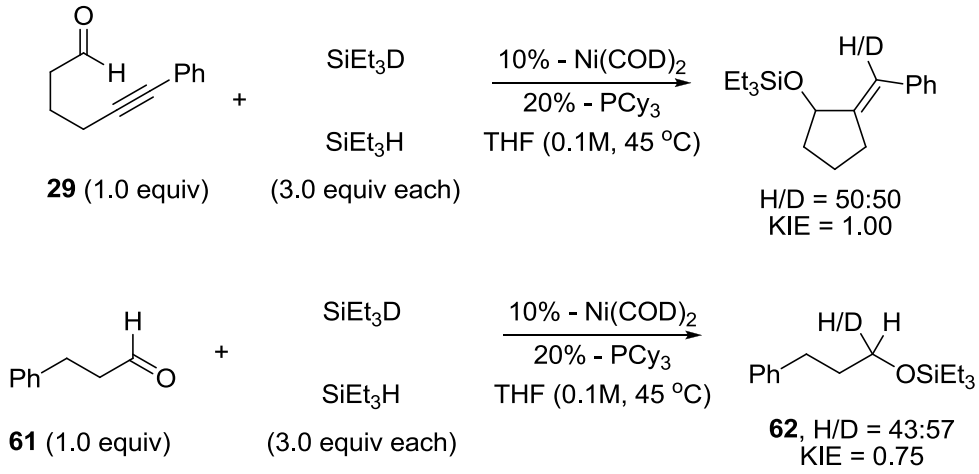


### 3.3 Summary of Mechanistic Evaluation of Intramolecular Nickel-Catalyzed Reductive Couplings of Aldehydes, Alkynes, and Trialkylsilanes

In summary, the kinetic behavior of nickel-catalyzed silane-mediated reductive cyclization of ynals has been studied. Rate data, along with crossover studies, DFT calculations, and kinetic isotope effects have been evaluated. The results of the rate study are consistent with a mechanism involving rate-determining oxidative cyclization to a metallacyclic intermediate, followed by rapid silane-mediated conversion to the observed product. Rate-limiting oxidative addition of the silane to Ni(0) can be ruled out on the basis of the rate data.

The lingering issue of the crossover results remains unsolved by kinetic studies. However, based on DFT calculations and experimental evidence discussed in Section 2.2.3, the viability of dimeric metallacyclic intermediates cannot be discounted. One potential explanation for the observed kinetic behavior coinciding with the observed crossover results is illustrated in Scheme 88.

**Scheme 88.** Mechanistic Rationale for Crossover Products Based on Kinetic Results

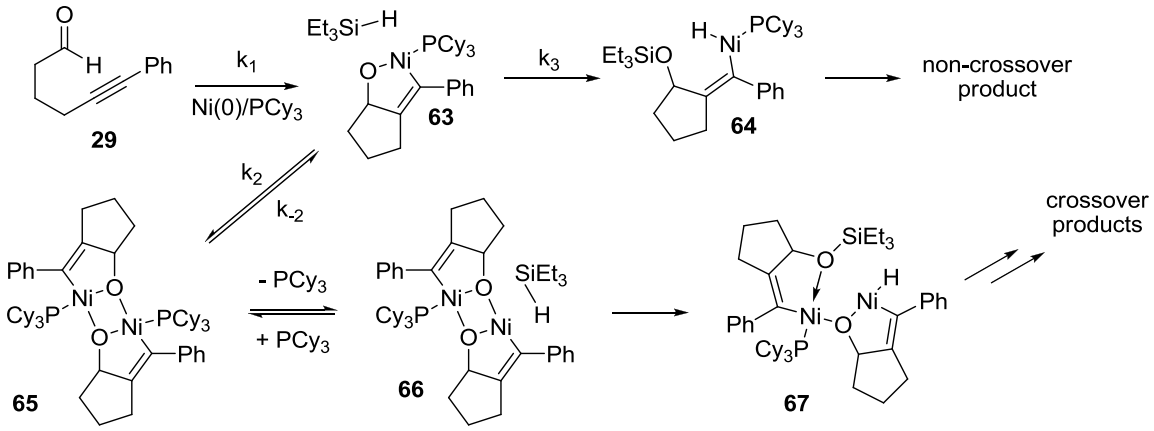


Rate-determining oxidative cyclization of **29** with the Ni(0) catalyst is supported by the observed first order rate dependence on [Ni(COD)$_2$] and [Ynal **29**], as well as the zero order rate dependence on [Et$_3$SiH], as its participation is exclusively post rate-limiting. Although it is theorized that large concentrations of dimeric metallacycle **65** inhibit product formation, if $k_2$ is sufficiently faster than $k_3$, it is still plausible that a small concentration may be built up during a productive reaction, leading to the small amounts of crossover products observed.

An ongoing computational collaboration with Houk and coworkers has supported the implication of intermediate **65** in the crossover pathway. Calculations suggest that that relative rate of $k_1$ to $k_3$ is critical for dimer formation. If $k_1$ is sufficiently fast, intermediate **63** may be present in a large enough concentration to allow for the rapid formation of dimeric intermediate **65** via $k_2$. However, when $k_3 >> k_1$, **63** may be present only in very small amounts, preventing the formation of **65**. These results suggest that the substrate dependent crossover effects observed in Scheme 72 and Scheme 74 may not be the result of diminishing ring strain in dimeric intermediates, but from a reduced rate

of oxidative cyclization. Current efforts are underway to correlate substrate steric effects with transition state barriers and observed crossover. It is theorized that varying the steric bulk of alkyne substituents on substrates analogous to **29** will have a significant effect on the amount of crossover observed. Experimental results will be supported by calculations of $k_1$, $k_2$, and $k_3$ by comparing $\Delta G^{\neq}$ values along the reaction landscape.

# Chapter 4

# Mechanistic Evaluation of Intermolecular Nickel-Catalyzed Reductive Couplings of Aldehydes, Alkynes, and Trialkylsilanes

## 4.1 Introduction

Of the various nickel-catalyzed coupling procedures that have been developed in the past two decades, intermolecular silane-mediated processes utilizing the unique structure and reactivity of NHC ligands have been arguably the most synthetically useful. While the stability of silane reducing agents has enhanced the ease and practicality of reductive couplings, the wide range of structural diversity readily accessible within the NHC ligand class has allowed for the development of highly stereoselective coupling processes. As described in Chapter 3, the development of sterically demanding asymmetric NHC ligands allowed for the production of chiral silyl-protected allylic alcohols (Scheme 60). As shown in Scheme 89, a wide variety of NHC ligands were synthesized and examined in the reductive coupling process.[29]

**Scheme 89.** Chiral *N*-Heterocyclic Carbenes used in Asymmetric Reductive Couplings

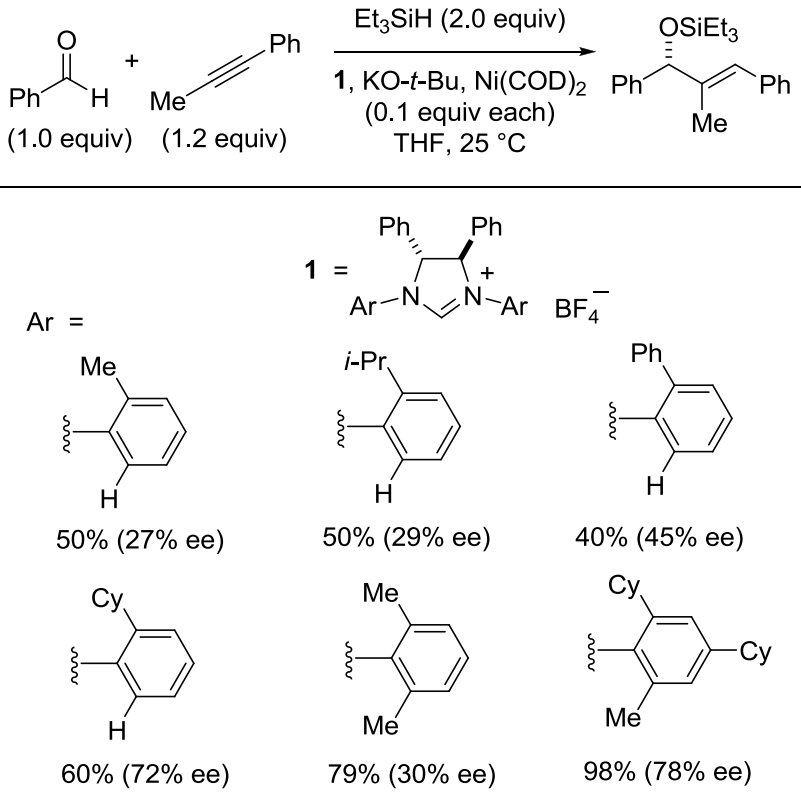


Also previously described were the highly regioselective coupling processes developed using a wide range of differentially sized NHC ligands (Scheme 62). These processes truly showcase the range of structural diversity that can be accessed within the NHC ligand class (Scheme 90).[46]

**Scheme 90.** Diverse *N*-Heterocyclic Carbenes used in Regioselective Reductive Couplings

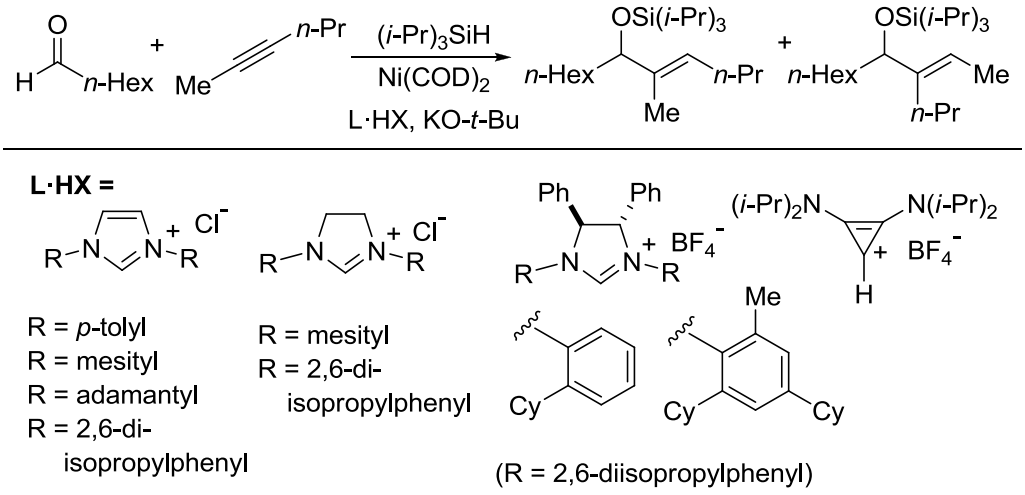


These powerful methods illustrate the synthetic utility of intermolecular silane-mediated aldehyde/alkyne couplings with NHC ligands. On this basis, we sought to carry out an initial rates study analogous to the one described in Sections 3.2.3 and 3.2.4 by examining intermolecular aldehyde/alkyne couplings using NHC ligands.

## 4.2 Results and Discussion

### 4.2.1 Preliminary Kinetic Results Using GCMS

The kinetic behavior of intermolecular nickel-catalyzed reductive couplings of aldehydes and alkynes was first studied by tracking the formation of silyl-protected allylic alcohols compared to an internal standard via GCMS (Scheme 91, Figure 14).

**Scheme 91.** Experimental Conditions for GC Analysis of Initial Rate

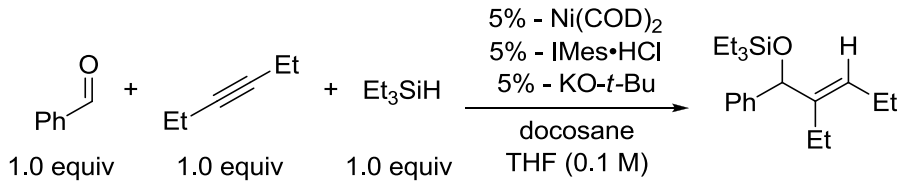


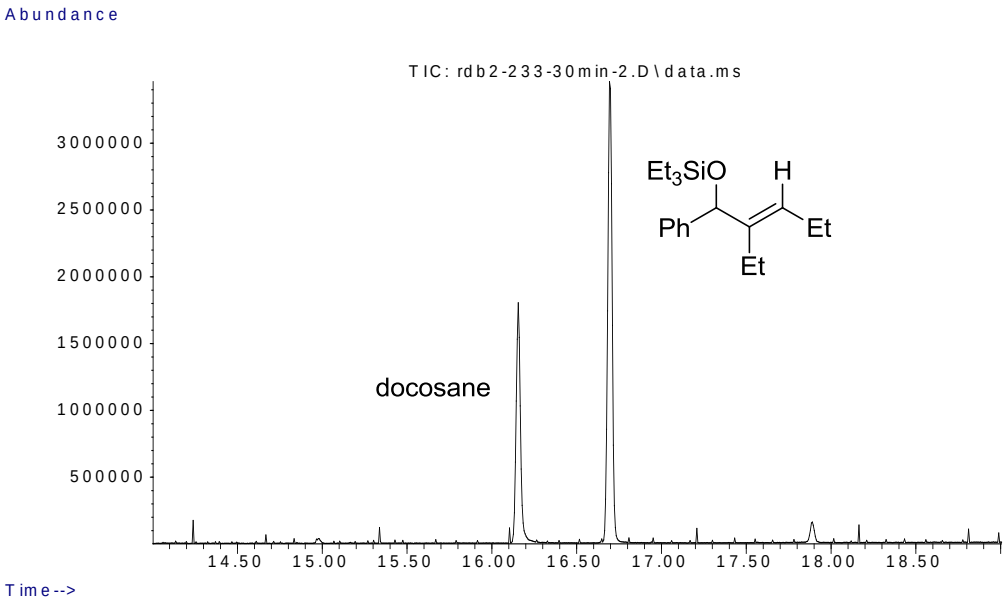


**Figure 14.** GC Trace Comparing Integrations of Coupling Product to Internal Standard

Plotting the ratio of product formation versus internal standard over the course of the reaction described in Scheme 91 yielded the reaction progression shown in Figure 15.

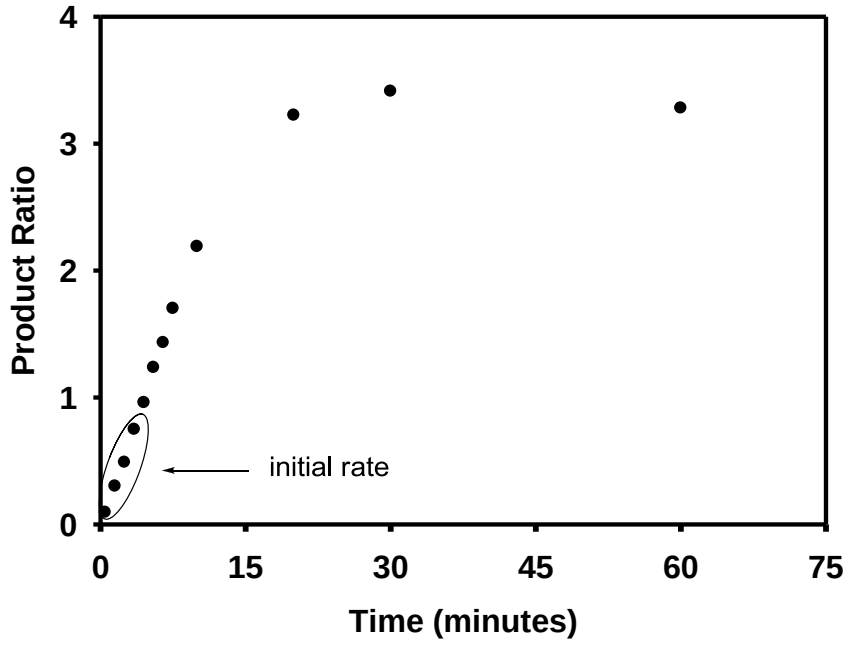


**Figure 15.** Reaction Progression as Measured by Product Ratio

An initial rate for this particular reaction was calculated by taking a line tangent to the reaction progression curve which included the first several data points. Under the conditions described in Scheme 92, [$Ni(COD)_2$] was varied between 5-15 mol% to yield the reaction progressions shown in Figure 16.

**Scheme 92.** Experimental Conditions for the Determination of Rate Dependence on [$Ni(COD)_2$] via GC Analysis

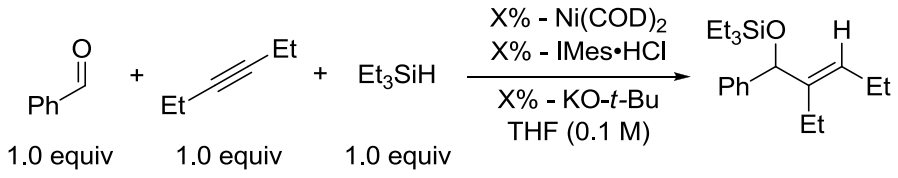

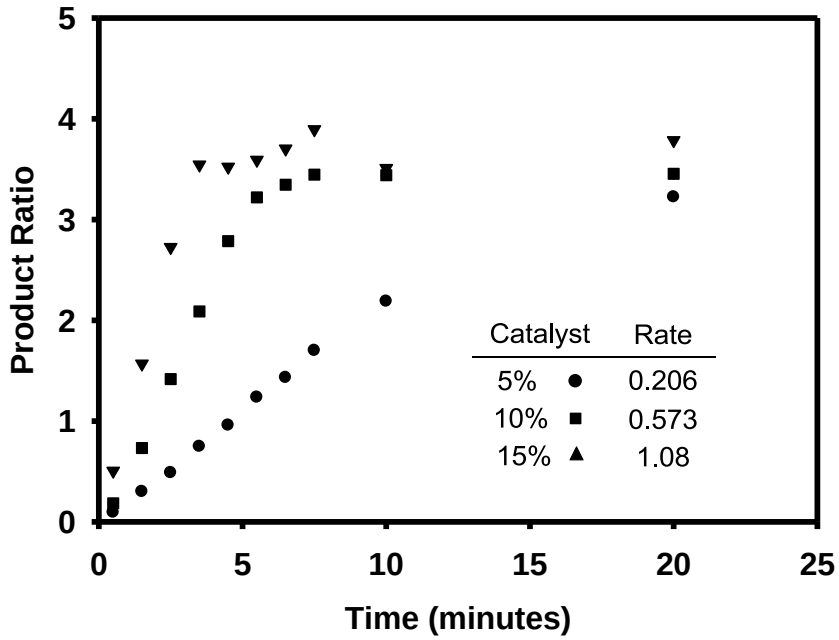


**Figure 16.** Reaction Progressions at Various [$Ni(COD)_2$]

As shown in Figure 16, changes in initial rate directly correlated to changes in [$Ni(COD)_2$], and seemed to indicate a slightly greater than first order dependence of reaction rate on catalyst concentration. However, at higher values of [$Ni(COD)_2$], reactions became too fast to accurately study using the manual sampling required for GC analysis. As illustrated in Figure 17, the difference of reaction progressions between 15% and 20% catalyst loading was negligible, and initial rates were calculated from data well past 50% reaction conversion.

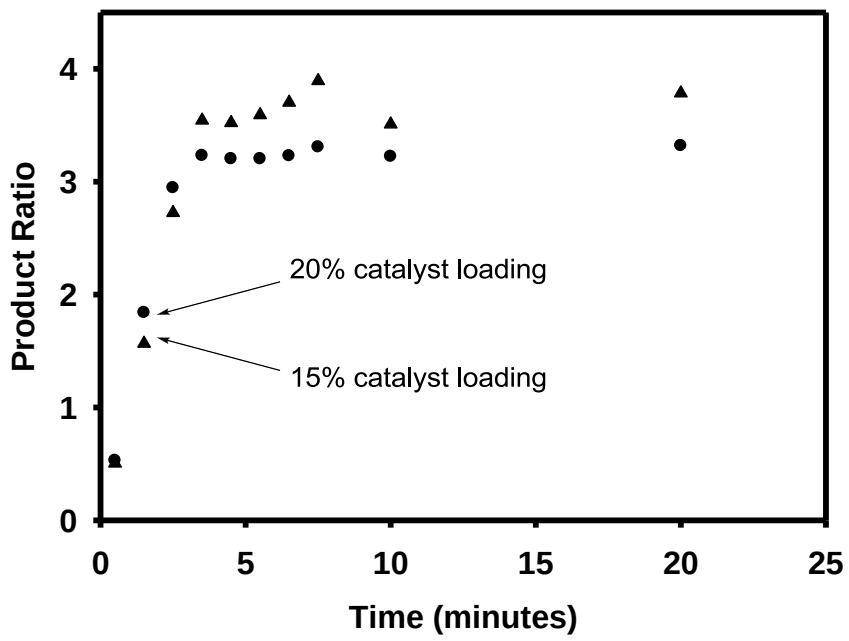


**Figure 17.** Reaction Progressions at Higher [$Ni(COD)_2$]

It was clear that lower catalyst loadings needed to be examined in order to obtain sufficient data for the comparison of initial rates. Reactions run with 2.5-5.0% catalyst were examined and an unexpected result appeared. A close look at the early stages of reaction revealed an induction period during which reactions were significantly slower than at later stages (Figure 18).

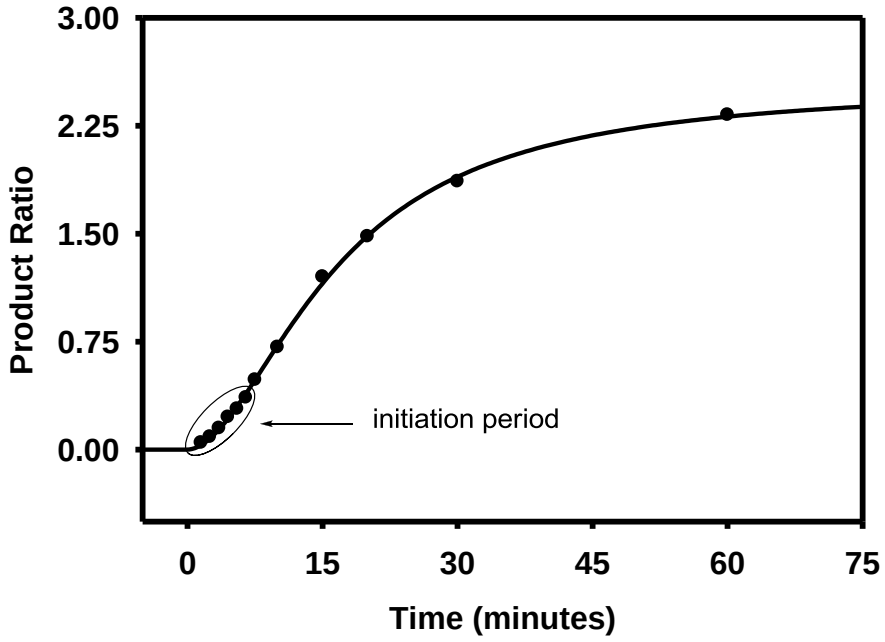


**Figure 18.** Reaction Progression at Low [$Ni(COD)_2$]

Because the length of induction periods were not consistent with varying [$Ni(COD)_2$], it was difficult to accurately compare initial rates. The origin of the induction period was not clear, but was thought to result either from poor reagent mixing due to such low catalyst concentrations, or the slow buildup of a reactive intermediate necessary at a minimum concentration for catalyst turnover. To further investigate this effect at synthetically relevant catalyst concentrations, the use of *in situ* reaction monitoring via IR was examined.

### 4.2.2 Initial Rate Study Using *In Situ* IR Monitoring

Using IR spectroscopy to monitor the reductive coupling *in situ*, reaction progression was expressed as the decreasing absorbance of the C=O stretch of benzaldehyde at 1708 $cm^{-1}$ (Scheme 93, Figure 19).

**Scheme 93.** Experimental Conditions for *In Situ* IR Analysis of Initial Rate

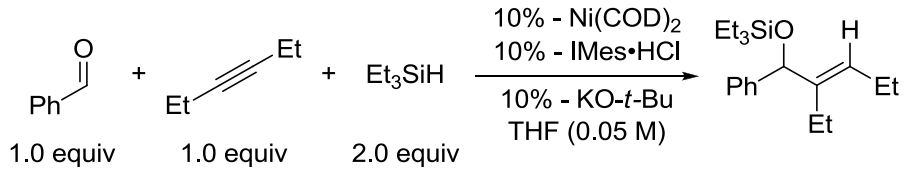


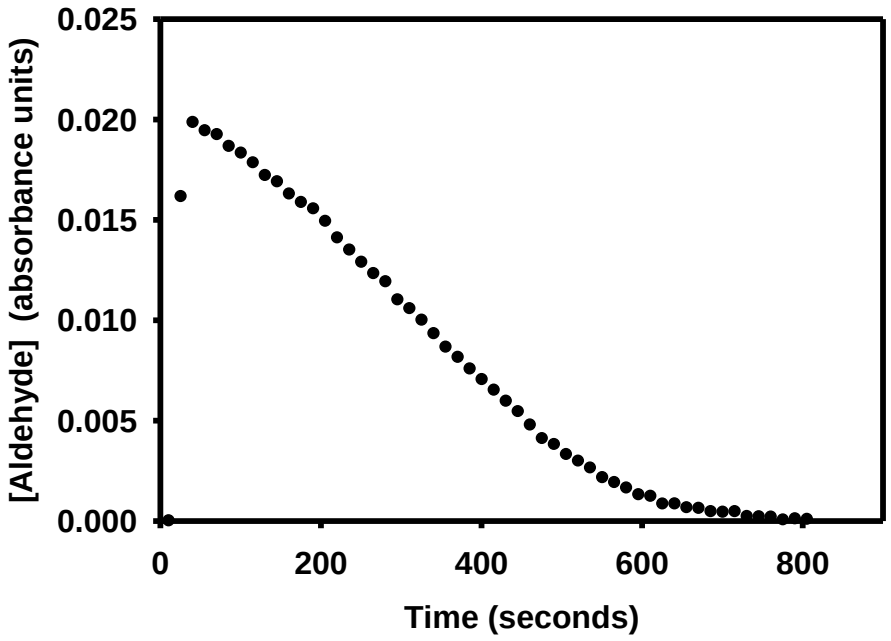


**Figure 19.** Reaction Progression as Measured by Aldehyde Absorbance

Under the conditions described in Scheme 94, the reaction rate between 0-30% conversion was shown to have a direct dependence on [$Ni(COD)_2$] between 5-20 mol% catalyst loading. However, the change in observed rates between different values of [$Ni(COD)_2$] did not follow a clear first order dependence. For example, doubling [$Ni(COD)_2$] from 5% to 10% nearly tripled the observed rate of reaction, but a less pronounced effect on reaction rate was observed when doubling the concentration again from 10-20 mol% (Figure 20).

**Scheme 94.** Experimental Conditions for the Determination of Rate Dependence on [Ni(COD)$_2$] via *In Situ* IR

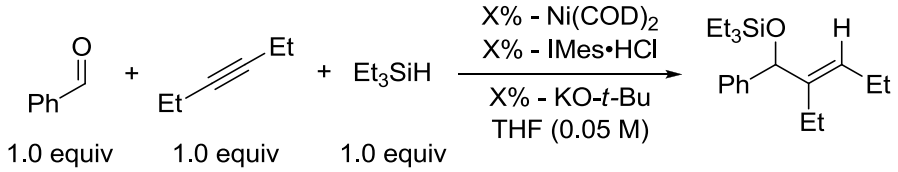


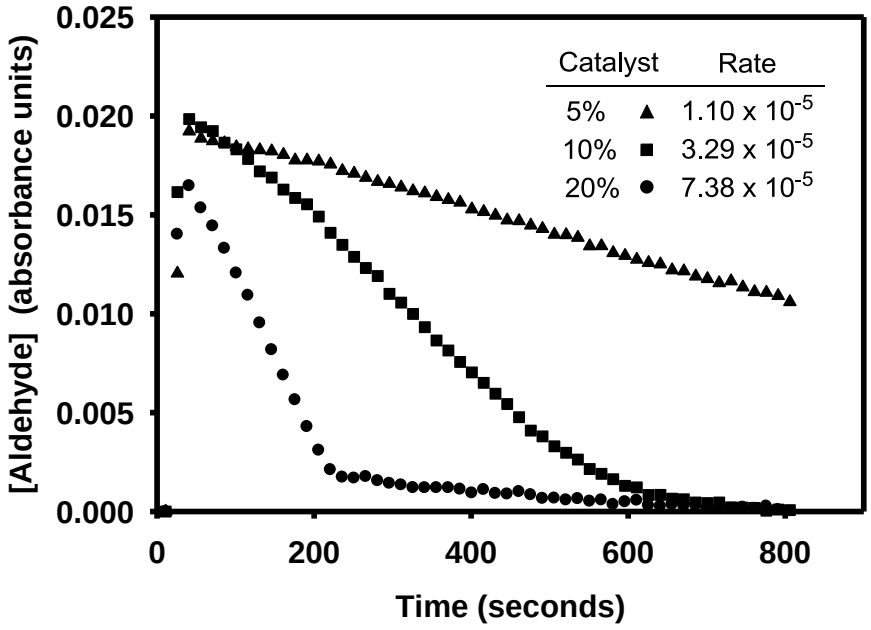


**Figure 20.** Reaction Progressions at Various Values of [Ni(COD)$_2$]

This non-linear relationship between initial rate and [Ni(COD)$_2$] may be a result from the initiation period still observed at the early stages of reaction. Illustrated in Figure 20, the induction period for a reaction using 10 mol% catalyst loading appears to continue through approximately 25% reaction conversion, at which point the rate increases to 4.09 x $10^{-5}$ between 25-50% reaction conversion (compared to 3.29 x $10^{-5}$ calculated from 0-30% conversion).

Under the conditions described in Scheme 95, no clear rate dependence on [benzaldehyde] between 1.0-4.0 equivalents was observed, although a slight inhibition of reaction rate was observed with increasing [benzaldehyde]. Interestingly, the reaction run with the highest concentration of benzaldehyde does not appear to contain a significant induction period, although the origin of this effect is not known (Figure 21).

**Scheme 95.** Experimental Conditions for the Determination of Rate Dependence on [Benzaldehyde] via *In Situ* IR

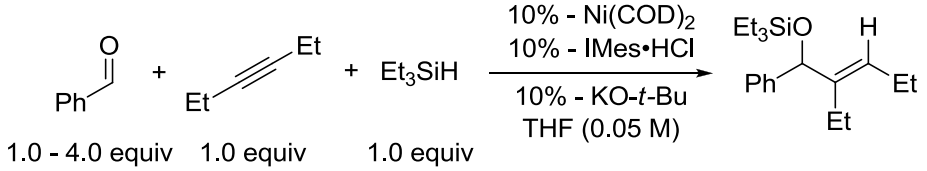


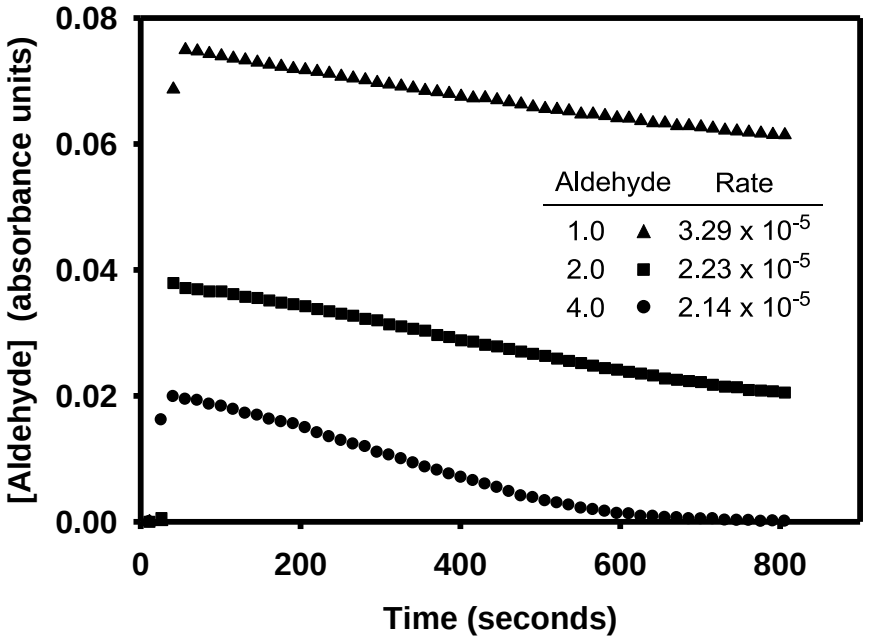


**Figure 21.** Reaction Progressions at Various Values of [Benzaldehyde]

Under the conditions described in Scheme 96, the reaction was shown to have no clear rate dependence on [3-hexyne] between 1.0-4.0 equivalents.

**Scheme 96.** Experimental Conditions for the Determination of Rate Dependence on [3-Hexyne] via *In Situ* IR

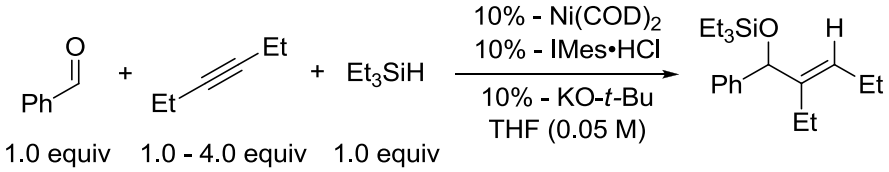


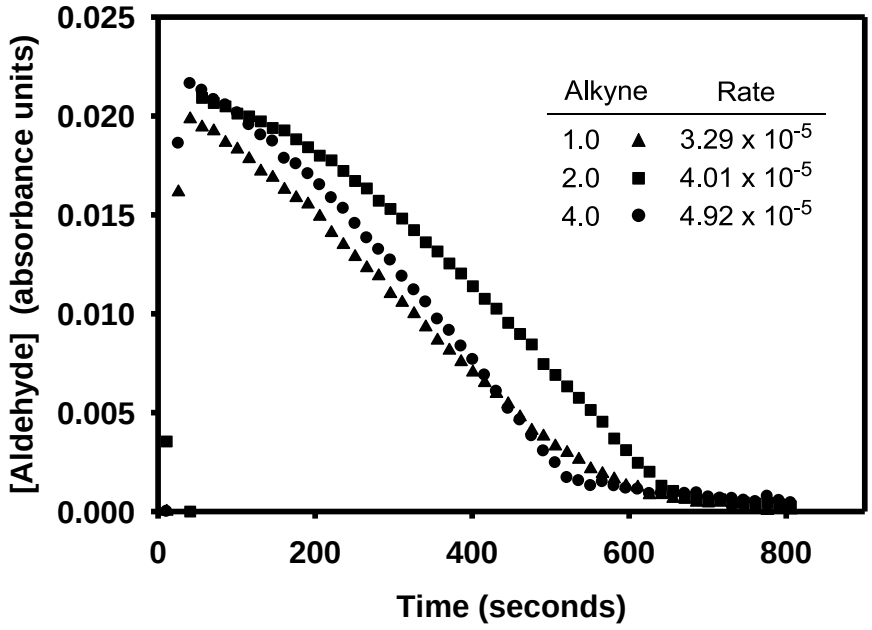


**Figure 22.** Reaction Progressions at Various Values of [3-Hexyne]

As illustrated in Figure 22, increasing [3-hexyne] appeared to affect of the significance of the induction periods observed at early stages of reaction. Although the variation of induction period made it difficult to compare initial rates in this regime, rates calculated between 0-30% reaction conversion showed that increasing [3-hexyne] increased reaction rates by a factor of 1.2 across the range of concentrations studied. These observations may be consistent with a complex network of equilibrating substrate-bound catalyst species. Based on the rate data observed with varying [benzaldehyde] and

[3-hexyne], it is likely that the large changes in reagent concentration necessary for rate study may be affecting the relative concentrations of equilibrating species contributing to the catalyst resting state.

Under the conditions described in Scheme 97, the reaction rate was shown to have a zero order dependence on [$Et_3SiH$] between 1.0-4.0 equivalents (Figure 23).

**Scheme 97.** Experimental Conditions for the Determination of Rate Dependence on [$Et_3SiH$] via *In Situ* IR

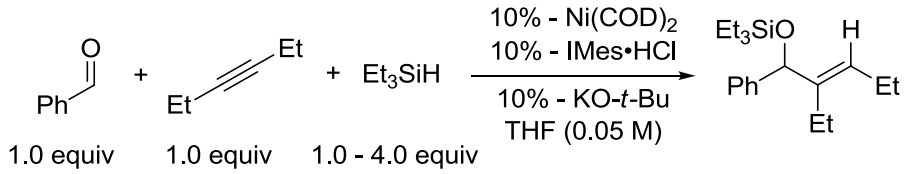


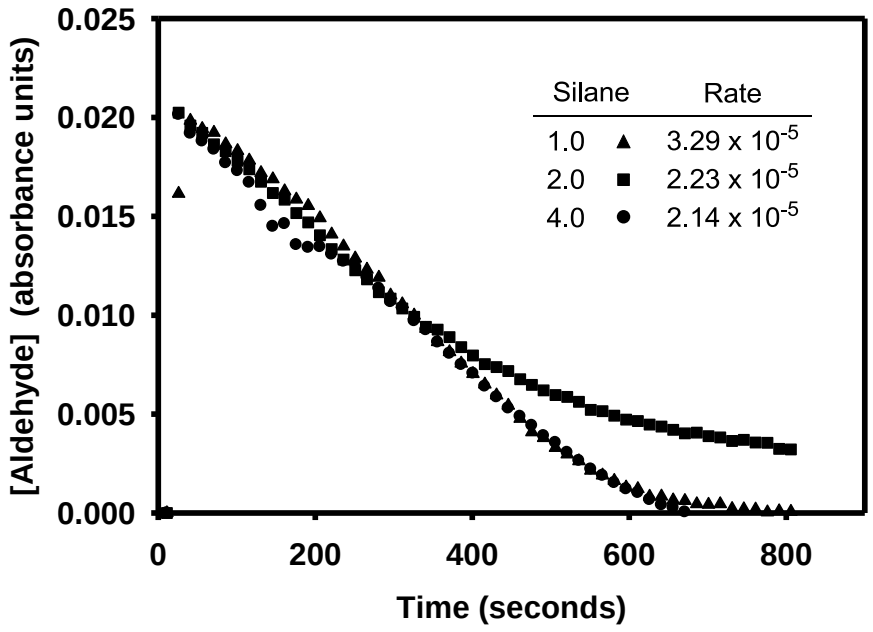


**Figure 23.** Reaction Progressions at Various Values of [$Et_3SiH$]

Similar to the observation made in the study of intramolecular silane-mediated reductive couplings with $PCy_3$, a zero-order dependence on [$Et_3SiH$] is indicative of silane participation after the turnover limiting step of the catalytic cycle.

### 4.2.3 Mechanistic Implications Kinetic and Crossover Data

Previously reported crossover results and initial rate studies described in this document support a metallacycle based mechanism in which the participation of the silane reducing agent occurs after the rate limiting step of the catalytic cycle. The direct relationship between reaction rate and [$Ni(COD)_2$] as well as the zero order rate dependence on [$Et_3SiH$] support a rate-determining oxidative cyclization to a metallacyclic intermediate followed by a rapid sequence involving $Et_3SiH$ (Scheme 98).

**Scheme 98.** Intermolecular Mechanism Consistent with Rate and Crossover Data

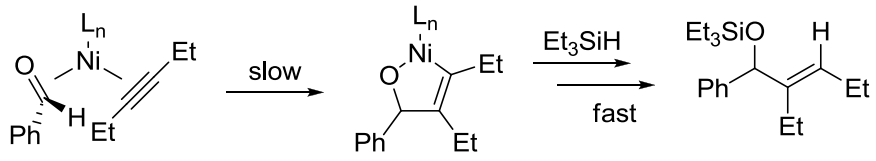


The non-integer rate dependence on [benzaldehyde] and [3-hexyne], as well as fluctuating induction periods suggest that the resting state of the catalyst may be one of several substrate-bound complexes whose relative concentrations are sensitive to fluctuations in both aldehyde and alkyne concentrations. Based on the computational work of Houk, it was proposed that catalyst resting state **51** was formed via equilibrating species **49** and **50** (Scheme 99).[49] Although transition from **51** to **52** was calculated as the pathway of minimum energy, it is easy to see that large changes in substrate

concentrations would have an effect on the relative concentrations of equilibrating species **49**, **50**, and **51** (Scheme 99).

**Scheme 99.** Equilibration of Substrate Bound Catalyst Complexes Prior to the Rate-Limiting Step

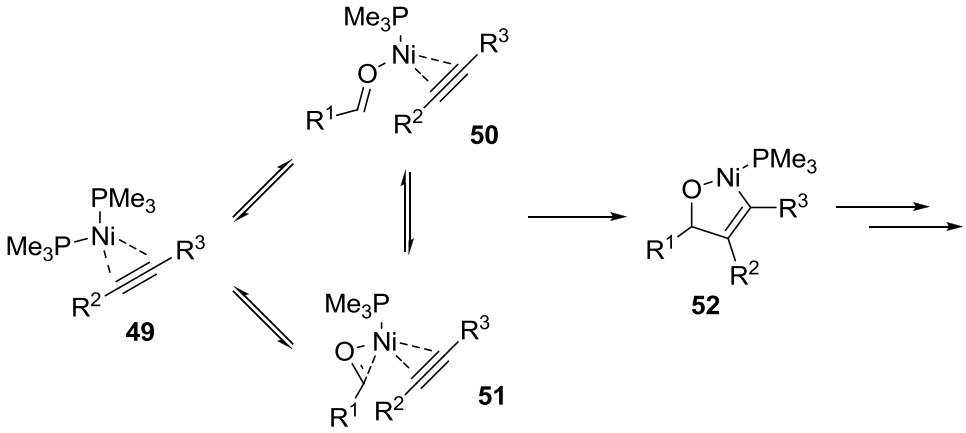


## 4.3 Summary of Mechanistic Evaluation of Intermolecular Nickel-Catalyzed Reductive Couplings of Aldehydes, Alkynes, and Trialkylsilanes

The kinetic evaluation of intermolecular nickel-catalyzed aldehyde/alkyne reductive couplings with NHC ligands was performed using both GC and *in situ* IR spectroscopy. Due to the speed of reductive coupling at room temperature, *in situ* IR is the preferred method of reaction monitoring. A comprehensive kinetic profile was not completed, but preliminary rate data support a metallacycle-based mechanism in which the participation of the silane reducing agent occurs after the rate-limiting step of the catalytic cycle. Based on the observed rate behavior with changing aldehyde and alkyne concentration, as well as fluctuating induction period effects, it is proposed that one of several potential equilibrating substrates-bound catalyst species may be implicated as the resting state of the catalytic cycle.

In order to accurately describe reaction behavior using the method of initial rates, future experimental efforts must identify catalyst/reagent interactions which lead to the observed initiation periods. Identification of the mechanism by which the initiation step occurs may lead to the development of reaction conditions by which initial rates can be accurately studied. For example, as shown in Figure 22, large excesses of aldehyde appear to eliminate an observable initiation period, suggesting that initial rates may be compared from a set of conditions which all contain large concentrations of aldehyde. However, this strategy may become problematic if consistent reaction behavior is not observed across the range of reagent and catalyst concentrations necessary for rate study. Alternatively, if initiation periods can be accurately correlated to catalyst concentration, future studies may examine the efficacy of monitoring reactions under very low catalyst loadings. If this strategy is successful, then initial rates can be compared at reaction conversions beyond the initiation period after several catalyst turnovers. For example, initial rates of reactions using 1-5 mol% catalyst loading may be compared between 15-30% reaction conversion assuming the reaction behavior and efficacy is maintained under these conditions.

# Chapter 5

# Experimental Section

## 5.1 Experimental Procedures and Spectral Data: Chapter 1

All reagents were used as received unless otherwise noted. Solvents were purified under nitrogen using a solvent purification system (Innovative Technology, inc., Model # SPS-400-3 and PS-400-3. Aldehydes were distilled prior to use. $Ni(COD)_2$ (Strem Chemicals, Inc., used as received), 1,3-Bis(2,4,6-trimethyl-phenyl)imidazolium chloride (IMes·HCl), 1,3-Bis(2,6-di-*iso*-propylphenyl)imidazolium chloride (IPr·HCl), $Al(O\text{-}i\text{-}Pr)_3$ (Sigma-Aldrich, used as received), and potassium *tert*-butoxide were stored and weighed in an inert atmosphere glovebox. All reactions were conducted in flame-dried glassware under nitrogen atmosphere. $^1H$ and $^{13}C$ spectra were obtained in $CDCl_3$ at rt (25 $^oC$), unless otherwise noted, on a Varian Mercury 400 or Varian Unity 500 MHz instrument. Chemical shifts of $^1H$ NMR spectra were recorded in parts per million (ppm) on the δ scale from an internal standard of residual chloroform (7.27 ppm). Chemical shifts of $^{13}C$ NMR spectra were recorded in ppm from the central peak of $CDCl_3$ (77.0 ppm) on the δ scale. High resolution mass spectra (HRMS) were obtained on a VG-70-250-s spectrometer manufactured by Micromass Corp. (Manchester UK) at the University of Michigan Mass Spectrometry Laboratory. Regioisomeric ratios were determined on crude reaction mixtures using NMR or GC. GC analyses were carried out

on an HP 6890 Series GC System with an HP-5MS column (30m x 0.252mm x 0.25 μm). Chiral HPLC analyses were carried out using an Agilent Technologies 1100 series instrument and chiralcel OD-H column from Chiral Technologies Inc.

### 5.1.1 General Procedure for Nickel Catalyzed Formation of Allylic Alkoxysilanes

$Ni(COD)_2$ (8.3 mg, 0.03 mmol, 0.1 equiv), 1,3-bis(2,4,6-trimethyl-phenyl)imidazolium chloride, (IMes·HCl) (10.2 mg, 0.03 mmol, 0.1 equiv), and KO-*t*-Bu (3.4 mg, 0.03 mmol, 0.1 equiv) were combined under inert atmosphere and dissolved in 2 mL of THF at rt. The aldehyde (0.3 mmol, 1.0 equiv), alkyne (0.33 mmol, 1.1 equiv) and silane (0.33 mmol, 1.1 equiv) were then added to the stirred catalyst mixture as a solution in 1 mL THF in a single portion. The progress of the reaction was monitored by TLC and GC. Upon completion, the reaction mixture was quenched with 10 mL $NaHCO_3$ (sat.) and extracted 3x each with 10 mL brine and $Et_2O$. The organic layer was dried with anhydrous $MgSO_4$, filtered, and solvent was removed by rotary evaporation. The crude reaction mixture was purified by silica gel chromatography using 98:2 Hexanes:$Et_2O$ (unless otherwise noted) and the products were isolated as colorless to pale yellow oils.

**(E)-di-tert-butyl(2-methyl-1,3-diphenylallyloxy)silane (Scheme 22, 10a)**

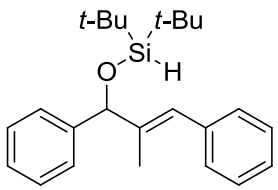


The general procedure was followed with benzaldehyde (0.032 g, 0.30 mmol), 1-phenyl-1-propyne (0.038 g, 0.33 mmol), and di-*tert*-butylsilane (0.047 g, 0.33 mmol).

Purification by column chromatography gave **10a** (0.041 g, 37%) as a 98:2 mixture of regioisomers. $^{1}$H (500 MHz, $CDCl_3$) δ 7.50-7.46 (m, 2H), 7.40-7.33 (m, 6H), 7.32-7.23 (m, 2H), 6.83 (s, 1H), 5.37 (s, 1H), 4.18 (s, 1H), 1.72 (d, *J* = 1.5 Hz, 3H), 1.11 (s, 9H), 1.00 (s, 9H); $^{13}$C (100 MHz, $CDCl_3$) δ 142.6, 139.7, 137.0, 129.0, 128.0, 127.9, 126.9, 126.3, 126.28, 126.0, 83.6, 27.3, 27.2, 20.2, 20.0, 13.4; IR (film, $cm^{-1}$) 2929, 2856, 2088, 1469, 1056; HRMS (EI) *m/z* calculated for $C_{24}H_{34}OSi$ $[M]^+$ 366.2379, found 366.2389.

**(E)-di-tert-butyl(1-cyclohexyl-2-methyl-3-phenylallyloxy)silane (Scheme 22, 10b)**

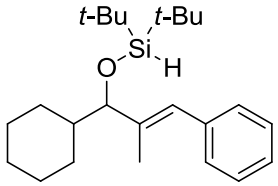


The general procedure was followed with cyclohexane carboxaldehyde (0.034 g, 0.30 mmol), 1-phenyl-1-propyne (0.038 g, 0.33 mmol), and di-*tert*-butylsilane (0.047 g, 0.33 mmol). Purification by column chromatography gave **10b** (0.028 g, 25%) as a 98:2 mixture of regioisomers. $^{1}$H (500 MHz, $CDCl_3$) δ 7.36-7.26 (m, 4H), 7.20-7.15 (m, 1H), 6.35 (s, 1H), 4.04 (s, 1H), 3.93 (d, *J* = 9 Hz, 2H), 2.04-2.00 (m, 1H), 1.78 (d, *J* = 2 Hz, 3H), 1.80-0.8 (m, 10H), 1.02 (m, 9H), 0.96 (m, 9H); $^{13}$C (100 MHz, $CDCl_3$) δ 138.4, 137.9, 128.9, 128.0, 127.4, 126.2, 85.9, 42.4, 29.7, 29.3, 27.8, 27.5, 26.6, 26.4, 26.3, 20.5, 20.2, 20.1, 13.8; IR (film, $cm^{-1}$) 2925, 2852, 2086, 1469, 1362, 1067, 824; HRMS (CI) *m/z* calculated for $C_{24}H_{22}OSi$ $[M-H]^+$ 371.2770, found 371.2755.

**(E)-(2-benzylidenecyclopentyloxy)di-tert-butylsilane (Scheme 22, 10c)**

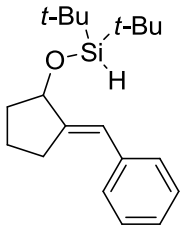


The general procedure was followed with 6-phenylhex-5-ynal (0.052 g, 0.33 mmol), and di-*tert*-butylsilane (0.047 g, 0.33 mmol). Purification by column chromatography gave **10c** (0.047 g, 49%). $^{1}$H (500 MHz, $CDCl_3$) δ 7.38-7.32 (m, 4H), 7.24-7.18 (m, 1H), 6.59 (q, *J* = 2.5 Hz, 1H), 4.66 (t, *J* = 2.5 Hz, 1H), 4.16 (s, 1H), 2.73-2.64 (m, 1H), 2.62-2.52 (m, 2H), 2.22-1.88 (m, 2H), 1.78- 1.62 (m, 2H), 1.05 (d, *J* = 0.5 Hz, 18H); $^{13}$C (125 MHz, $CDCl_3$) δ 146.7, 138.1, 128.447, 126.2, 122.8, 80.6, 34.4, 28.5, 27.41, 27.40, 21.9, 20.3, 20.0.

**2,2-di-tert-butyl-5-cyclohexyl-4-methyl-3-phenyl-2,5-dihydro-1,2-oxasilole (Scheme 25, 12)**

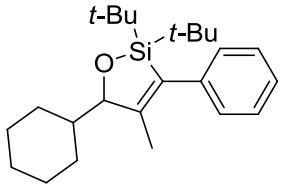


The general procedure was followed with cyclohexane carboxaldehyde (0.034 g, 0.30 mmol), 1-phenyl-1-propyne (0.038 g, 0.33 mmol), di-*tert*-butylsilane (0.047 g, 0.33 mmol), and Ti(O-*i*-Pr)$_4$ (0.128 g, 0.45 mmol) as a Lewis acidic additive. Purification by column chromatography gave **10b** (0.047 g, 42%) and **12** (0.047 g, 42%) as a 50:50 mixture. Spectral data for **12**: $^{1}$H (400 MHz, $CDCl_3$) δ 7.30-7.25 (m, 2H), 7.16-7.06 (m,

3H), 4.38 (s, 1H), (s, 9H), 1.80-1.11 (m, 10H), 1.00 (t, $J$ = 1.6 Hz, 18H); $^{13}$C (100 MHz, $CDCl_3$) δ 155.0, 141.4, 136.1, 128.3, 128.1, 125.2, 89.1, 41.9, 31.0, 28.5, 27.9, 26.9, 26.63, 26.60, 26.3, 22.9, 21.2, 14.6; IR (film, $cm^{-1}$) 2930, 2855, 2361, 1603, 1490, 1471, 1112; HRMS (EI) *m/z* calculated for $C_{24}H_{38}OSi$ $[M]^+$ 370.2692, found 370.2679.

### 5.1.2 General Procedure for Nickel Catalyzed Oxasilacyclopentene Formation

$Ni(COD)_2$ (8.3 mg, 0.03 mmol, 0.1 equiv), 1,3-bis(2,4,6-trimethyl-phenyl)imidazolium chloride, (IMes·HCl) (10.2 mg, 0.03 mmol, 0.1 equiv), and KO-*t*-Bu (3.4 mg, 0.03 mmol, 0.1 equiv) were combined under inert atmosphere and dissolved in 1 mL of THF at rt. $Al(O\text{-}i\text{-}Pr)_3$ (92 mg, 0.45 mmol, 1.5 equiv) was dissolved in 0.5 mL of toluene and was added to the stirred catalyst mixture via syringe. The aldehyde (0.3 mmol, 1.0 equiv) was added as a solution in 0.5 mL THF. The alkyne (0.33 mmol, 1.1 equiv) and silane (0.33 mmol, 1.1 equiv) were then added as a solution in 1 mL THF over 60 min via syringe-pump. The progress of the reaction was monitored by TLC and GC. Upon completion, the reaction mixture was quenched with 10 mL $NaHCO_3$ (sat.) and extracted 3x each with 10 mL brine and $Et_2O$. The organic layer was dried with anhydrous $MgSO_4$, filtered, and solvent was removed by rotary evaporation. The crude reaction mixture was purified by silica gel chromatography using 98:2 Hexanes:$Et_2O$ (unless otherwise noted) and the products were isolated as colorless to pale yellow oils.

**2,2-diethyl-4-methyl-3,5-diphenyl-2,5-dihydro-1,2-oxasilole (Table 3, 13a)**

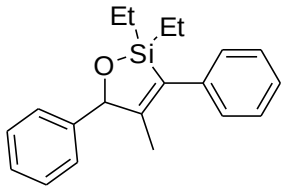

The general procedure was followed with benzaldehyde (0.032 g, 0.30 mmol), 1-phenyl-1-propyne (0.038 g, 0.33 mmol), and diethylsilane (0.030 g, 0.33 mmol). Purification by column chromatography gave **13a** (0.060 g, 65%) as a 98:2 mixture of regioisomers. $^{1}$H (500 MHz, $CDCl_3$) δ 7.40-7.28 (m, 7H), 7.24-7.20 (m, 1H), 7.16-7.12 (m, 2H), 5.54 (s, 1H), 1.61 (d, *J* = 1.0 Hz, 3H), 1.03 (t, *J* = 8.0 Hz, 3H), 1.00 (t, *J* = 9.0 Hz, 3H), 0.94-0.74 (m, 4H), diagnostic peak for minor regioisomer, 5.90 (q, *J* = 1.5 Hz); $^{13}$C (100 MHz, $CDCl_3$) δ 153.9, 142.0, 139.3, 134.8, 128.5, 128.4, 127.9, 127.8, 127.4, 125.8, 88.2, 14.8, 7.5, 7.2, 7.0, 6.5; IR (film, $cm^{-1}$) 3028, 2956, 2875, 1602, 1492, 1454; HRMS (EI) *m/z* calculated for $C_{20}H_{24}OSi$ $[M]^+$ 308.1596, found 308.159

**2,2,3,4-tetraethyl-5-phenyl-2,5-dihydro-1,2-oxasilole (Table 3, 13b)**

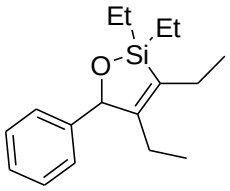


The general procedure was followed with benzaldehyde (0.032 g, 0.30 mmol), 3-hexyne (0.027 g, 0.33 mmol), and diethylsilane (0.030 g, 0.33 mmol). Purification by column chromatography gave **13b** (0.047 g, 56%). $^{1}$H (500 MHz, $CDCl_3$) δ 7.36-7.33 (m, 2H), 7.32-7.27 (m, 3H), 5.53 (s, 1H), 2.33-2.28 (m, 2H), 2.22 (dq, *J* = 15, 7.5 Hz, 1H), 1.73 (dq, *J* = 16, 8.0 Hz, 1H), 1.12 (t, *J* = 8.0 Hz, 3H), 1.07 (t, *J* = 7.5 Hz, 3H), 1.00 (t, *J* = 8.0 Hz, 3H), 0.92-0.78 (m, 6H), 0.67 (dq, *J* = 16, 7.5, 1H); $^{13}$C (125 MHz, $CDCl_3$) δ 157.2, 142.5, 134.1, 128.3, 127.7, 127.5, 86.2, 21.2, 20.8, 15.0, 13.3, 8.1, 7.6, 7.2, 6.6; IR (film, $cm^{-1}$) 2961, 2361, 2336, 1653, 1456; HRMS (EI) *m/z* calculated for $C_{17}H_{26}OSi$ $[M]^+$ 274.1753, found 274.1750.

**5-cyclohexyl-2,2-diethyl-4-methyl-3-phenyl-2,5-dihydro-1,2-oxasilole (Table 3, 13c)**

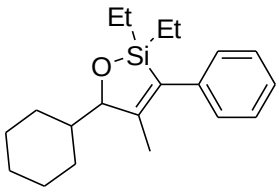


The general procedure was followed with cyclohexane carboxaldehyde (0.034 g, 0.30 mmol), 1-phenyl-1-propyne (0.038 g, 0.33 mmol), and diethylsilane (0.030 g, 0.33 mmol). Purification by column chromatography gave **13c** (0.061 g, 65%) as a 94:6 mixture of regioisomers. $^{1}$H (500 MHz, $CDCl_3$) δ 7.36-7.31 (m, 2H), 7.22-7.18 (m, 1H), 7.10-7.07 (m, 2H), 4.55 (s, 1H), 1.88-1.54 (m, 6H), 1.76 (s, 3H), 1.42-1.30 (m, 2H), 1.22-1.09 (m, 3H) 0.98 (t, *J* = 7.5 Hz, 3H), 0.95 (t, *J* = 8.0 Hz, 3H), 0.93-0.68 (m, 4H), diagnostic peak for minor regioisomer, 4.92 (quint, *J* = 2.0 Hz); $^{13}$C (100 MHz, $CDCl_3$) δ 153.6, 139.8, 135.0, 128.2, 127.8, 125.4, 89.7, 41.3, 30.9, 26.9, 26.48, 26.42, 24.6, 14.4, 7.3, 7.1, 6.9, 6.5; IR (film, $cm^{-1}$) 2929, 2874, 2361, 1450; HRMS (EI) *m/z* calculated for $C_{20}H_{30}OSi$ $[M]^+$ 314.2066, found 314.2051.

**2,2,4-triethyl-5-phenyl-3-(prop-1-en-2-yl)-2,5-dihydro-1,2-oxasilole (Table 3, 13d)**

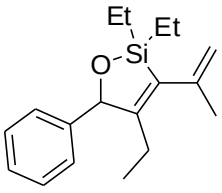


The general procedure was followed with benzaldehyde (0.032 g, 0.30 mmol), 2-methyl-1-hexen-3-yne (0.031 g, 0.33 mmol), and diethylsilane (0.030 g, 0.33 mmol). Purification by column chromatography gave **13d** (0.058 g, 69%) as a >95:5 mixture of regioisomers. $^{1}$H (500 MHz, $CDCl_3$) δ 7.38-7.28 (m, 5H), 5.6 (s, 1H), 4.93 (dq, *J* = 4.0,

1.5 Hz, 1H), 4.66 (m, 1H), 2.40 (dq, *J* = 15.0, 7.5 Hz, 1H), 1.92 (t, *J* = 1.0 Hz, 3H), 1.71 (dq, *J* = 15.0, 7.0 Hz, 1H), 1.06 (t, *J* = 8.0 Hz, 3H), 1.02 (t, *J* = 8.0 Hz, 3H), 0.89 (t, *J* = 7.5 Hz, 3H), 0.92-0.66 (m, 4H); $^{13}$C (100 MHz, $CDCl_3$) δ 158.0, 143.2, 142.1, 136.5, 128.4, 127.8, 127.4, 111.2, 86.0, 24.2, 21.7, 13.7, 7.6, 7.1, 7.0, 6.4; IR (film, $cm^{-1}$) 3076, 3028, 2959, 2874, 1631, 1593, 1453; HRMS (ESI+) *m/z* calculated for $C_{18}H_{26}OSi[M]^+$ 287.1831, found 287.1824.

**2,2-diethyl-3-hexyl-5-phenyl-2,5-dihydro-1,2-oxasilole (Table 3, 13e)**

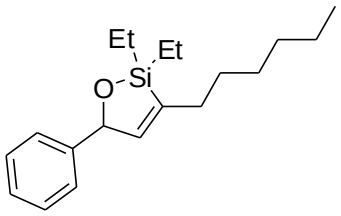


The general procedure was followed with benzaldehyde (0.032 g, 0.30 mmol), 1-octyne (0.036 g, 0.33 mmol), and diethylsilane (0.030 g, 0.33 mmol). Purification by column chromatography gave **13e** (0.058 g, 64%) as a >95:5 mixture of regioisomers. $^1$H (500 MHz, $CDCl_3$) δ 7.35-7.28 (m, 4H), 7.27-7.22 (m, 1H), 6.47 (q, 1H), 5.63 (q, *J* = 1.5 Hz, 1H), 2.25 (m, 2H), 1.50-1.41 (m, 2H), 1.36-1.24 (m, 6H), 1.01 (t, *J* = 7.6 Hz, 3H), 1.00 (t, *J* = 8.0 Hz, 3H), 0.91-0.62 (m, 4H), 0.88 (t, *J* = 6.8 Hz, 3H); $^{13}$C (100 MHz, $CDCl_3$) δ 145.3, 142.9, 140.6, 128.4, 127.4, 126.2, 83.6, 31.7, 31.5, 29.6, 29.4, 22.7, 14.1, 7.5, 7.0, 6.9, 6.6; IR (film, $cm^{-1}$) 2926, 2875, 2361, 2336, 1456; HRMS (EI) *m/z* calculated for $C_{19}H_{30}OSi[M]^+$ 302.2066, found 302.2057.

**2,2-diethyl-4-methyl-3-phenyl-5-propyl-2,5-dihydro-1,2-oxasilole (Table 3, 13f)**

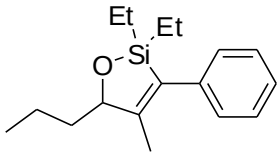


The general procedure was followed with butyraldehyde (0.022 g, 0.30 mmol), 1-phenyl-1-propyne (0.038 g, 0.33 mmol), and diethylsilane (0.030 g, 0.33 mmol). Purification by column chromatography gave **13f** (0.044 g, 53%) as a 94:6 mixture of regioisomers. $^{1}$H (400 MHz, $CDCl_3$) δ 7.27-7.21 (m, 2H), 7.23-7.07 (m, 1H), 7.01-6.96 (m, 2H), 4.56 (dd, *J* = 8.0, 3.6 Hz, 1H), 1.77-1.68 (m, 1H), 1.68 (d, *J* = 0.8 Hz, 3H), 1.50-1.30 (m, 3H), 0.89 (t, *J* = 7.2 Hz, 3H), 0.88 (t, *J* = 7.6 Hz, 3H), 0.84 (t, *J* = 8.0 Hz, 3H), 0.80-0.51 (m, 4H), diagnostic peak for minor regioisomer, 4.91 (dquint, *J* = 7.5, 1.5 Hz); $^{13}$C (125 MHz, $CDCl_3$) δ 155.1, 139.8, 133.5, 128.3, 127.9, 125.5, 85.5, 38.3, 18.2, 14.4, 14.3, 7.4, 7.2, 6.9, 6.6; IR (film, $cm^{-1}$) 3025, 2957, 1610, 1490, 1458; HRMS (EI) *m/z* calculated for $C_{17}H_{26}OSi$ $[M]^+$ 274.1753, found 274.1742.

**5-cyclohexyl-2,2,3,4-tetraethyl-2,5-dihydro-1,2-oxasilole (Table 3, 13g)**

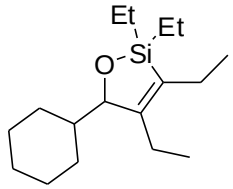


The general procedure was followed with cyclohexane carboxaldehyde (0.034 g, 0.30 mmol), 3-hexyne (0.027 g, 0.33 mmol), and diethylsilane (0.030 g, 0.33 mmol). Purification by column chromatography gave **13g** (0.048 g, 57%). $^{1}$H (500 MHz, $CDCl_3$) δ 4.50 (s, 1H), 2.34-2.15 (m, 3H), 2.00-1.90 (m, 1H), 1.84-1.08 (m, 11H), 1.06-0.94 (m,

9H), 0.89 (t, *J* = 7.0 Hz, 3H), 0.82-0.66 (m, 3H), 0.57 (dq, *J* = 15.0, 7.5 Hz, 1H); $^{13}$C (100 MHz, $CDCl_3$) δ 156.2, 134.1, 87.7, 41.0, 31.2, 27.0, 26.5, 26.4, 24.8, 21.0, 20.5, 15.0, 13.3, 8.0, 7.1, 7.0, 6.5; IR (film, $cm^{-1}$) 2958, 2925, 1600, 1450, 1232; HRMS (EI) *m/z* calculated for $C_{17}H_{32}OSi$ $[M]^+$ 280.2222, found 280.2213.

**5-cyclohexyl-2,2-diethyl-4-methyl-3-pentyl-2,5-dihydro-1,2-oxasilole (Table 3, 13h)**

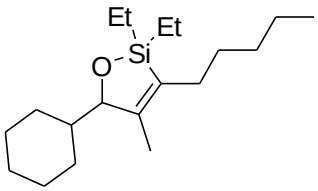


The general procedure was followed with cyclohexane carboxaldehyde (0.034 g, 0.30 mmol), 2-octyne (0.036 g, 0.33 mmol), and diethylsilane (0.030 g, 0.33 mmol). Purification by column chromatography gave **13h** (0.060 g, 65%) as a 62:38 mixture of regioisomers. $^1$H (500 MHz, $CDCl_3$) δ 4.49 (s, $1H_{minor}$), 4.37 (s, $1H_{major}$), 2.35-2.27 (m, $1H_{minor}$), 2.22-2.10 (m, $2H_{major}$), 1.94-1.86 (m, $1H_{minor}$), 1.84-1.77 (m, $1H_{major}$ + $1H_{minor}$), 1.74 (d, J = 1.5 Hz, $3H_{minor}$), 1.72-1.08 (m, $16H_{major}$ + $16H_{minor}$), 1.64 (s, $3H_{major}$), 1.06-0.99 (m, $3H_{major}$ + $3H_{minor}$), 0.94-0.86 (m, $6H_{major}$ + $6H_{minor}$), 0.81-0.54 (m, $4H_{major}$ + $4H_{minor}$); $^{13}$C (100 MHz, $CDCl_3$) δ 155.4, 150.8, 133.3, 127.6, 89.5, 88.3, 41.1, 41.0, 32.1, 31.9, 31.1, 30.9, 29.9, 28.3, 27.8, 27.2, 27.1, 27.0, 26.6, 26.57, 26.52, 26.4, 24.9, 24.6, 22.52, 22.50, 14.1, 14.0, 13.0, 12.7, 7.8, 7.03, 7.00, 6.9, 6.59, 6.55, 6.2; IR (film, $cm^{-1}$) 2925, 2852, 1608, 1450; HRMS (EI) *m/z* calculated for $C_{19}H_{36}OSi[M]^+$ 308.2535, found 308.2536.

**5-(1-(*tert*-butyldimethylsilyloxy)hexyl)-2,2-diethyl-4-methyl-3-phenyl-2,5-dihydro-1,2-oxasilole (2i Table 3, 13i)**

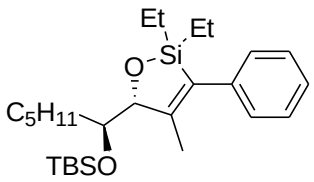


The general procedure was followed with 2-(*tert*-butyldimethylsilyloxy)heptanal (0.073g, 0.3 mmol), 1-phenyl-1-propyne (0.038 g, 0.33 mmol), and diethylsilane (0.030 g, 0.33 mmol). Purification by column chromatography gave **13i** (0.114 g, 85%) as a 73:27 mixture of diastereomers. Deprotection with TBAF (1M in THF) followed by acetonide formation showed the anti-isomer to be the major product. $^{1}$H (400 MHz, $CDCl_3$) δ 7.32-7.26 (m, $2H_{major}$ + $2H_{minor}$), 7.19-7.13 (m, $1H_{major}$ + $1H_{minor}$), 7.07-7.00 (m, $2H_{major}$ + $2H_{minor}$), 4.72 (m, $1H_{major}$), 4.60 (m, $1H_{minor}$), 3.93 (dt, *J* = 11, 3.5 Hz, $1H_{major}$), 3.89-3.85 (m, $1H_{minor}$), 1.82 (d, *J* = 1.0 Hz, $3H_{minor}$), 1.74 (d, *J* = 0.5 Hz, $3H_{major}$), 1.66-1.18 ($8H_{major}$ + $8H_{minor}$), 0.97-0.82 (m, $9H_{major}$ + $9H_{minor}$), 0.92 (s, $9H_{major}$), 0.87 (s, $9H_{minor}$), 0.81-0.63 (m, $4H_{major}$ + $4H_{minor}$), 0.12 (s, $3H_{major}$), 0.11 (s, $3H_{major}$), 0.07 (s, $3H_{minor}$), 0.06 (s, $3H_{minor}$), diagnostic peak for minor regioisomer present in less than 5%, 5.09 (dq, *J* = 2.5, 2.5 Hz); $^{13}$C (100 MHz, $CDCl_3$) δ 153.1, 152.2, 139.7, 139.6, 136.0, 135.8, 128.3, 128.2, 127.9, 127.7, 125.6, 125.5, 89.8, 87.4, 74.8, 74.6, 32.0, 31.9, 31.8, 30.4, 26.1, 25.9, 25.7, 22.7, 18.5, 18.1, 15.2, 15.0, 14.1, 14.0, 7.4, 7.37, 7.32, 7.1, 6.9, 6.8, 6.5, 6.4, -4.1, -4.11, -4.14, -4.7; IR (film, $cm^{-1}$) 2955, 2856, 1740, 1461; HRMS (ESI+) *m/z* calculated for $C_{26}H_{46}O_2Si_2$ $[M + Na]^+$ 469.2934, found 469.2922 .

**Acetonide Formation from 13i**

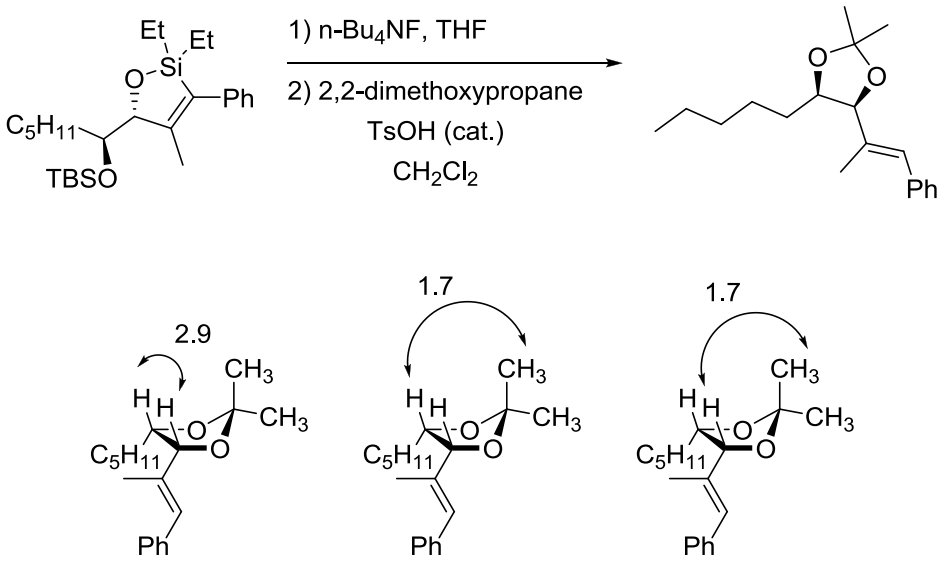


**5-cyclohexyl-2,2-diethyl-3-methyl-4-pentyl-2,5-dihydro-1,2-oxasilole (13j)**

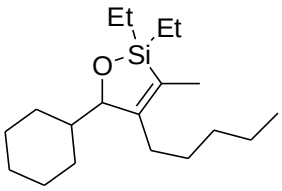


The general procedure was followed with cyclohexane carboxaldehyde (0.056 g, 0.50 mmol), 2-octyne (0.061 g, 0.55 mmol), and diethylsilane (0.049 g, 0.55 mmol). IPr·HCl (0.021 g, 0.05 mmol) was used as the ligand in place of IMes·HCl and required 20 minutes of stirring before adding Al(O-*i*-Pr)$_3$. Purification by column chromatography gave **13j** (0.058 g, 38%) as an 88:12 mixture of regioisomers. Further purification gave **13j** as a single regioisomer. **13j**$_{major}$: $^1$H (500 MHz, $CDCl_3$) δ 4.48 (s, 1H), 2.35-2.26 (m, 1H), 1.94-1.87 (m, 1H), 1.83-1.76 (m, 1H), 1.74-1.68 (m, 1H), 1.72 (dd, *J* = 2.0, 0.5 Hz, 3H), 1.67-1.60 (m, 2H), 1.56-1.09 (m, 13H), 1.00 (t, *J* = 8.0 Hz, 3H), 0.92-0.85 (m, 6H), 0.76-0.65 (m, 4H); $^{13}$C (100 MHz, $CDCl_3$) δ 155.4, 127.5, 88.2, 41.0, 31.8, 31.1, 27.7,

27.1, 27.0, 26.5, 26.3, 24.8, 22.4, 14.0, 12.6, 7.0, 6.9, 6.5, 6.1; IR (film, $cm^{-1}$) 2926, 2852, 1608, 1450, 1107; HRMS (ESI+) *m/z* calculated for $C_{19}H_{36}OSi$ $[M+H]^+$ 309.2614, found 309.2605.

**Scheme 29. Regioselectivity of Aldehyde, Alkyne, Silane Couplings**

The general procedure was followed for all reactions involving IMes·HCl. Reactions involving IPr·HCl were stirred for 20 minutes prior to adding $Al(O\text{-}i\text{-}Pr)_3$. Regiochemical comparisons were made by NMR on crude reaction mixtures after filtering through a short plug of silica gel.

**(*E*)-(1-cyclohexyl-2-methyloct-2-enyloxy)triethylsilane (Scheme 29, 15a)**

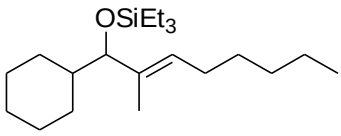


The general procedure was followed with cyclohexane carboxaldehyde (0.028 g, 0.25 mmol), 2-octyne (0.031 g, 0.28 mmol), and triethylsilane (0.033 g, 0.28 mmol). Purification by column chromatography (100% Hexanes) afforded pure **15a** and **15b** (0.064 g, 76% combined in a 63:37 ratio of **15a:15b**). **15a** major: $^1$H (500 MHz, Tol-$d_8$) δ 5.28 (t, *J* = 7.0 Hz, 1H), 3.62 (d, *J* = 8.5 Hz, 1H), 2.26-2.19 (m, 1H), 2.11-2.07 (m, 1H), 2.04-1.94 (m, 2H), 1.83-1.76 (m, 1H), 1.74-1.6 (m, 1H), 1.66-1.62 (m, 1H) 1.61 (s, 3H), 1.53-1.44 (m, 2H), 1.40-1.10 (m, 8H), 1.04 (t, *J* = 6.0 Hz, 9H), 1.01-0.93 (m, 1H), 0.91 (t, *J* = 6.0 Hz, 3H), 0.87-0.76 (m, 1H), 0.65 (q, *J* = 8.0 Hz, 6H); $^{13}$C (100 MHz, Tol-$d_8$) δ 136.9, 127.5, 84.5, 41.9, 32.1, 30.4, 30.0, 29.7, 27.8, 27.1, 26.7, 26.6, 23.0, 14.3, 11.3,

7.3, 5.4; IR (film, $cm^{-1}$) 2952, 2921, 1449, 1237, 1054; HRMS (EI) *m/z* calculated for $C_{21}H_{42}OSi$ $[M]^+$ 338.3005, found 338.3006.

**(E)-(1-cyclohexyl-2-ethylideneheptyloxy)triethylsilane (15b)**

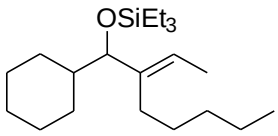


The general procedure was followed with cyclohexane carboxaldehyde (0.028 g, 0.25 mmol), 2-octyne (0.031 g, 0.28 mmol), and triethylsilane (0.033 g, 0.28 mmol). IPr·HCl (0.011 g, 0.025 mmol) was used as the ligand in place of IMes·HCl and required 20 minutes of stirring before adding $Al(O\text{-}i\text{-}Pr)_3$. Purification by column chromatography (100% Hexanes) afforded pure **15b** and **15a** (0.049 g, 58% combined in a 90:10 ratio). **15b**$_{major}$: $^1H$ (500 MHz, Tol-$d_8$) δ 5.37 (q, *J* = 6.5 Hz, 1H), 3.70 (d, *J* = 7.5 Hz, 1H), 2.16-2.02 (m, 4H), 1.83-1.76 (m, 1H), 1.75-1.69 (m, 1H), 1.68-1.62 (m, 1H), 1.62-1.56 (m, 1H), 1.60 (d, *J* = 7.0 Hz, 3H), 1.54-1.10 (m, 10H), 1.04 (t, *J* = 8.0 Hz, 9H), 1.00-0.94 (m, 1H), 0.91 (t, *J* = 6.0 Hz, 3H), 0.65 (q, *J* = 8.0 Hz, 6H); $^{13}C$ (100 MHz, Tol-$d_8$) δ 141.7, 121.3, 83.2, 42.0, 32.8, 30.4, 29.3, 29.1, 27.1, 26.8, 26.4, 22.6, 14.0, 12.8, 7.0, 5.1; IR (film, $cm^{-1}$) 2952, 2927, 1450, 1237; HRMS (EI) *m/z* calculated for $C_{21}H_{42}OSi$ $[M]^+$ 338.3005, found 338.3019.

**Observation of $H_2$ via sealed-tube NMR experiment**

To avoid the requirement of syringe-pumping reagents, di-*tert*-butylsilane was used as the reducing agent in the coupling of benzaldehyde and 1-phenyl-propyne. $Ni(COD)_2$ (5.5 mg, 0.02 mmol, 0.05 equiv), 1,3-bis(2,4,6-trimethyl-phenyl)imidazolium

chloride (IMes·HCl) (6.8 mg, 0.02 mmol, 0.05 equiv), and KO-*t*-Bu (2.2 mg, 0.02 mmol, 0.05 equiv) were combined in an inert atmosphere and dissolved in 1.0 mL of toluene-$d_8$ at rt. The catalyst mixture was transferred via syringe to an NMR-tube sealed by a screw-cap fitted with a septum. Al(O-*i*-Pr)$_3$ (92 mg, 0.45 mmol, 1.13 equiv) was dissolved in 0.5 mL of toluene-$d_8$ and added to the catalyst mixture via syringe. Benzaldehyde (0.042 g, 0.40 mmol), 1-phenyl-1-propyne (0.046 g, 0.40 mmol), and di-*tert*-butylsilane (0.058 g, 0.40 mmol) were added to the reaction mixture in a single portion as a solution in 0.5 mL of toluene-$d_8$. The reaction was agitated by inverting the NMR-tube several times before acquiring spectra. The chemical shift of $H_2$ (4.5 ppm in toluene-$d_8$) was identified by bubbling $H_2$ gas through a blank sample of toluene-$d_8$. The stacked plot below shows the presence of $H_2$(g) upon completion of the reaction (60 minutes). Bubbling $N_2$(g) through the reaction vessel purges $H_2$(g) from the mixture as evidenced by the disappearance of the diagnostic peak at 4.5 ppm. The peak can be made to reappear upon bubbling $H_2$(g) through the reaction vessel.

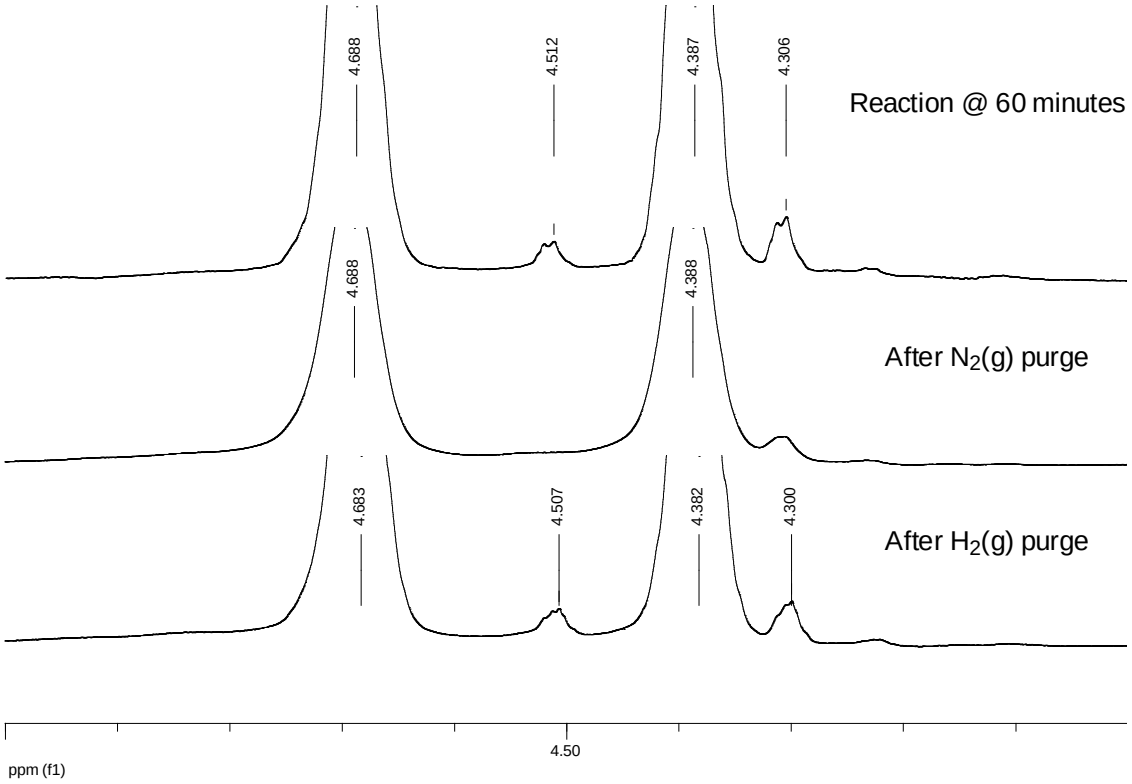


The following two compounds were prepared and isolated by a separate procedure to verify the identity of products arising from the coupling of benzaldehyde, 1-phenyl-1-propyne, and di-*tert*-butylsilane during a sealed-tube NMR experiment.

**(*E*)-di-*tert*-butyl(2-methyl-1,3-diphenylallyloxy)silane**

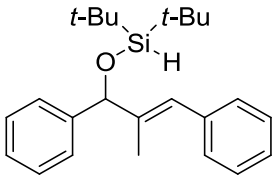


$Ni(COD)_2$ (13.8 mg, 0.05 mmol, 0.1 equiv), IMes·HCl (17.1 mg, 0.05 mmol, 0.1 equiv), and KO-*t*-Bu (5.6 mg, 0.05 mmol, 0.1 equiv) were combined in an inert atmosphere and dissolved in 3.0 mL of THF at rt. $Al(O\text{-}i\text{-}Pr)_3$ (0.152 g, 0.75 mmol, 1.5 equiv) was dissolved in 0.8 mL of toluene and added to the catalyst mixture via syringe.

Di-*tert*-butylsilane (0.079 g, 0.55 mmol), benzaldehyde (0.053 g, 0.50 mmol) and 1-phenyl-1-propyne (0.064 g, 0.55 mmol) were added as a solution in 1.2 mL THF. The reaction was stirred for one hour before being judged complete by TLC analysis. The mixture was quenched with 5 mL $NaHCO_3$ (sat.) and extracted 3x each with 5 mL brine and $Et_2O$. The organic layer was dried with anhydrous $MgSO_4$, filtered, and the solvent was removed by rotary evaporation. Column chromatography (100% Hex) yielded the acyclic (0.056 g, 33%) and cyclic products (0.021 g, 12%) as colorless oils. Spectral data for the acyclic silane: $^1$H (500 MHz, $CDCl_3$) δ 7.50-7.46 (m, 2H), 7.40-7.33 (m, 6H), 7.32-7.23 (m, 2H), 6.83 (s, 1H), 5.37 (s, 1H), 4.18 (s, 1H), 1.72 (d, *J* = 1.5 Hz, 3H), 1.11 (s, 9H), 1.00 (s, 9H); $^{13}$C (100 MHz, $CDCl_3$) δ 142.6, 139.7, 137.0, 129.0, 128.0, 127.9, 126.9, 126.3, 126.28, 126.0, 83.6, 27.3, 27.2, 20.2, 20.0, 13.4; IR (film, $cm^{-1}$) 2929, 2856, 2088, 1469, 1056; HRMS (EI) *m/z* calculated for $C_{24}H_{34}OSi$ $[M]^+$ 366.2379, found 366.2389.

**2,2-di-tert-butyl-4-methyl-3,5-diphenyl-2,5-dihydro-1,2-oxasilole**

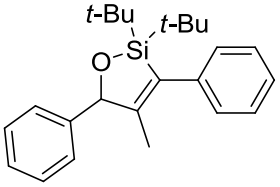


Spectral data for the cyclic silane: $^1$H (400 MHz, $CDCl_3$) δ 7.46-7.30 (m, 7H), 7.26-7.20 (m, 3H), 5.52 (s, 1H), 1.54 (s, 3H), 1.12 (s, 9H), 1.11(s, 9H); $^{13}$C (100 MHz, $CDCl_3$) δ 154.6, 141.7, 141.0, 136.3, 128.5, 128.3, 128.26, 128.24, 128.0, 125.6, 88.2, 28.4, 28.0, 22.7, 21.1, 15.1; IR (film, $cm^{-1}$); 2932, 2855, 1471, 1044; HRMS (EI) *m/z* calculated for $C_{24}H_{32}OSi$ $[M]^+$ 364.2222, found 364.2214.

**Procedure for the asymmetric production of 13c**

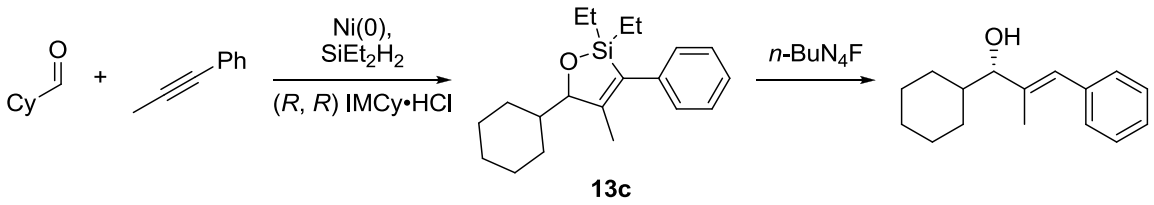


**13c**

$Ni(COD)_2$ (8.3 mg, 0.03 mmol, 0.1 equiv), (*R,R*) IMCy·HCl, (24.6 mg, 0.03 mmol, 0.1 equiv), and KO-*t*-Bu (3.4 mg, 0.03 mmol, 0.1 equiv) were combined in an inert atmosphere and dissolved in 1.0 mL of THF at rt. $Al(O\text{-}i\text{-}Pr)_3$ (92 mg, 0.45 mmol, 1.5 equiv) was dissolved in 0.5 mL of toluene and added to the catalyst mixture via syringe. Cyclohexane carboxaldehyde (0.034 g, 0.30 mmol) was added to the stirred solution before beginning a 60 min. syringe-pump addition of 1-phenyl-1-propyne (0.038 g, 0.33 mmol) and diethylsilane (0.030 g, 0.33 mmol) in 1.5 mL THF. The reaction was quenched with 5 mL $NaHCO_3$ (sat.) and extracted 3x each with 5 mL brine and $Et_2O$. The organic layer was dried with anhydrous $MgSO_4$, filtered, and the solvent was removed by rotary evaporation. Column chromatography (98:2 Hex:$Et_2O$) gave **13c** (0.052 g, 55%) as a colorless oil. Chiral HPLC analysis was performed on the allylic alcohol resulting from *n*-$BuN_4F$ (1M soln. in THF, 1.7 mL, 10 equiv) deprotection of **13c**. Compound 13c was formed in 56% enantiomeric excess as the (*S*) enantiomer. Absolute configuration was assigned based on comparison to the same allylic alcohol resulting from coupling with triethylsilane.[29]

## Chiral HPLC Traces from Asymmetric Preparation of 13c

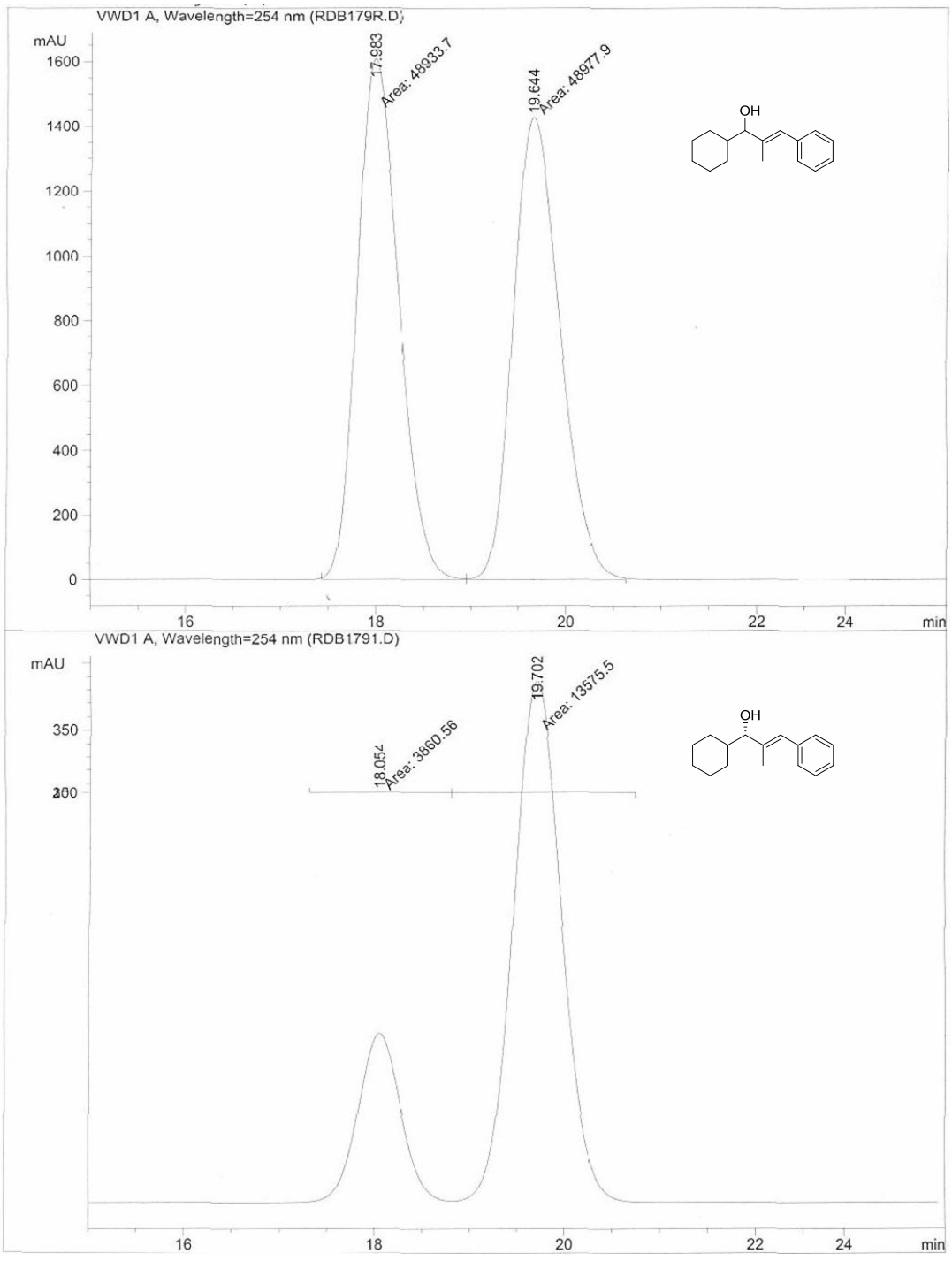

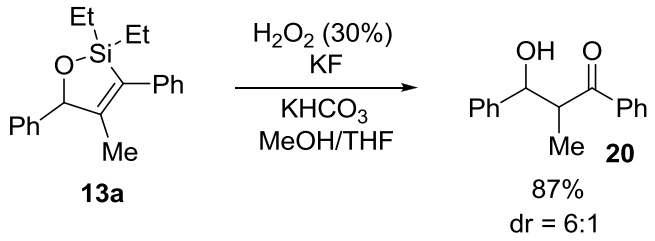


Silacycle **13a** (62 mg, 0.20 mmol), was dissolved in 1.7 ml MeOH and 0.85 ml THF. Solid KF (58 mg, 1.0 mmol) was added to the stirred reaction mixture. Solid $KHCO_3$ (100 mg, 1.0 mmol) was added to the stirred reaction mixture. Hydrogen peroxide (1.7 ml of a 30% by weight solution, 15 mmol) was added to the stirred reaction mixture via a gas-tight syringe; the reaction was allowed to stir for 12 hours. Solid $Na_2S_2O_3$ was added portionwise to the stirred reaction mixture (CAUTION: highly exothermic, induction period prior to exotherm). The crude reaction mixture was diluted with $Et_2O$, washed with NaCl (sat.) and extracted with $Et_2O$ before drying with $MgSO_4$. The crude material was purifed via column chromatography using 20% EtOAc in Hexanes to yield desired product **20** (42 mg, 87%). Spectral data were identical to previous reports.[53]

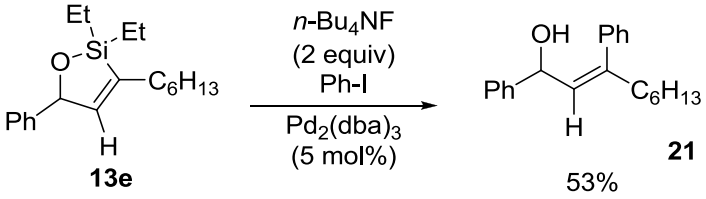


Silacycle **13e** (192 mg, 0.64 mmol) was dissolved in 1.16 ml *n*-$Bu_4NF$ (1 mol/L in THF) and stirred for 2 minutes at room temperature. Iodobenzene (30 mg, 0.15 mmol) and $Pd_2(dba)_3$ (14 mg, 0.015 mmol) were added to the stirred reaction mixture. After 3 hours, an additional portion of iodobenzene (30 mg, 0.15 mmol) and $Pd_2(dba)_3$ (14 mg,

0.015 mmol) were added to the stirred reaction mixture. This procedure was repeated two additional times (four total reagent additions, each with a 3 hour stirring period between additions). After all reagents have been added, the reaction was stirred for an additional 24 hours. The crude reaction mixture was filtered through a short plug of silica gel (70:30 Hex:EtOAc) before being purified via column chromatography using 20% EtOAc in Hexanes to yield desired allylic alcohol **21** (91.2 mg, 53%). $^{1}$H (500 MHz, $CDCl_3$) δ 7.45-7.20 (m, 10H), 5.72 (dd, *J* = 9, 0.5 Hz, 1H), 5.15 (d, *J* = 9.5, 1H), 2.38 (t, *J* = 7.5 Hz, 2H), 1.77 (s, 1H), 1.40-1.20 (m, 6H), 0.86 (t, *J* = 7.0 Hz, 3H); $^{13}$C (100 MHz, $CDCl_3$) δ 144.5, 143.9, 140.3, 128.45, 128.43, 127.3, 127.0, 126.0, 71.2, 39.2, 31.6, 29.7, 28.8, 27.7, 22.5, 14.0; IR (film, $cm^{-1}$); 3380, 3026, 2925, 1599, 1492, 1453, 1376; HRMS (ESI+) *m/z* calculated for $C_{21}H_{26}O$ $[M+Na]^+$ 317.1881, found 317.1877.

## 5.2 Experimental Procedures and Spectral Data: Chapter 2

All reagents were used as received unless otherwise noted. Solvents were purified under nitrogen using a solvent purification system (Innovative Technology, inc., Model # SPS-400-3 and PS-400-3). Aldehydes were distilled prior to use; ynals were prepared and purified (by column chromatography) immediately before use. $Ni(COD)_2$ (Strem Chemicals, Inc., used as received) and tricyclohexyl phosphine were stored and weighed in an inert atmosphere glovebox. All reactions were conducted in flame-dried glassware under nitrogen atmosphere. Microwave reactions were carried out using a Biotage Initiator™ model 2.0. $^{1}$H and $^{13}$C spectra were obtained in $CDCl_3$ at rt (22 $^{o}$C), unless otherwise noted, on a Varian Mercury 400 or Varian Unity 500 MHz instrument. Chemical shifts of $^{1}$H NMR spectra were recorded in parts per million (ppm) on the δ scale from an internal standard of residual chloroform (7.27 ppm). Chemical shifts of $^{13}$C

NMR spectra were recorded in ppm from the central peak of $CDCl_3$ (77.0 ppm) on the δ scale. High resolution mass spectra (HRMS) were obtained on a VG-70-250-s spectrometer manufactured by Micromass Corp. (Manchester UK) at the University of Michigan Mass Spectrometry Laboratory. Gas chromatographs were acquired on an HP 6890 Series GC System with an HP-5MS column (30m x 0.252mm x 0.25 μm) attached to a an HP 5973N Series Mass Selective Detector. For GC analysis, aliquots of crude reactions were quenched by filtering through a short plug of silica gel. Product ratios were determined by comparing substrate integration to a known amount of docosane ($C_{22}H_{46}$) as an internal standard.

### 5.2.1 General Procedure for Intramolecular Hydroacylation of Alkynes with Ni(COD)/$PCy_3$ Under Thermal Conditions

$Ni(COD)_2$ (7.0 mg, 0.025 mmol, 0.1 equiv) and tricyclohexylphosphine (14.0 mg, 0.05 mmol, 0.2 equiv) were combined under inert atmosphere. The catalyst mixture was solvated in 2ml of THF and stirred until completely dissolved before being immersed in an oil bath heated to 45 $^oC$. The ynal substrate (0.25 mmol) was dissolved in 3ml THF and added to the reaction over 60 minutes via syringe-drive. The progress of the reaction was monitored by TLC and GC. After 18 hours, the reaction mixture was quenched with 10 mL $NaHCO_3$ (sat.) and extracted 3x each with 10 mL brine and $Et_2O$. The organic layer was dried with anhydrous $MgSO_4$, filtered, and solvent was removed by rotary evaporation. The crude reaction mixture was purified via a short plug of silica gel using 100% Hexanes (unless otherwise noted) and the product was isolated as colorless to pale yellow oil.

**(E)-2-benzylidenecyclopentanone (Scheme 47, 30)**

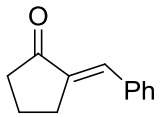


The general procedure was followed with 6-phenylhex-5-ynal (0.040 g, 0.25 mmol). Purification by column chromatography gave **30** (0.028 g, 63%). Spectral data is identical to previous reports.[54]

**(E)-2-benzylidenecycloheptanone (Scheme 48, 34)**

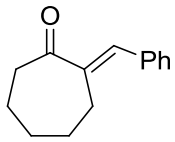


The general procedure was followed with 8-phenyloct-7-ynal (0.050 g, 0.25 mmol). Purification by column chromatography gave **34** (0.010 g, 20%). Spectral data is identical to previous reports.[54]

**(E)-2-(4-methoxybenzylidene)cyclopentanone (Scheme 53, 37)**

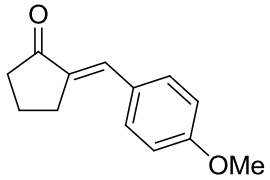


The general procedure was followed with 6-(4-methoxyphenyl)hex-5-ynal (0.0X0 g, 0.25 mmol). Purification by column chromatography gave **37** (0.030 g, 64%). Spectral data is identical to previous reports.[55]

### 5.2.2 General Procedure for Intermolecular Hydroacylation of Alkynes with Ni(COD)/$PCy_3$ Under Microwave Conditions

$Ni(COD)_2$ (7.0 mg, 0.025 mmol, 0.1 equiv) and tricyclohexylphosphine (14.0 mg, 0.05 mmol, 0.2 equiv) were combined under inert atmosphere in a 5ml microwave reaction vial equipped with a small teflon-coated stir bar. The catalyst mixture was solvated in 2ml of THF and stirred until completely dissolved. The aldehyde (0.25 mmol, 1.0 equiv) and alkyne (0.38 mmol, 1.5 equiv) were combined in 2ml THF and added to the reaction vessel in one portion via syringe. The reaction vessel was then placed into the microwave reactor and heated to 100-150 $^{o}$C for 15 minutes. Upon cooling, the reaction vessel was removed from the microwave reactor and the reaction mixture was filtered through a short plug of silica gel. This crude mixture was purified by silica gel chromatography using a gradient from 100:0 to 95:5 Hexanes:EtOAc (unless otherwise noted) and the products were isolated as colorless to pale yellow oils.

**(E)-2-methyl-1-phenylnon-1-en-3-one (Scheme 50)**

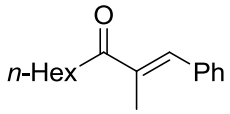


The general procedure was followed with heptanal (29 mg, 0.25 mmol, 1.0 equiv) and phenyl propyne (44 mg, 0.38 mmol, 1.5 equiv). Purification by column chromatography gave the desired product (0.030 g, 53%). Spectral data is identical to previous reports.[56]

**(E)-1-phenyl-2-propylhex-2-en-1-one (Scheme 52, 35a)**

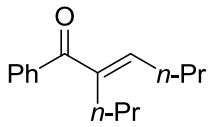


The general procedure was followed with benzaldehyde (27 mg, 0.25 mmol, 1.0 equiv) and 4-octyne (44 mg, 0.38 mmol, 1.5 equiv). Purification by column chromatography gave **35a** (0.041 g, 76%). Spectral data is identical to previous reports.[39]

**(E)-2-methyl-1-phenyloct-2-en-1-one (Scheme 52, 35b)**

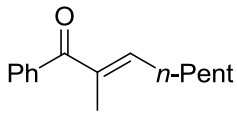


The general procedure was followed with benzaldehyde (27 mg, 0.25 mmol, 1.0 equiv) and 2-octyne (44 mg, 0.38 mmol, 1.5 equiv). Purification by column chromatography gave **35b** (0.017 g, 47%). Spectral data is identical to previous reports.[57]

**(E)-2-ethyl-1-phenylpent-2-en-1-one (Scheme 52, 35c)**

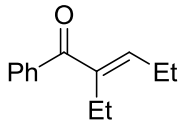


The general procedure was followed with benzaldehyde (27 mg, 0.25 mmol, 1.0 equiv) and 3-hexyne (42 mg, 0.38 mmol, 1.5 equiv). Purification by column chromatography gave **35c** (0.027 g, 57%).[58]

**(E)-2-methyl-1-phenylhex-2-en-1-one (Scheme 52, 35d)**

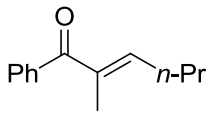


The general procedure was followed with benzaldehyde (27 mg, 0.25 mmol, 1.0 equiv) and 2-hexyne (42 mg, 0.38 mmol, 1.5 equiv). Purification by column chromatography gave **35d** (0.015 g, 31%). Spectral data is identical to previous reports.[59]

**(E)-5-propyldodec-4-en-6-one (Scheme 52, 35g)**

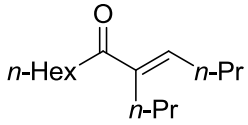


The general procedure was followed with heptanal (29 mg, 0.25 mmol, 1.0 equiv) and 4-octyne (44 mg, 0.38 mmol, 1.5 equiv). Purification by column chromatography gave **35g** (0.019 g, 54%). $^1$H (500 MHz, $CDCl_3$) δ 6.50 (t, *J* = 7.5 Hz, 1H), 2.55 (t, *J* = 7.5 Hz, 2H), 2.35 (dt, *J* = 7.5, 2.0 Hz, 2H), 2.2-2.1 (m, 4H), 1.82 (q, *J* = 7.5 Hz, 4H), 1.30-1.20 (m, 6H), 1.19 (t, *J* = 7.5 Hz, 3H), 0.9 (t, *J* = 7.5 Hz, 3H), 0.8 (t, *J* = 7.5 Hz, 3H).

### 5.2.3 Intramolecular Crossover Under Thermal Conditions

Using the general procedure for intramolecular hydroacylation, ynals **36** (0.25 mmol, 0.5 equiv) and **37** (0.25 mmol, 0.5 equiv) were combined and heated to 45 $^{o}$C for 12 hours. Upon completion of the reaction, the crude mixture was quenched with 10 ml of a saturated $NaHCO_3$ solution. The organic layer was extracted with EtOAc, washed with a saturated NaCl solution, dried with anhydrous $MgSO_4$, filtered, and solvent was

removed by rotary evaporation. The crude reaction mixture was purified by silica gel chromatography using 95:5 Hexanes:EtOAc to yield the products as separate isotopic mixtures. The relative percentage of hydrogen incorporation at the product alkene position was determined by comparing the integration of peaks at 7.19 and 2.12 ppm for the phenyl compound (in $CDCl_3$), and peaks at 7.28 and 2.57 ppm for the para-methoxy phenyl compound (in Toluene-$d_8$).

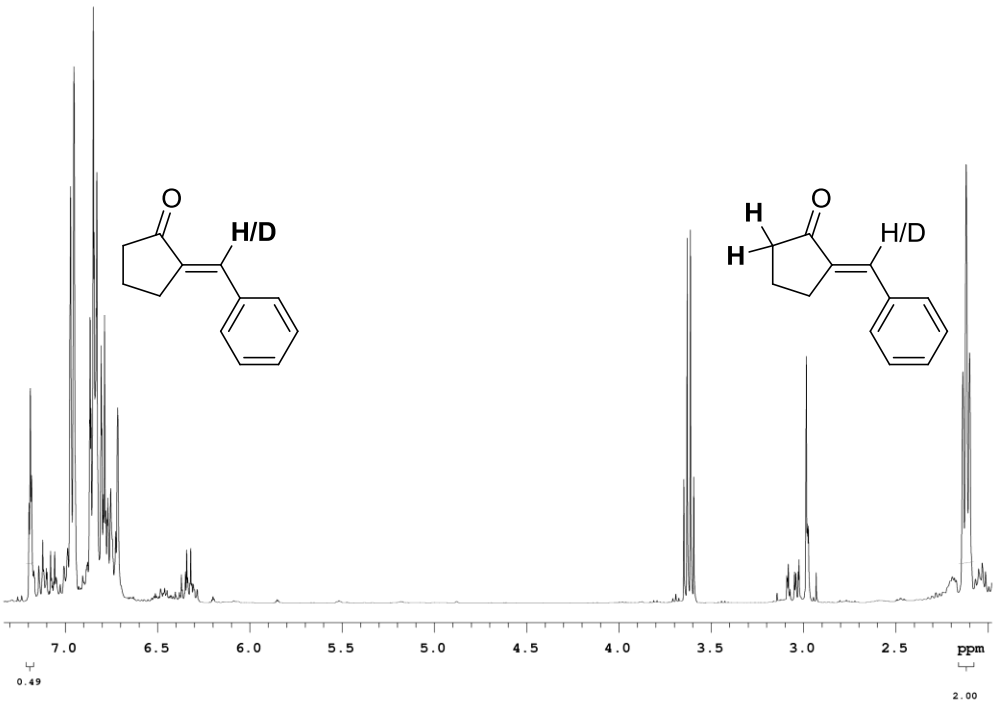

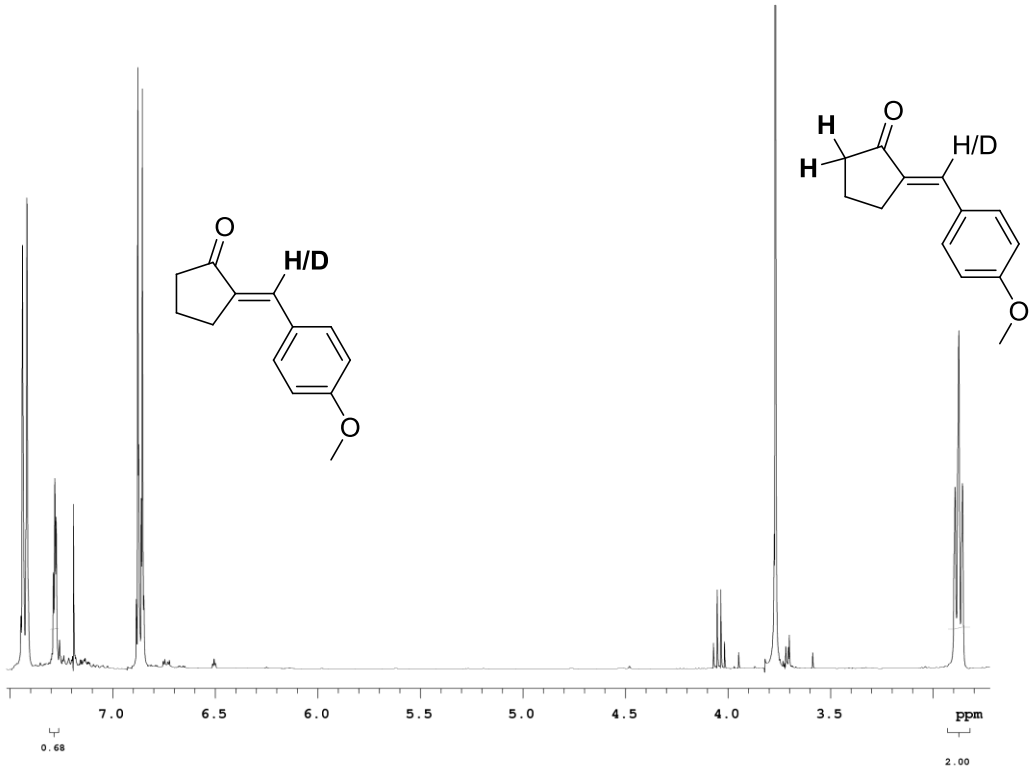


### 5.2.4 DFT Calculations of Dimeric Metallacycles

Calculations were performed on Gaussian 03 and 09 via remote computer clusters owned by the Center for Advanced Computing at the University of Michigan - Ann Arbor. Molecular geometries of optimized structures were visualized using Gaussview 4.1.2 software. All of the geometry optimizations and frequency calculations were performed with the B3LYP functional implemented in Gaussian 03 (Frisch, M. J.; et al. *Gaussian 03*, revision D.01; Gaussian, Inc.: Pittsburgh, PA, 2004). The LANL2DZ basis set was used for nickel and the 6-31G(d) basis set for the other atoms.

**Structure 38 (Monomer)**

Zero-point correction= 0.325333
(Hartree/Particle)
Thermal correction to Energy= 0.345442
Thermal correction to Enthalpy= 0.346386
Thermal correction to Gibbs Free Energy= 0.275686
Sum of electronic and zero-point Energies= -1169.784485
Sum of electronic and thermal Energies= -1169.764376
Sum of electronic and thermal Enthalpies= -1169.763432
Sum of electronic and thermal Free Energies= -1169.834132

| Center Number | Atomic Number | Atomic Type | Coordinates (Angstroms) X | Y | Z |
|---|---|---|---|---|---|
| 1 | 28 | 0 | 0.004509 | -1.486449 | -0.162218 |
| 2 | 8 | 0 | 1.650924 | -2.159139 | -0.257465 |
| 3 | 6 | 0 | 0.768465 | 0.222298 | 0.128078 |
| 4 | 6 | 0 | 2.088229 | 0.085990 | 0.368748 |
| 5 | 6 | 0 | 2.637147 | -1.305374 | 0.265879 |
| 6 | 1 | 0 | 2.961265 | -1.674845 | 1.259656 |
| 7 | 6 | 0 | 3.219088 | 1.100668 | 0.388777 |
| 8 | 1 | 0 | 3.034685 | 1.905337 | -0.333278 |
| 9 | 1 | 0 | 3.350220 | 1.583730 | 1.365659 |
| 10 | 6 | 0 | 4.469502 | 0.243227 | 0.004313 |
| 11 | 1 | 0 | 5.137214 | 0.766486 | -0.688074 |
| 12 | 1 | 0 | 5.056229 | 0.021854 | 0.904723 |
| 13 | 6 | 0 | 0.040309 | 1.494038 | 0.003264 |
| 14 | 6 | 0 | -0.560474 | 1.874906 | -1.213811 |
| 15 | 6 | 0 | -0.062203 | 2.382302 | 1.092954 |
| 16 | 6 | 0 | -1.228402 | 3.093330 | -1.337916 |
| 17 | 1 | 0 | -0.476977 | 1.205479 | -2.066305 |
| 18 | 6 | 0 | -0.731389 | 3.601160 | 0.969027 |
| 19 | 1 | 0 | 0.394330 | 2.103694 | 2.038869 |
| 20 | 6 | 0 | -1.320297 | 3.961269 | -0.245408 |
| 21 | 1 | 0 | -1.670065 | 3.371940 | -2.291779 |
| 22 | 1 | 0 | -0.792523 | 4.271244 | 1.823156 |
| 23 | 1 | 0 | -1.841693 | 4.909871 | -0.341695 |
| 24 | 6 | 0 | 3.902841 | -1.070417 | -0.585065 |
| 25 | 1 | 0 | 4.615315 | -1.901919 | -0.550835 |
| 26 | 1 | 0 | 3.592269 | -0.929346 | -1.628353 |
| 27 | 15 | 0 | -2.222573 | -1.212575 | 0.093379 |
| 28 | 6 | 0 | -2.742293 | -0.266870 | 1.589799 |
| 29 | 1 | 0 | -3.832823 | -0.253758 | 1.695461 |
| 30 | 1 | 0 | -2.299008 | -0.726567 | 2.478506 |
| 31 | 1 | 0 | -2.369904 | 0.758643 | 1.516610 |
| 32 | 6 | 0 | -3.014191 | -2.868382 | 0.363884 |
| 33 | 1 | 0 | -2.538852 | -3.370634 | 1.212340 |
| 34 | 1 | 0 | -4.087379 | -2.771551 | 0.563452 |
| 35 | 1 | 0 | -2.875883 | -3.495435 | -0.523135 |
| 36 | 6 | 0 | -3.281236 | -0.491960 | -1.240128 |
| 37 | 1 | 0 | -2.990355 | 0.548518 | -1.407560 |
| 38 | 1 | 0 | -3.129274 | -1.046718 | -2.171478 |
| 39 | 1 | 0 | -4.342420 | -0.530841 | -0.969169 |

**Structure 39 (Dimer)**

Zero-point correction= 0.653265
(Hartree/Particle)
Thermal correction to Energy= 0.694594
Thermal correction to Enthalpy= 0.695538
Thermal correction to Gibbs Free Energy= 0.577426
Sum of electronic and zero-point Energies= -2339.642382
Sum of electronic and thermal Energies= -2339.601053
Sum of electronic and thermal Enthalpies= -2339.600109
Sum of electronic and thermal Free Energies= -2339.718221

| Center Number | Atomic Number | Atomic Type | Coordinates (Angstroms) X | Y | Z |
|---|---|---|---|---|---|
| 1 | 8 | 0 | 0.298846 | -1.191823 | 0.295417 |
| 2 | 6 | 0 | 2.881047 | -0.907106 | -0.079909 |
| 3 | 6 | 0 | 2.429630 | -2.177302 | -0.028926 |
| 4 | 6 | 0 | 0.980524 | -2.416706 | 0.314788 |
| 5 | 1 | 0 | 0.898910 | -2.884094 | 1.316719 |
| 6 | 6 | 0 | 3.032356 | -3.464496 | -0.580376 |
| 7 | 1 | 0 | 3.561228 | -3.270128 | -1.521333 |
| 8 | 1 | 0 | 3.766878 | -3.920550 | 0.095689 |
| 9 | 6 | 0 | 1.803903 | -4.401370 | -0.788527 |
| 10 | 1 | 0 | 1.863786 | -4.974953 | -1.719444 |
| 11 | 1 | 0 | 1.746629 | -5.130633 | 0.029885 |
| 12 | 6 | 0 | 4.212613 | -0.596607 | -0.645024 |
| 13 | 6 | 0 | 4.333512 | 0.248468 | -1.766829 |
| 14 | 6 | 0 | 5.397529 | -1.152228 | -0.121953 |
| 15 | 6 | 0 | 5.576364 | 0.522688 | -2.339551 |
| 16 | 1 | 0 | 3.429373 | 0.674047 | -2.195852 |
| 17 | 6 | 0 | 6.642919 | -0.872754 | -0.688096 |
| 18 | 1 | 0 | 5.330866 | -1.807171 | 0.742991 |
| 19 | 6 | 0 | 6.739945 | -0.032487 | -1.799482 |
| 20 | 1 | 0 | 5.636402 | 1.166663 | -3.214011 |
| 21 | 1 | 0 | 7.539749 | -1.315312 | -0.260747 |
| 22 | 1 | 0 | 7.708625 | 0.183557 | -2.242323 |
| 23 | 6 | 0 | 0.576032 | -3.468141 | -0.740399 |
| 24 | 1 | 0 | -0.352603 | -4.002501 | -0.505575 |
| 25 | 1 | 0 | 0.437170 | -2.949813 | -1.697736 |
| 26 | 15 | 0 | 2.747838 | 1.996732 | 1.066468 |
| 27 | 28 | 0 | 1.458966 | 0.323476 | 0.330788 |
| 28 | 8 | 0 | -0.298803 | 1.191779 | 0.295134 |
| 29 | 28 | 0 | -1.458939 | -0.323500 | 0.330796 |
| 30 | 6 | 0 | -2.881034 | 0.907096 | -0.079842 |
| 31 | 6 | 0 | -2.429602 | 2.177288 | -0.028900 |
| 32 | 6 | 0 | -4.212655 | 0.596625 | -0.644849 |
| 33 | 6 | 0 | -5.397517 | 1.152238 | -0.121649 |
| 34 | 6 | 0 | -4.333661 | -0.248396 | -1.766681 |
| 35 | 6 | 0 | -6.642961 | 0.872802 | -0.687694 |
| 36 | 1 | 0 | -5.330769 | 1.807144 | 0.743316 |
| 37 | 6 | 0 | -5.576568 | -0.522579 | -2.339305 |
| 38 | 1 | 0 | -3.429565 | -0.673963 | -2.195808 |
| 39 | 6 | 0 | -6.740094 | 0.032584 | -1.799107 |
| 40 | 1 | 0 | -7.539748 | 1.315352 | -0.260247 |
| 41 | 1 | 0 | -5.636689 | -1.166514 | -3.213789 |
| 42 | 1 | 0 | -7.708816 | -0.183429 | -2.241873 |

| | | | | | |
|---|---|---|---|---|---|
| 43 | 6 | 0 | -1.803944 | 4.401409 | -0.788399 |
| 44 | 1 | 0 | -1.863880 | 4.975083 | -1.719255 |
| 45 | 1 | 0 | -1.746649 | 5.130592 | 0.030083 |
| 46 | 6 | 0 | -3.032368 | 3.464492 | -0.580282 |
| 47 | 1 | 0 | -3.561234 | 3.270153 | -1.521249 |
| 48 | 1 | 0 | -3.766904 | 3.920493 | 0.095802 |
| 49 | 15 | 0 | -2.747778 | -1.996766 | 1.066530 |
| 50 | 6 | 0 | -0.576055 | 3.468197 | -0.740417 |
| 51 | 1 | 0 | 0.352585 | 4.002553 | -0.505603 |
| 52 | 1 | 0 | -0.437241 | 2.949949 | -1.697804 |
| 53 | 6 | 0 | -0.980468 | 2.416668 | 0.314705 |
| 54 | 1 | 0 | -0.898764 | 2.883951 | 1.316676 |
| 55 | 6 | 0 | 4.220489 | 1.493022 | 2.060036 |
| 56 | 1 | 0 | 4.715188 | 2.372749 | 2.487555 |
| 57 | 1 | 0 | 3.896475 | 0.833311 | 2.870955 |
| 58 | 1 | 0 | 4.929341 | 0.945516 | 1.436434 |
| 59 | 6 | 0 | 1.856758 | 3.047716 | 2.301891 |
| 60 | 1 | 0 | 1.429837 | 2.408742 | 3.080954 |
| 61 | 1 | 0 | 2.542238 | 3.767889 | 2.763177 |
| 62 | 1 | 0 | 1.038572 | 3.588465 | 1.823334 |
| 63 | 6 | 0 | 3.454806 | 3.257237 | -0.087328 |
| 64 | 1 | 0 | 4.152930 | 2.768417 | -0.772111 |
| 65 | 1 | 0 | 2.650332 | 3.708610 | -0.675148 |
| 66 | 1 | 0 | 3.982061 | 4.043020 | 0.465549 |
| 67 | 6 | 0 | -1.856651 | -3.047792 | 2.301882 |
| 68 | 1 | 0 | -1.038470 | -3.588506 | 1.823280 |
| 69 | 1 | 0 | -1.429721 | -2.408846 | 3.080961 |
| 70 | 1 | 0 | -2.542110 | -3.767996 | 2.763152 |
| 71 | 6 | 0 | -4.220394 | -1.493102 | 2.060173 |
| 72 | 1 | 0 | -4.715076 | -2.372852 | 2.487666 |
| 73 | 1 | 0 | -3.896353 | -0.833434 | 2.871116 |
| 74 | 1 | 0 | -4.929268 | -0.945567 | 1.436624 |
| 75 | 6 | 0 | -3.454789 | -3.257216 | -0.087300 |
| 76 | 1 | 0 | -4.152934 | -2.768355 | -0.772033 |
| 77 | 1 | 0 | -2.650341 | -3.708566 | -0.675170 |
| 78 | 1 | 0 | -3.982031 | -4.043021 | 0.465558 |

## 5.3 Experimental Procedures and Spectral Data: Chapter 3

All reagents were used as received unless otherwise noted. Solvents were purified under nitrogen using a solvent purification system (Innovative Technology, inc., Model # SPS-400-3 and PS-400-3). Ynal **29** was prepared from the corresponding alcohol using standard PCC oxidation conditions, filtered through a short plug of layered silica/alumina/celite, and purified via column chromatography (80:20 Hexanes:EtOAc) immediately before each use. Nickel cyclooctadiene ($Ni(COD)_2$, Strem Chemicals, Inc),

tricyclohexyl phosphine ($PCy_3$, Aldrich), 1,3-Bis(2,4,6-trimethyl-phenyl)imidazolium chloride (IMes·HCl), 1,3-Bis(2,6-di-*iso*-propylphenyl)imidazolium chloride (IPr·HCl), $Al(O\text{-}i\text{-}Pr)_3$ (Sigma-Aldrich, used as received), and potassium *tert*-butoxide were stored and weighed in an inert atmosphere glovebox. Triethylsilane (Aldrich) was passed over a plug of basic alumina and stored under an inert atmosphere. Triethylsilane-d (Aldrich) was stored under an inert atmosphere and used as received. All reactions were conducted in flame-dried glassware under a nitrogen atmosphere. NMR spectra were obtained in $CDCl_3$ at room temperature (22 $^oC$), unless otherwise noted, on a Varian Inova 400MHz, or Unity 500 MHz instrument. Chemical shifts of $^1H$ NMR spectra were recorded in parts per million (ppm) on the δ scale from an internal standard of tetramethylsilane (TMS, 0.0 ppm). *In situ* FTIR rate data were acquired on a Mettler-Toledo React-IR$^{TM}$ 45m module fitted with a 9.5mm diamond-tipped probe; silane monitoring experiments were performed using a 9.5mm silicon-composite probe.

### 5.3.1 Ligand Dependent Crossover and KIE Experiments (Scheme 71)

**Crossover Experiment: Determination of Isotopic Distribution of Products From Couplings Using $Et_3SiD/Pr_3SiH$**

Pure samples of products derived from $Et_3SiH$, $Et_3SiD$, and $Pr_3SiH$ were independently prepared, and GCMS analysis was performed. For substrates examined in previous crossover studies, spectral data of all compounds were identical to our previous report.[1] Based on the similarity of the molecular ion regions of the $Et_3SiH$ and $Et_3SiD$-derived products, the molecular ion region of the $Pr_3SiD$-derived product was assumed to appear as the molecular ion region of the $Pr_3SiH$-derived product, shifted by one mass unit. Relative peak heights in the molecular ion region of the spectra of each pure

compound were normalized, with a value of 1 assigned to the base peak. In the crude product of an experiment that employed one equivalent each of $Et_3SiD$ and $Pr_3SiH$, the ratio of $Et_3Si$ products to $Pr_3Si$ products was determined by GC and verified by NMR integration. From the GCMS of the crude sample, the relative intensity of the 289 and 330 peaks were normalized, with a value of 1 assigned to the base peak. The ratio of the $Et_3Si$-(H) product to the $Et_3Si$-(D) product was determined as follows:

$$\frac{\text{intensity of 288 peak in crossover experiment}}{\text{intensity of 289 peak in crossover experiment}} = \frac{[X] \times [\text{rel height of 288 peak in pure } Et_3Si\text{-(H) product}] + [Y] \times [\text{rel height of 288 peak in pure } Et_3Si\text{-(D) product}]}{[X] \times [\text{rel height of 289 peak in pure } Et_3Si\text{-(H) product}] + [Y] \times [\text{rel height of 289 peak in pure } Et_3Si\text{-(D) product}]}$$

X = 1/100 x relative % of $Et_3Si$-(H) product
Y = 1/100 x relative % of $Et_3Si$-(D) product = 1 - X

In the above equation, after substitution of [1 – X] for [Y], the experimental values were inserted and the equation was solved for [X]. The ratio of the $Pr_3Si$-(H) product to the $Pr_3Si$-(D) product was determined in a similar fashion.

**Crossover with a $Ni(COD)_2$/IMes Catalyst System**

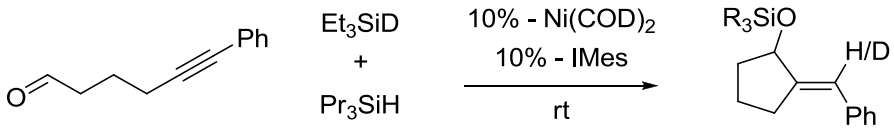


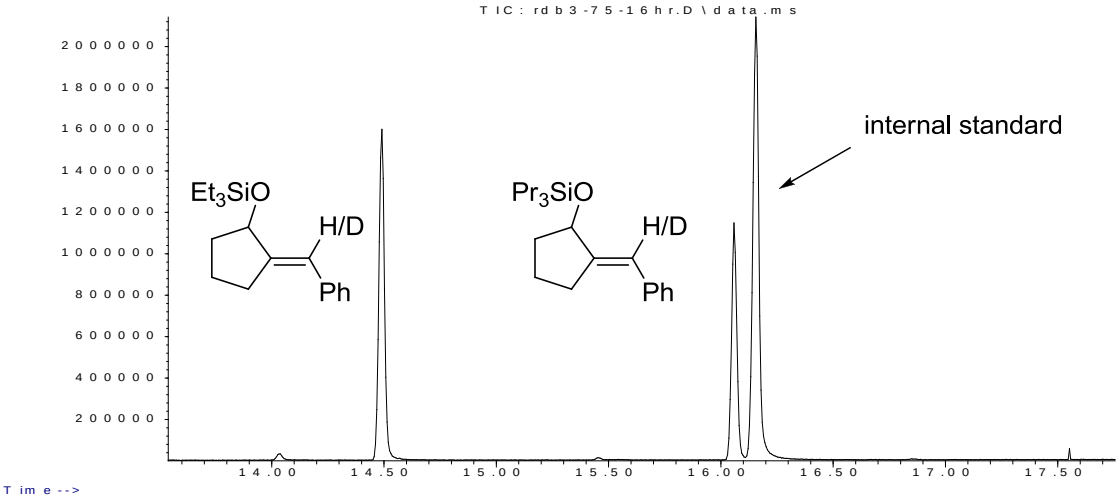


Signal : TIC: rdb3-75-16hr.D\data.ms

| peak # | R.T. min | first scan | max scan | last scan | PK TY | peak height | corr. area | corr. % max. | % of total |
|---|---|---|---|---|---|---|---|---|---|
| 1 | 14.491 | 1986 | 1994 | 2006 | M | 1603610 | 27811898 | 100.00% | 59.577% |
| 2 | 16.058 | 2258 | 2268 | 2278 | M | 1145135 | 18870590 | 67.85% | 40.423% |

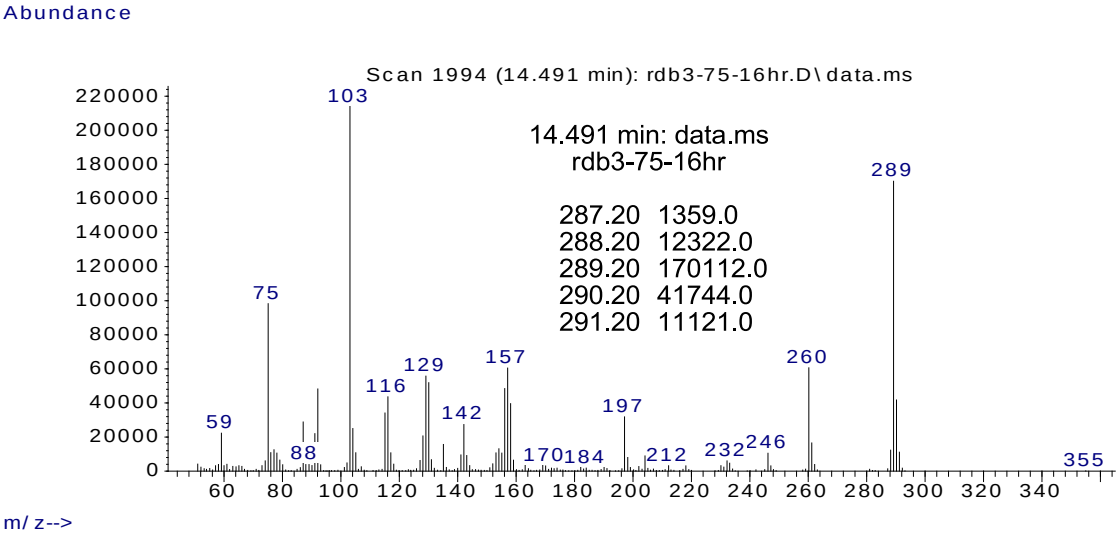

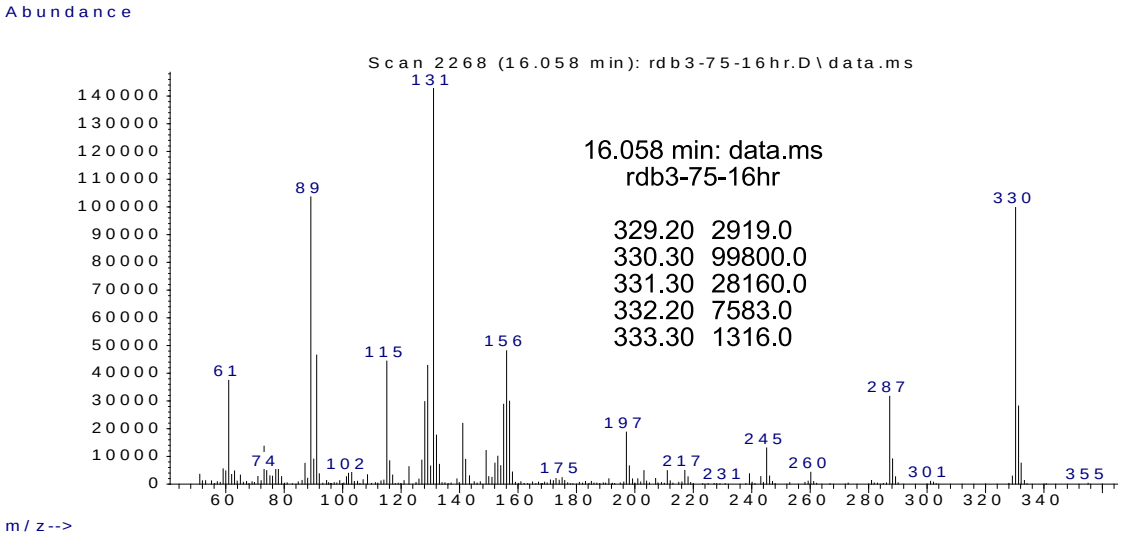
Abundance
Scan 2268 (16.058 min): rdb3-75-16hr.D\data.ms
16.058 min: data.ms
rdb3-75-16hr
329.20 2919.0
330.30 99800.0
331.30 28160.0
332.20 7583.0
333.30 1316.0
131
89
330
115
156
61
287
197
245
74
102
175
217
231
260
301
355
m/z-->

## Crossover with a $Ni(COD)_2/PBu_3$ Catalyst System, 45 °C

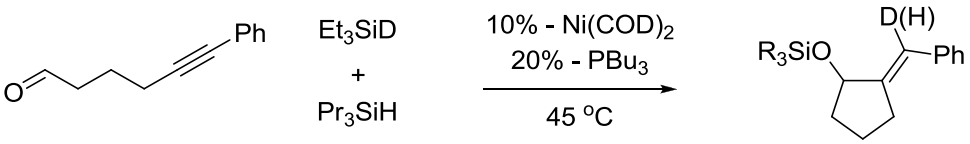


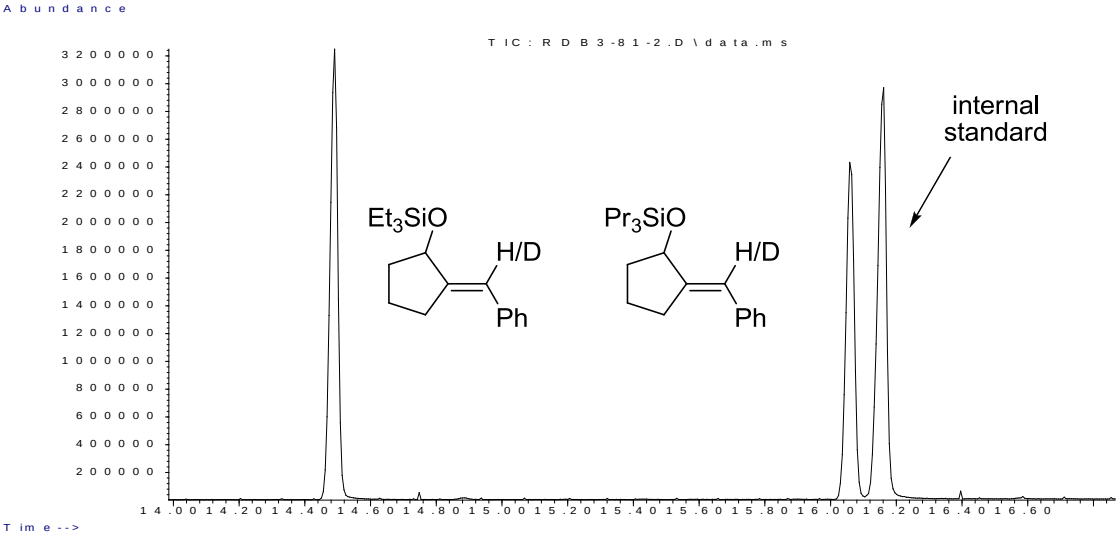


Signal : TIC: RDB3-81-2.D\data.ms

| peak # | R.T. min | first scan | max scan | last scan | PK TY | peak height | corr. area | corr. % max. | % of total |
|---|---|---|---|---|---|---|---|---|---|
| 1 | 14.491 | 1986 | 1994 | 2007 | M | 3256491 | 53671336 | 100.00% | 55.199% |
| 2 | 16.058 | 2259 | 2268 | 2276 | M | 2457693 | 43561293 | 81.16% | 44.801% |

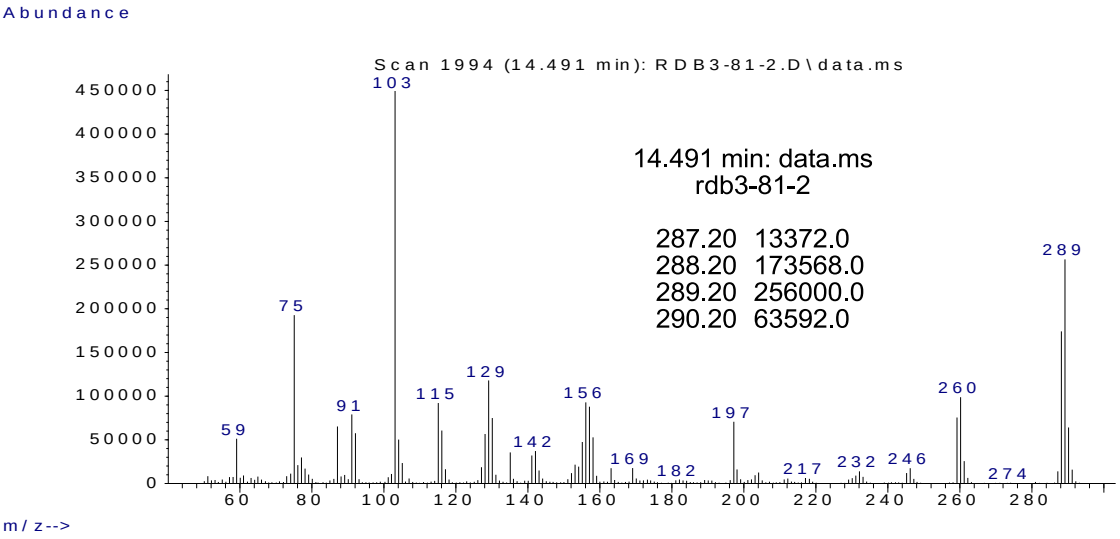

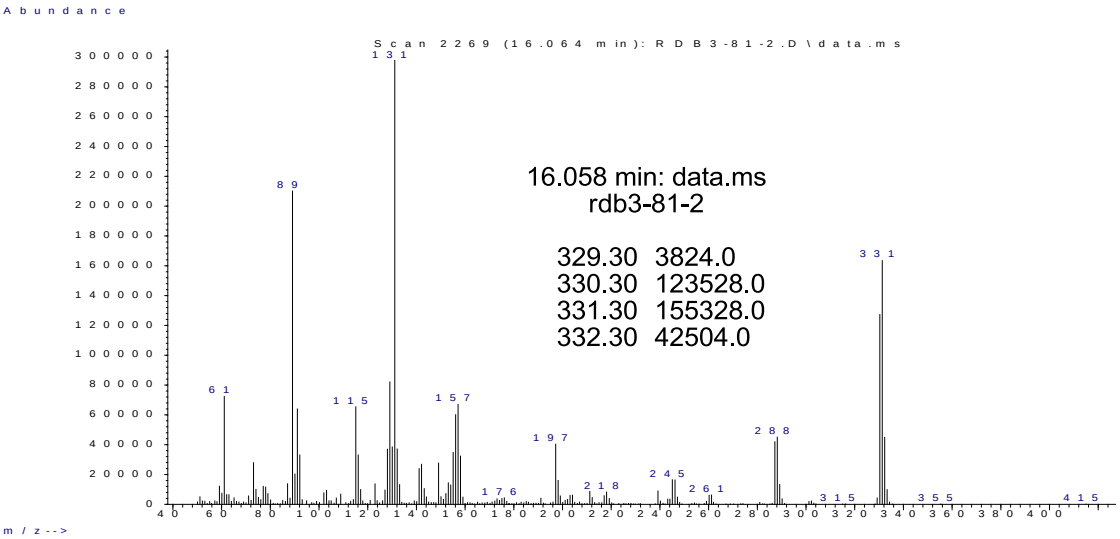
Abundance
Scan 2269 (16.064 min): RDB3-81-2.D\data.ms
16.058 min: data.ms
rdb3-81-2
329.30 3824.0
330.30 123528.0
331.30 155328.0
332.30 42504.0
m/z-->

## Crossover with a $Ni(COD)_2/PCy_3$ Catalyst System

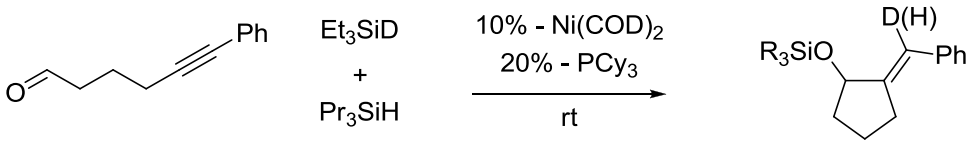


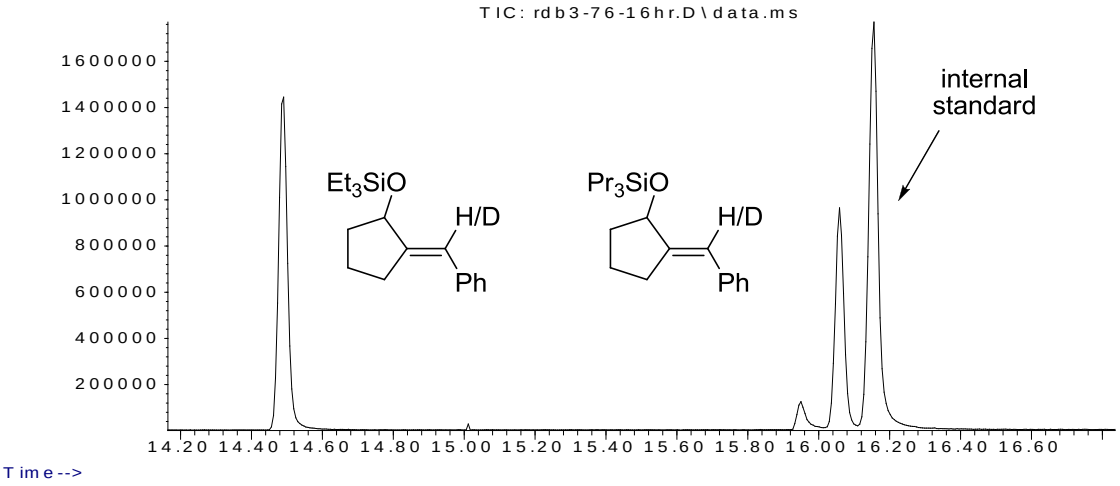


Signal : TIC: rdb3-76-16hr.D\data.ms

| peak # | R.T. min | first scan | max scan | last scan | PK TY | peak height | corr. area | corr. % max. | % of total |
|---|---|---|---|---|---|---|---|---|---|
| 1 | 14.491 | 1987 | 1994 | 2010 | M | 1471976 | 25647207 | 100.00% | 60.631% |
| 2 | 16.058 | 2258 | 2268 | 2278 | M | 957377 | 16653031 | 64.93% | 39.369% |

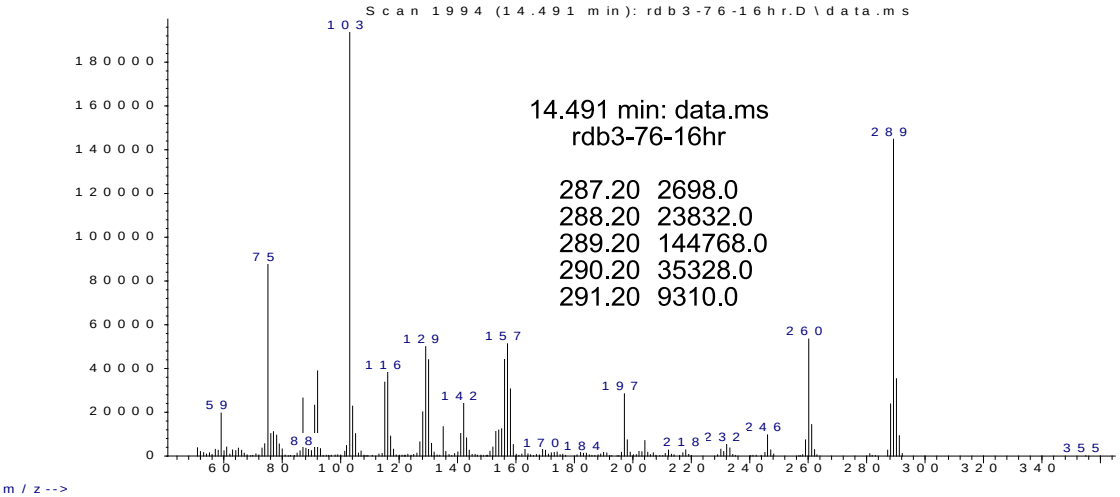

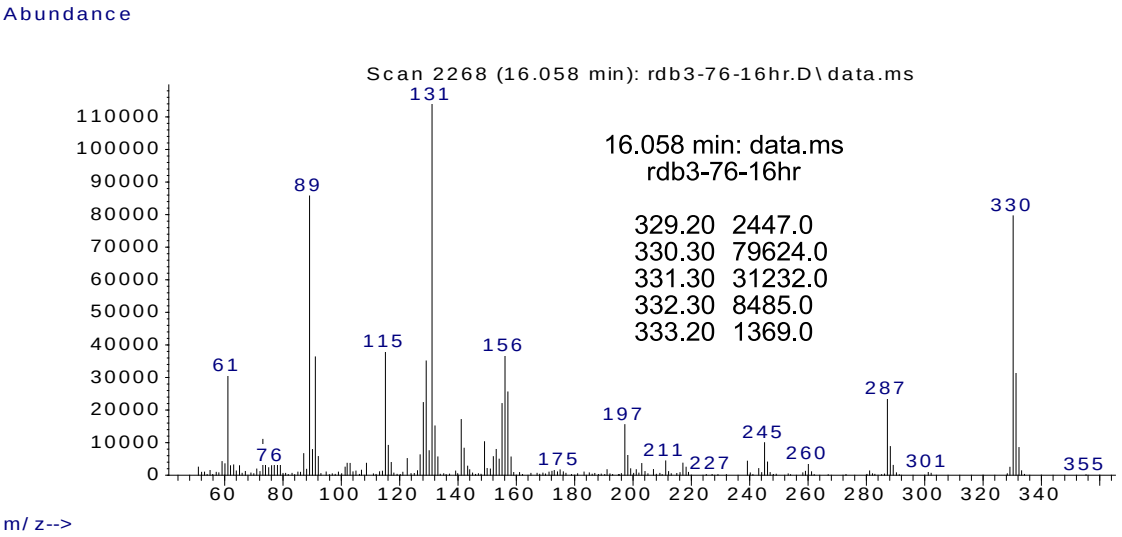


**NMR Determination of the Kinetic Isotope Effect with Respect to Triethylsilane**

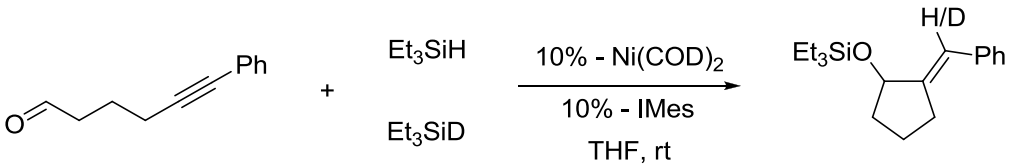


Following the general preparative procedure for nickel-catlayzed ynal **29** (86 mg, 0.50 mmol, 1.0 equiv) was cyclized in the presence of $Ni(COD)_2$/IMes, $Et_3SiH$ (174 mg, 1.5 mmol, 3.0 equiv) and $Et_3SiD$ (176 mg, 1.5 mmol, 3.0 equiv) at room temperature. After aqueous workup, the crude reaction mixture was flushed through a plug of silica gel using 100% Hexanes to yield the desired product as an inseparable isotopic mixture. This material was analyzed by NMR, and the integration of the vinylic proton was diagnostic for the percentage of hydrogen incorporation in the product.

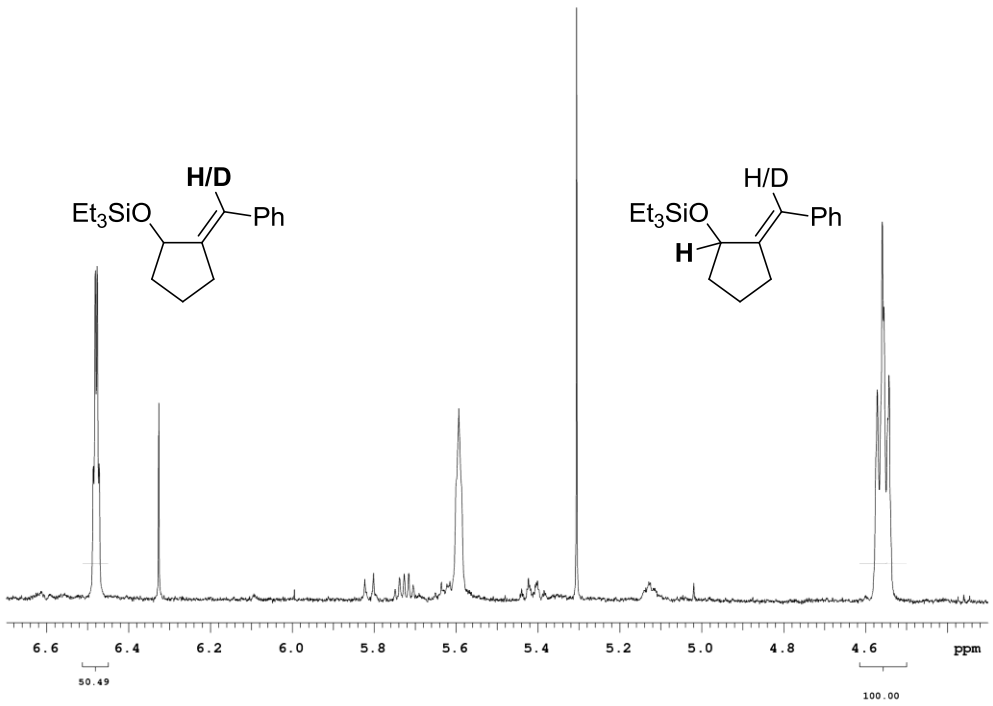


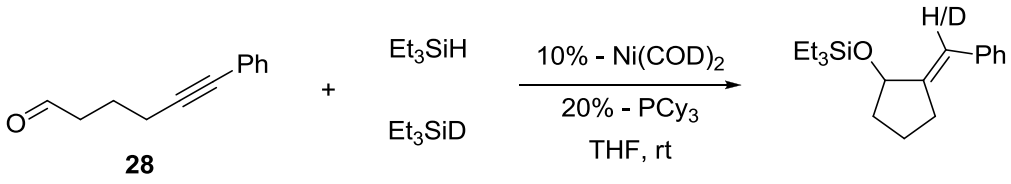


Following the general preparative procedure for nickel-catlayzed ynal cyclization, ynal **29** (86 mg, 0.50 mmol, 1.0 equiv) was cyclized in the presence of $Ni(COD)_2/PCy_3$, $Et_3SiH$ (174 mg, 1.5 mmol, 3.0 equiv) and $Et_3SiD$ (176 mg, 1.5 mmol, 3.0 equiv) at room temperature. After aqueous workup, the crude reaction mixture was flushed through a plug of silica gel using 100% Hexanes to yield the desired product as an inseparable isotopic mixture. This material was analyzed by NMR, and the integration of the vinylic proton was diagnostic for the percentage of hydrogen incorporation in the product.

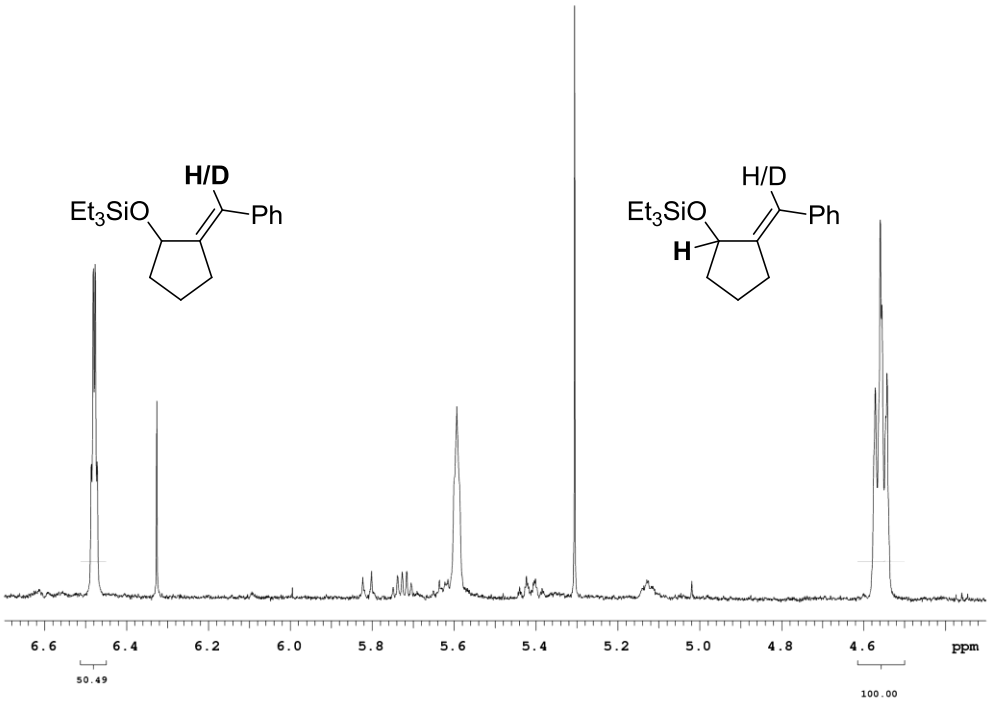


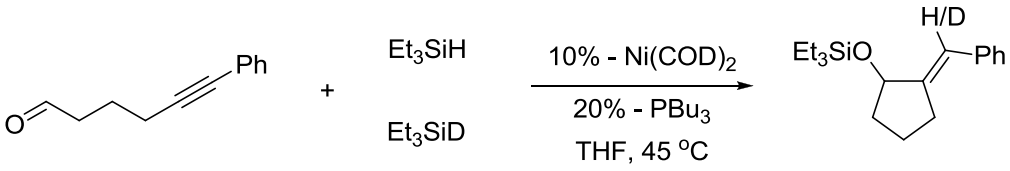


Following the general preparative procedure for nickel-catlayzed ynal **29** (86 mg, 0.50 mmol, 1.0 equiv) was cyclized in the presence of $Ni(COD)_2/PBu_3$, $Et_3SiH$ (174 mg, 1.5 mmol, 3.0 equiv) and $Et_3SiD$ (176 mg, 1.5 mmol, 3.0 equiv) at 45 $^oC$. After aqueous workup, the crude reaction mixture was flushed through a plug of silica gel using 100% Hexanes to yield the desired product as an inseparable isotopic mixture. This material was analyzed by NMR, and the integration of the vinylic proton was diagnostic for the percentage of hydrogen incorporation in the product.

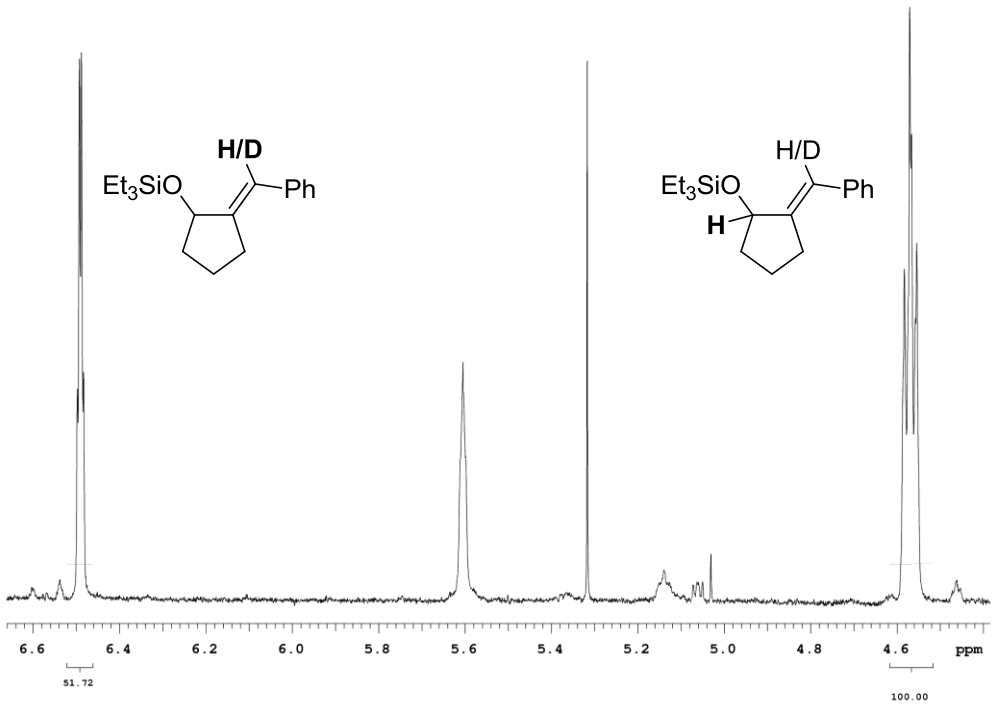
H/D
Et3SiO
Ph
H/D
Et3SiO
H
Ph
6.6
6.4
6.2
6.0
5.8
5.6
5.4
5.2
5.0
4.8
4.6
ppm
51.72
100.00

## 5.3.2 Substrate Dependent Crossover Experiments (Scheme 72)

## Authentic Sample

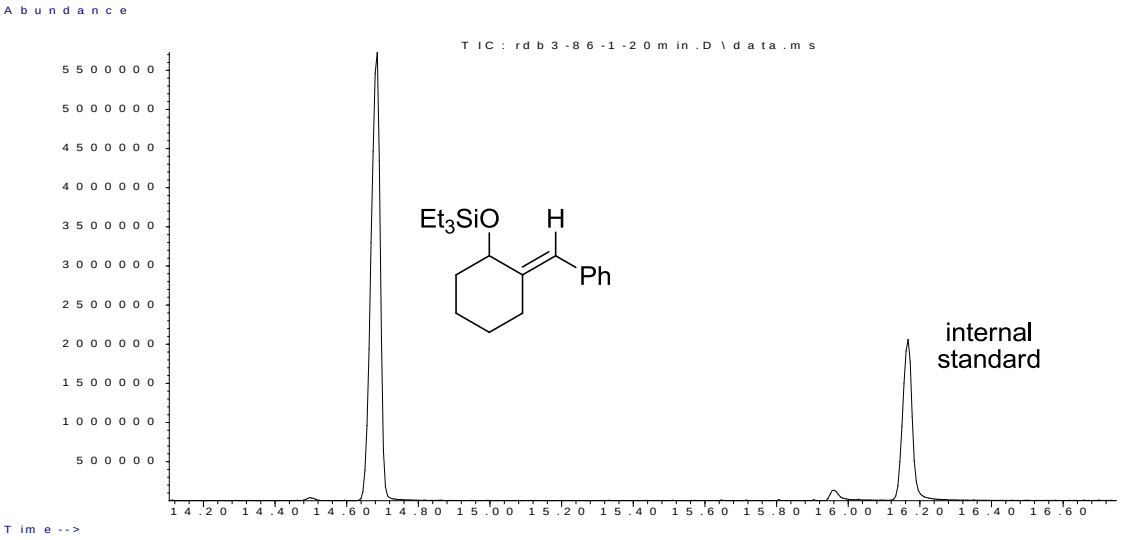


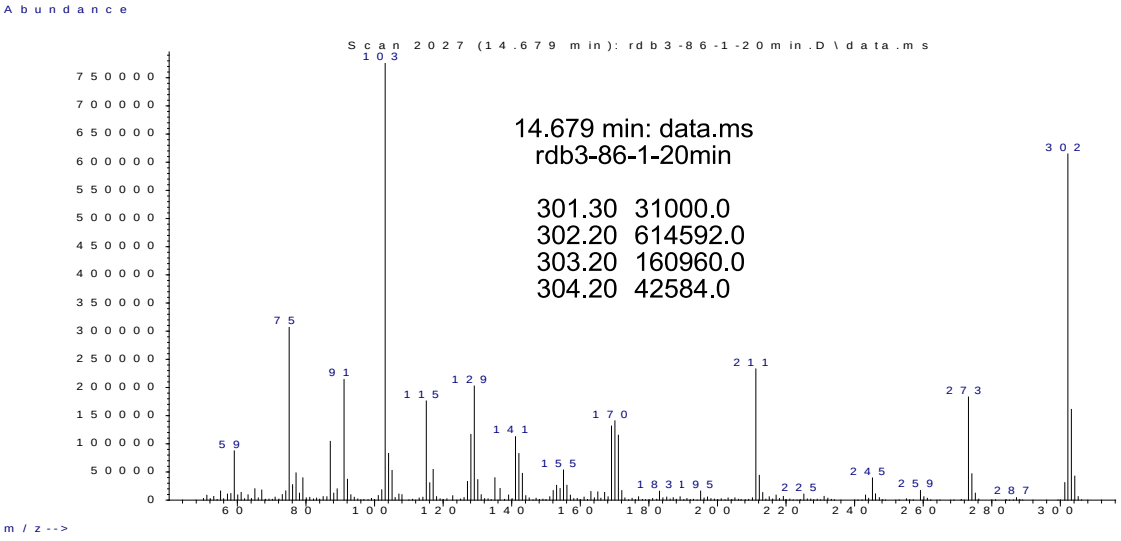

## Authentic Sample

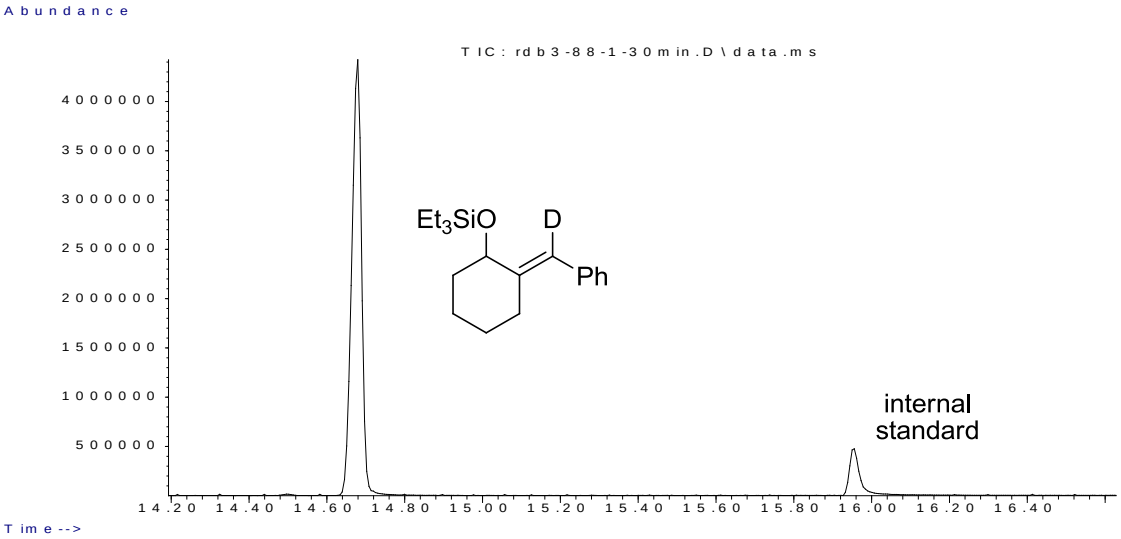


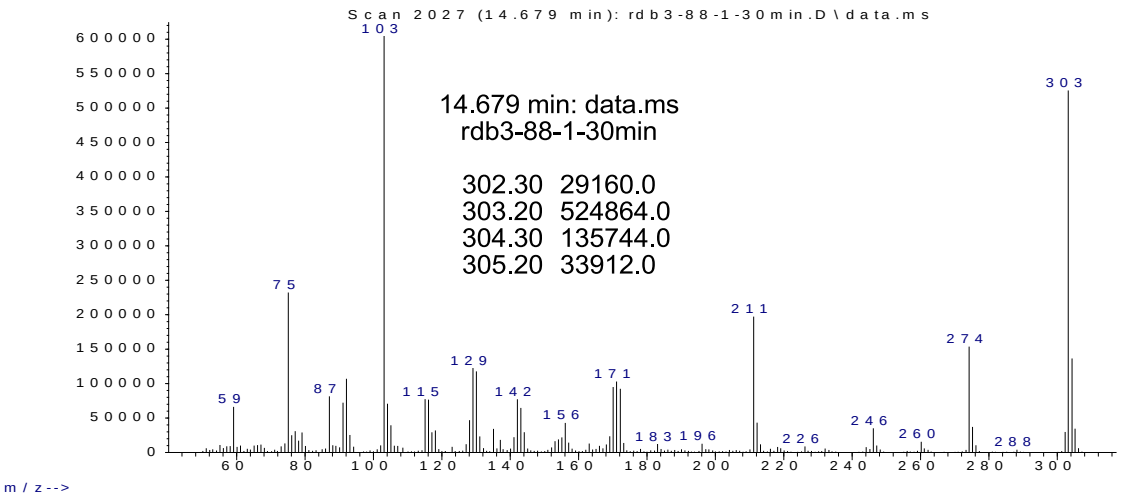

## Authentic Sample

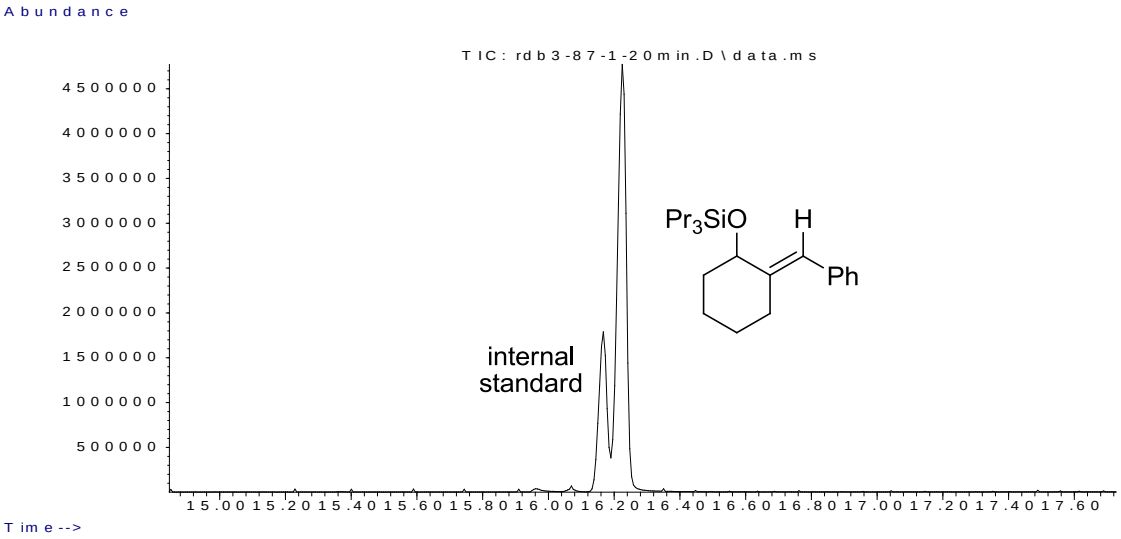


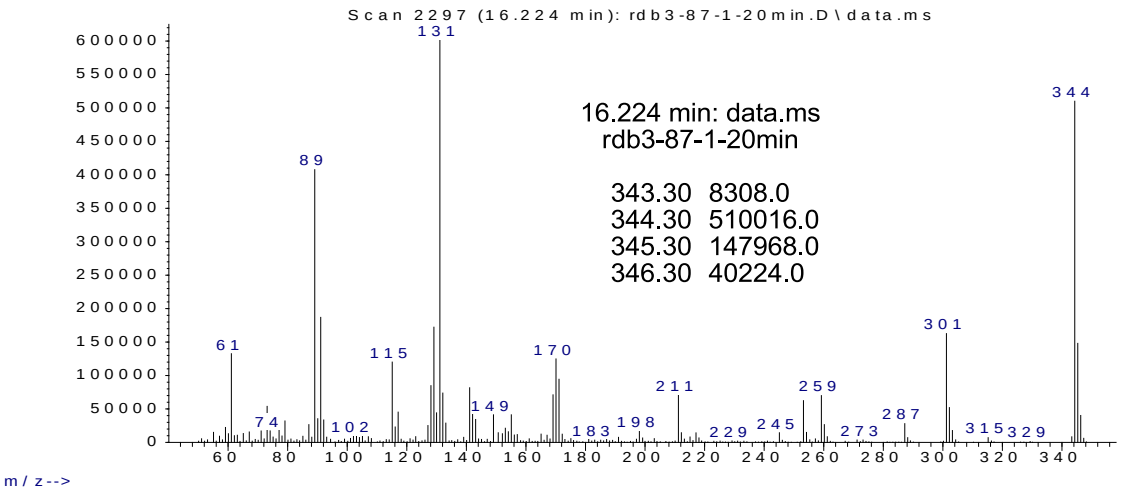

## Crossover with a $Ni(COD)_2/PCy_3$ Catalyst System: 6-Membered Ring Product

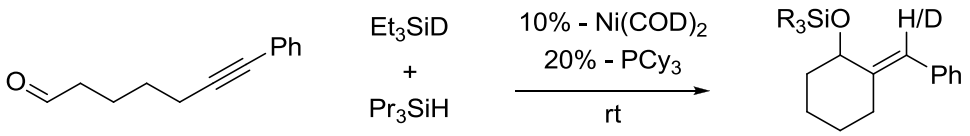


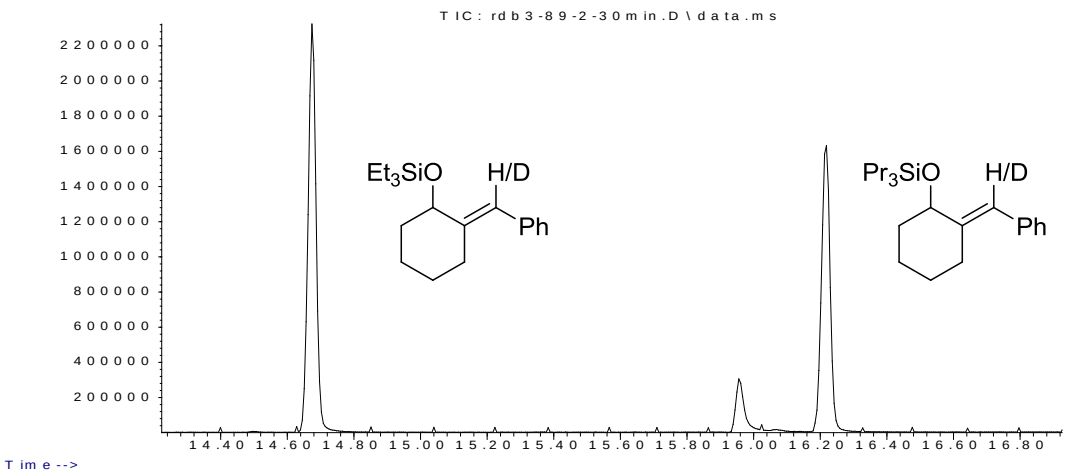


Signal : TIC: rdb3-89-2-30min.D\data.ms

| peak # | R.T. min | first scan | max scan | last scan | PK TY | peak height | corr. area | corr. % max. | % of total |
|---|---|---|---|---|---|---|---|---|---|
| 1 | 14.674 | 2019 | 2026 | 2042 | M | 2331922 | 38743233 | 100.00% | 56.870% |
| 2 | 16.219 | 2288 | 2296 | 2307 | M | 1646751 | 29382749 | 75.84% | 43.130% |

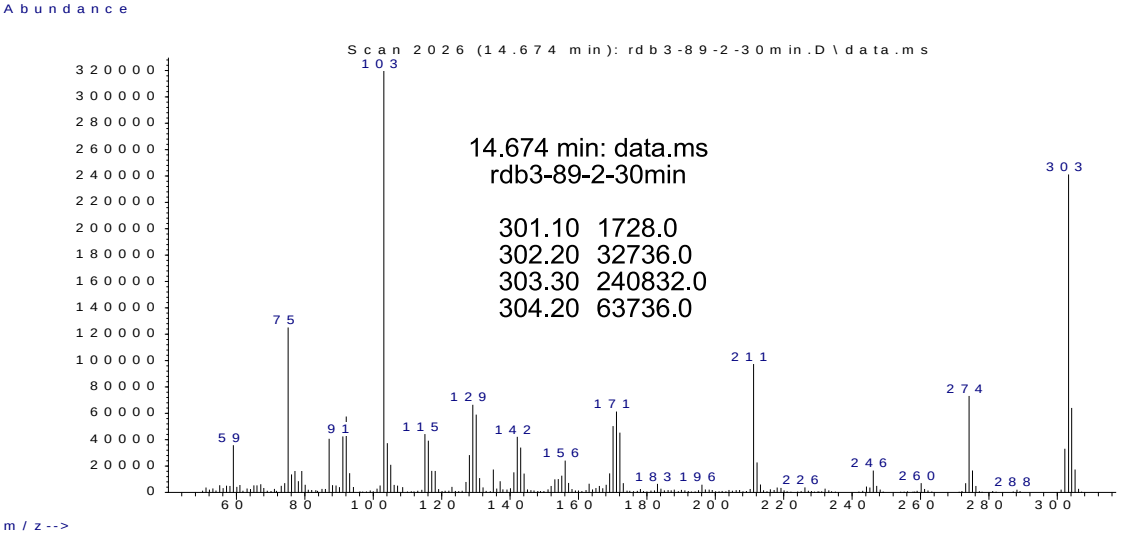

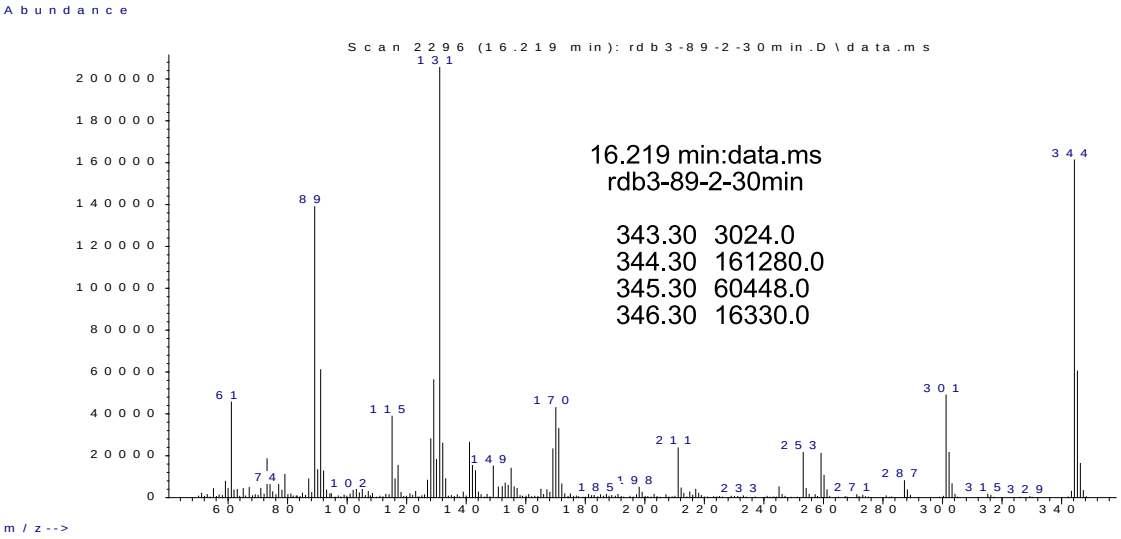
Abundance
Scan 2296 (16.219 min): rdb3-89-2-30min.D\data.ms
16.219 min:data.ms
rdb3-89-2-30min
343.30 3024.0
344.30 161280.0
345.30 60448.0
346.30 16330.0
131
89
344
61
115
170
301
211
253
149
74
102
185
198
233
271
287
315
329
m/z-->

## Authentic Sample

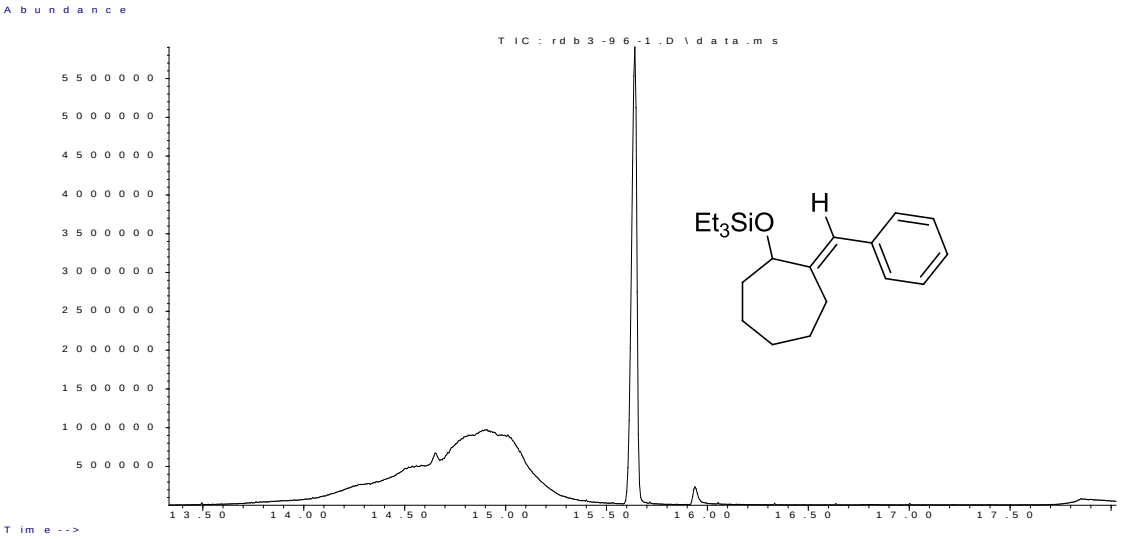


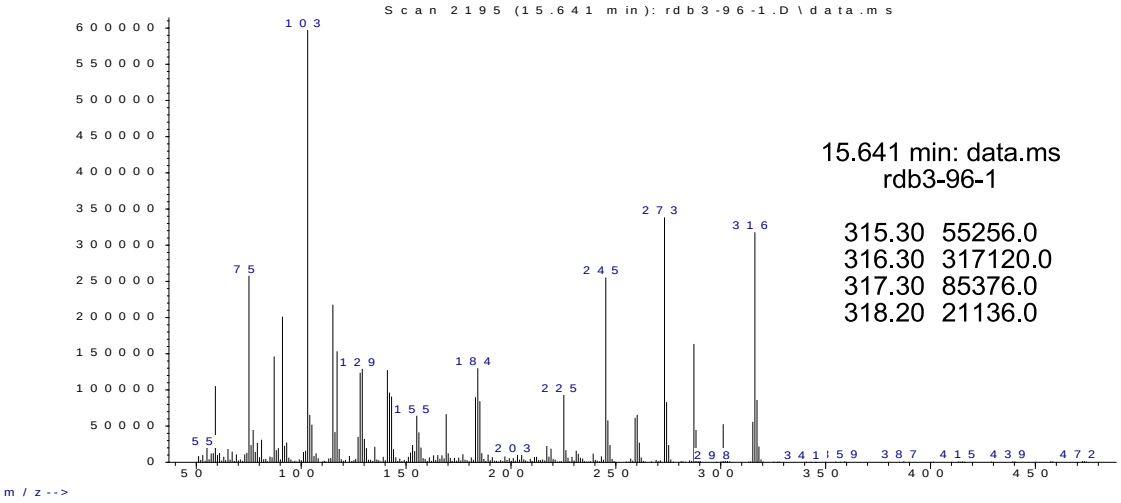

## Authentic Sample

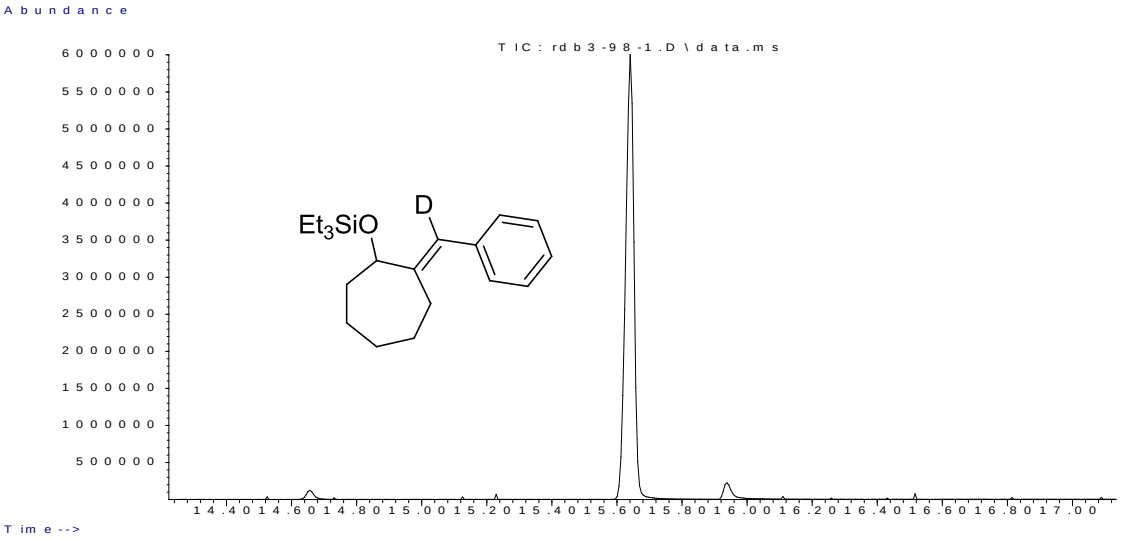


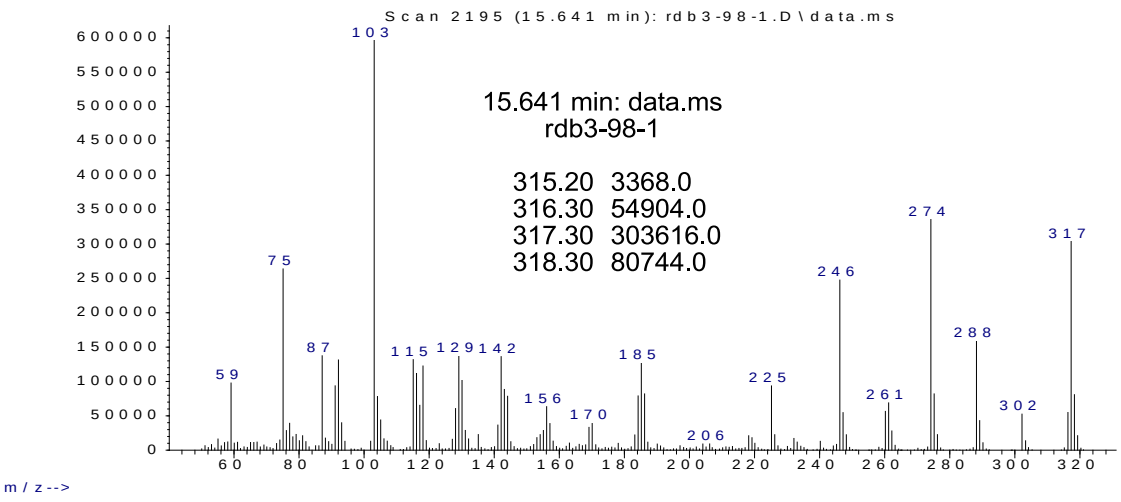

## Authentic Sample

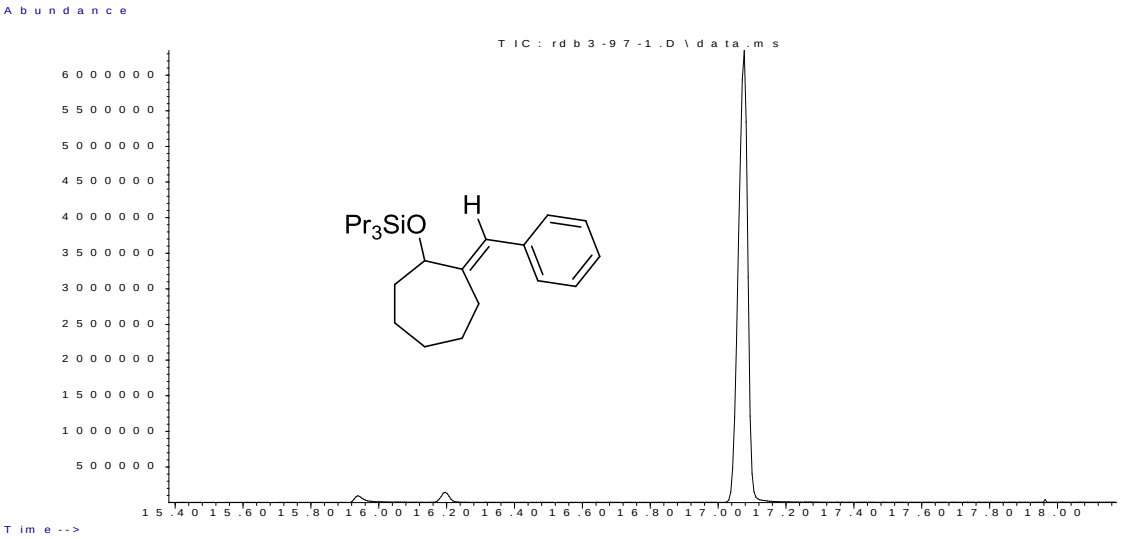


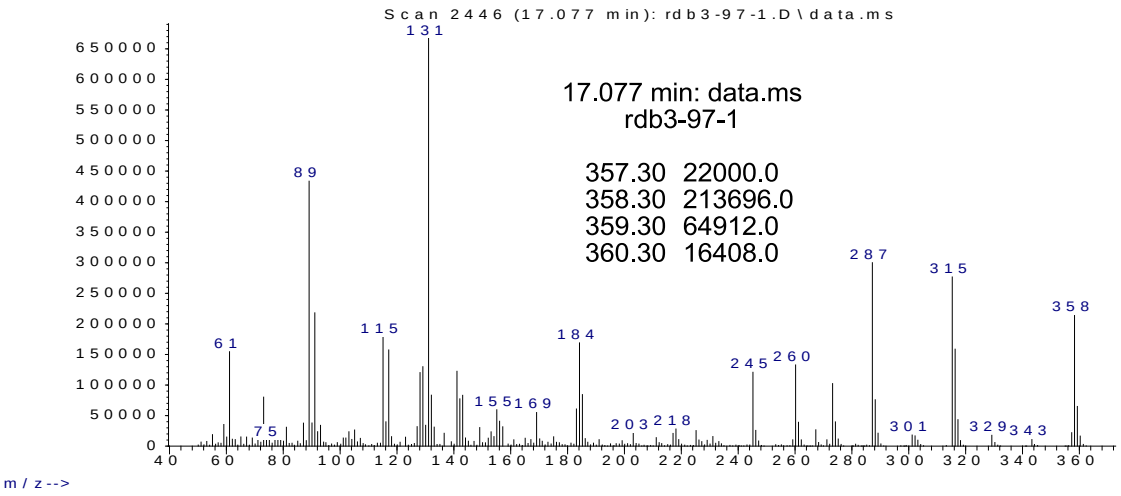

## Crossover with a $Ni(COD)_2/PCy_3$ Catalyst System: 7-Membered Ring Product

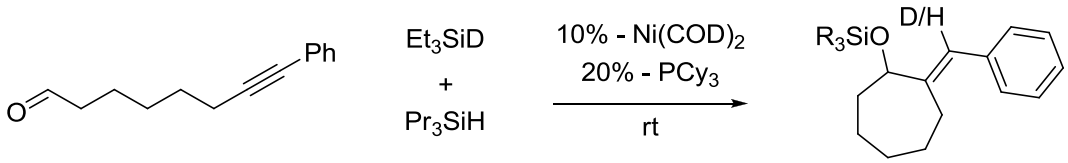


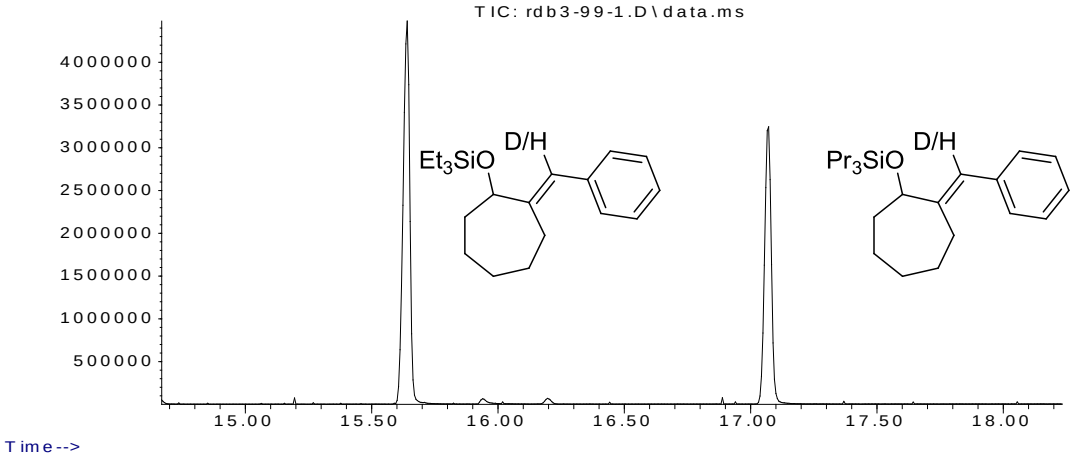


Signal : TIC: rdb3-99-1.D\data.ms

| peak # | R.T. min | first scan | max scan | last scan | PK TY | peak height | corr. area | corr. % max. | % of total |
|---|---|---|---|---|---|---|---|---|---|
| 1 | 15.641 | 2184 | 2195 | 2212 | M | 4509431 | 82777251 | 100.00% | 57.849% |
| 2 | 17.071 | 2435 | 2445 | 2465 | M | 3306839 | 60314339 | 72.86% | 42.151% |

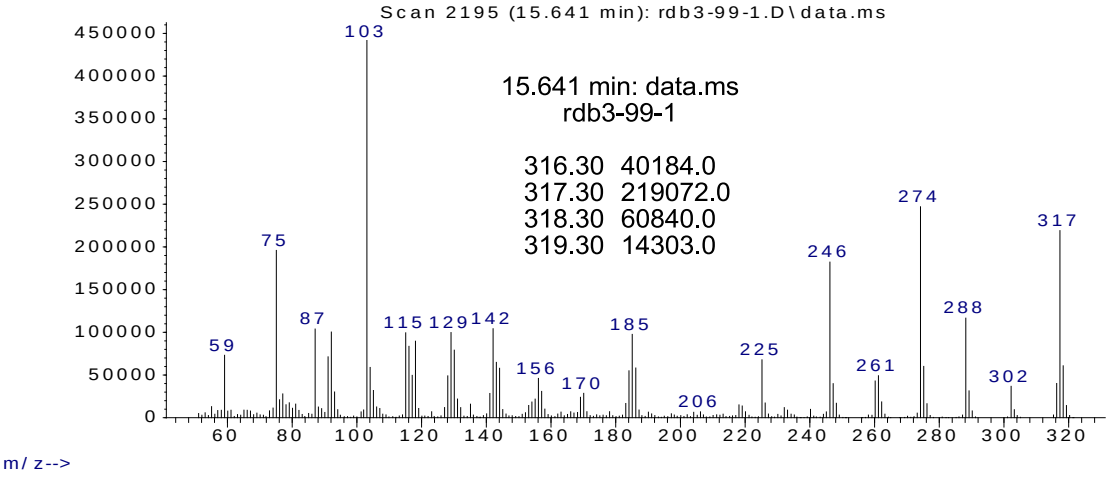

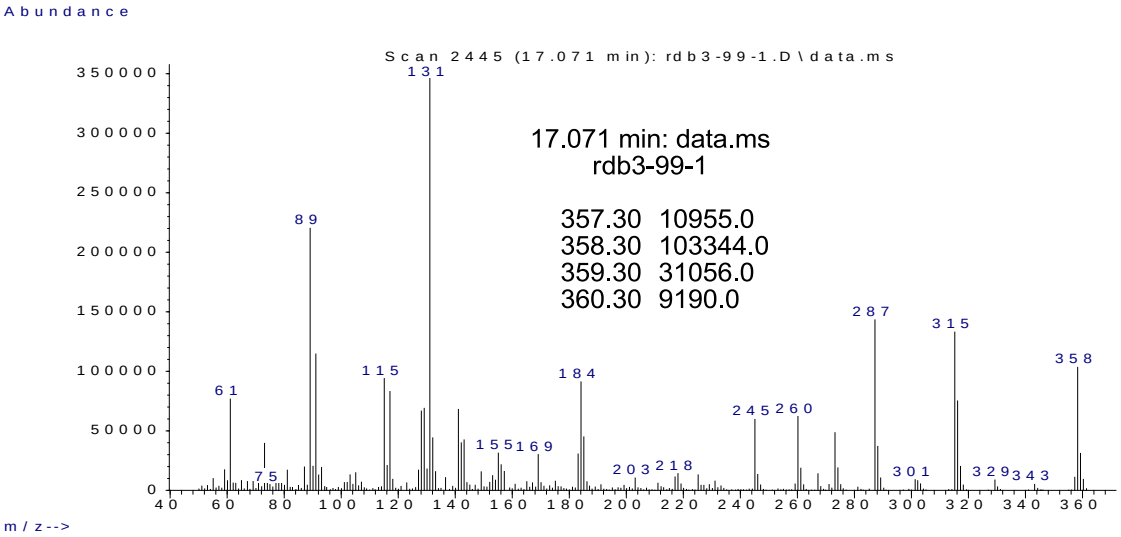
Abundance
Scan 2445 (17.071 min): rdb3-99-1.D\data.ms
17.071 min: data.ms
rdb3-99-1
357.30 10955.0
358.30 103344.0
359.30 31056.0
360.30 9190.0
m/z-->

### 5.3.3 Crossover Experiments Under Various Conditions (Scheme 73)

**Crossover with a $Ni(COD)_2/PCy_3$ Catalyst System: -25 °C**

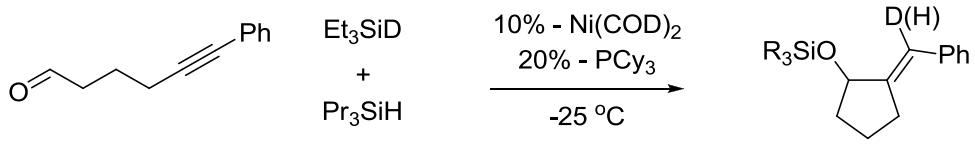


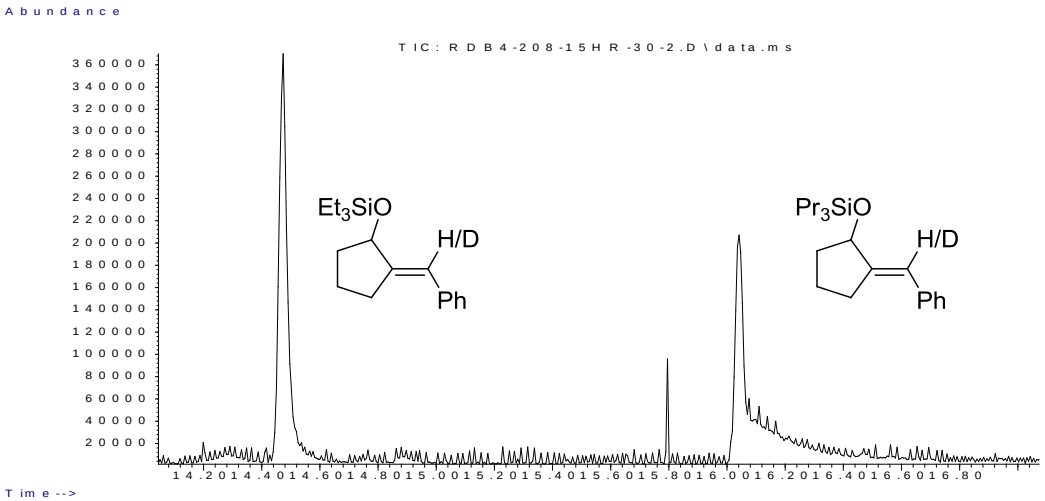


Signal : TIC: RDB4-208-15HR-30-2.D\data.ms

| peak # | R.T. min | first scan | max scan | last scan | PK TY | peak height | corr. area | corr. % max. | % of total |
|---|---|---|---|---|---|---|---|---|---|
| 1 | 14.474 | 1983 | 1991 | 2019 | M | 366316 | 7648694 | 100.00% | 62.891% |
| 2 | 16.041 | 2259 | 2265 | 2274 | M2 | 205829 | 4513066 | 59.00% | 37.109% |

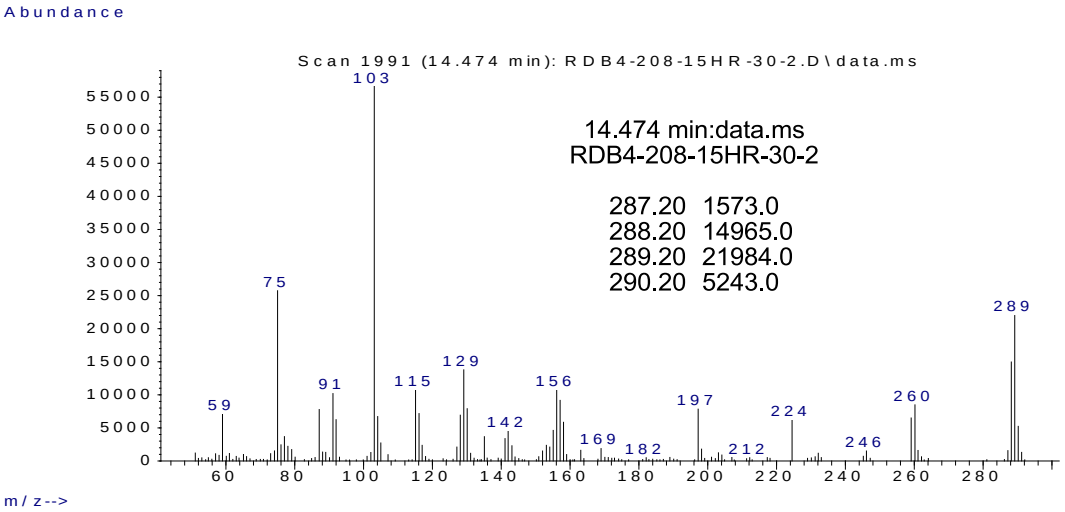

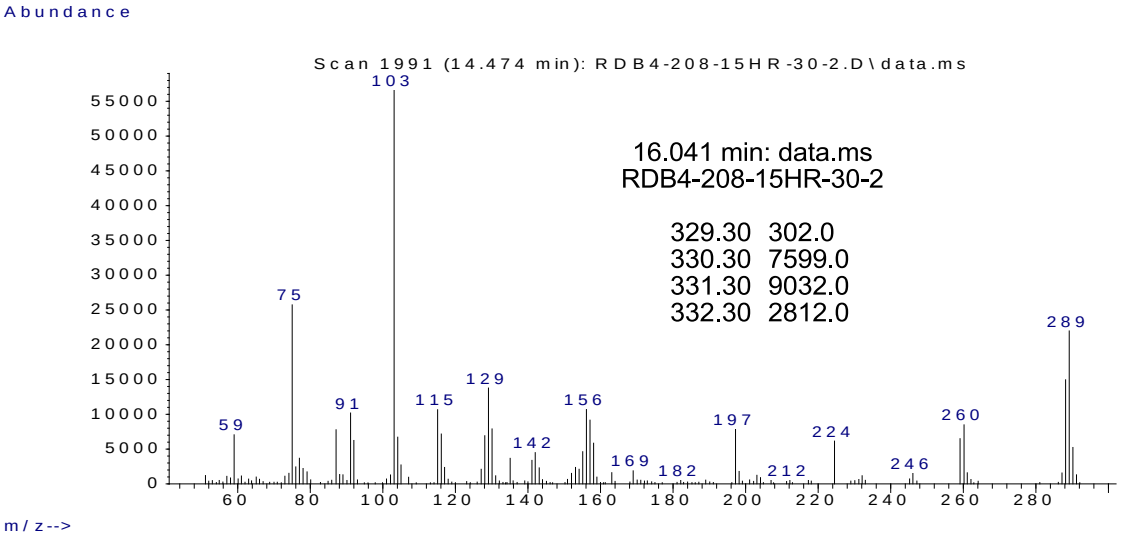
Abundance
Scan 1991 (14.474 min): RDB4-208-15HR-30-2.D\data.ms
16.041 min: data.ms
RDB4-208-15HR-30-2
329.30 302.0
330.30 7599.0
331.30 9032.0
332.30 2812.0
m/z-->

## Crossover with a $Ni(COD)_2/PCy_3$ Catalyst System: 0 °C

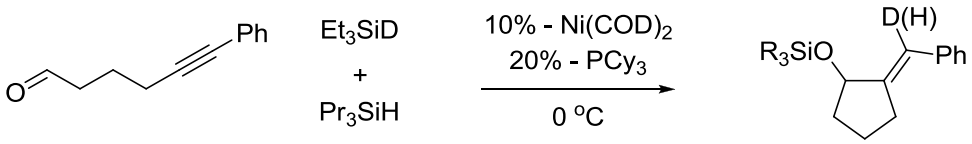


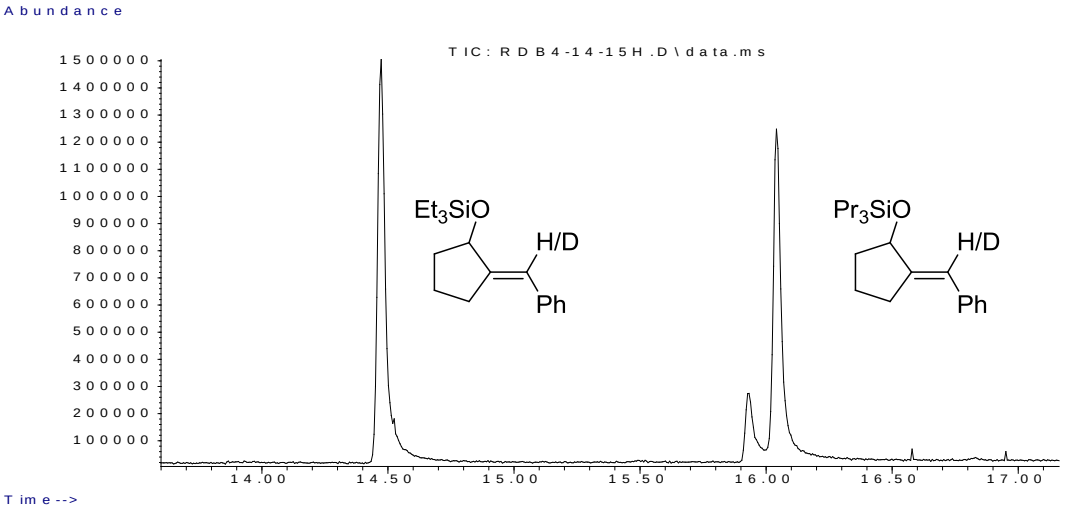


Signal : TIC: RDB4-14-15H.D\data.ms

| peak # | R.T. min | first scan | max scan | last scan | PK TY | peak height | corr. area | corr. % max. | % of total |
|---|---|---|---|---|---|---|---|---|---|
| 1 | 14.473 | 1983 | 1991 | 2042 | M | 1497752 | 36756063 | 100.00% | 50.564% |
| 2 | 16.041 | 2254 | 2265 | 2331 | M2 | 1242897 | 35936103 | 97.77% | 49.436% |

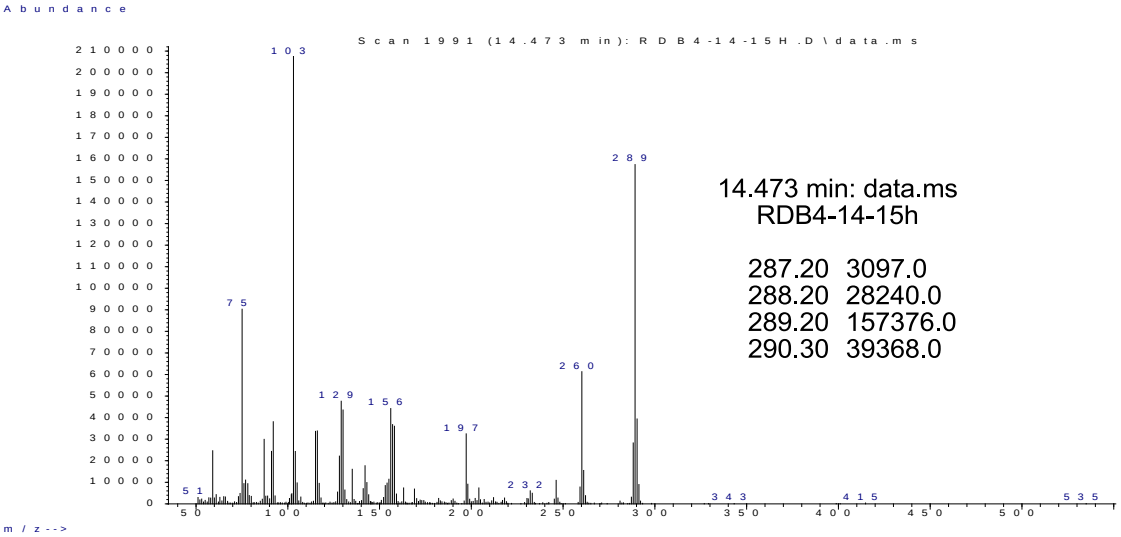

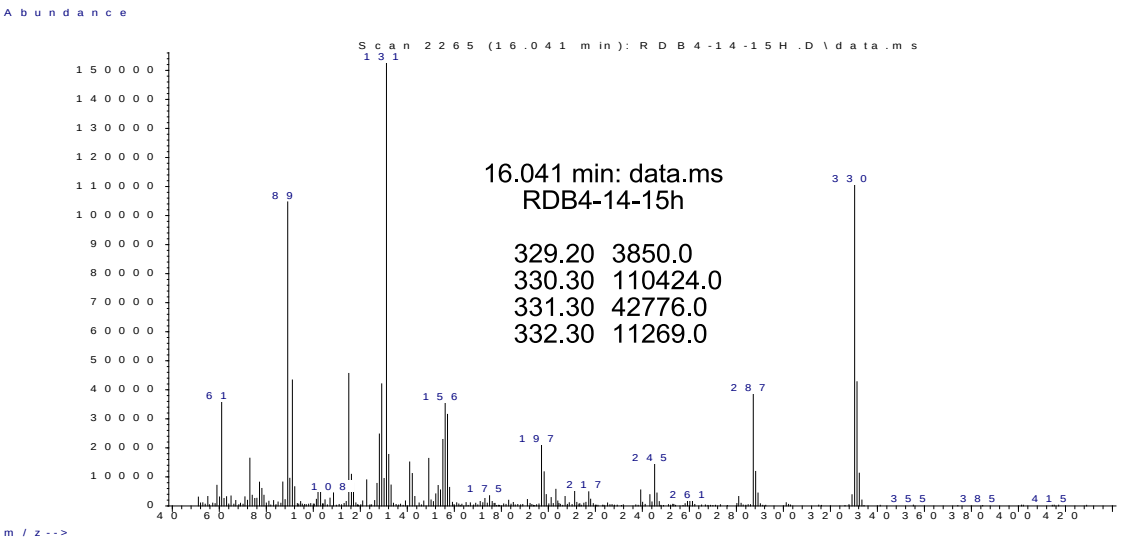
Abundance
Scan 2265 (16.041 min): RDB4-14-15H.D\data.ms
16.041 min: data.ms
RDB4-14-15h
329.20 3850.0
330.30 110424.0
331.30 42776.0
332.30 11269.0
m/z-->

## Crossover with a $Ni(COD)_2/PCy_3$ Catalyst System: 45 °C

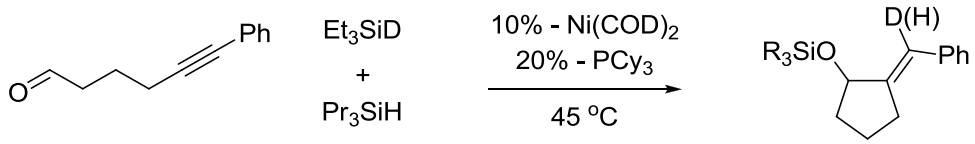


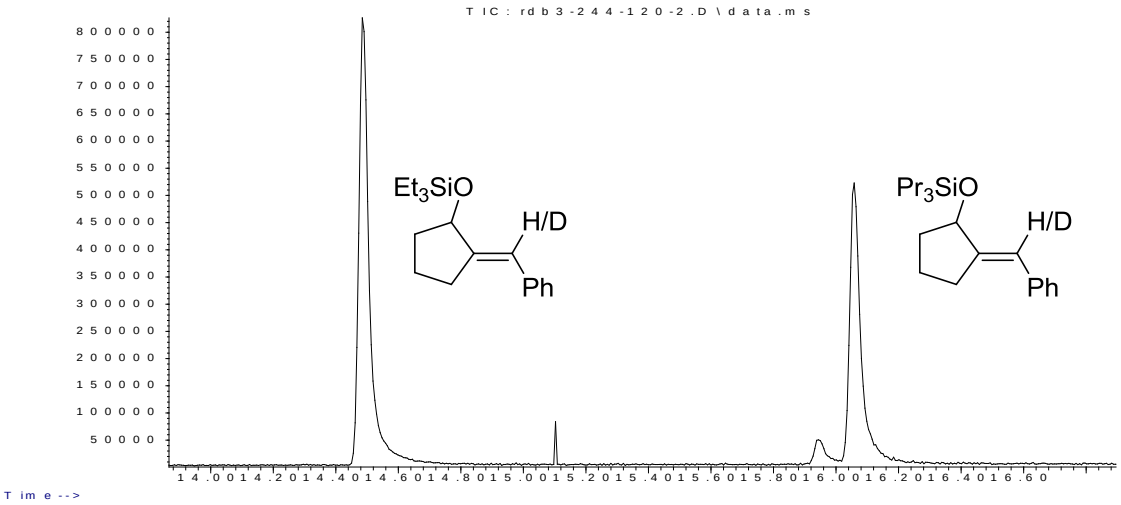


Signal : TIC: rdb3-244-120-2.D\data.ms

| peak # | R.T. min | first scan | max scan | last scan | PK TY | peak height | corr. area | corr. % max. | % of total |
|---|---|---|---|---|---|---|---|---|---|
| 1 | 14.485 | 1986 | 1993 | 2038 | M | 837995 | 20334729 | 100.00% | 59.428% |
| 2 | 16.058 | 2259 | 2268 | 2323 | M2 | 519867 | 13882815 | 68.27% | 40.572% |

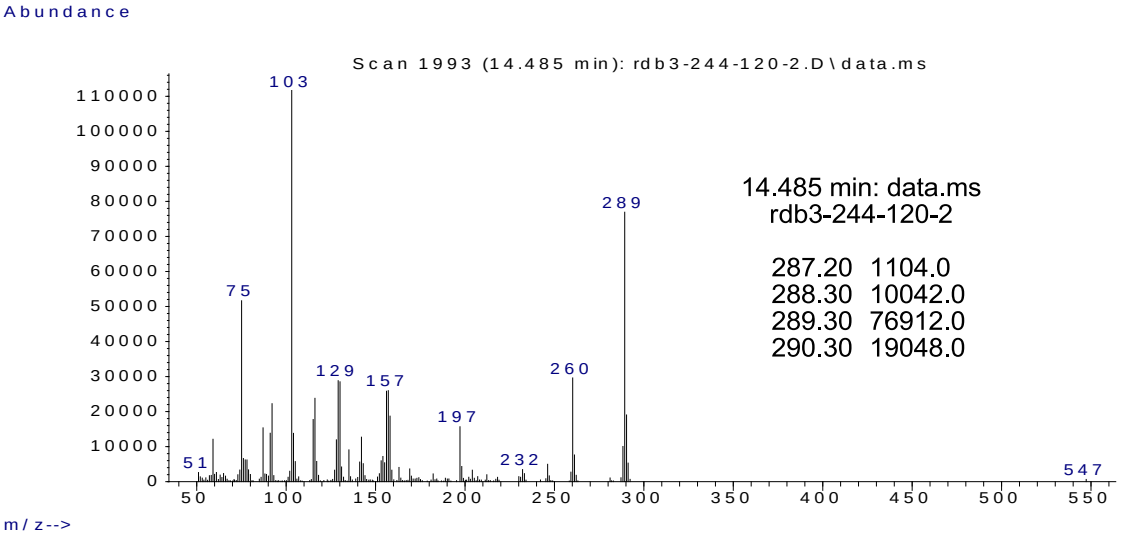

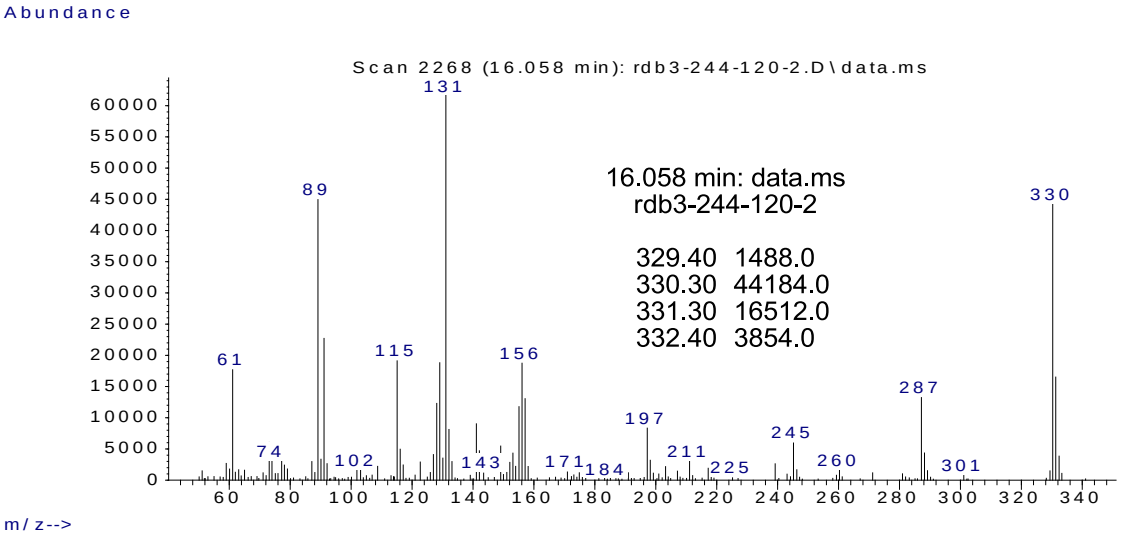
Abundance
Scan 2268 (16.058 min): rdb3-244-120-2.D\data.ms
16.058 min: data.ms
rdb3-244-120-2
329.40 1488.0
330.30 44184.0
331.30 16512.0
332.40 3854.0
131
89
330
61
115
156
287
197
245
74
102
143
171
184
211
225
260
301
m/z-->

**Crossover with a $Ni(COD)_2/PBu_3$ Catalyst System: -25 °C, 6-membered Ring Product**

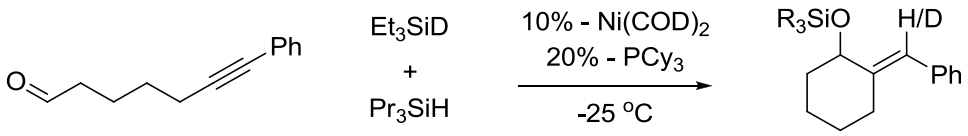


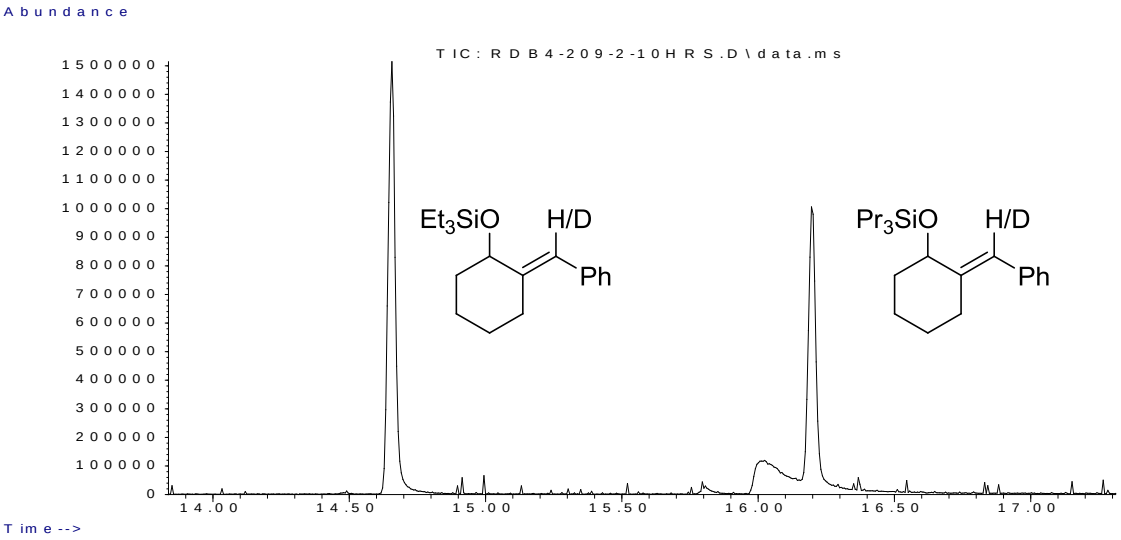


Signal : TIC: RDB4-209-2-10HRS.D\data.ms

| peak # | R.T. min | first scan | max scan | last scan | PK TY | peak height | corr. area | corr. % max. | % of total |
|---|---|---|---|---|---|---|---|---|---|
| 1 | 14.657 | 2013 | 2023 | 2045 | M | 1514974 | 28640314 | 100.00% | 55.948% |
| 2 | 16.196 | 2285 | 2292 | 2324 | M2 | 1020026 | 22550623 | 78.74% | 44.052% |

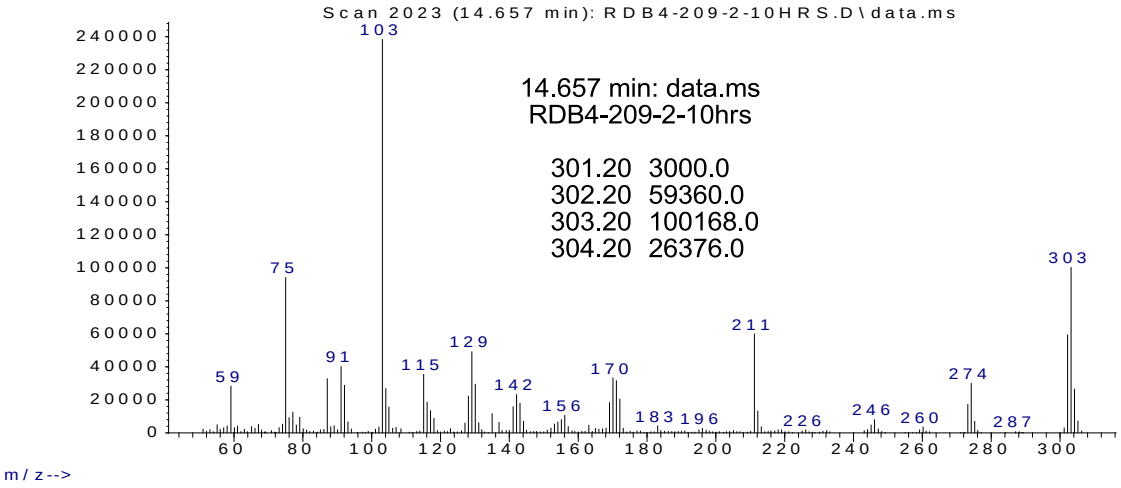

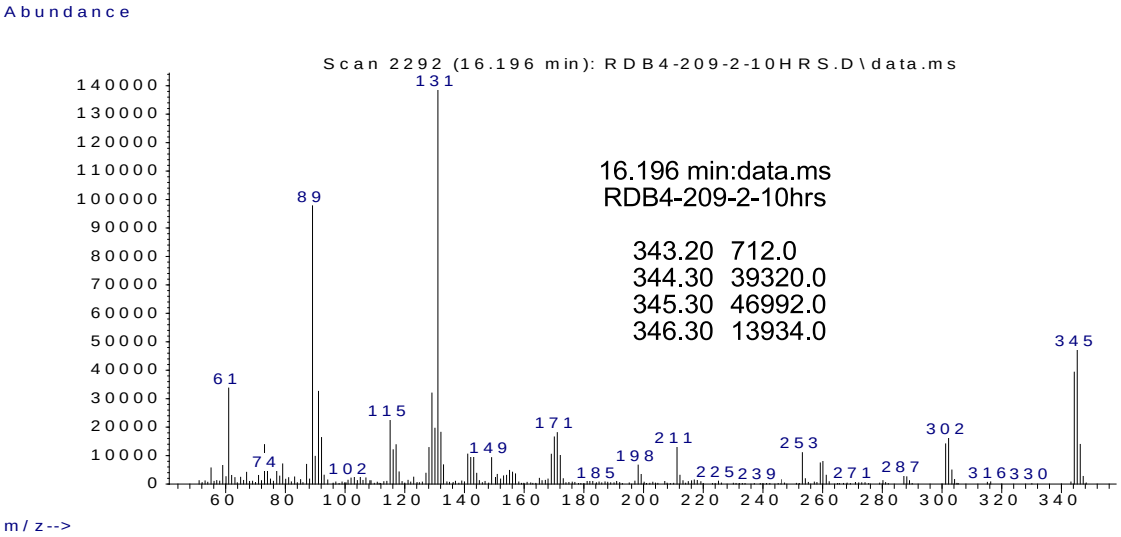
Abundance
Scan 2292 (16.196 min): RDB4-209-2-10HRS.D\data.ms
16.196 min:data.ms
RDB4-209-2-10hrs
343.20 712.0
344.30 39320.0
345.30 46992.0
346.30 13934.0
m/z-->

**Crossover with a $Ni(COD)_2/PBu_3$ Catalyst System: 45 °C, 6-membered Ring Product**

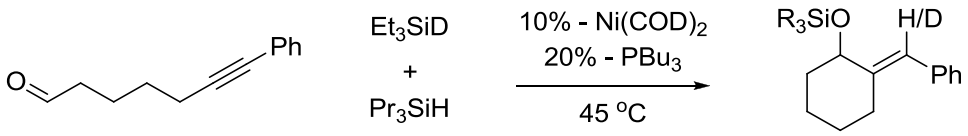


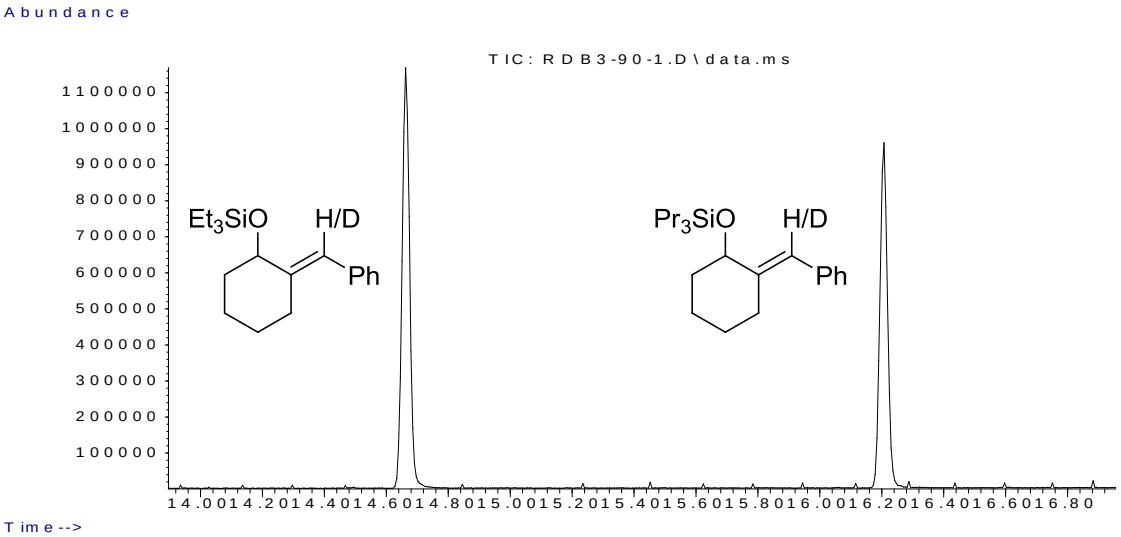


Signal : TIC: RDB3-90-1.D\data.ms

| peak # | R.T. min | first scan | max scan | last scan | PK TY | peak height | corr. area | corr. % max. | % of total |
|---|---|---|---|---|---|---|---|---|---|
| 1 | 14.662 | 2015 | 2024 | 2039 | M | 1168347 | 19724680 | 100.00% | 54.465% |
| 2 | 16.207 | 2286 | 2294 | 2304 | M | 964966 | 16490561 | 83.60% | 45.535% |

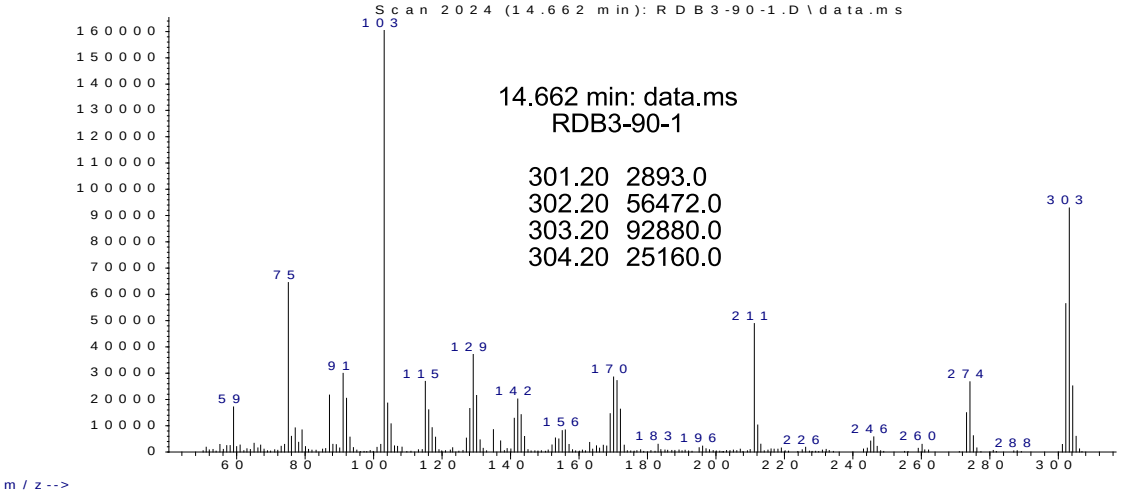

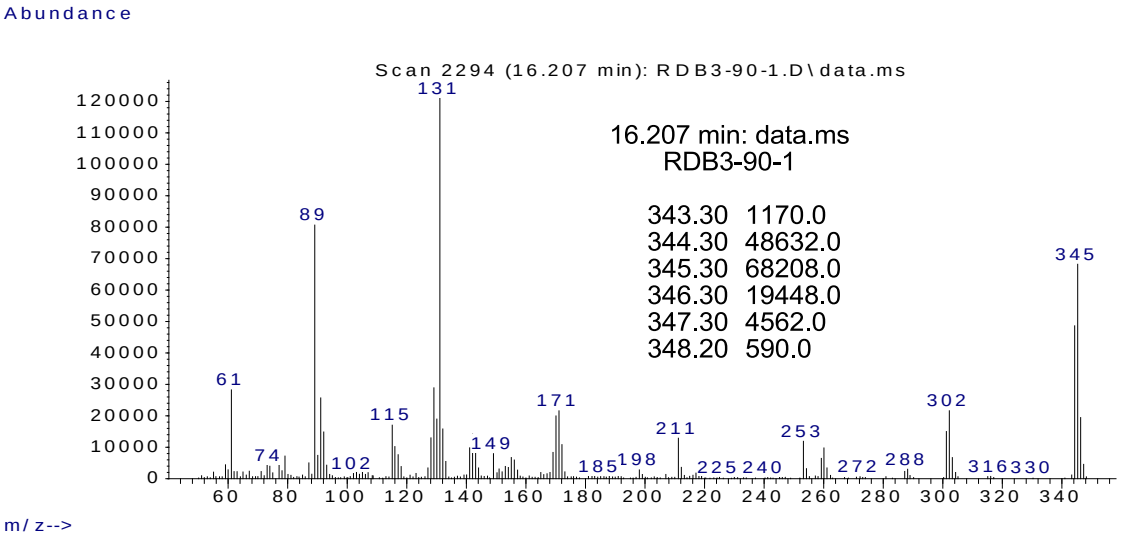
Abundance
Scan 2294 (16.207 min): RDB3-90-1.D\data.ms
16.207 min: data.ms
RDB3-90-1
343.30 1170.0
344.30 48632.0
345.30 68208.0
346.30 19448.0
347.30 4562.0
348.20 590.0
m/z-->

**Crossover with a $Ni(COD)_2/PBu_3$ Catalyst System: -25 °C, 7-membered Ring Product**

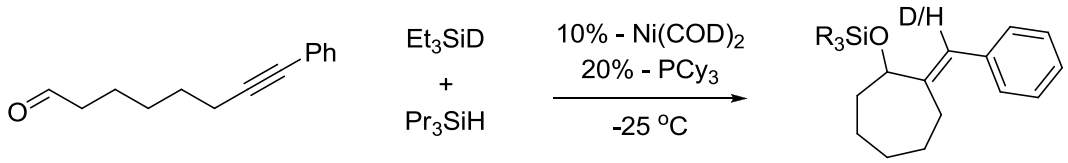


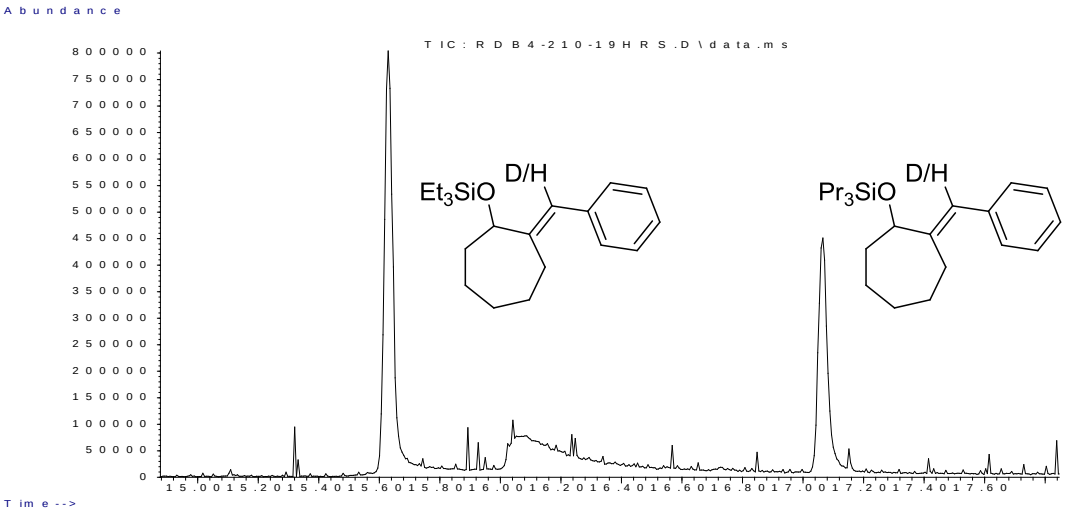


Signal : TIC: RDB4-210-19HRS.D\data.ms

| peak # | R.T. min | first scan | max scan | last scan | PK TY | peak height | corr. area | corr. % max. | % of total |
|---|---|---|---|---|---|---|---|---|---|
| 1 | 15.629 | 2182 | 2193 | 2218 | M4 | 801489 | 17201219 | 100.00% | 62.214% |
| 2 | 17.066 | 2435 | 2444 | 2466 | M3 | 448952 | 10447134 | 60.73% | 37.786% |

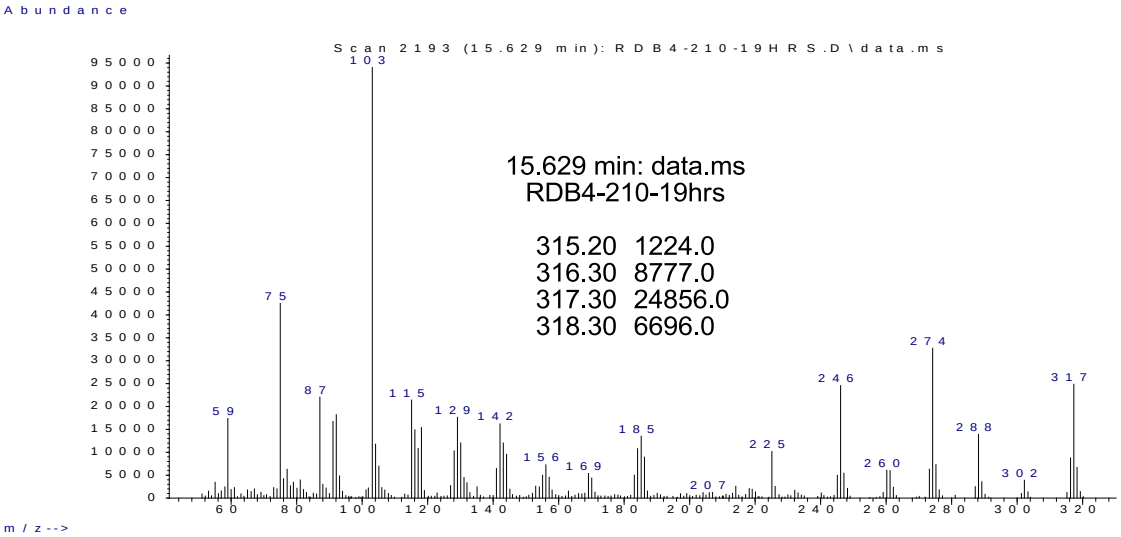

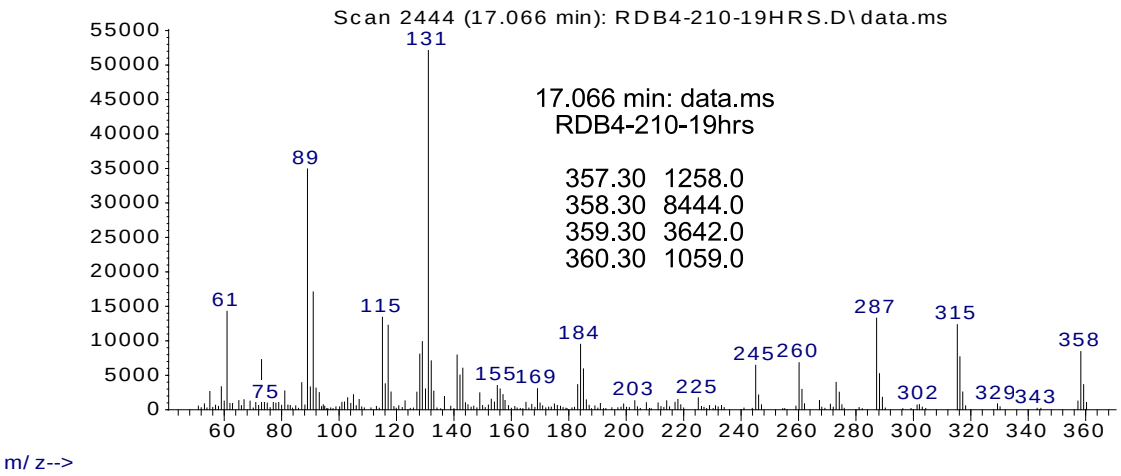
Abundance
Scan 2444 (17.066 min): RDB4-210-19HRS.D\data.ms
17.066 min: data.ms
RDB4-210-19hrs
357.30 1258.0
358.30 8444.0
359.30 3642.0
360.30 1059.0
m/z-->

**Crossover with a $Ni(COD)_2/PCy_3$ Catalyst System: Intermolecular Coupling, Room Temperature**

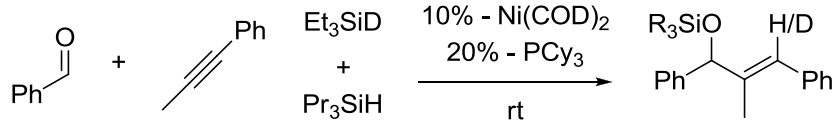


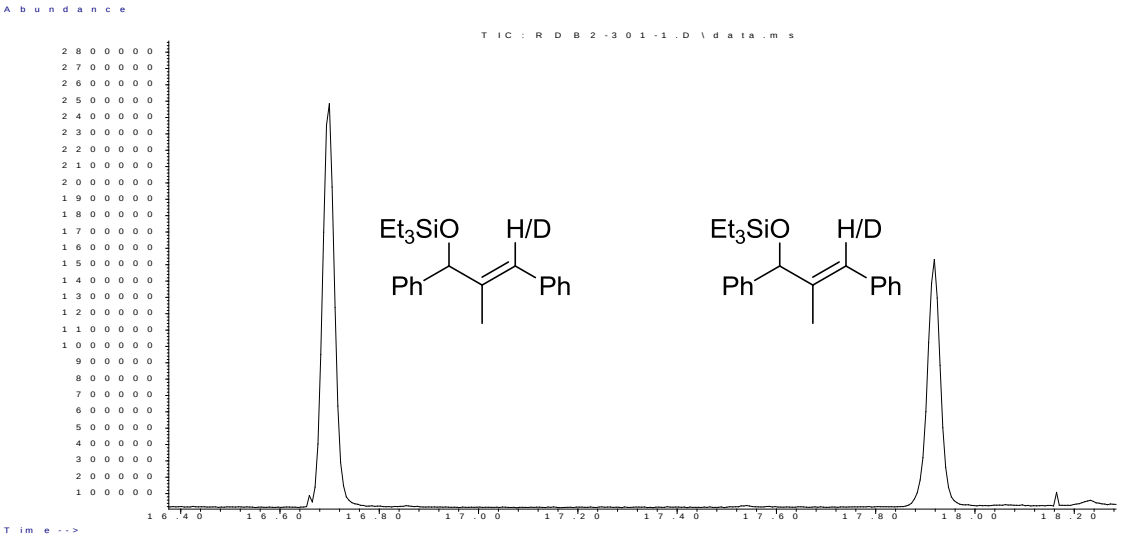


Signal : TIC: RDB2-301-1.D\data.ms

| peak # | R.T. min | first scan | max scan | last scan | PK TY | peak height | corr. area | corr. % max. | % of total |
|---|---|---|---|---|---|---|---|---|---|
| 1 | 16.699 | 2374 | 2380 | 2398 | M | 2496549 | 42599897 | 100.00% | 59.492% |
| 2 | 17.918 | 2581 | 2593 | 2605 | M | 1524273 | 29005873 | 68.09% | 40.508% |

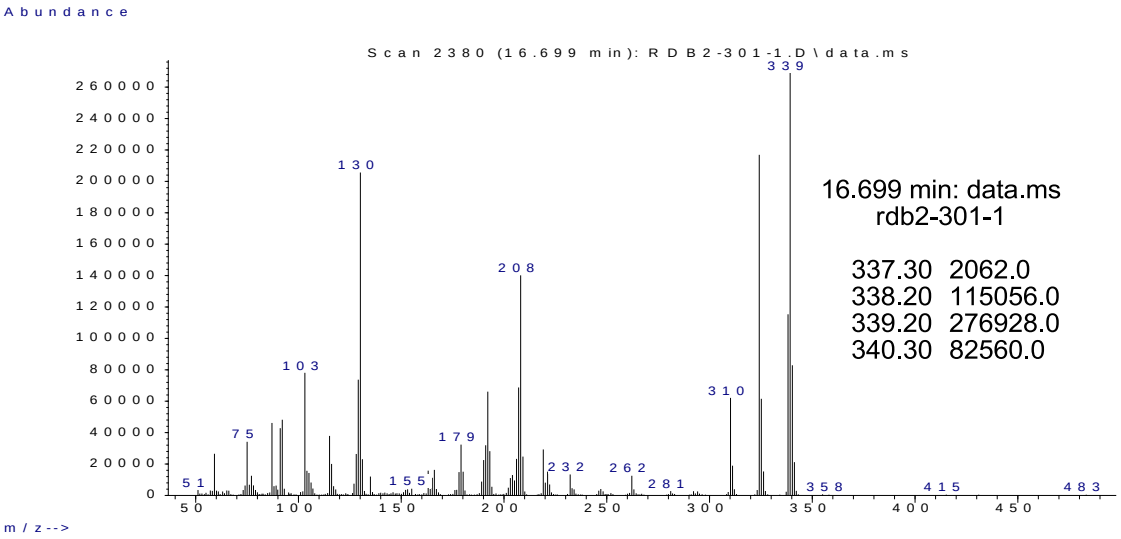

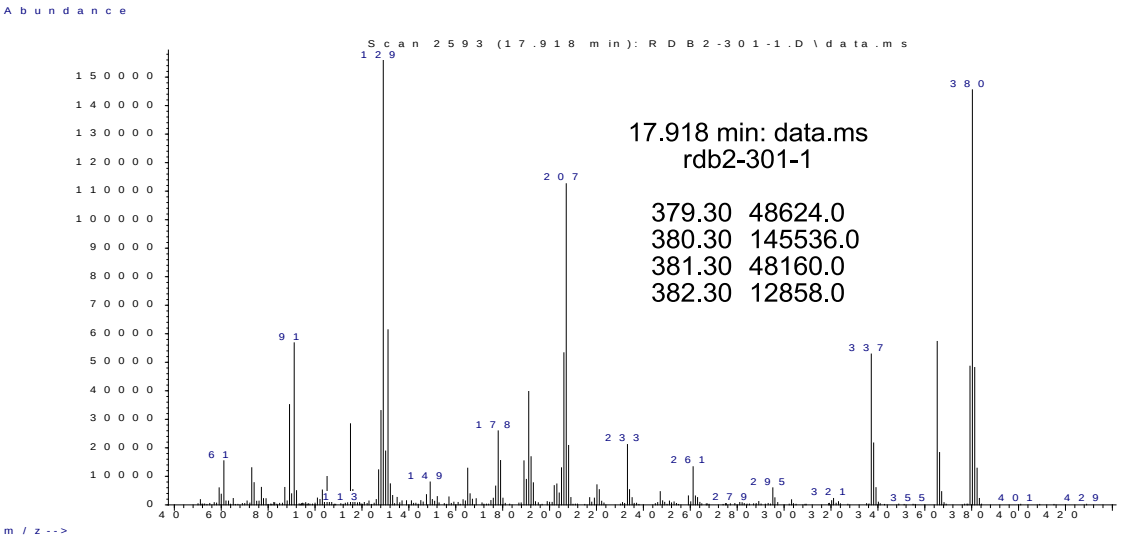
Abundance
Scan 2593 (17.918 min): RDB2-301-1.D\data.ms
17.918 min: data.ms
rdb2-301-1
379.30 48624.0
380.30 145536.0
381.30 48160.0
382.30 12858.0
m/z-->

## Crossover with a $Ni(COD)_2/PCy_3$ Catalyst System: Intermolecular Coupling -25 $^oC$

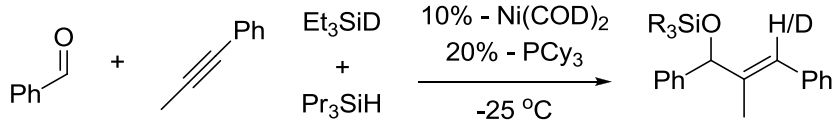


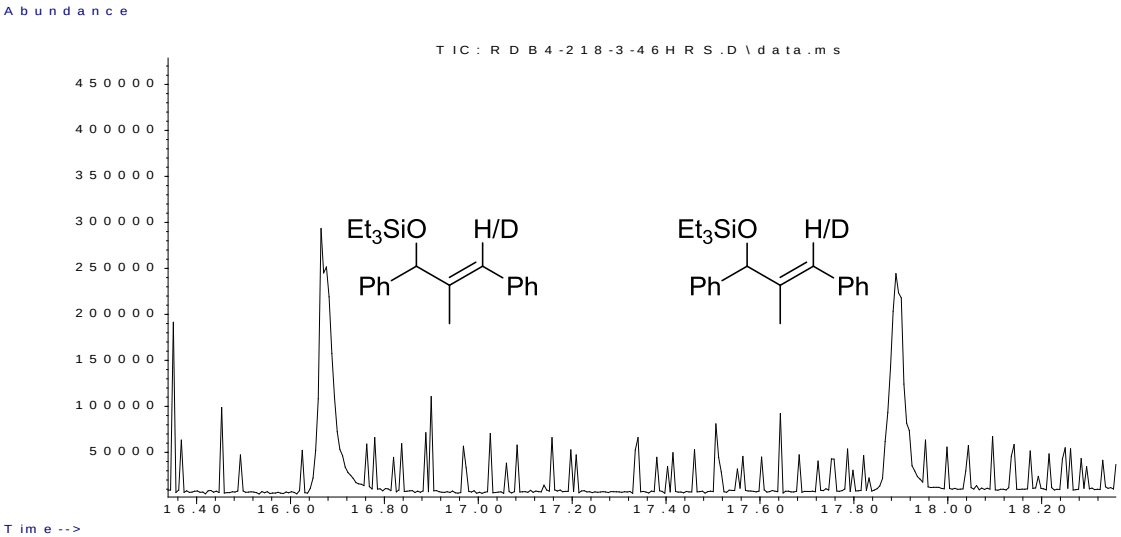


Signal : TIC: RDB4-218-3-46HRS.D\data.ms

| peak # | R.T. min | first scan | max scan | last scan | PK TY | peak height | corr. area | corr. % max. | % of total |
|---|---|---|---|---|---|---|---|---|---|
| 1 | 16.665 | 2369 | 2374 | 2396 | M2 | 300039 | 6496744 | 100.00% | 53.541% |
| 2 | 17.890 | 2579 | 2588 | 2605 | M2 | 239956 | 5637391 | 86.77% | 46.459% |

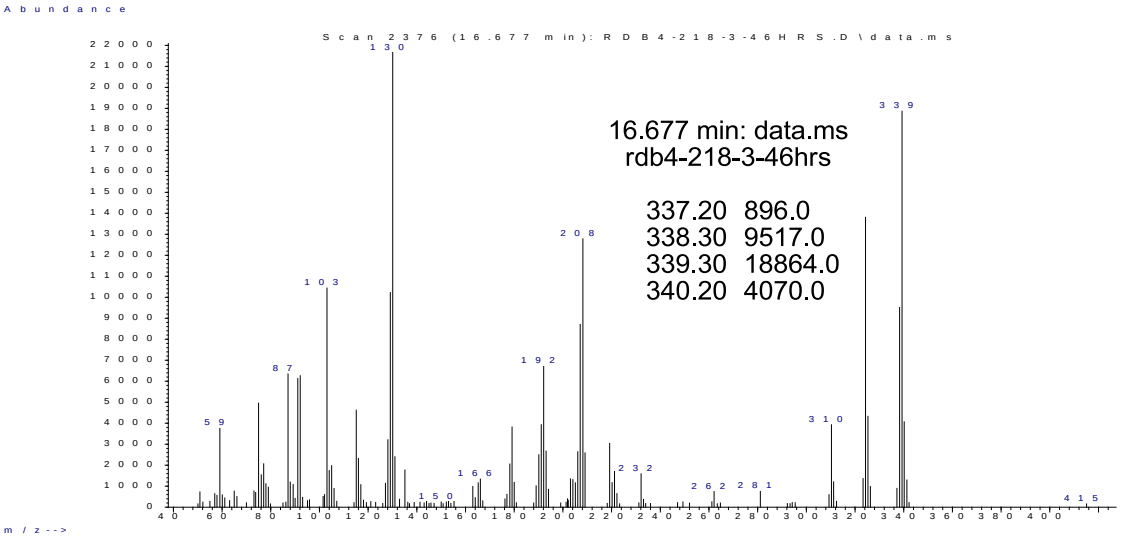

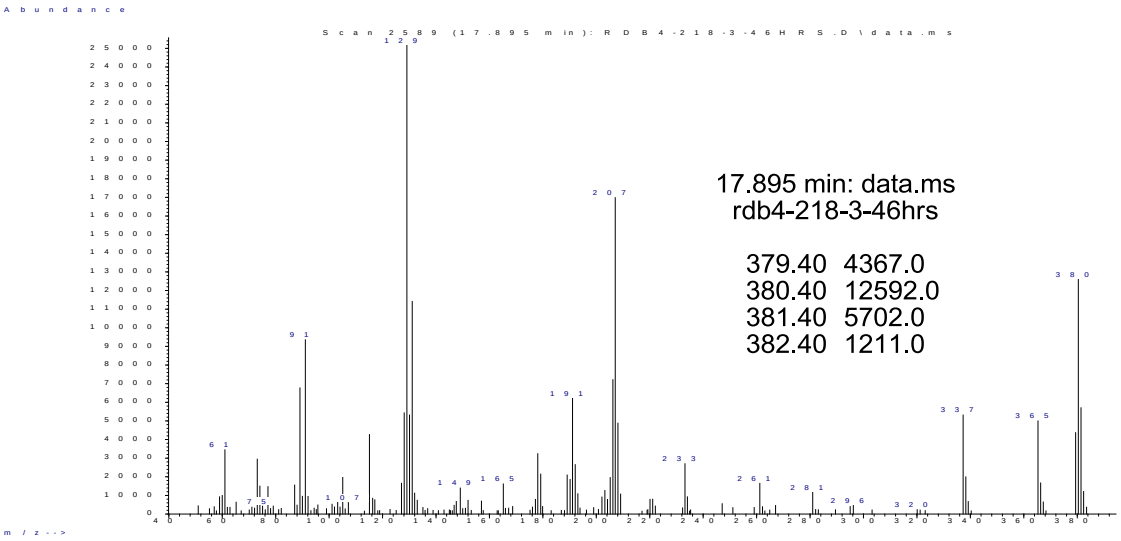


### 5.3.4 DFT Calculations of Possible Reaction Pathways

Calculations were performed on Gaussian 03 and 09 via remote computer clusters owned by the Center for Advanced Computing at the University of Michigan - Ann Arbor. Molecular geometries of optimized structures were visualized using Gaussview 4.1.2 software. All of the geometry optimizations and frequency calculations were performed with the B3LYP functional implemented in Gaussian 03 (Frisch, M. J.; et al. *Gaussian 03*, revision D.01; Gaussian, Inc.: Pittsburgh, PA, 2004). The LANL2DZ basis set was used for nickel and the 6-31G(d) basis set for the other atoms.

**Structure 58 (Alkyne Bound)**

```
Zero-point correction=                           0.436996
(Hartree/Particle)
 Thermal correction to Energy=                    0.467273
 Thermal correction to Enthalpy=                  0.468217
 Thermal correction to Gibbs Free Energy=         0.370191
 Sum of electronic and zero-point Energies=          -1630.781458
 Sum of electronic and thermal Energies=             -1630.751182
 Sum of electronic and thermal Enthalpies=           -1630.750237
 Sum of electronic and thermal Free Energies=        -1630.848264
 Center     Atomic     Atomic              Coordinates (Angstroms)
```

| Number | Number | Type | X | Y | Z |
|---|---|---|---|---|---|
| 1 | 6 | 0 | -0.895503 | 0.501329 | -0.698036 |
| 2 | 6 | 0 | 0.190004 | 1.128017 | -0.400070 |
| 3 | 6 | 0 | 0.882684 | 2.400983 | -0.313983 |
| 4 | 6 | 0 | 1.495796 | 2.972351 | -1.447391 |
| 5 | 6 | 0 | 0.966660 | 3.102006 | 0.905987 |
| 6 | 6 | 0 | 2.161270 | 4.194845 | -1.362427 |
| 7 | 1 | 0 | 1.442032 | 2.443828 | -2.395417 |
| 8 | 6 | 0 | 1.630250 | 4.325706 | 0.985549 |
| 9 | 1 | 0 | 0.499558 | 2.674911 | 1.789506 |
| 10 | 6 | 0 | 2.234066 | 4.879149 | -0.146438 |
| 11 | 1 | 0 | 2.623652 | 4.616246 | -2.252032 |
| 12 | 1 | 0 | 1.675272 | 4.849891 | 1.937325 |
| 13 | 1 | 0 | 2.753930 | 5.831291 | -0.081916 |
| 14 | 6 | 0 | -2.303627 | 0.730643 | -1.140433 |
| 15 | 1 | 0 | -2.335281 | 1.595664 | -1.821438 |
| 16 | 1 | 0 | -2.677466 | -0.127363 | -1.717930 |
| 17 | 6 | 0 | -3.257440 | 0.992437 | 0.042020 |
| 18 | 1 | 0 | -3.237489 | 0.140594 | 0.730466 |
| 19 | 1 | 0 | -2.894329 | 1.851336 | 0.617114 |
| 20 | 6 | 0 | -4.695331 | 1.250952 | -0.409792 |
| 21 | 1 | 0 | -4.761703 | 2.139087 | -1.058648 |
| 22 | 1 | 0 | -5.076250 | 0.423735 | -1.032519 |
| 23 | 8 | 0 | -5.417285 | 1.359745 | 1.897722 |
| 24 | 6 | 0 | -5.683500 | 1.440792 | 0.718607 |
| 25 | 1 | 0 | -6.725221 | 1.666348 | 0.390617 |
| 26 | 28 | 0 | 0.415394 | -0.751903 | -0.136562 |
| 27 | 6 | 0 | -2.327833 | -2.860354 | 0.234274 |
| 28 | 1 | 0 | -2.923258 | -2.121306 | -0.308452 |
| 29 | 1 | 0 | -2.741041 | -3.859486 | 0.050586 |
| 30 | 1 | 0 | -2.404790 | -2.633028 | 1.302400 |
| 31 | 6 | 0 | -0.675701 | -3.371080 | -2.043700 |
| 32 | 1 | 0 | 0.328074 | -3.475873 | -2.467698 |
| 33 | 1 | 0 | -1.189401 | -4.338771 | -2.097756 |
| 34 | 1 | 0 | -1.219294 | -2.641701 | -2.652466 |
| 35 | 6 | 0 | 0.128632 | -4.244629 | 0.555198 |
| 36 | 1 | 0 | 0.157259 | -4.072492 | 1.636305 |
| 37 | 1 | 0 | -0.477476 | -5.136933 | 0.357612 |
| 38 | 1 | 0 | 1.151854 | -4.435350 | 0.214962 |
| 39 | 6 | 0 | 3.586191 | -2.143756 | -0.559326 |
| 40 | 1 | 0 | 4.603479 | -2.241733 | -0.161562 |
| 41 | 1 | 0 | 3.146404 | -3.142170 | -0.653362 |
| 42 | 1 | 0 | 3.639609 | -1.704666 | -1.560973 |
| 43 | 6 | 0 | 2.781311 | -1.877480 | 2.179612 |
| 44 | 1 | 0 | 2.318507 | -2.868920 | 2.193042 |
| 45 | 1 | 0 | 3.846479 | -1.979002 | 2.420293 |
| 46 | 1 | 0 | 2.300133 | -1.271317 | 2.954134 |
| 47 | 6 | 0 | 3.611427 | 0.410875 | 0.697281 |
| 48 | 1 | 0 | 3.176417 | 1.105165 | 1.421815 |
| 49 | 1 | 0 | 4.621900 | 0.133325 | 1.020018 |
| 50 | 1 | 0 | 3.667396 | 0.937748 | -0.259815 |
| 51 | 15 | 0 | -0.554694 | -2.738233 | -0.300602 |
| 52 | 15 | 0 | 2.517504 | -1.073796 | 0.523681 |

**Structure 59 (Ald/Alk bound)**

Zero-point correction= 0.322650
(Hartree/Particle)
Thermal correction to Energy= 0.344068
Thermal correction to Enthalpy= 0.345012
Thermal correction to Gibbs Free Energy= 0.270815
Sum of electronic and zero-point Energies= -1169.776053
Sum of electronic and thermal Energies= -1169.754636
Sum of electronic and thermal Enthalpies= -1169.753692
Sum of electronic and thermal Free Energies= -1169.827889

| Center Number | Atomic Number | Atomic Type | Coordinates (Angstroms) X | Y | Z |
|---|---|---|---|---|---|
| 1 | 28 | 0 | -0.921392 | 0.034445 | -0.198788 |
| 2 | 6 | 0 | 0.788523 | -0.819574 | -0.230067 |
| 3 | 6 | 0 | -0.168742 | -1.665102 | -0.386463 |
| 4 | 6 | 0 | 2.219232 | -0.607184 | -0.107393 |
| 5 | 6 | 0 | 3.047153 | -1.592119 | 0.470209 |
| 6 | 6 | 0 | 2.825419 | 0.582146 | -0.554146 |
| 7 | 6 | 0 | 4.420273 | -1.392048 | 0.595047 |
| 8 | 1 | 0 | 2.594432 | -2.512978 | 0.827692 |
| 9 | 6 | 0 | 4.200681 | 0.777592 | -0.437571 |
| 10 | 1 | 0 | 2.198681 | 1.343564 | -1.009395 |
| 11 | 6 | 0 | 5.005898 | -0.206760 | 0.140977 |
| 12 | 1 | 0 | 5.037289 | -2.164868 | 1.047451 |
| 13 | 1 | 0 | 4.646272 | 1.701533 | -0.798598 |
| 14 | 1 | 0 | 6.077251 | -0.052103 | 0.238215 |
| 15 | 6 | 0 | -0.741329 | -2.994378 | -0.715468 |
| 16 | 1 | 0 | -1.242083 | -2.910803 | -1.692416 |
| 17 | 1 | 0 | 0.036320 | -3.763187 | -0.836154 |
| 18 | 6 | 0 | -1.782737 | -3.507891 | 0.310853 |
| 19 | 1 | 0 | -2.378156 | -4.302566 | -0.155683 |
| 20 | 1 | 0 | -1.269858 | -3.961026 | 1.167847 |
| 21 | 6 | 0 | -2.719241 | -2.413743 | 0.894679 |
| 22 | 1 | 0 | -3.509809 | -2.904651 | 1.477520 |
| 23 | 1 | 0 | -2.130910 | -1.768375 | 1.556359 |
| 24 | 6 | 0 | -2.540321 | 3.035028 | 0.640705 |
| 25 | 1 | 0 | -2.442291 | 4.120716 | 0.759643 |
| 26 | 1 | 0 | -3.305107 | 2.826645 | -0.114700 |
| 27 | 1 | 0 | -2.880109 | 2.604753 | 1.588731 |
| 28 | 6 | 0 | -0.472100 | 3.304945 | -1.309179 |
| 29 | 1 | 0 | -1.163647 | 3.118830 | -2.137417 |
| 30 | 1 | 0 | -0.496035 | 4.371895 | -1.055893 |
| 31 | 1 | 0 | 0.533997 | 3.042637 | -1.650629 |
| 32 | 6 | 0 | 0.203996 | 2.882644 | 1.444981 |
| 33 | 1 | 0 | 0.178853 | 3.977218 | 1.510974 |
| 34 | 1 | 0 | -0.080229 | 2.460735 | 2.414596 |
| 35 | 1 | 0 | 1.225502 | 2.555806 | 1.227879 |
| 36 | 15 | 0 | -0.939876 | 2.234520 | 0.136028 |
| 37 | 6 | 0 | -3.355748 | -1.521275 | -0.132713 |
| 38 | 1 | 0 | -4.314453 | -1.841741 | -0.580323 |
| 39 | 8 | 0 | -2.875568 | -0.449748 | -0.500844 |

### 5.3.5 Procedure for Manipulating and Interpreting Rate Data Using *In Situ* React-IR™

*In situ* React-IR™ was used to monitor the progression of intramolecular nickel-catalyzed reductive aldehyde/alkyne couplings for the purpose of determining initial rates. This method of reaction monitoring was preferred over GC analysis for two important reasons. First, the rapid rate of reaction precluded accurate measurements of initial rates via GC due to the inefficiency of manual sampling (no more than one aliquot per minute could consistently be removed by hand). Second, due to the air- and moisture sensitivity of nickel-catalyzed processes, *in situ* reaction monitoring was preferred over manual removal of reaction aliquots by syringe to maintain the integrity of reactions.

For the intramolecular nickel-catalyzed reductive coupling of ynals with silane reducing agents, reaction rates were determined by tracking the disappearance of starting material via the distinctive IR stretching frequency of the aldehyde C=O bond of **29** at 1728 $cm^{-1}$ (Scheme 100). No distinctive IR stretches were observed in the silyl-protected allylic alcohol that would allow for determination of initial rates by tracking product appearance.

**Scheme 100.** Intramolecular Nickel-Catalyzed Aldehyde/Alkyne Coupling

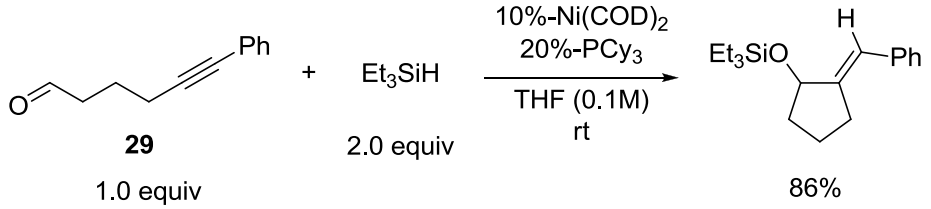


A solvent subtracted spectrum of ynal starting material **29** is shown in Figure 24. The aldehyde C=O stretch at 1728 $cm^{-1}$ meets two important criteria for choosing an

appropriate peak to monitor via React-IR$^{TM}$; it exhibits a strong absorbance that can be easily separated from background noise, and appears at a location in the spectrum that is not confounded by overlapping peaks arising from other species in the reaction medium.

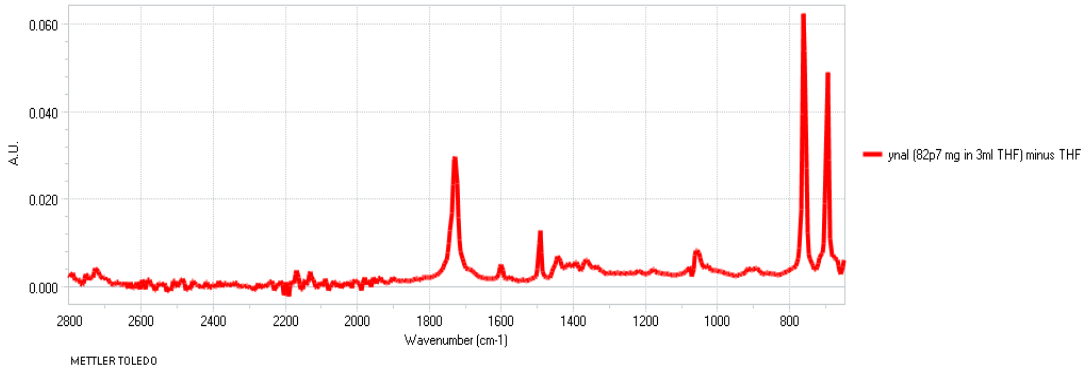


**Figure 24.** Spectrum of Ynal Starting Material (THF subtracted)

For this particular reaction, it was necessary to acquire data at low temperature due to the rapid rate of starting material consumption. In this case, the reaction vessel was placed in a Neslab CB-60 Cryobath set to -30$^{o}$C and allowed to stir until the internal temperature had equilibrated before the injection of organic reagents. For experimental setup, see Figure 25.

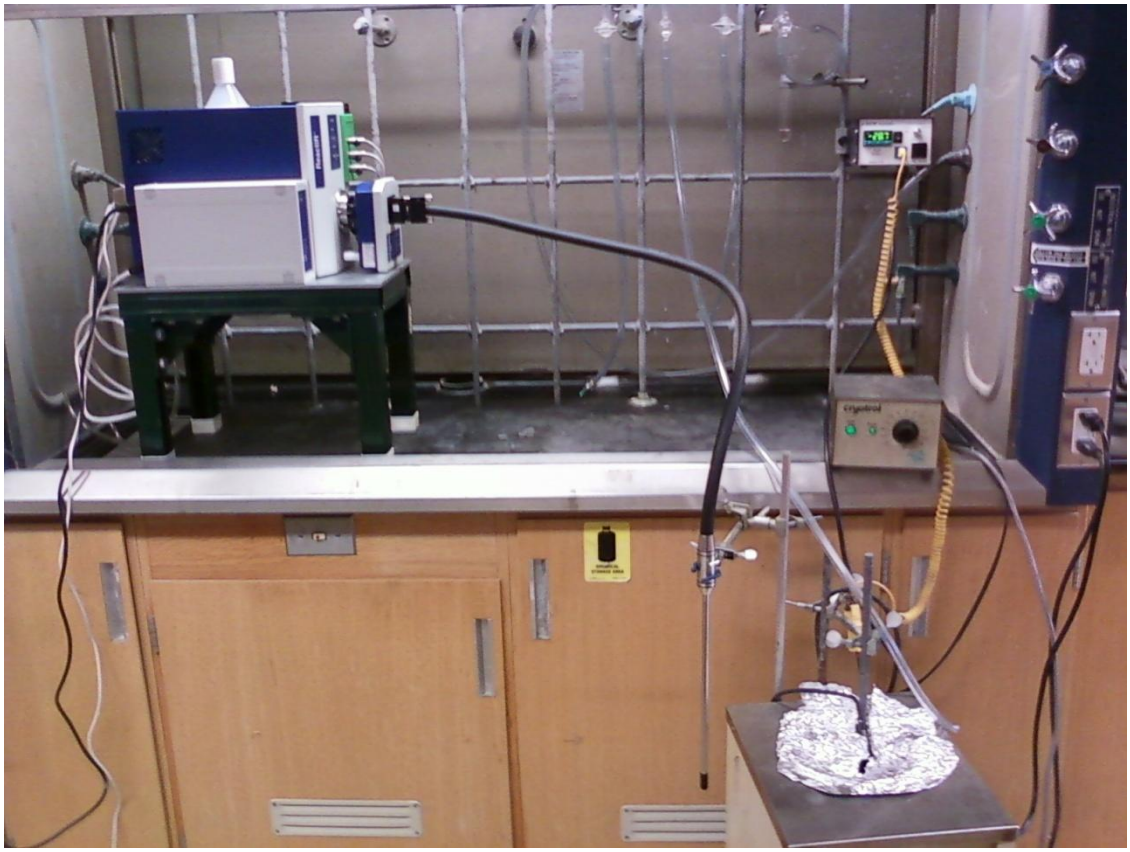

**Figure 25.** Experimental Setup for Low Temperature Reaction Monitoring via React-IR™

In all cases, the cryobath temperature was monitored using an external J-Kem thermocouple probe (readout in upper right corner of Figure 25). Internal reaction temperature was monitored directly via the React-IR probe and visualized in the "Trends" window as "RTD1" in the iC software package that runs the React-IR from an externally connected PC. As stated previously, the internal temperature of the reaction vessel was allowed to equilibrate before starting the reaction; this equilibration is shown in Figure 26.

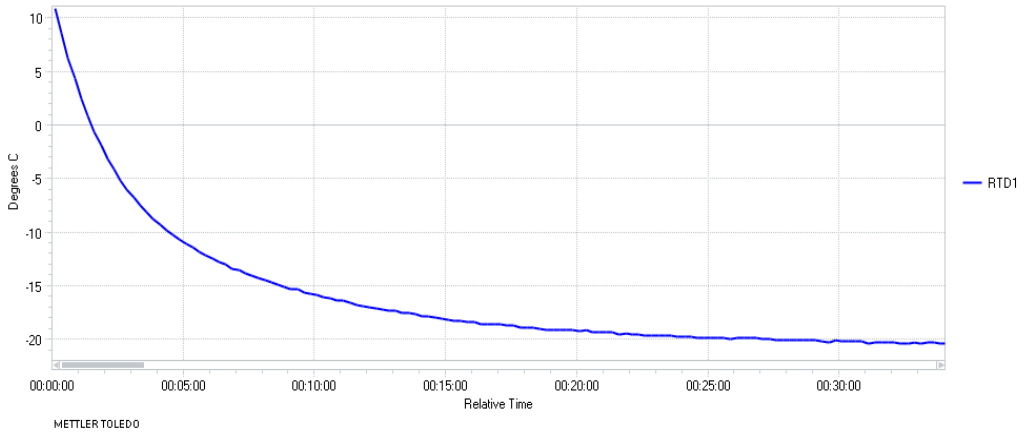


**Figure 26.** Equilibration of Internal Temperature

As seen in Figure 26, it takes approximately 35-40 minutes for a 0.02 M catalyst solution in THF (4ml total volume) to stabilize. Once the internal temperature has stabilized, the organic reagents were added via syringe to the reaction vessel and allowed to react. The absorbance of the C=O ynal stretch could then be monitored by "pinning" the peak at 1728 $cm^{-1}$ from a solvent subtracted spectrum in the "Spectra" window of the iC software (spectra are acquired at timed intervals that are determined during experimental setup). Peaks at any wavelength can be pinned either during a reaction or after the experiment has completed. Once a peak has been pinned it's absorbance will be graphed as a function of time in the "Trends" window of the iC software. A solvent subtracted spectrum acquired shortly after the addition of organic reagents is shown in Figure 27. The vertical highlighted bar at 1728 $cm^{-1}$ shows that the aldehyde peak has been pinned. The change in aldehyde absorbance as a function of time is shown in Figure 28.

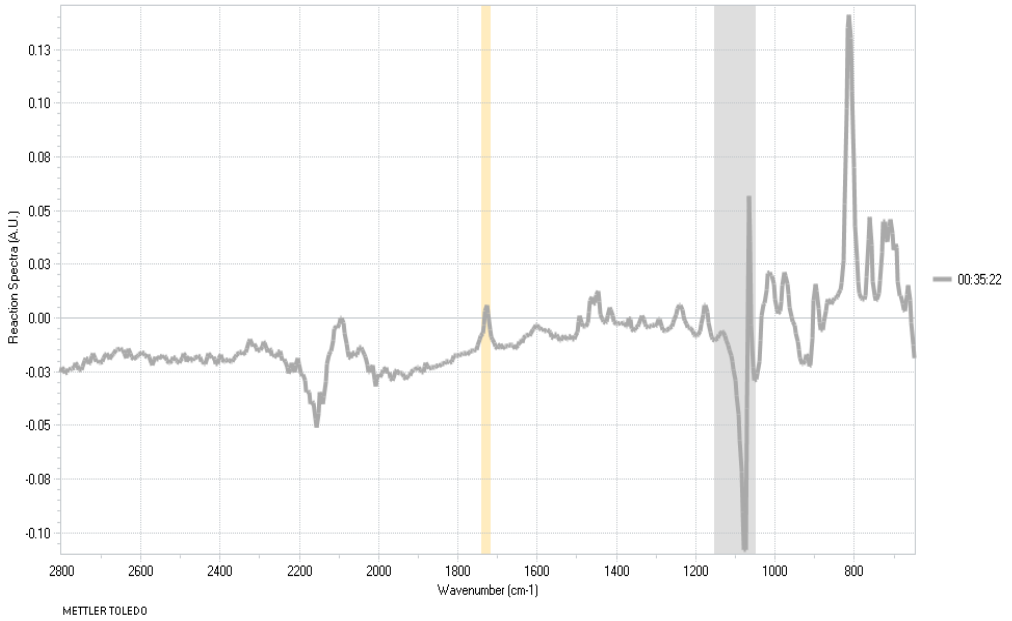


**Figure 27.** Solvent Subtracted Spectrum of Reaction Mixture

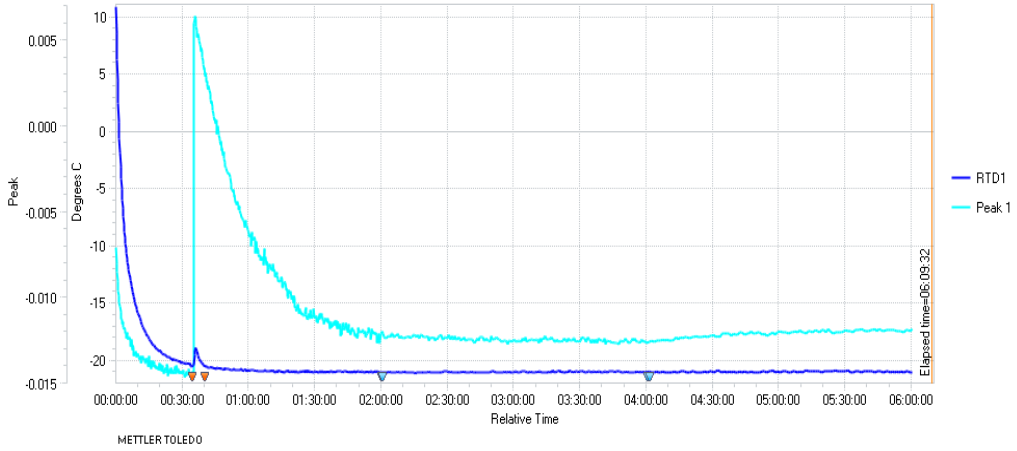


**Figure 28.** "Trends" of Internal Temperature and Aldehyde Absorbance as a Function of Time

The internal temperature of the reaction increases approximately 1.5 $^{o}$C upon the addition of the organic reagents but rapidly stabilizes and remains consistent through the remainder of the experiment. As seen in Figure 28, the absolute value of the absorbance at 1728 cm$^{-1}$ equilibrates to a minimum value as the internal temperature of the reaction

vessel stabilizes. To standardize the absorbance values at 1728 $cm^{-1}$, a baseline correction is performed by choosing a wavelength within the spectral window (shown to be stable in the raw data throughout the reaction) as an artificial 'zero' for every spectrum (in "data treatments" window of software). This ensures that instrumental fluctuations are accounted for. The absorbance values of the ynal C=O stretch can then be imported into Excel for analysis by right-clicking the desired signal from the "Trends" window and copying to the clipboard, pasting into a word or notepad file and transferring to a personal computer (usually via a USB jump drive). This data can then be pasted into an Excel spreadsheet to assign a numerical value to the initial rate (Δynal/Δtime) of the reaction being studied (Figure 29).

| 198-20% | Peak 1 |
|---|---|
| 0:00:06 | -0.0042 |
| 0:00:21 | -0.00197 |
| 0:00:36 | -0.00673 |
| 0:00:51 | -0.00864 |
| 0:01:06 | -0.01082 |
| 0:01:21 | -0.01285 |

**Figure 29.** Absorbance Values of Peak at 1728 $cm^{-1}$ Imported Into Excel

For kinetic interpretation, the absorbance value at the time point prior to addition of the ynal is given a value of zero in excel, and subsequent absorbance values are corrected by the same factor (Figure 30). This correction factor is necessary since the chosen value for the baseline corrected value may not be a 'true zero' when measuring the baseline to peak height value of the peak at 1728 $cm^{-1}$.

| | | |
|---|---|---|
| 0:34:21 | -0.02221 | 7.75007E-05 |
| 0:34:36 | -0.022 | 0.000289607 |
| 0:34:51 | -0.02241 | -0.000126406 |
| 0:35:06 | -0.02229 | 0 |
| 0:35:21 | -0.0173 | 0.00498777 |
| 0:35:36 | -0.00169 | 0.020591465 |
| 0:35:51 | -0.00178 | 0.020502638 |
| 0:36:06 | -0.00196 | 0.020322897 |
| 0:36:21 | -0.00207 | 0.020212581 |

**Figure 30.** Baseline Corrected Absorbance Values at 1728 $cm^{-1}$

As shown in Figure 30, the only mathematical manipulation of the absorbance data is the addition of a numerical constant. Reaction rates calculated from either data set would necessarily yield identical values. The correction is done for the purpose of overlaying graphs acquired from separate reactions, allowing for direct comparison of absolute absorbance values.

Generally, only the first 10-20% of a reaction is studied for the purposes of comparing initial rates. To obtain an initial rate from the data shown in Figure 30, a straight line is plotted between the maximum absorbance and the point that represents 10-20% consumption of ynal starting material (Figure 31). Whatever percent conversion is chosen for the calculation of initial rates, it is important to remain consistent when examining differing reaction conditions. The slope of this line shown in Figure 31 is the initial rate for this particular set of reaction conditions (in units of change in absorbance per unit time) and can be compared to the initial rates of other reactions when varying one of the reactive components (note that the x-axis is plotted in units of seconds instead of the 'hours:minutes:seconds' format given by the IR software).

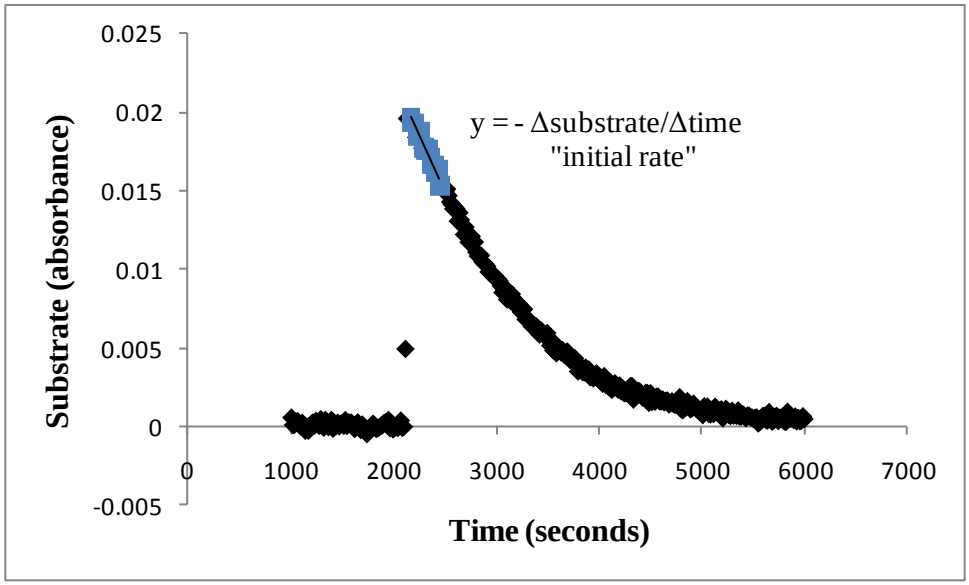


**Figure 31.** Initial Rate Superimposed on Reaction Progression Plot

In this way, by varying the concentration of the starting catalyst mixture while holding the concentrations of the ynal substrate and silane constant, one can gain insight into the affect catalyst concentration has on the rate of reaction across a range of catalyst concentrations. Traditionally, this data is used to determine the molecularity of the reactive components that participate in a given reaction. A graph of initial rate versus the concentration of the species being varied will give an indication of whether reaction order with respect to this species is greater than, equal to, or less than one (Figure 32).

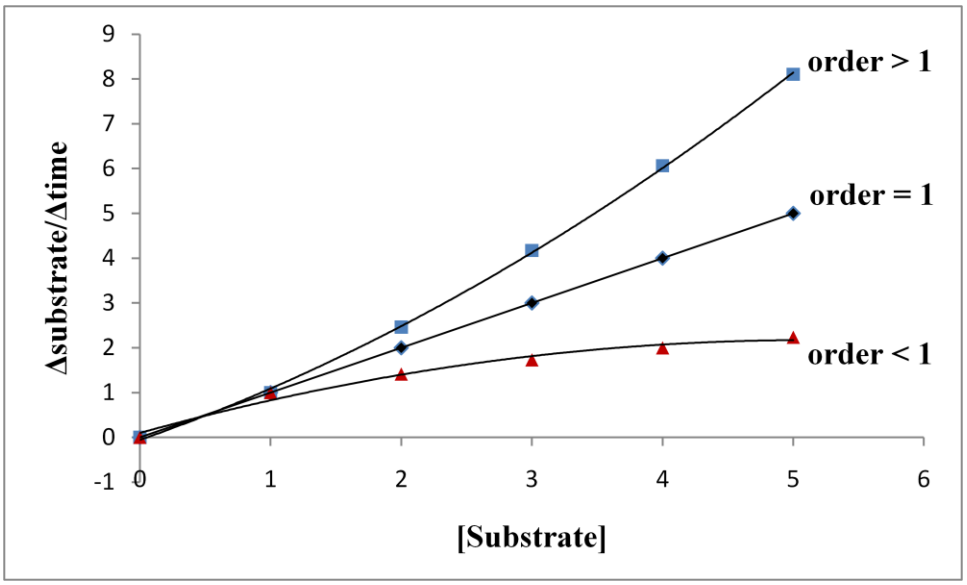


**Figure 32.** Graph Shape Changing with Substrate Order

The absolute value for the order in a given substrate can be determined directly by graphing the natural log of the observed rates versus the natural log of the substrate concentrations (due to the mathematical relationship between the natural log function and d[substrate]/dt) (Figure 33).

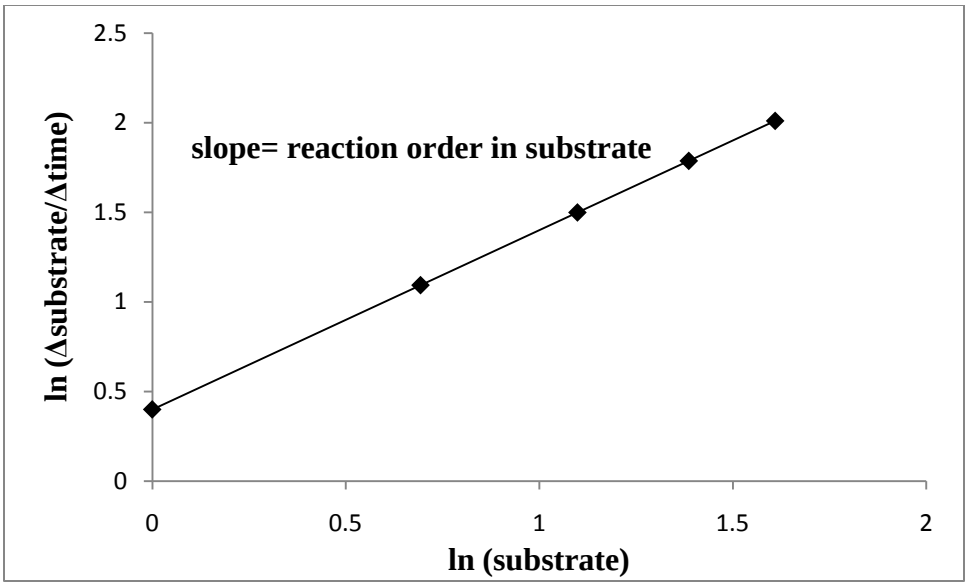


**Figure 33.** Natural Log Plot Yielding Reaction Order

Conversely, the order with respect to a reactive species can be calculated from a graph analogous to Figure 32 by plotting observed rates of reaction at various concentrations of the species being studied and fitting the data to a line with the equation y = ax^b + c. Solving for the value of 'b' yields the reaction order with respect to the species being varied (done in the plotting program SigmaPlot).

In scientific literature, reaction rates are generally expressed as a change in concentration per unit time. Because the infrared absorbance of an organic species is directly related to its concentration by Beer's Law, a simple calibration factor is all that's necessary to convert absorbance values to molar concentration. To ensure that there exists a linear dependence between ynal concentration and absorbance across the concentration range being studied in this particular reaction, it was necessary to create a calibration curve from a series of stock solutions of known substrate concentration.

Using the 'Spectral Library' feature of the iC software, a series of individual solvent-subtracted spectra were obtained (Figure 34).

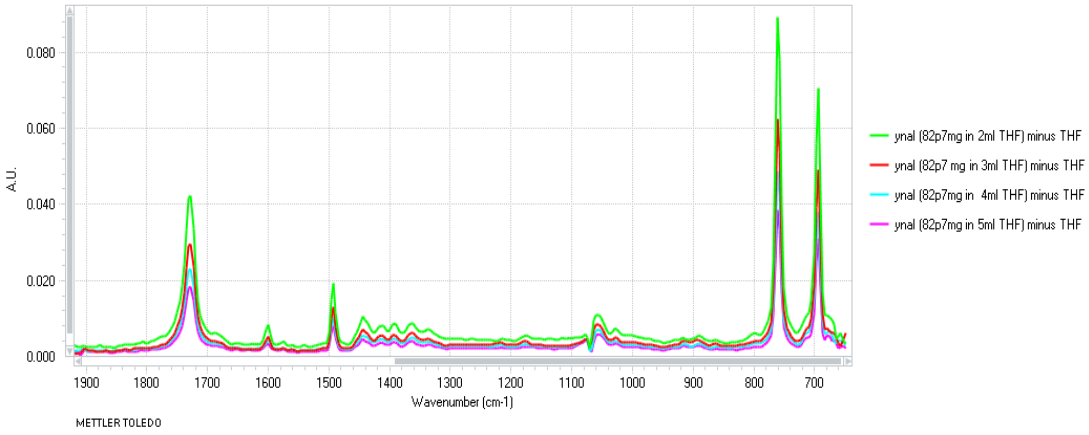


**Figure 34.** Spectra of Ynal Generated From Stock Solutions of Known Concentration

Graphing absorbance values (maximum peak value at 1728 $cm^{-1}$ minus baseline value) versus molar concentration yields a straight line with a high $R^2$ value showing that absorbance is directly related to concentration via a liner relationship in the desired concentration range (Figure 35).

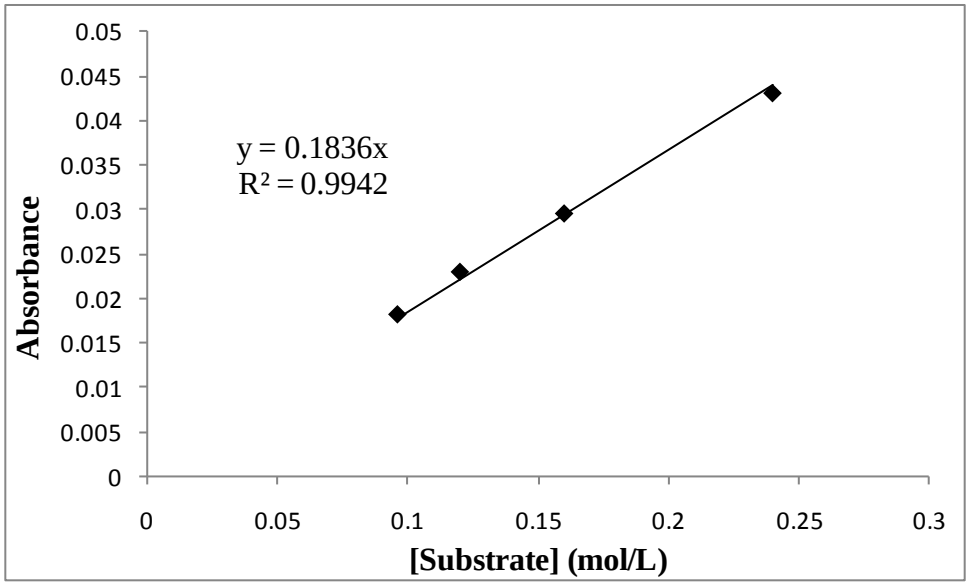


**Figure 35.** Graph of Absorbance versus Molar Concentration of Substrate

Analogous to the baseline correction factor, changing from absorbance to molar concentration will not affect the comparison of rate data from one reaction to the next; the relative difference in rates will remain the same whether d[substrate]/dt is measured in absorbance or molar concentration (only the *absolute* values of initial rate will change).

Throughout the course of studying the effect of varying substrate concentration on the rate of reductive coupling, initial absorbance values of various substrate concentrations at early stages of reaction will effectively yield the same calibration data described in Figure 34 and Figure 35. Across the range of concentrations studied for this particular reaction, the calibration curve generated from experimental data is in agreement with the one generated from stock solutions (Figure 36).

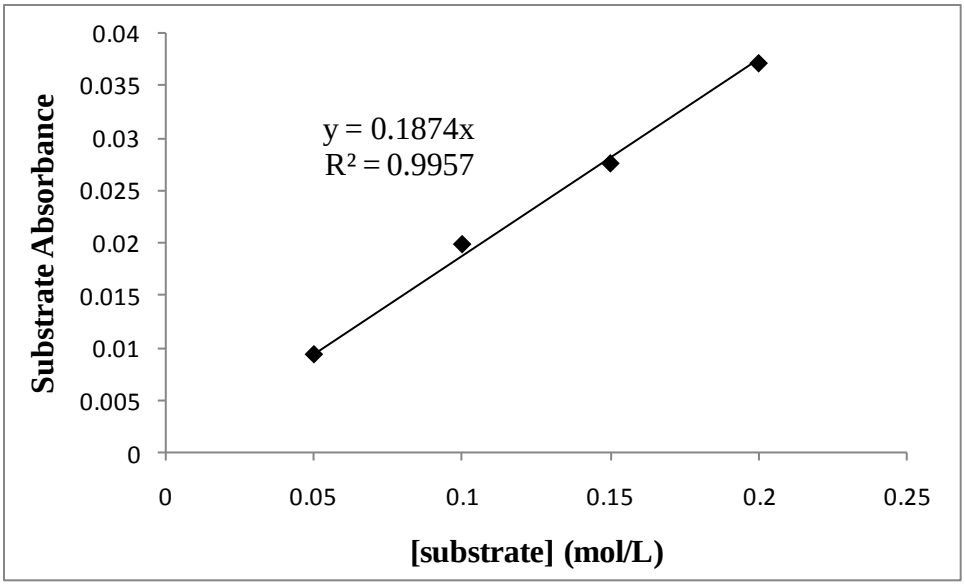


**Figure 36.** Calibration Curve Generated from Experimental Data

From either calibration curve, changes in absorbance per unit time can be converted into changes in concentration per unit time by the correction factor indicated by the slope of the line.

### 5.3.6 Experimental Procedures and Spectral Data for Mechanistic Study Under Synthetic Conditions

All reagents were used as received unless otherwise noted. Solvents were purified under nitrogen using a solvent purification system (Innovative Technology, inc., Model # SPS-400-3 and PS-400-3). Ynal **29** was prepared from the corresponding alcohol using standard PCC oxidation conditions, filtered through a short plug of layered silica/alumina/celite, and purified via column chromatography (80:20 Hexanes:EtOAc) immediately before each use. Nickel cyclooctadiene ($Ni(COD)_2$, Strem Chemicals, Inc) and tricyclohexyl phosphine ($PCy_3$, Aldrich) were stored and weighed in an inert atmosphere glovebox. Triethylsilane (Aldrich) was passed over a plug of basic alumina and stored under an inert atmosphere. Triethylsilane-d (Aldrich) was stored under an inert

atmosphere and used as received. All reactions were conducted in flame-dried glassware under a nitrogen atmosphere. NMR spectra were obtained in $CDCl_3$ at room temperature (22 $^oC$), unless otherwise noted, on a Varian Inova 400MHz, or Unity 500 MHz instrument. Chemical shifts of $^1H$ NMR spectra were recorded in parts per million (ppm) on the δ scale from an internal standard of tetramethylsilane (TMS, 0.0 ppm). *In situ* FTIR rate data were acquired on a Mettler-Toledo React-IR$^{TM}$ 45m module fitted with a 9.5mm diamond-tipped probe; silane monitoring experiments were performed using a 9.5mm silicon-composite probe. Rate data was manipulated as described in Section 5.3.3.

#### 5.3.6.1 General Preparative Procedure: $Ni(COD)_2/PCy_3$-Catalyzed Intramolecular Aldehyde/Alkyne (Ynal) Coupling

$Ni(COD)_2$ (13.8 mg, 0.05 mmol, 0.1 equiv) and tricyclohexylphosphine (28 mg, 0.1 mmol, 0.2 equiv) were combined under an inert atmosphere and dissolved in 4 mL of THF at room temperature. Ynal substrate **29** (86 mg, 0.5 mmol, 1.0 equiv) and triethylsilane (116 mg, 1.0 mmol, 2.0 equiv) were combined in 1 mL of THF and added to the catalyst mixture as a single portion via syringe. Upon completion, the reaction mixture was quenched with 10 mL $NaHCO_3$ (sat.) and extracted 3x each with 10 mL brine and EtOAc. The organic layer was dried with anhydrous $MgSO_4$, filtered, and solvent was removed by rotary evaporation. The crude reaction mixture was purified via silica gel chromatography using 98:2 Hexanes:EtOAc to yield the desired silylated allylic alcohol (124 mg, 86%) as a colorless oil. Spectral data were identical to previous reports.[1]

### 5.3.6.2 General Procedure for Kinetic Analysis: *In Situ* IR Monitoring of Ynal Cyclization with $Ni(COD)_2/PCy_3/Et_3SiH$

$Ni(COD)_2$ (13.8 mg, 0.05 mmol, 0.1 equiv) and tricyclohexylphosphine (28.0 mg, 0.10 mmol, 0.2 equiv) were combined under an inert atmosphere in a 10 mL three-necked round-bottomed flask equipped with a three-way valve, two septa, and a teflon coated stirbar. The IR probe was inserted through the center neck of the flask via a nitrogen-purged teflon adapter under positive nitrogen pressure before adding 4 mL of THF to the catalyst mixture. The stirred catalyst mixture was then immersed in a Neslab Cryobath CB-60 at -25 $^{o}$C. Solvent subtracted spectra were acquired at 15 second intervals for approximately 35 minutes until the baseline of the IR spectrum at 1728 $cm^{-1}$ (ynal C=O peak) and internal temperature had stabilized at approximately -25 $^{o}$C. Ynal **29** (86.0 mg, 0.50 mmol, 1.0 equiv) and triethylsilane (116 mg, 1.0 mmol, 2.0 equiv) were combined in 1 mL of THF and added to the stirred catalyst as a single portion via syringe. Reaction progression was monitored by the decreasing absorbance of the ynal C=O stretch as a function of time. Correlation of ynal disappearance to product appearance was confirmed by GCMS analysis using docosane ($C_{22}H_{46}$) as an internal standard. Absolute absorbance values were determined by the peak height at 1728 $cm^{-1}$ relative to a baseline zeroed value at 1559 $cm^{-1}$ (shown to be stable throughout the reaction). Absorbance values were converted to concentrations via a calibration curve to express rates as a change in molar concentration with respect to time. For the purpose of determining initial rates, reactions were monitored up to 30% conversion to ensure data was collected beyond at least one catalyst turnover. Analogous changes in relative rates were observed when reactions were monitored to 15% conversion.

**Data for Initial Rate vs. Concentration of Ynal 29**

Following the general procedure for kinetic analysis, $Ni(COD)_2$ (0.10 mmol) and $PCy_3$ (0.20 mmol) were reacted with ynal **29** (0.25-1.0 mmol) and $Et_3SiH$ (1.0 mmol) in 5 mL THF. Each reaction was carried out multiple times; reported values are given as the average of three runs with error expressed as the standard deviation between individual runs. Representative examples at each set of conditions are displayed below.

| [Ynal] (mol/L) | $\Delta$Ynal/$\Delta$t (M/sec) x $10^{-5}$ | Avg.$\Delta$Ynal/$\Delta$t | Std. Dev. |
|---|---|---|---|
| 0.05 | 3.56 | 3.75 | 0.33 |
| | 3.54 | | |
| | 4.13 | | |
| 0.075 | 6.24 | 5.50 | 0.58 |
| | 5.88 | | |
| | 5.11 | | |
| 0.10 | 7.60 | 7.32 | 0.26 |
| | 7.09 | | |
| | 7.27 | | |
| 0.125 | 9.65 | 9.11 | 0.76 |
| | 8.56 | | |
| | 8.07 | | |

0.05 mol/L **29**: initial rate = 3.54 x $10^{-5}$ M/sec, $R^2$ = 0.949

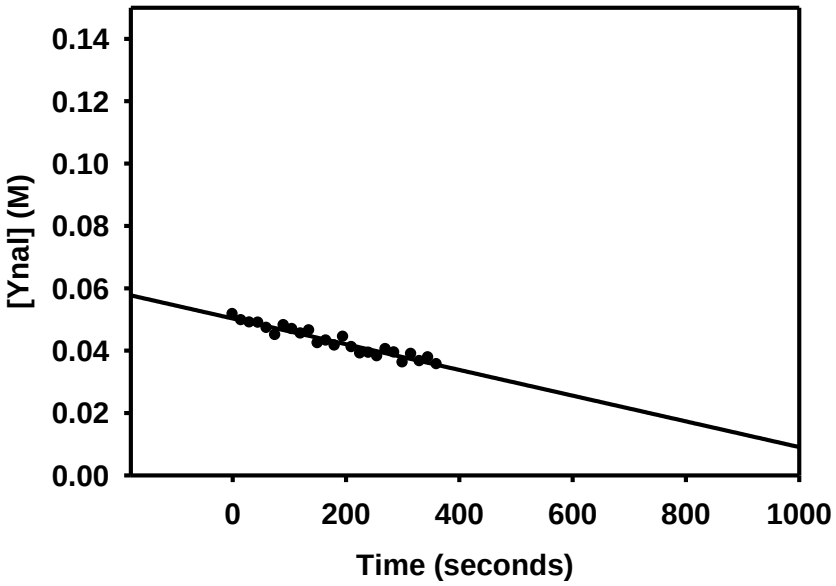


0.075 mol/L **29**: initial rate = 5.88 x $10^{-5}$ M/sec, $R^2$ = 0.932

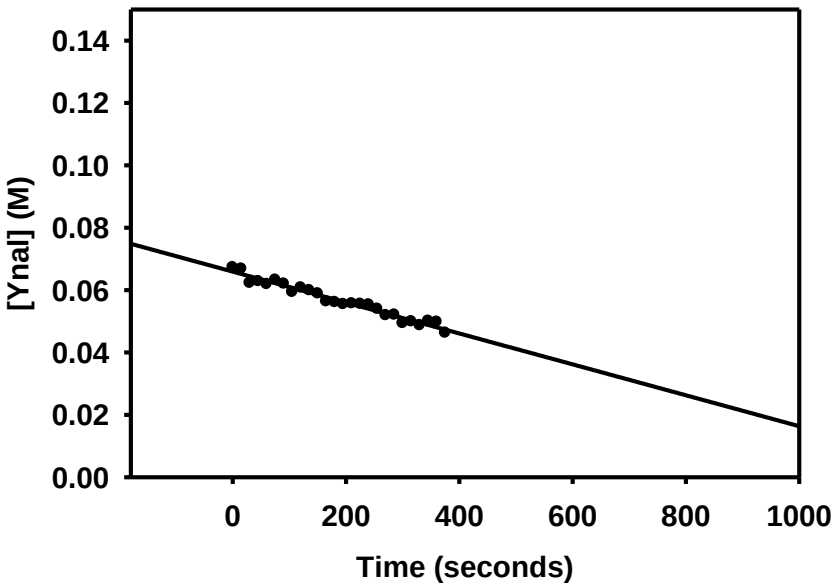

0.10 mol/L **29**: initial rate = 7.27 x $10^{-5}$ M/sec, $R^2$ = 0.984

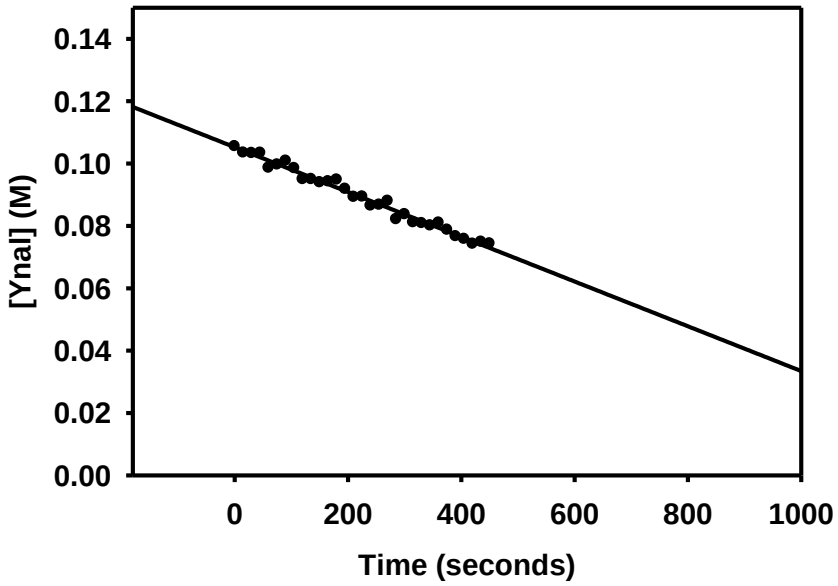


0.125 mol/L **29**: initial rate = 8.56 x $10^{-5}$ M/sec, $R^2$ = 0.938

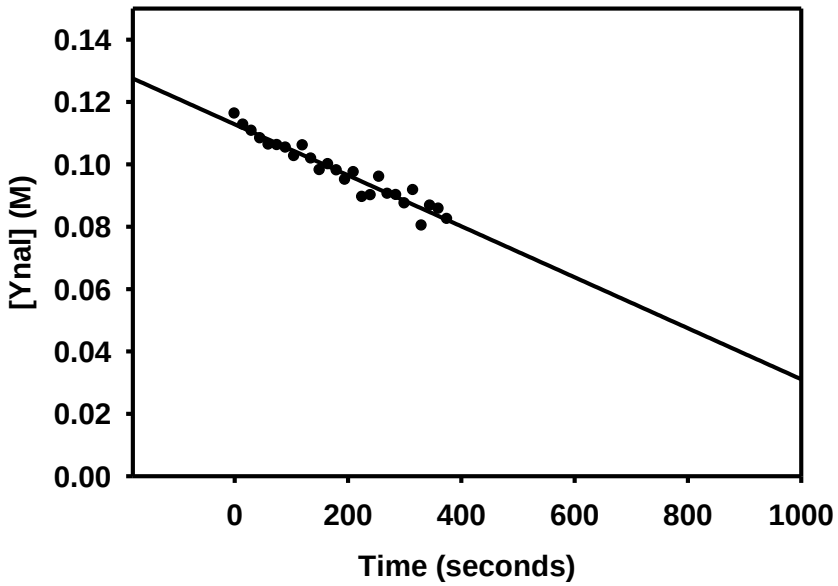

**Data for Initial Rate vs. Concentration of $Ni(COD)_2/PCy_3$**

Following the general procedure for kinetic analysis, $Ni(COD)_2$ (0.05-0.125 mmol) and $PCy_3$ (0.10-0.25 mmol) were reacted with ynal **29** (0.50 mmol) and $Et_3SiH$ (1.0 mmol) in 5 mL THF. Each reaction was carried out multiple times; reported values are given as the average of three runs with error expressed as the standard deviation between individual runs. Representative examples at each set of conditions are displayed below.

| $[Ni(COD)_2]$ (mol/L) | $\Delta$Ynal/$\Delta$t (M/sec) x $10^{-5}$ | Avg.$\Delta$Ynal/$\Delta$t | Std. Dev. |
|---|---|---|---|
| 0.01 | 3.86 | 3.83 | 0.04 |
| | 3.83 | | |
| | 3.78 | | |
| 0.015 | 5.89 | 5.56 | 0.46 |
| | 5.69 | | |
| | 5.10 | | |
| 0.02 | 7.60 | 7.32 | 0.26 |
| | 7.09 | | |
| | 7.27 | | |
| 0.025 | 9.12 | 8.96 | 0.15 |
| | 8.83 | | |
| | 8.95 | | |

0.01 mol/L $Ni(COD)_2$, 0.02 mol/L $PCy_3$: initial rate = $3.83 \times 10^{-5}$ M/sec, $R^2 = 0.979$

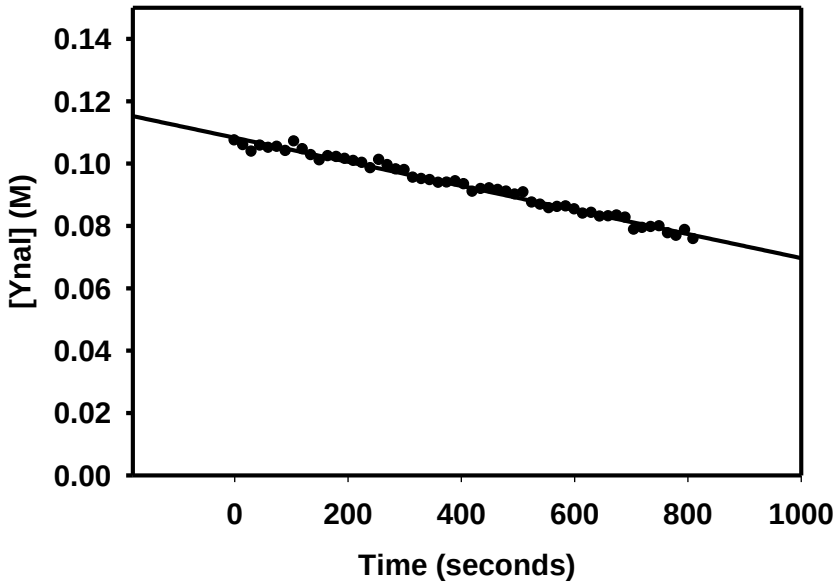


0.015 mol/L $Ni(COD)_2$, 0.30 mol/L $PCy_3$: initial rate = $5.89 \times 10^{-5}$ M/sec, $R^2 = 0.985$

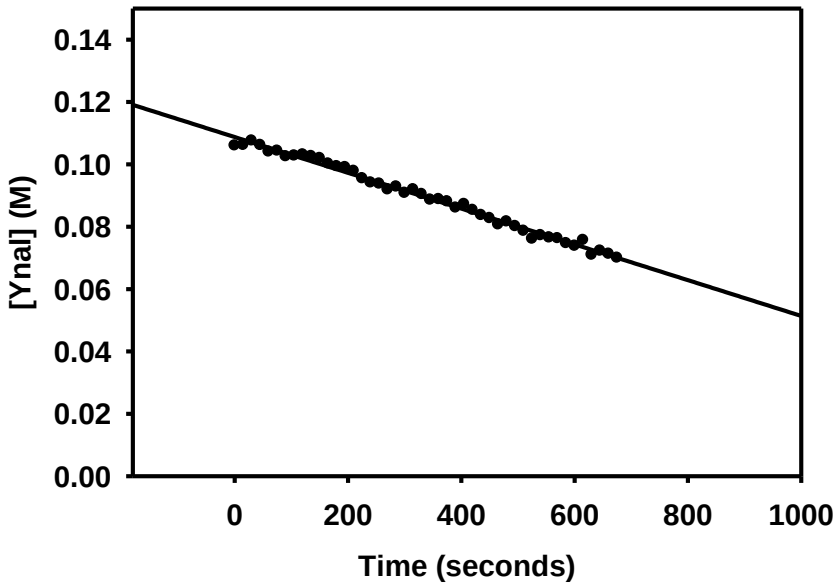

0.02 mol/L $Ni(COD)_2$, 0.04 mol/L $PCy_3$: initial rate = 7.27 x $10^{-5}$ M/sec, $R^2$ = 0.984

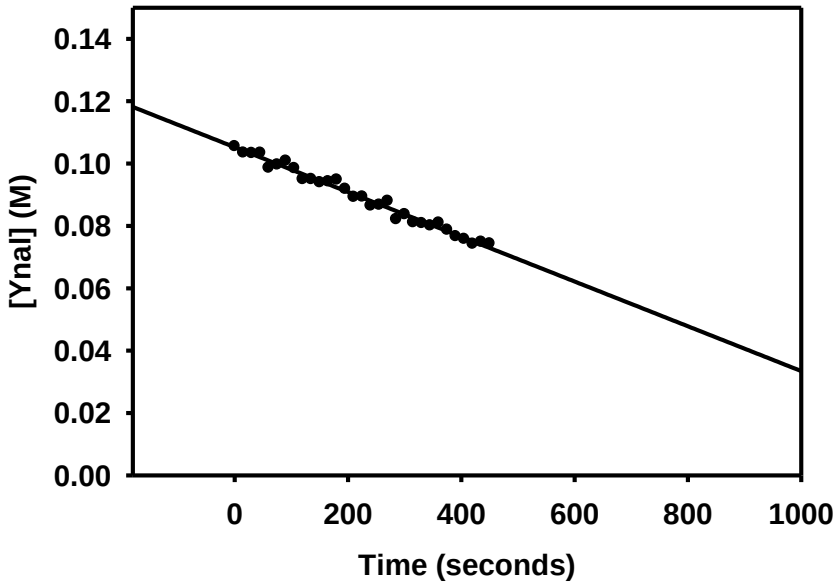


0.025 mol/L $Ni(COD)_2$, 0.05 mol/L $PCy_3$: initial rate = 8.95 x $10^{-5}$ M/sec, $R^2$ = 0.987

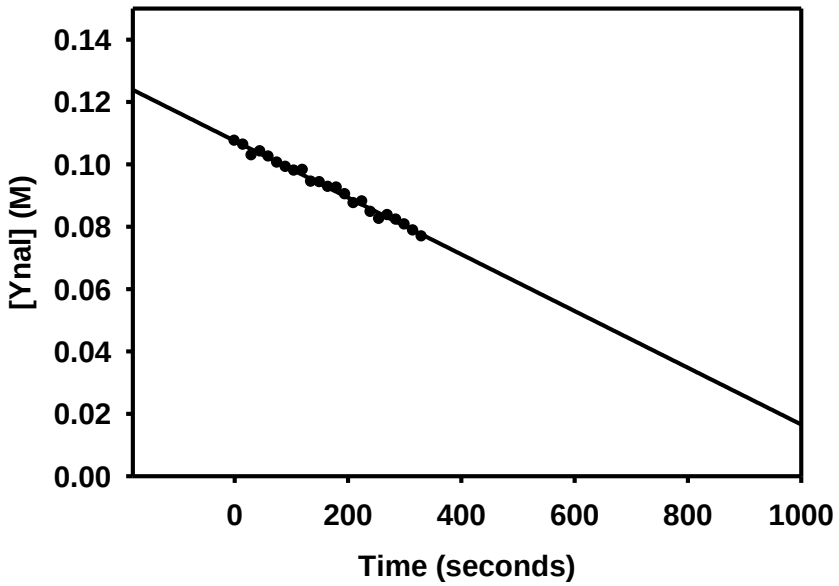

**Data for Initial Rate vs. Concentration of $Et_3SiH$**

Following the general procedure for kinetic analysis, $Ni(COD)_2$ (0.10 mmol) and $PCy_3$ (0.20 mmol) were reacted with ynal **29** (0.50 mmol) and $Et_3SiH$ (0.5-2.0 mmol) in 5 mL THF. Each reaction was carried out multiple times; reported values are given as the average of three runs with error expressed as the standard deviation between individual runs. Representative examples at each set of conditions are displayed below.

| $[Et_3SiH]$ (mol/L) | $\Delta$Ynal/$\Delta$t (M/sec) x $10^{-5}$ | Avg.$\Delta$Ynal/$\Delta$t | Std. Dev. |
|---|---|---|---|
| 0.10 | 7.08 | 7.13 | 0.05 |
| | 7.14 | | |
| | 7.18 | | |
| 0.20 | 7.60 | 7.32 | 0.26 |
| | 7.09 | | |
| | 7.27 | | |
| 0.30 | 7.60 | 7.99 | 0.60 |
| | 7.36 | | |
| | 8.46 | | |
| 0.40 | 7.23 | 7.16 | 0.15 |
| | 7.02 | | |
| | 7.23 | | |

0.10 mol/L $Et_3SiH$: initial rate = 7.14 x $10^{-5}$ M/sec, $R^2$ = 0.980

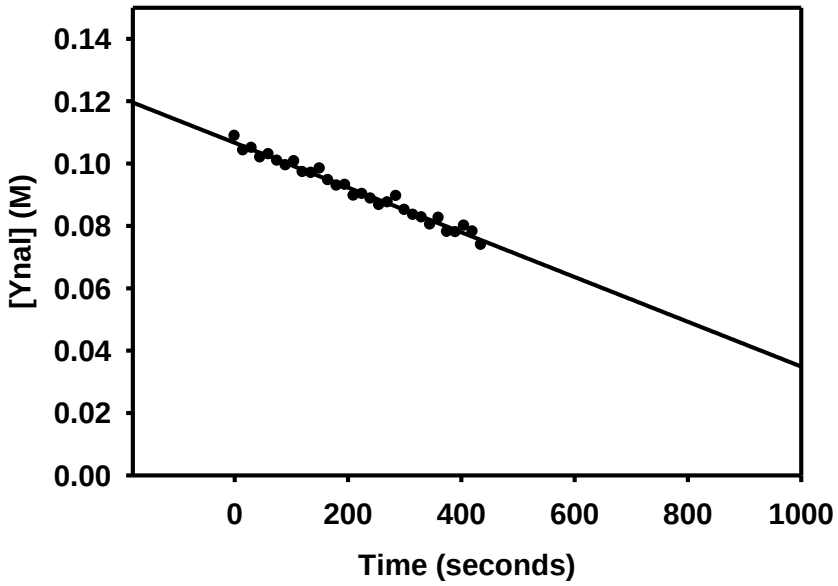


0.20 mol/L $Et_3SiH$: initial rate = 7.27 x $10^{-5}$ M/sec, $R^2$ = 0.984

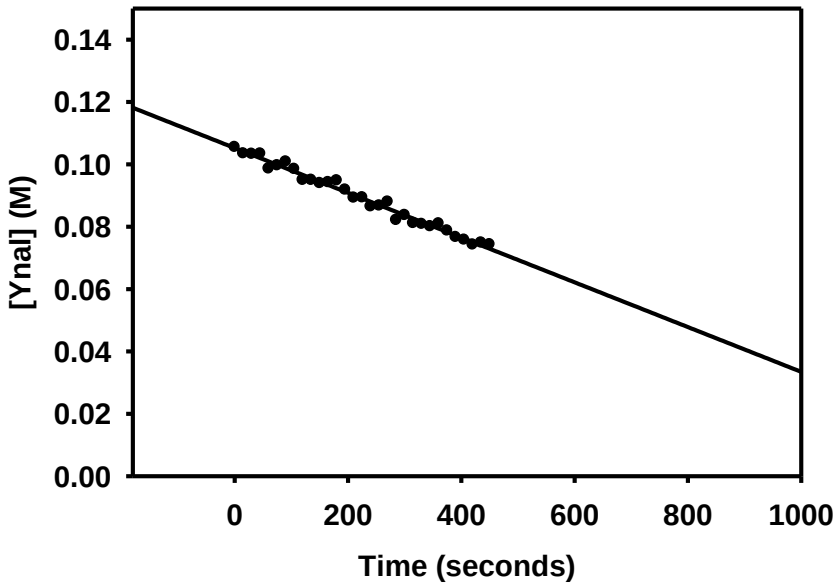

0.30 mol/L $Et_3SiH$: initial rate = 7.60 x $10^{-5}$ M/sec, $R^2$ = 0.970

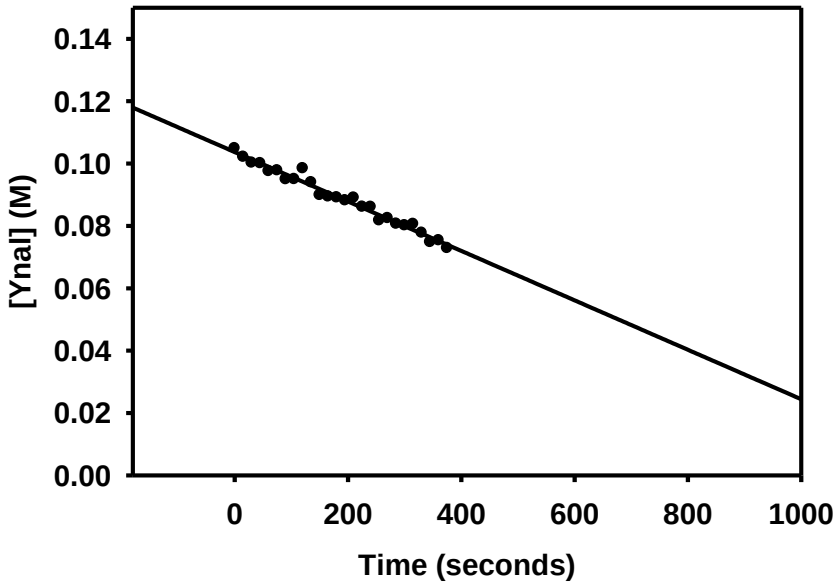


0.40 mol/L $Et_3SiH$: initial rate = 7.23 x $10^{-5}$ M/sec, $R^2$ = 0.979

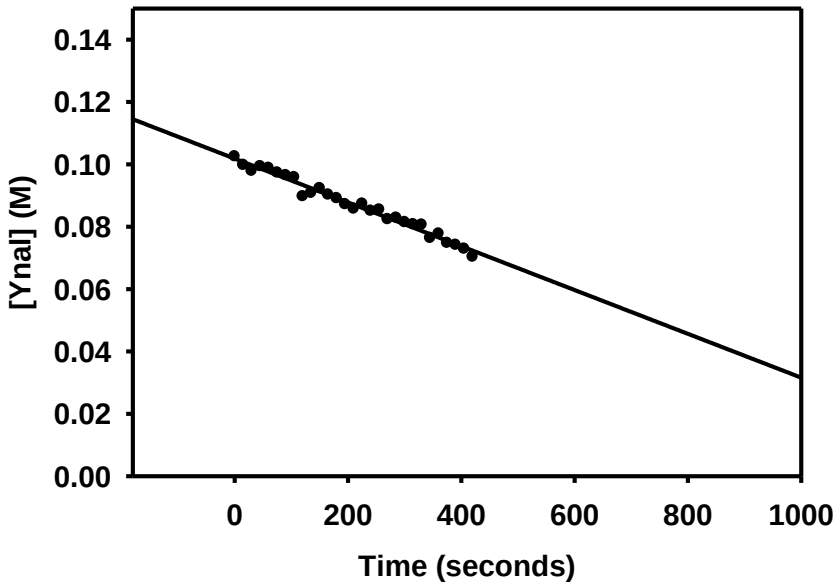

### 5.3.6.3 NMR Determination of the Kinetic Isotope Effect with Respect to Triethylsilane for Ynal Cyclization Using $Ni(COD)_2/PCy_3$

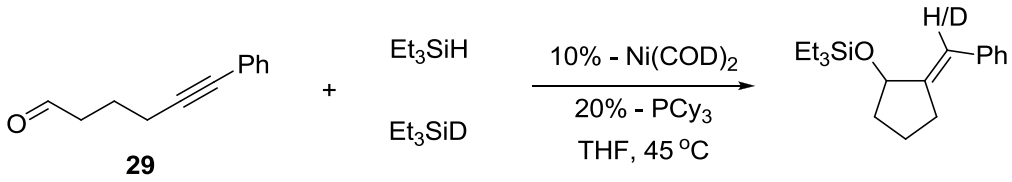


Following the general preparative procedure for nickel-catlayzed ynal **29** (86 mg, 0.50 mmol, 1.0 equiv) was cyclized in the presence of $Et_3SiH$ (174 mg, 1.5 mmol, 3.0 equiv) and $Et_3SiD$ (176 mg, 1.5 mmol, 3.0 equiv) at 45 $^oC$. After aqueous workup, the crude reaction mixture was flushed through a plug of silica gel using 100% Hexanes to yield the desired product (120 mg, 83%) as a colorless oil; spectral data were identical to previous reports.[1] This material was analyzed by NMR, and the integration of the vinylic proton was diagnostic for the percentage of hydrogen incorporation in the product.

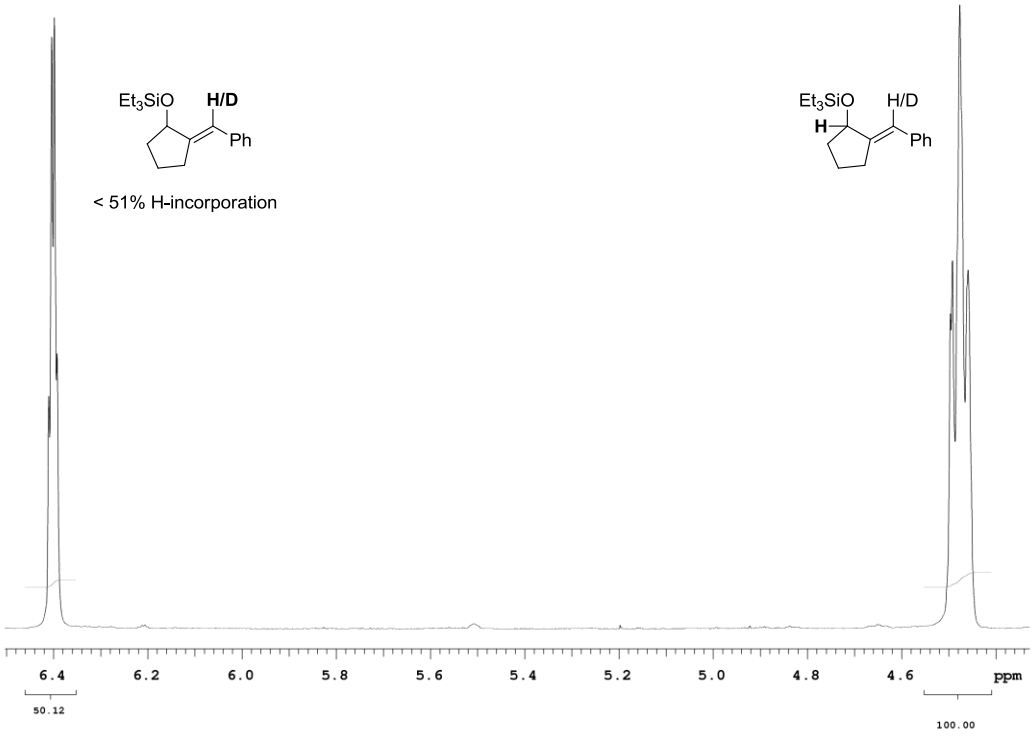


**NMR Determination of the Kinetic Isotope Effect with Respect to Triethylsilane for Aldehyde Hydrosilylation Using $Ni(COD)_2/PCy_3$**

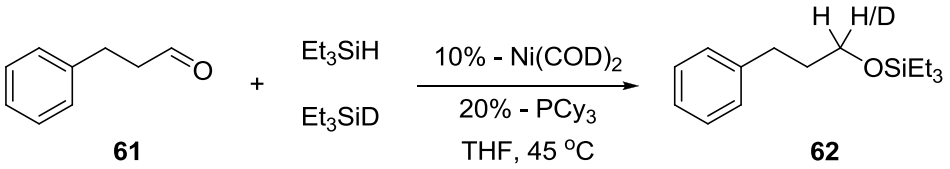


**61** **62**

$Ni(COD)_2$ (13.8 mg, 0.05 mmol, 0.1 equiv) and tricyclohexylphosphine (28 mg, 0.1 mmol, 0.2 equiv) were combined under an inert atmosphere and dissolved in 4 mL of THF at room temperature before being immersed in a 45 $^{o}$C oil bath. Triethylsilane (174 mg, 1.5 mmol, 3.0 equiv) and triethylsilane-d (0.176, 1.5 mmol, 3.0 equiv) were combined in 0.5 mL of THF and added to the stirred reaction mixture. Aldehyde **61** (68 mg, 0.5 mmol, 1.0 equiv) was dissolved in 0.5 mL of THF and added to the stirred

reaction mixture. After 12 hours the reaction mixture was cooled to room temperature, quenched with 10 mL $NaHCO_3$ (sat.) and extracted 3x each with 10 mL brine and EtOAc. The organic layer was dried with anhydrous $MgSO_4$, filtered, and solvent was removed by rotary evaporation. The crude reaction mixture was flushed through a plug of silica gel using 100% Hexanes to yield silyl ether product **62** (84 mg, 67%) as a colorless oil; spectral data were identical to previous reports.[60] This material was analyzed by NMR to determine the percent of hydrogen incorporation at the methylene position adjacent to oxygen. Relevant NMR peaks of the authentic samples are shown below for comparison.

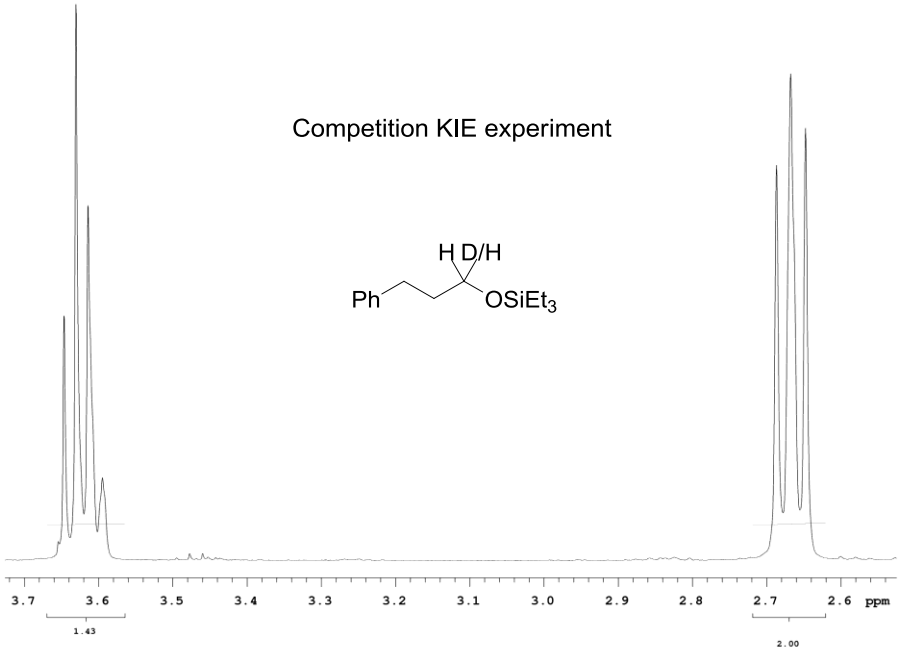

Authentic sample of unlabelled hydrosilylation product

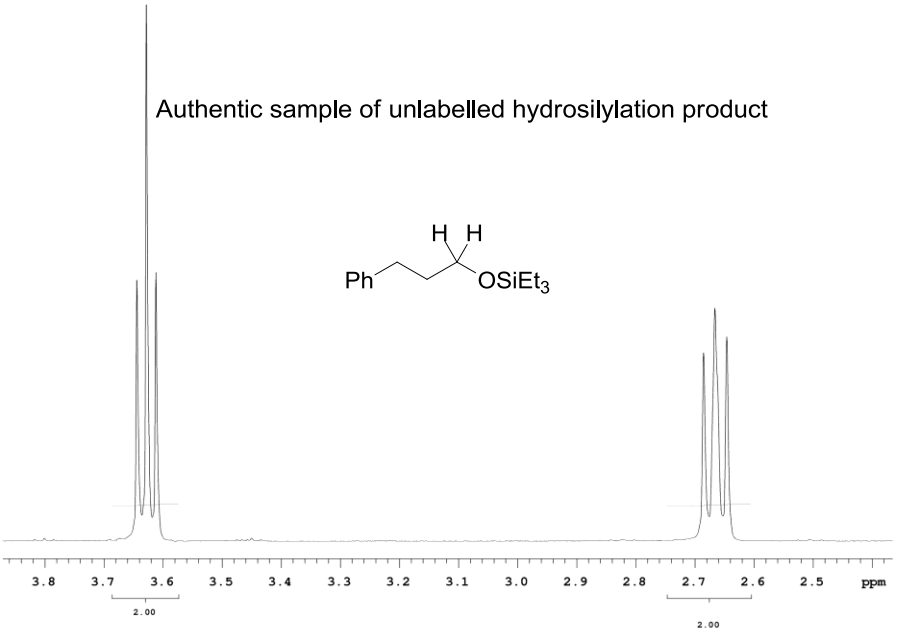


Authentic sample of mono-deuterated hydrosilylation product

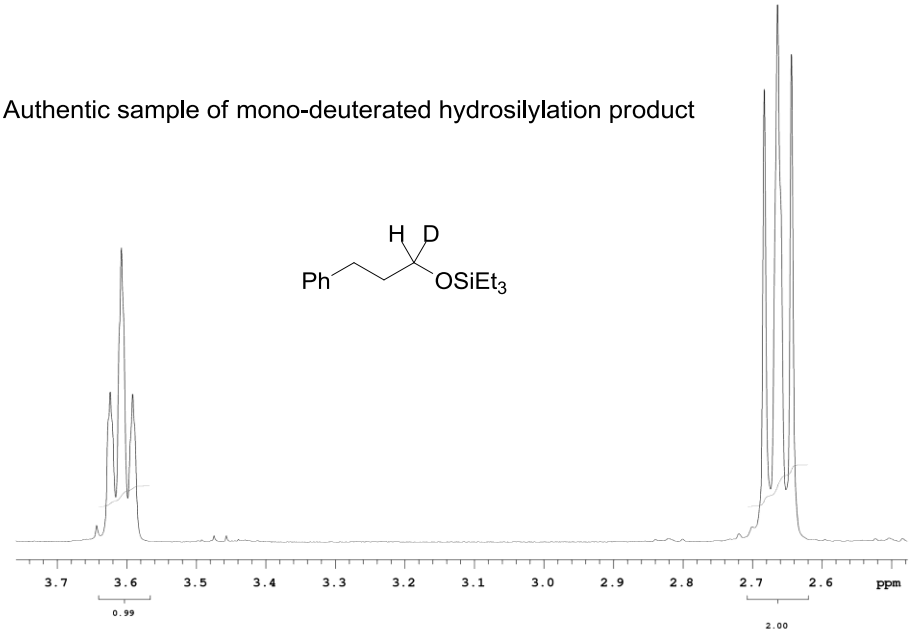

**5.3.6.5 Treatment of $Et_3SiH$ with a Stoichiometric Amount of $Ni(COD)_2/PCy_3$: Tracking Silane Si-H by *In Situ* IR**

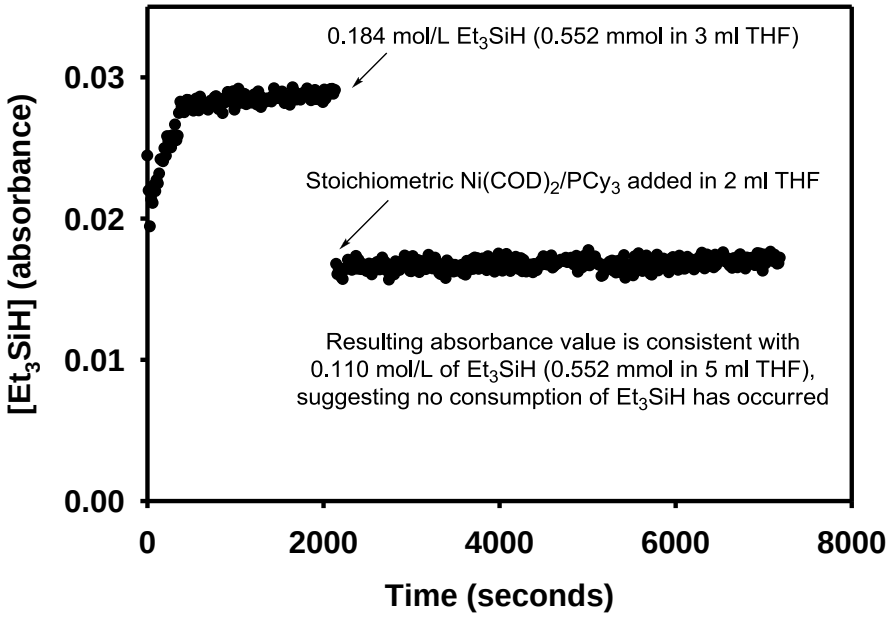


**Calibration Curve for $Et_3SiH$ at Various Concentrations**

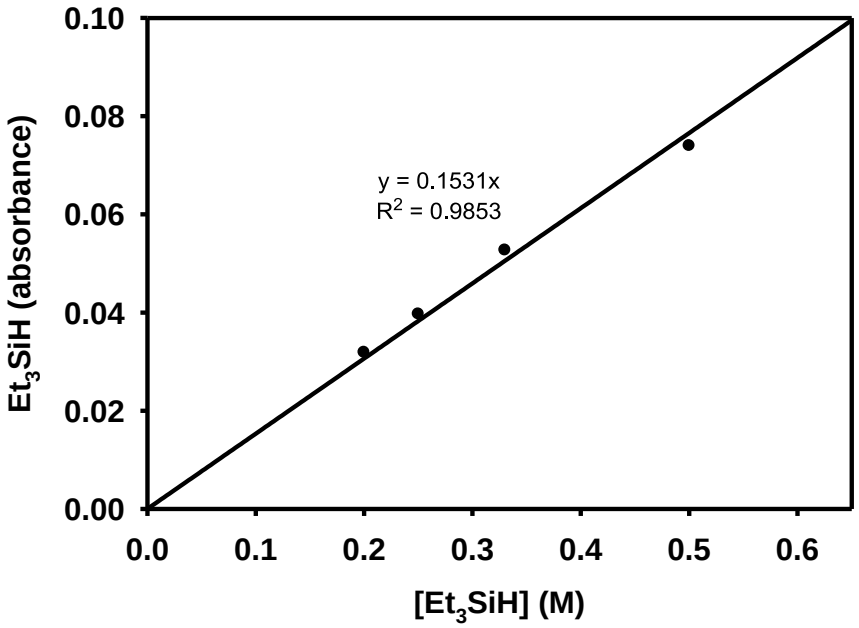

## 5.4 Experimental Procedures and Spectral Data: Chapter 4

All reagents were used as received unless otherwise noted. Solvents were purified under nitrogen using a solvent purification system (Innovative Technology, inc., Model # SPS-400-3 and PS-400-3. Aldehydes were distilled prior to use. $Ni(COD)_2$ (Strem Chemicals, Inc., used as received), 1,3-Bis(2,4,6-trimethyl-phenyl)imidazolium chloride (IMes·HCl), and potassium *tert*-butoxide were stored and weighed in an inert atmosphere glovebox. Triethylsilane was passed over a plug of alumina and stored under an inert atmosphere. Triethylsilane-$d_{15}$ was stored under an inert atmosphere and used as received. All reactions were conducted in flame-dried glassware under nitrogen atmosphere. $^{1}H$ and $^{13}C$ spectra were obtained in $CDCl_3$ at rt (22 $^{o}C$), unless otherwise noted, on a Varian Mercury 400 or Varian Unity 500 MHz instrument. Chemical shifts of $^{1}H$ NMR spectra were recorded in parts per million (ppm) on the δ scale from an internal standard of residual chloroform (7.27 ppm). Chemical shifts of $^{13}C$ NMR spectra were recorded in ppm from the central peak of $CDCl_3$ (77.0 ppm) on the δ scale. Gas chromatographs were acquired on an HP 6890 Series GC System with an HP-5MS column (30m x 0.252mm x 0.25 μm) attached to a an HP 5973N Series Mass Selective Detector. For GC analysis of kinetics, aliquots of crude reactions were quenched by filtering through a short plug of silica gel. Product ratios were determined by comparing substrate integration to a known amount of docosane ($C_{22}H_{46}$) as an internal standard. *In situ* FTIR data was acquired on a Mettler-Toledo ic10 ReactIR$^{TM}$ fitted with a 6mm diamond-tipped probe.

**General Procedure for Intermolecular Reductive Couplings of Aldehydes and Alkynes with IMes·HCl**

$Ni(COD)_2$ (13.8 mg, 0.05 mmol, 0.1 equiv), 1,3-bis(2,4,6-trimethyl-phenyl)imidazolium chloride, (IMes·HCl) (17.1 mg, 0.05 mmol, 0.1 equiv), and KO-*t*-Bu (5.6 mg, 0.05 mmol, 0.1 equiv) were combined under inert atmosphere and dissolved in 5 mL of THF at rt. Benzaldehyde (0.5 mmol, 1.0 equiv), 3-hexyne (0.5 mmol, 1.0 equiv), triethylsilane (0.5 mmol, 1.0 equiv), and internal standard (docosane, 0.25 mmol, 0.5 equiv) were combined in 1 ml of THF and added to the catalyst as a single portion via syringe. The progress of the reaction was monitored by TLC and GC. Upon completion, the reaction mixture was quenched with 10 mL $NaHCO_3$ (sat.) and extracted 3x each with 10 mL brine and EtOAc. The organic layer was dried with anhydrous $MgSO_4$, filtered, and solvent was removed by rotary evaporation. The crude reaction mixture was purified by silica gel chromatography using 98:2 Hexanes:EtOAc and the product was isolated as a colorless to pale yellow oil. Spectral data matched previous reports.[29]

**General Procedure for Kinetic Analysis: *In Situ* IR Monitoring of Intermolecular Coupling with $Ni(COD)_2$/IMes/$Et_3SiH$**

$Ni(COD)_2$ (0.05 mmol, 0.1 equiv), 1,3-bis(2,4,6-trimethyl-phenyl)imidazolium chloride, (IMes·HCl) (0.05 mmol, 0.1 equiv), and KO-*t*-Bu (0.05 mmol, 0.1 equiv) were combined under an inert atmosphere in a 10 mL three-necked round-bottomed flask equipped with a three-way valve, two septa, and a teflon coated stirbar. The IR probe was inserted through the center neck of the flask via a nitrogen-purged teflon adapter under positive nitrogen pressure before adding 8 mL of THF to the catalyst mixture. The stirred catalyst mixture was then immersed in a water/ice bath and stirred. Solvent subtracted spectra were acquired at 15 second intervals for approximately 15 minutes until the

baseline of the IR spectrum at 1708 $cm^{-1}$ (aldehyde C=O peak) had stabilized. Benzaldehyde (0.50 mmol, 1.0 equiv), 3-hexyne (0.50 mmol, 1.0 equiv) and triethylsilane (0.5 mmol, 1.0 equiv) were combined in 2 mL of THF and added to the stirred catalyst as a single portion via syringe. Reaction progression was monitored by the decreasing absorbance of the aldehyde C=O stretch as a function of time. Correlation of aldehyde disappearance to product appearance was confirmed by GCMS analysis using docosane ($C_{22}H_{46}$) as an internal standard. Absolute absorbance values were determined by the peak height at 1708 $cm^{-1}$ relative to a baseline zeroed value at 1700 $cm^{-1}$. For the purpose of determining initial rates, reactions were monitored up to 30% conversion to ensure data was collected beyond at least one catalyst turnover. Rate data was manipulated in an analogous fashion to that described in Section 5.3.3.

# References


(1) Mahandru, G. M.; Liu, G.; Montgomery, J. *J. Am. Chem. Soc.* **2004**, *126*, 3698.

(2) Oblinger, E.; Montgomery, J. *J. Am. Chem. Soc.* **1997**, *119*, 9065.

(3) Huang, W. S.; Chan, J.; Jamison, T. F. *Org. Lett.* **2000**, *2*, 4221.

(4) Wipf, P. In *Comprehensive Organic Synthesis*; Trost, B. M., Ed.; Pergamon Press: Oxford, 1991; Vol. 5, p 827.

(5) Hoveyda, A. H.; Evans, D. A.; Fu, G. C. *Chem. Rev.* **1993**, *93*, 1307.

(6) Godleski, S. A. In *Comprehensive Organic Synthesis*; Trost, B. M., Ed.; Pergamon Press: Oxford, 1991; Vol. 4, p 585.

(7) Jin, H.; Uenishi, J.; Christ, W. J.; Kishi, Y. *J. Am. Chem. Soc.* **1986**, *108*, 5644.

(8) Takai, K.; Tagashira, M.; Kuroda, T.; Oshima, K.; Utimoto, K.; Nozaki, H. *J. Am. Chem. Soc.* **1986**, *108*, 6048.

(9) Srebnik, M. *Tetrahedron Letters* **1991**, *32*, 2449.

(10) Montgomery, J.; Savchenko, A. V. *J. Am. Chem. Soc.* **1996**, *118*, 2099.

(11) Tang, X.-Q.; Montgomery, J. *J. Am. Chem. Soc.* **1999**, *121*, 6098.

(12) Tang, X.-Q.; Montgomery, J. *J. Am. Chem. Soc.* **2000**, *122*, 6950.

(13) Franz, A. K.; Woerpel, K. A. *Acc. Chem. Res.* **2000**, *33*, 813.

(14) Denmark, S. E.; Pan, W. *Org. Lett.* **2001**, *3*, 61.

(15) Tamao, K.; Akita, M.; Kumada, M. *J. Organomet. Chem.* **1983**, *254*, 13.

(16) *Strategic Applications of Named Reactions in Organic Synthesis*; Elsevier, 2005.

(17) Marshall, J. A.; Yanik, M. M. *J. Org. Chem.* **2001**, *66*, 1373.

(18) Bergens, S. H.; Noheda, P.; Whelan, J.; Bosnich, B. *J. Am. Chem. Soc.* **1992**, *114*, 2121.

(19) Chalk, A. J.; Harrod, J. F. *J. Am. Chem. Soc.* **1965**, *87*, 16.

(20) Murai, S.; Sonoda, N. *Angew. Chem. Int. Ed. Engl.* **1979**, *18*, 837.

(21) Leighton, J. L.; Chapman, E. *J. Am. Chem. Soc.* **1997**, *119*, 12416.

(22) O'Malley, S. J.; Leighton, J. L. *Angew. Chem. Int. Ed. Engl.* **2001**, *40*, 2915.

(23) Clark, T. B.; Woerpel, K. A. *J. Am. Chem. Soc.* **2004**, *126*, 9522.

(24) Driver, T. G.; Woerpel, K. A. *J. Am. Chem. Soc.* **2004**, *126*, 9993.

(25) Franz, A. K.; Woerpel, K. A. *J. Am. Chem. Soc.* **1999**, *121*, 949.

(26) Ravikumar, P. C.; Yao, L.; Fleming, F. F. *J. Org. Chem.* **2009**, *74*, 7249.

(27) Amarasinghe, K. K. D.; Montgomery, J. *J. Am. Chem. Soc.* **2002**, *124*, 9366.

(28) Baxter, R. D.; Montgomery, J. *J. Am. Chem. Soc.* **2008**, *130*, 9662.

(29) Chaulagain, M. R.; Sormunen, G. J.; Montgomery, J. *J. Am. Chem. Soc.* **2007**, *129*, 9568.

(30) Noyori, R.; Suzuki, M. *Science* **1993**, *259*, 44.

(31) Dobbs, D. A.; Vanhessche, K. P. M.; Brazi, E.; Rautenstrauch, V.; Lenoir, J.-Y.; Genet, J.-P.; Wiles, J.; Bergens, S. J. *Angew. Chem. Int. Ed. Engl.* **2000**, *39*, 1992.

(32) Seepersaud, M.; Al-Abed, Y. *Tetrahedron Lett.* **2000**, *41*, 4291.

(33) Larock, R. C.; Oertle, K.; Potter, G. F. *J. Am. Chem. Soc.* **1980**, *102*, 190.

(34) Tanaka, K.; Fu, G. C. *J. Am. Chem. Soc.* **2001**, *123*, 11492.

(35) Willis, M. C. *Chem. Rev.* **2010**, *110*, 725.

(36) Takeishi, K.; Sugishama, K.; Sasaki, K.; Tanaka, K. *Chem. Eur. J.* **2004**, *10*, 5681.

(37) Jun, C.-H.; Lee, H.; Hong, J.-B.; Kwon, B.-I. *Angew. Chem. Int. Ed. Engl.* **2002**, *41*.

(38) Williams, V. M.; Leung, J. C.; Patman, R. L.; J., K. M. *Tetrahedron* **2009**, *65*, 5024.

(39) Tsuda, T.; Kiyoi, T.; Saegusa, T. *J. Org. Chem.* **1990**, *55*, 2554.

(40) Ogoshi, S.; Arai, T.; Ohashi, M.; Kurosawa, H. *Chem. Comm.* **2008**, 1347.

(41) Crabtree, R. H. *The Organometallic Chemistry of the Transition Metals*; Wiley-Interscience: Hoboken, 2005.

(42) Montgomery, J.; Sormunen, G. J. In *Metal Catalyzed Reductive C-C Bond Formation: A Departure from Preformed Organometallic Reagents*; Krische, M. J., Ed.; Springer: Berlin, 2007; Vol. 279, p 1.

(43) Moslin, R. M.; Miller-Moslin, K.; Jamison, T. F. *Chem. Comm.* **2007**, 4441.

(44) Ikeda, S. *Angew. Chem. Int. Ed. Engl.* **2003**, *42*, 5120.

(45) Malik, H. A.; Baxter, R. D.; Montgomery, J. In *Catalysis Without Precious Metals*; Bullock, R. M., Ed.; Wiley: 2010, p 181-212.

(46) Malik, H. A.; Sormunen, G. J.; Montgomery, J. *J. Am. Chem. Soc.* **2010**, *132*, 5966.

(47) Kablaoui, N. M.; Buchwald, S. L. *J. Am. Chem. Soc.* **1996**, *118*.

(48) Crowe, W. E.; Rachita, M. J. *J. Am. Chem. Soc.* **1995**, *117*.

(49) McCarren, P. R.; Liu, P.; Cheong, P., H-Y.; Jamison, T. F.; Houk, K. N. *J. Am. Chem. Soc.* **2009**, *131*, 6654.

(50) Cheng, T. Y.; Bullock, R. M. *J. Am. Chem. Soc.* **1999**, *121*, 3150.

(51) Jones, W. D. *Acc. Chem. Res.* **2003**, *36*, 140.

(52) Schneider, N.; Finger, M.; Haferkemper, C.; Bellemin-Laponnaz, S.; Hofmann, P.; Gade, L. H. *Chem. Eur. J.* **2009**, *15*, 11515.

(53) Denmark, S. E.; Wong, K.-T.; Stavenger, R. A. *J. Am. Chem. Soc.* **1997**, *119*, 2333.

(54) Falck, J. R.; He, A.; Reddy, M.; Kundu, A.; Barma, D. B.; Bandyopadhyay, A.; Kamila, S.; Akella, R.; Bejot, R.; Mioskowski, C. *Org. Lett.* **2006**, *8*, 4645.

(55) Kreher, U. P.; Rosamilia, A. E.; Raston, C. L.; Scott, J. L.; Strauss, C. R. *Org. Lett.* **2003**, *5*, 3107.

(56) Lee, D.-Y.; Moon, C. W.; Jun, C.-H. *J. Org. Chem.* **2002**, *67*, 3945.

(57) Bellina, F.; Carpita, A.; Ciucci, D.; De Santis, M.; Rossi, R. *Tetrahedron* **1993**, *49*, 4677.

(58) Hojo, M.; Sakata, K.; Ushioda, N.; Watanabe, T.; Nishikori, H.; Hosomi, A. *Organometallics* **2001**, *20*, 5014.

(59) Ishihara, K.; Kurihara, H.; Yamamoto, H. *Synlett* **1997**, *5*, 597.

(60) Yeom, C.-E.; Kim, Y. J.; Lee, S. Y.; Shin, Y. J.; Kim, B. M. *Tetrahedron* **2005**, *61*, 12227.